CRANFIELD UNIVERSITY

AQEEL SHAMSUL

A BIOCUBESAT COMPATIBLE PAYLOAD FOR FUTURE SPACE SYSTEMS: DEVELOPMENT OF A SECOND GENERATION BAMMSAT PAYLOAD FOR STRATOSPHERIC BALLOON FLIGHT

SCHOOL OF AEROSPACE, TRANSPORT AND MANUFACTURING
Space Research Group

PhD

Academic Year: 2017 - 2022

First Supervisor: Professor David C. Cullen
Second Supervisor: Dr. Stephen Hobbs
February 2022

CRANFIELD UNIVERSITY

SCHOOL OF AEROSPACE, TRANSPORT AND MANUFACTURING
Space Research Group

PhD

Academic Year 2017 - 2022

AQEEL SHAMSUL

A BIOCUBESAT COMPATIBLE PAYLOAD FOR FUTURE SPACE SYSTEMS: DEVELOPMENT OF A SECOND GENERATION BAMMSAT PAYLOAD FOR STRATOSPHERIC BALLOON FLIGHT

First Supervisor: Professor David C. Cullen
Second Supervisor: Dr. Stephen Hobbs
February 2022

This thesis is submitted in partial fulfilment of the requirements for the degree of Doctor of Philosophy

© Cranfield University 2022. All rights reserved. No part of this publication may be reproduced without the written permission of the copyright owner.

ABSTRACT

National space agencies have announced planned long-duration crewed missions beyond Low Earth Orbit. It is critical to understand the impact of long-duration microgravity and especially deep-space radiation exposure on humans. There is a knowledge gap concerning the effects of the space environment on humans, our human microbiome and associated Earth biology needed to support human activities in space.

There is also a renaissance in the space industry, as seen in increased space activities and commercialisation. This is driven by the growing international activities, shifting funding landscape, and change in commercialisation activities. It is thought that the space industry is at an inflexion point for a full-scale microgravity research programme (DiFrancesco & Olson, 2015). With a newfound interest in life science and microgravity, there is a need for validating data on space-based biological models for terrestrial and space applications. These biological studies require frequent access and many discrete samples before they can be understood and accepted by the scientific community.

CubeSats offer opportunities to improve spaceflight access with reduced development time using standardised components, more frequent flight opportunities, and reduced mission costs. Over the last decade, a series of seven bioCubeSats have been launched into orbit by NASA and SpacePharma: GeneSat, PharmaSat, O/OREOS, SporeSat, Dido-2, EcAMSat and Dido-3. The term bioCubeSat refers to a CubeSat with a biological payload onboard. These bioCubeSats proved the feasibility and de-risk the concept of performing a biological experiment on CubeSat. However, these bioCubeSats have design limitation that inhibits the types of organisms and experiments that could be performed onboard. The design limitation affects the number of independent discrete samples, pre-flight handling capability, and sensor types within its system.

Cranfield University has been developing an alternative bioCubeSat concept named BAMMsat, for application in LEO and beyond LEO. BAMMsat stands for

Bioscience, Astrobiology, Medical, and Material science on CubeSats. The versatile platform builds upon the typical experiment need of these scientific fields, such as i) the need to house multiple samples, ii) the need to maintain viable samples in an appropriate space environment, iii) the need to artificially perturb the samples and (iv) the need to monitor the samples. BAMMsat was developed to address the knowledge gap to fly a broader range of organisms and experiments enabled by its Rotary Valve, Multi-Chamber Sample Disc, and richer sensor offering.

BAMMsat could be an asset to provide autonomous and high-throughput experiments as an R&D instrument for space bioscience and biotechnology. At a lower entry cost combined with the capability to perform an autonomous in-situ data measurement, BAMMsat could increase life science in microgravity either for using space for a terrestrial application and supporting future human exploration of the Moon and Mars.

The PhD thesis reports on PhD research performed to advance the BAMMsat concept developing the 1st gen. laboratory breadboard (TRL 4) into a 2nd gen. technology demonstration hardware (TRL 5/6) and bridging the gap towards a 3rd gen. spaceflight mission, currently planned to be on-board the ISS. During the PhD, five different subsystems were developed: the multi-chamber sample disc, rotary valve, compact brightfield microscope, fluidic subsystem, Geneva gear mechanism, and mechanical housing. These subsystems were packaged into a 2U CubeSat payload version of BAMMsat. The 2U CubeSat payload was flown under the BAMMsat-on-BEXUS (BoB) mission. BoB mission was an experiment using live *C. elegans* from Cranfield University and the University of Exeter, performing a technology and operation demonstration of a 2nd gen. design of BAMMsat hosted on a stratospheric balloon at an altitude of ~28 km above the ground under the BEXUS programme.

Keywords:

CubeSat, C. elegans, bioscience, astrobiology, material, medicine, nanosatellite, BEXUS, stratosphere, technology demonstration.

ACKNOWLEDGEMENTS

I would like to thank Cranfield University for the support provided throughout the PhD research. The output of this research is only possible with a good infrastructure and support system behind the PhD programme.

I would like to especially thank Prof David C. Cullen for his excellent guidance and supervision throughout the PhD. They say supervisor makes or breaks a PhD, and you make them. It was evident that you go above and beyond to support your students. The PhD would not have advanced thus far without your generous guidance, knowledge sharing, intellectual discussion, and support.

Thanks to the Space Research Group for various insights, discussions, and feedback for this PhD research. The group certainly made an enjoyable research environment.

Thanks to Mr Jarryd Braithwaite, Specialist Technical Officer, for his support with the lab facilities and design development.

Many thanks to my sponsor, the Majlis Amanah Rakyat, for covering the PhD tuition fees and Cranfield University for the PhD tuition fees and bursary. Without the funding, the advancement of this research would not have been possible.

I would also like to thank the Swedish National Space Agency (SNSA), German Aerospace Centre (DLR), and European Space Agency (ESA) for their ongoing support in the BEXUS programme. You are making a difference in the space industry.

A special thanks to all the BAMMsat-on-BEXUS team members who went above and beyond. Even after your MSc studies, your hard work and support for the project were admirable and key to its success. In no particular order, thanks to M. Zalasiewicz, G. Sinclair, A. Bolliand, M. Cooke, A. Chabi, M. Martinez De Bujo, N. Shetti, R. Giraud, S. Raj, H. Lleo, J. Lucero, and R. Panchal. BoB was an incredible experience that will shape my thought process throughout my career.

Thank you to the entire SATM Cranfield Workshop team; meeting the BEXUS milestones would have been impossible without their expertise and care to produce a quick turnaround of high-quality parts.

A well overdue thanks to my parents and family. To my parents, Shamsul Salim and Dr Anis Amira Ab Rahman, thanks for your unconditional support in helping us achieve our goals. To my brothers, Arif, Amir, Aniq, and Danish, who are always there for our family.

Thanks to Momo and Dun Dun for their emotional support.

A warm and special thanks to my dear partner, Selena Zang, who has been through thick and thin throughout the PhD. Your many supports were key to the PhD, and I am truly lucky. Both of us went through our PhDs at the same time, and we share unique and great memories that not many can experience.

TABLE OF CONTENTS

ABSTRACT iii
ACKNOWLEDGEMENTS v
LIST OF FIGURES xiii
LIST OF TABLES xx
LIST OF EQUATIONS xxii
LIST OF ABBREVIATIONS xxiii
1 Background and Introduction 1
1.1 The motivation behind the PhD research 1
1.2 A brief history of BAMMsat 4
1.3 Introduction to the BAMMsat-on-BEXUS (BoB) mission 8
1.3.1 Introduction to the REXUS/BEXUS programme 9
1.3.2 Brief overview of the BoB mission, system, and payload 10
1.4 PhD research aim and objectives 14
1.4.1 Aim 14
1.4.2 Objectives 14
1.5 Narrative of the PhD research 17
1.6 Contributions to knowledge 21
1.7 Structure of the thesis documents 24
1.7.1 Chapter 1 24
1.7.2 Chapter 2 24
1.7.3 Chapter 3 25
1.7.4 Chapter 4 25
1.7.5 Chapter 5 25
1.7.6 Chapter 6 25
1.7.7 Chapter 7 26
1.7.8 Chapter 8 26
1.7.9 Chapter 9 26
1.7.10 Chapter 10 26
2 Literature Review 27
2.1 Introduction 27
2.2 Aim and objectives 28
2.3 Literature review research methodology 29
2.3.1 List of literature resources 29
2.3.2 List of search strings 30
2.4 Results and analysis from literature review 33
2.4.1 Establishing the background knowledge for bioCubeSat 33
2.4.2 Establishing the current state of the art technology 37
2.4.3 Establishing the current public domain knowledge on stratospheric balloon testing for technology demonstration 60

2.5 Discussion and conclusion 62
3 Subsystem level – 2nd gen. MCSD and RV subsystems: Design, manufacture, and test 64
3.1 Introduction to the chapter 64
3.2 Introduction to the MCSD and RV concept 65
3.3 Aim and objectives 66
3.4 Overview of the 1st gen. MCSD and RV 67
3.4.1 Introduction to the 1st gen. design 67
3.4.2 Evaluation and critiques on 1st gen. design 70
3.5 List of design needs for the 2nd gen. 72
3.6 Preliminary design concept and material selection for the 2nd gen. 75
3.6.1 Preliminary design - MCSD and RV material selection 76
3.6.2 Preliminary design - Geneva mechanism sizing and material selection 86
3.7 Manufacturing techniques 88
3.7.1 CNC machining 88
3.8 Initial design (V1) of the 2nd gen. MCSD and RV 93
3.8.1 Overview of the initial design 93
3.8.2 Discussion on leaking issue in the initial design 96
3.8.3 Design improvement on leaking issue 98
3.9 Final design (V2) of 2nd gen. MCSD and RV 101
3.9.1 Overview of the final design (V2) 101
3.9.2 Testing performed on the 2nd gen. MCSD and RV (V2) 104
3.10 Discussion, conclusion, and future work 109
3.10.1 Discussion and conclusion 109
3.10.2 Future work 114
4 Subsystem level – Compact brightfield microscope: Design, manufacture, and test 116
4.1 Introduction 116
4.2 Aim and objectives 117
4.3 Overview of the 1st gen. BAMMsat microscope 118
4.3.1 Introduction to the 1st gen. design 118
4.3.2 Evaluation and critique on 1st gen. design 121
4.4 List of requirements for the compact brightfield microscope for the BoB mission 123
4.5 Preliminary design for the compact brightfield microscope 125
4.5.1 Preliminary design concept 125
4.5.2 Justification for using Raspberry Pi (RPi) V2.1 camera 126
4.5.3 Sizing the *C. elegans* against the IMX219 RPi camera sensor 127
4.5.4 Lens selection 128
4.6 Initial design and test (V1) 133

4.6.1 Initial design (V1) 133
4.6.2 Initial test – Resolving *C. elegans* 134
4.7 Final design and test (V2) 140
4.7.1 Summary of the final design 140
4.7.2 Characterising the optical performance 141
4.8 Verification matrix 145
4.9 Discussion, conclusion, and future work 146
4.9.1 Discussion and conclusion 146
4.9.2 Future work 150
5 Subsystem level – 2nd gen. fluidics subsystem: Design, manufacture, and test 152
5.1 Introduction 152
5.2 Aim and objectives 153
5.3 Overview of 1st gen. fluidic subsystem 154
5.3.1 Introduction to the 1st gen. design 154
5.3.2 Evaluation and critiques on the 1st gen. design 157
5.4 List of requirements for the 2nd gen. fluidic subsystem for the BoB mission 161
5.5 Description of the design process 163
5.6 Characterising the mp6 pump performance with the MCSD and RV 166
5.6.1 Results from initial characterisation testing of the mp6 pump 167
5.6.2 Results from initial pumping into the MCSD and RV 170
5.6.3 Results from testing to find the lowest possible flow rate 171
5.6.4 Results from testing on pulling vs pushing the liquids 175
5.7 Characterising the LPG10 flow sensor performance 177
5.7.1 Result from the flow sensor verification test 177
5.8 Design and manufacture of the 2nd gen. selector valve manifold 180
5.9 Verification matrix 183
5.10 Discussion, conclusion, and future work 184
5.10.1 Discussion and conclusion 184
5.10.2 Future work 186
6 Subsystem level – 2nd gen. Geneva gear mechanism: Design, manufacture, and test 188
6.1 Introduction 188
6.2 Aim and objectives 189
6.3 Overview of the 1st gen. Geneva gear mechanism 190
6.3.1 Introduction to the 1st gen. design 190
6.3.2 Evaluation and critiques of the 1st gen. design 192
6.4 List of requirements for the 2nd gen. Geneva gear mechanism for the BoB mission 194
6.5 Description on the design process 195

6.6 Motor selection for the Geneva gear mechanism 196
6.6.1 Characterising the estimated torque to rotate the MCSD once bolted 196
6.6.2 Estimating the torque translated at the motor from the MCSD 197
6.6.3 Motor selection trade-off analysis 199
6.7 Final design and manufacture of Geneva gear and motor housing 202
6.8 2nd gen. Geneva gear mechanism test 205
6.9 Verification matrix 207
6.10 Discussion, conclusion, and future work 208
6.10.1 Discussion and conclusion 208
6.10.2 Future work 210
7 Subsystem level – Mechanical support: Design, manufacture and test 212
7.1 Introduction 212
7.2 Aim and objectives 213
7.3 Overview of the 1st gen. mechanical support 214
7.3.1 Introduction to the 1st gen. design 214
7.3.2 Evaluation and critiques of the 1st gen. design 215
7.4 List of requirements for the 2nd gen. mechanical support 216
7.5 Discussion on the design and manufacturing process 217
7.6 Issue during the initial mechanical assembly test 219
7.7 Verification matrix 221
7.8 Discussion, conclusion, and future work 222
7.8.1 Discussion and conclusion 222
7.8.2 Future work 224
8 System level – 2nd gen. BAMMsat bioCubeSat payload: Assembly, Integration, and Testing (AIT) 225
8.1 Introduction 225
8.2 Aim and objectives 228
8.3 Overview of BoB system (3U) initial design 229
8.4 Overview of the 2nd gen. BAMMsat bioCubeSat payload (2U) initial design 233
8.5 Core functionalities of the 2nd gen. BAMMsat bioCubeSat payload for BoB mission 236
8.6 List of requirements for the BoB system 239
8.7 AIT of the 2nd gen. BAMMsat bioCubeSat payload (2U) into the BoB system (3U) 240
8.7.1 Description of the planned AIT process 240
8.7.2 Implementation of AIT process 241
8.8 Final design of the BoB system, ready for BoB flight campaign 249
8.9 Verification matrix 251
8.10 Discussion, summary, and future work 252

8.10.1 Discussion and summary 252
8.10.2 Future work 252
9 BAMMsat-on-BEXUS: Flight campaign summary, preliminary analysis of the flight results and lessons learnt 255
9.1 Introduction 255
9.1.1 Why BEXUS? 257
9.1.2 BEXUS system and gondola 259
9.1.3 The environment experienced by the BoB system during pre-flight and flight operations 260
9.1.4 Why *C. elegans on BAMMsat-on-BEXUS mission*? 263
9.2 BAMMsat-on-BEXUS mission aim and objectives 265
9.3 BAMMsat-on-BEXUS: The team, roles, management, and challenges 269
9.3.1 Work packages and responsible personnel 269
9.3.2 Challenges in project management 272
9.4 Final flight design and operations 275
9.4.1 Imaging problems and modification at Esrange space centre 279
9.4.2 Leakage issue and increased number of housed samples inside the 2nd gen. MCSD as a mitigation strategy 282
9.5 Preliminary analysis of BAMMsat-on-BEXUS flight results 286
9.5.1 Summary of flight timeline and flight path 286
9.5.2 Comparison between flight environment and internal BoB environment and its impact on the BoB system 289
9.5.3 Flight results analysis 297
9.6 Flight campaign discussion, conclusion and lessons learnt 304
9.6.1 Flight campaign discussion 304
9.6.2 Flight campaign conclusion 311
9.6.3 Future work and lessons learnt 314
10 Final discussion, future work, and conclusion 318
10.1 Final discussion 318
10.2 Future work 333
10.3 Conclusion 333
REFERENCES 335
APPENDICES 349
Appendix A BAMMsat-on-BEXUS requirements and constraints 349
Appendix B BAMMsat-on-BEXUS verification matrix 360
Appendix C Thorlabs MAP051919-A datasheet 385
Appendix D BoB custom lens assembly 386
Appendix E BoB custom camera mount 387
Appendix F BoB custom lens tube 388
Appendix G List of publications by the author throughout the PhD research 389

Appendix H Bartels Mikrotechnik mp6 datasheet 390
Appendix I Sensirion LPG10 datasheet 396
Appendix J Sensirion LPG10 Basic Performance Check..... 401

LIST OF FIGURES

Figure 1-1. Timeline representing the BAMMsat development alongside the successfully launched bioCubeSat to date. 4

Figure 1-2. BAMMsat NSTP-2 integrated fluidic and microscope breadboard of 1st generation BAMMSat (Image courtesy of Prof Cullen). 5

Figure 1-3. BAMMsat NSTP-2 fluidics network, actuators, and sensor subsystem (Image courtesy of Prof Cullen). 5

Figure 1-4. Images of BEXUS large stratospheric balloon and BAMMsat-on-BEXUS. 9

Figure 1-5. (Top) Rendered CAD showing the 3U BoB system. (Bottom) 3U BoB system during the full-system test without the 2U pressure vessel. 13

Figure 1-6. Block diagram of the overall BAMMsat-on-BEXUS system. The diagram represents the interface between the sensors and actuators. 13

Figure 1-7. Image showing the correlation between the ten chapters and the evolution of the subsystems into a flight model. 24

Figure 2-1. Various images of GeneSat. 38

Figure 2-2. Various images of 2U PharmaSat bioCubeSat payload. 42

Figure 2-3. Various images of O/OREOS. 46

Figure 2-4. Various images of SporeSat. 50

Figure 2-5. EcAMSat 2U bioCubeSat payload with the pressure vessel. Left image (Boone et al., 2014). Right image (M. Padgen, 2017). 52

Figure 2-6. Various images of SpacePharma's SPmg lab. 54

Figure 2-7. Images of CubeLab by Space Tango. Images from their website (Space Tango, 2022). 56

Figure 2-8. Various images of the SpacePharma Advanced Lab (SPad). Images extracted from (Glick, 2018). 57

Figure 2-9. Various images of Experiment Shells by Yuri. Images extracted from their website (Yuri, 2022) 58

Figure 2-10. Various images of 2U MisST payload. 59

Figure 3-1. Image of 1st gen. MCSD (Image courtesy of Prof Cullen with minor editing). 67

Figure 3-2. Image of the 1st gen. MCSD and RV. (Image courtesy of Prof Cullen with minor editing). 68

Figure 3-3. (Top) Image of the BAMMsat 1st gen. RV (Image courtesy of Prof Cullen with minor editing). 69

Figure 3-4. (Left) Glass fibre filter vs (Right) Track-etched membrane filter. Credit (Merck) 84

Figure 3-5. Cross-section image of NASA BioSentinel fluidic µwell with the sample filters (A J Ricco et al., 2016). 85

Figure 3-6. Mathematical relationship of Geneva gear size and resulting MCSD dimensions. 86

Figure 3-7. Images of PSA material cut using CO_2 and UV laser cutter. 90

Figure 3-8. Left – CO_2 laser cut polycarbonate. Right – UV laser cut polycarbonate. 92

Figure 3-9. Left – Exploded view of the 2nd gen. MCSD, detailing the 13 layers and their respective materials. Right – Fully assembled 2nd gen. MCSD .. 93

Figure 3-10. Demonstration of the key concept in the 2nd gen. MCSD and RV included the ability to access the sample chamber easily. 94

Figure 3-11. Cross-section cut view of the entire assembly of the initial design of the 2nd gen MCSD and RV. 95

Figure 3-12. Left - Image of the 2nd gen. MCSD in Configuration 1 with the sample chamber opened. Right – Diagnosis test was performed to record the leak (red arrows) from the sample chambers. 96

Figure 3-13. Finite element analysis and lab testing on the impact of bolting. . 97

Figure 3-14. FEA was performed on the ¼ of MCSD to evaluate the impact of adding compression ridges. 98

Figure 3-15. Results from testing the compression ridges. 99

Figure 3-16. Cross-section cut view of the modified 2nd gen. rotary valve without the MCSD. 100

Figure 3-17. Final design and assembly of the 2nd gen. MCSD and RV. 101

Figure 3-18. Various images of issues associated with CO_2 laser cutting silicone. 102

Figure 3-19. Images of leaking on the side of the MCSD due to the misalignment of the fluidic channels. 103

Figure 3-20. Experiment setup for 7-day water retention testing. 105

Figure 3-21. Example of images with bubble and condensation formation on the MCSD. 106

Figure 4-1. Various images of 1st gen. microscope. 119

Figure 4-2. Example of white light fluorescent images taken using BAMMsat 1st gen. epi-fluorescent microscope during NSTP project (images courtesy of Prof Cullen with minor editing). 120

Figure 4-3. Earliest conceptualisation of the compact brightfield microscope for BoB inside a 2U pressure vessel (note the axes). 125

Figure 4-4. Image of RPi v2.1 camera with original lens removed to expose the IMX219 sensor. 127

Figure 4-5. Image showing the relationship between working distance (WD) or object distance, focal length, and image distance (Edmund Optics, 2022b). 130

Figure 4-6. The illustration describes an extension of the relationship shown in Figure 4-5 (Hollows & James, 2022). 130

Figure 4-7. Illustration made to visualise the distance between two 1:1 image relay lenses for comparison. 131

Figure 4-8. Left – CAD image of the initial design of the compact brightfield microscope (v1) inside the 2nd gen. BAMMsat bioCubeSat payload. Right – Optical test bench setup. 133

Figure 4-9. Images of result from capturing micrometre test slide and *C. elegans*. 135

Figure 4-10. Images highlighting the issue with focusing distance. 137

Figure 4-11. Images of custom compact brightfield microscope housing. 138

Figure 4-12. Left – Image of the fully assembled compact brightfield microscope. Right - Mechanical fit check and image capture test assembled in the 2nd gen. BAMMSat bioCubeSat payload. 140

Figure 4-13. Brightness test captured with flight model LED (CREE) at an LED supply voltage ranging from 2.4 V to 4.2 V. 141

Figure 4-14. Optimised optical setup to focus the object with the required FOV. 142

Figure 4-15. Depth of field test with an image taken at an increment of 0.01 mm. 143

Figure 4-16. Cropped and zoomed-in image of dried down *C. elegans* microscopic slide. 148

Figure 5-1. (Left) Image of 1st fluidic subsystems flatsat breadboard. (Right) Image of 1st generation selector valves manifold. Images courtesy of Prof Cullen with minor editing. 154

Figure 5-2. Initial fluidic network design for the 2nd gen. fluidic subsystem. 163

Figure 5-3. mp6 pump electrical schematic in the mp6 datasheet. 166

Figure 5-4. Images of mp6 pump initial test result. 168

Figure 5-5. Graph and image of the pressure difference across mp6 pump. . 168

Figure 5-6. Left – Disassemble RV layer showing liquid dispersion across the layer. Right – Test setup and the resulting leak occurred during pumping. 170

Figure 5-7. Left - Graph of the measured flow rate with V_{dd} at 5 V and 3.3 V to evaluate the flow rate difference. Right – Test setup with mp6 pulling liquid from the reservoir to the flow sensor, which is opened to the atmosphere. 172

Figure 5-8. Graph of the measured flow rate with varying the AMPLITUDE (Vpump) of the mp6 pump..... 172

Figure 5-9. Graph of the measured flow rate with varying the CLOCK of the mp6 pump. 173

Figure 5-10. Test result showing bubble formation when pulling the liquid. ... 175

Figure 5-11. Various images of 2nd gen. selector valve manifold. 181

Figure 5-12. Left – Image of fully assembled selector valves manifold. Right – Top view of the manifold with viewable hidden fluidic network. 181

Figure 6-1. (Left) Image of 1st gen. Geneva gear mechanism. (Right) Alternative gear system explored during the NSTP programme. Images courtesy of Prof Cullen with minor editing. 190

Figure 6-2. The Geneva gear mechanism was designed during the packaging exercise for a fit check. 191

Figure 6-3. A simple sketch of the gearing mechanism. 192

Figure 6-4. Images of torque determination test and result 196

Figure 6-5. Image of the initial Geneva gear mechanism design highlighting the three gear reductions. 197

Figure 6-6. An exploded view of the Geneva gear mechanism. 202

Figure 6-7. Image showing alpha-numeric code based on the ISO system of limits and fits for the tolerance fitting required by various components. 202

Figure 6-8. Left and top-right images show the complete assembly of the Geneva gear mechanism, and the bottom-right image shows a twisted Geneva drive crescent due to misalignment..... 203

Figure 6-9. Various images of 2nd gen. Geneva gear mechanism bench test. 205

Figure 6-10. Graph of the current measurement for an increasing torque (0.1 Nm to 0.4 Nm) applied to bolt the MCSD and RV. 206

Figure 7-1. Two projections of the CubeSat payload assembly with vessel cover removed. Images courtesy of Prof Cullen. 214

Figure 7-2. The mechanical support for the 2nd gen. BAMMsat bioCubeSat payload was manufactured and assembled during a mechanical fit check. 217

Figure 7-3. Top view CAD image showing the MCSD and the compact brightfield microscope lens. 218

Figure 7-4. Damage was incurred on one of the rails during a mechanical fit check. 220

Figure 7-5. The modified rails are custom-fitted to each square hole on the pressure vessel lid to accommodate the design issue with each square end of the rail. 220

Figure 7-6. Top view image of the MCSD bolted to the RV and the compact brightfield microscope and Geneva drive shaft. 223

Figure 8-1. Block diagram of the BoB system during CDR stage with the associated interfaces for electrical, communication protocol and power. 230

Figure 8-2. (Left) Labelled exploded CAD overview of the 3U BoB system with a 1U bus and 2U BAMMsat bioCubeSat payload. (Right – top and bottom) Labelled 2U BAMMsat bioCubeSat payload. 230

Figure 8-3. An initial fluidic network designed for the BoB fluidics subsystem at the CDR stage of the BoB mission. 233

Figure 8-4. The location of the five different *C. elegans* phenotypes and their replicates. 239

Figure 8-5. Images illustrating Step 1 to Step 4 of the assembly process. 242

Figure 8-6. Images illustrating Step 5 to step 7 of the assembly process. 242

Figure 8-7. Images illustrating Step 8 to Step 12 of the assembly process. ... 243

Figure 8-8. Images illustrating Step 13 to Step 15 of the assembly process. . 243

Figure 8-9. Images illustrating Step 16 to Step 19 of the assembly process. . 243

Figure 8-10. Left – Fully assembled BoB system without the pressure vessel. Right – CAD image showing the location of the fluidic T-junction 244

Figure 8-11. The compressive force from the bolting caused the polymer underneath to crack and cause leakage. It also caused the adhesive to seep and block the fluidic channel. 245

Figure 8-12. Left – Leaking at connector since sealing had to be judged by hand. Right – Polymer cracked during testing and caused fluidic leaking. 245

Figure 8-13. Snapshot of each quadrant of the MCSD during a full system rotation test with *C. elegans*. 247

Figure 8-14. The issue with structural bending from bolting the MCSD and RV. The image on the right has an exaggerated tilting of the MCSD for visual purposes. 248

Figure 8-15. Block diagram of the BoB system ready to be shipped to the BoB flight campaign. 249

Figure 8-16. The fluidic subsystem's fluidic pathways; ready to be shipped for the BoB flight campaign. 250

Figure 9-1. Image of the BEXUS 19 flight campaign during take-off at ESRANGE Space Centre in 2014. 259

Figure 9-2. Image of the BEXUS 30 Gondola on the launch site preparing for launch..... 260

Figure 9-3. BEXUS nominal flight profile. 261

Figure 9-4. Previous BEXUS flight PTU (pressure, temperature, humidity) sondes flight data compared to Standard Atmosphere 1976 (Frenea-Schmidt, 2021). 262

Figure 9-5. The local temperature around the Gondola can vary depending on its position across the Gondola (Frenea-Schmidt, 2021). 262

Figure 9-6. Image of the Dome building at ESRANGE on the left where all pre-flight operations were performed, i.e., assemble, integration, and verification. 278

Figure 9-7. Uncropped images of Chamber 5 were taken during the Interference test via an autonomous operation on 27/09/2021. 279

Figure 9-8. (Left) Compact brightfield microscope designed for the BoB system with the custom lens. (Right) An RPi v2.1 camera with its original lens. . 280

Figure 9-9. Captured image of chamber 3 showing *C. elegans* after aborted FCT. 281

Figure 9-10. Left - A fully assembled MCSD ready for flight with leakage on the underside of one of the chambers. 283

Figure 9-11. The final flight configuration with an increased number of sample chambers with *C. elegans* and the addition of a "dye" chamber. 285

Figure 9-12. Summary of BEXUS 30 flight paths. 288

Figure 9-13. Pressure profile vs altitude of the BEXUS 30 flight during the ascent phase. 289

Figure 9-14. The pressure inside the 2U pressure vessel. 290

Figure 9-15. Graph of the external temperature vs altitude during the ascent phase of the BEXUS 30 flight. 291

Figure 9-16. Temperature readings for all RTDs inside the 2U pressure vessel. 292

Figure 9-17. The RTD3 temperature sensor values in the four different phases during the flight. 294

Figure 9-18. Temperature test results in the pseudo thermal vacuum chamber of the active thermal subsystem before the flight campaign for comparison (Bolliand, 2020). 294

Figure 9-19. Extracted frame by frame video of Chamber 37 captured at 0.03 seconds apart (30 fps). 297

Figure 9-20. Example of three chambers with motile *C. elegans* captured at various stages during the float phase of the flight. 299

Figure 9-21. Uncropped images of Chamber 2 during the flight before and after fluidic pumping. 300

Figure 9-22. The relative humidity and temperature inside the 2U pressure vessel. 301

Figure 9-23. Images showing obstruction due to bubbles or water droplets... 301

Figure 9-24. The temperature profile of the six RTDs inside the 2U pressure vessel across to flight campaign events during FTC (29/09/2021) and flight (30/09/2021) 306

Figure 9-25. The temperature profile of the six RTDs inside the 2U pressure vessel during FCT. 306

Figure 9-26. *C. elegans* progeny was found in one of the fluidic channels along Chamber 6 extracted, and placed on a petri dish. 308

Figure 9-27. Images of post-flight analysis of the Rotary Valve demonstrating damage from leaking. 309

LIST OF TABLES

Table 2-1. List of pattern search result. 35

Table 3-1. Material properties and design functions of PTFE, PCTFE, and PEEK. 78

Table 3-2. Trade-off analysis result for material for MCSD and RV..... 79

Table 3-3. Polycarbonate vs PMMA 82

Table 3-4. The result from CO_2 laser cutting and UV laser cutting of materials under consideration for the 2nd gen. MCSD. 91

Table 3-5. Observational results from the 7-days liquid retention test. 105

Table 3-6. Permeability properties of FEP and PMP film. 111

Table 3-7. Summary of research performed against MCSD and RV design drivers. 113

Table 4-1. Summary of key parameters to compare the two 1:1 image relay lens. 132

Table 4-2. Verification matrix for compact brightfield microscope. 145

Table 5-1. Summary of the evaluation and critique with a suggested solution for the 2nd gen. fluidic subsystem 158

Table 5-2. The LPG10 flow sensor verification test was taken at four different times. 179

Table 5-3. Verification matrix for 2nd gen. fluidic subsystem. 183

Table 6-1. Weighted parameter used during trade-off analysis. 199

Table 6-2. Result from trade-off analysis..... 201

Table 6-3. Verification matrix for 2nd gen. Geneva gear mechanism. 207

Table 7-1. Verification matrix for mechanical support subsystem..... 221

Table 8-1. *C. elegans* strain on-board BAMMsat-on-BEXUS flight..... 237

Table 8-2. Different media used in BoB mission..... 238

Table 8-3. List of AIT processes for the BoB system..... 241

Table 9-1. BAMMsat-on-BEXUS mission's milestones and dates within the BEXUS programme..... 258

Table 9-2. The various late access timing for current launch vehicles for CubeSats or CubeSat compatible missions. 266

Table 9-3. Overview of the activities and challenges experienced during the BEXUS 30 flight campaign. 276

Table 9-4. The table provides the extracted time for key events during the launch sequence on 30/09/2021. 287

Table 9-5. Chamber position of motile *C. elegans* in the MCSD and its respective phenotypes. 304

LIST OF EQUATIONS

Equation 3.1 97
Equation 4.1 129
Equation 4.2 129

LIST OF ABBREVIATIONS

AIT	Assembly, Integration, Testing
AIV	Assembly, Integration, Verification
AFOV	Angular field of view
ASE	Astronautics and Space Engineering
BAMMsat	Bioscience, Astrobiology, Material, Medicine science on CubeSat
BEXUS	Balloon Experiments for University Students
BFL	Back focal length
BoB	BAMMsat-on-BEXUS
CAD	Computer-aided design
CCD	Charge-coupled device
CDR	Critical Design Review
CMOS	Complementary metal–oxide–semiconductor
CNC	Computer numerical control
COTS	Commercial off-the-shelf
DLR	The German Aerospace Center (Deutsches Zentrum für Luft- und Raumfahrt)
EAR	Experiment Acceptance Review
EcAMSat	E. coli AntiMicrobial Satellite
ECLSS	Environmental Control and Life Support System
EPS	Electrical Power System
ESA	European Space Agency
ESTEC	European Space Research and Technology Centre
FEA	Finite Element Analysis
FEP	Fluorinated ethylene propylene
FKM	Fluorocarbon elastomers, commonly known as FKM
FM	Flight model
FOV	Field of view
GNSS	Global Navigation Satellite System
IMU	Inertial measurement unit
IPR	Integration Progress Review
ISIS	Innovative Solutions In Space

ISS	International Space Station
LED	Light emitting diodes
LEO	Low Earth Orbit
LOC	Lab-on-a-chip
MCSD	Multi-chamber sample disc
MisST	Microsatellite In-Situ Technologies
MORABA	Mobile Rocket Base (Mobile Raketenbasis)
MSc	Master of Science
MTF	Modular Transfer Function
NASA	National Aeronautics and Space Administration
NSTP	National Space Technology Programme
OBDH	On-board Data Handling
O/OREOS	Organism/Organic Exposure to Orbital Stresses
PCB	Printed Circuit Board
PDR	Preliminary Design Review
PEEK	Polyether ether ketone
PET	Polyethylene terephthalate
PMMA	Poly (methyl methacrylate)
PMP	Polymethylpentene
PS	Polystyrene
PSA	Pressure-sensitive adhesive
PTFE	Polytetrafluoroethylene
PTCFE	Polychlorotrifluoroethylene
PTU	Pressure, temperature, and humidity
REXUS	Rocket Experiments for University Students
RPi	Raspberry Pi
RTD	Resistance Temperature Detector
R&D	Research & Development
RV	Rotary valve
SED	Student Experiment Document
SESLO	Space Environment Survivability of Live Organisms
SEVO	Space Environment Viability of Organics
SPAd	SpacePharma Advanced Lab

SPmg	SpacePharma microgravity lab
SPuMP	Space Pharma Microgravity miniaturised pump
SNSA	Swedish National Space Agency
SSC	Swedish Space Corporation
UKSA	UK Space Agency
WD	Working Distance
ZARM	Center of Applied Space Technology and Microgravity (Zentrum für Angewandte Raumfahrttechnologie und Mikrogravitation)

1 Background and Introduction

1.1 The motivation behind the PhD research

The PhD research revolves around the concept of a CubeSat compatible bioCubeSat payload for future space systems. The research builds upon Cranfield University's BAMMsat concept. BAMMsat stands for Bioscience, Astrobiology, Material, Medicine science on CubeSat. The BAMMsat concept aims to leverage the CubeSat miniaturisation and standardisation paradigm to develop an autonomous miniaturised scientific laboratory to improve space research access for astrobiology, biological, materials and medical science.

For readers who are not familiar with CubeSats, a CubeSat is classified under the nanosatellite mass class. It has a standard size and form factor defined in Units, often abbreviated as 'U'. A 10 cm x 10 cm x 10 cm cube with a mass of up to 1.33 kg is classified as 1U (California Polytechnic State University, 2015). Historically, traditional access to space has been limited due to the high cost, infrequent flight opportunities, and long lead time. The CubeSat approach has democratised access with lower development and launch costs, more frequent flight opportunities, and shorter lead times.

This thesis uses the term bioCubeSat to refer to a CubeSat with a biological payload. Note that a widely accepted terminology could not be established during the literature review. The concept of CubeSat and biology has been de-risk and proven in orbit with seven free-flying bioCubeSats launched by NASA and SpacePharma. See section 2.4.2.1 later in the thesis. It is also increasingly used as a system onboard a larger platform. The simplified and standardised nature of the CubeSat format enabled it to be easily interfaced on board a larger platform such as the International Space Station (ISS). Commercial entities such as Space Application Services with its ICE Cubes facility, NanoRacks with its Nanolabs, and Space Tango with its TangoLab have been providing commercial space access for scientific experiments on board the ISS (Crombrugghe & Pletser, 2017).

The space industry has been experiencing renewed growth since the Apollo programme. DiFrancesco & Olson (2015) have made a case from an economic perspective that the space industry is at an inflexion point for a full-scale microgravity research programme. This is driven by the growing international activities, shifting funding landscape, and changes in commercialisation activities (DiFrancesco & Olson, 2015). The reduction in the barrier of entry also supports growth. An analysis by Jones in 2018 stated that the launch cost to Low Earth Orbit (LEO) had been reduced from $54,500/kg onboard NASA's Space Shuttle to $2,720/kg onboard SpaceX's Falcon 9 (Jones, 2018). The reduced cost means that the capacity to move to and from LEO increases.

It can be argued that in the short term, the primary motivation to perform R&D in space is to access sustained microgravity. In recent years, the case for microgravity has increased. A pharmaceutical company, Merck, has leveraged microgravity's unique effects of reduced sedimentation and convective forces to learn how to produce higher yield protein crystallisation in microgravity. The results were translated to Merck's earth application on protein crystallisation to increase its production value with a higher yield protein (Reichert et al., 2019).

A similar argument can also be made for drug development. Amgen, a US-based biotechnology company, has leveraged microgravity to study bone atrophy and wasting. Their activities have resulted in an FDA-approved drug, denosumab, marketed under Prolia (Cohen & Stodieck, 2016). A review has been published on a range of possibilities of using microgravity to support drug development. The study made a case for leveraging microgravity to assist in finding biological, biochemical, and molecular pathways for drug development (Braddock, 2019).

The space industry's growth enables research in sustained microgravity at a new scale, opening a new market such as space biomanufacturing. A recent study performed a preliminary market analysis and predicted that the market size for LEO-based biomanufacturing could reach $2.87B in 2035, from $308M in 2026, at a CAGR of 25%, for the period between 2026-2035 (Sharma et al., 2021).

However, one critical bottleneck is the lack of data to validate space-based models for terrestrial applications (Sharma et al., 2021).

A bioCubeSat could be an asset to provide autonomous and high-throughput experiments as an early R&D tool for the growing LEO economy alongside supporting basic research. BioCubeSat, such as BAMMsat, could be the bridge to a sustainable LEO economy with its functionalities to perform an autonomous in-situ measurement in space. At a lower entry cost, it could support the R&D in space bioscience and biotechnology en route to commercialisation, either for using space for Earth-based application and supporting future human exploration of the Moon and Mars

1.2 A brief history of BAMMsat

This section aims to provide the reader with a historical context of the BAMMsat programme and the technological status at the start of the PhD. The BAMMsat programme began in 2012 after the launch of GeneSat, PharmaSat and O/OREOS by NASA Ames. The development started with a 3-month system-level concept study to de-risk and develop a baseline mission for future spaceflight (see Figure 1-1). The study resulted in BAMMsat. After the initial study, Cranfield University received a one-year UKSA NSTP funding in 2015 to produce a functionally representative laboratory breadboard version that brought it up to TRL 4. See Figure 1-2 and Figure 1-3.

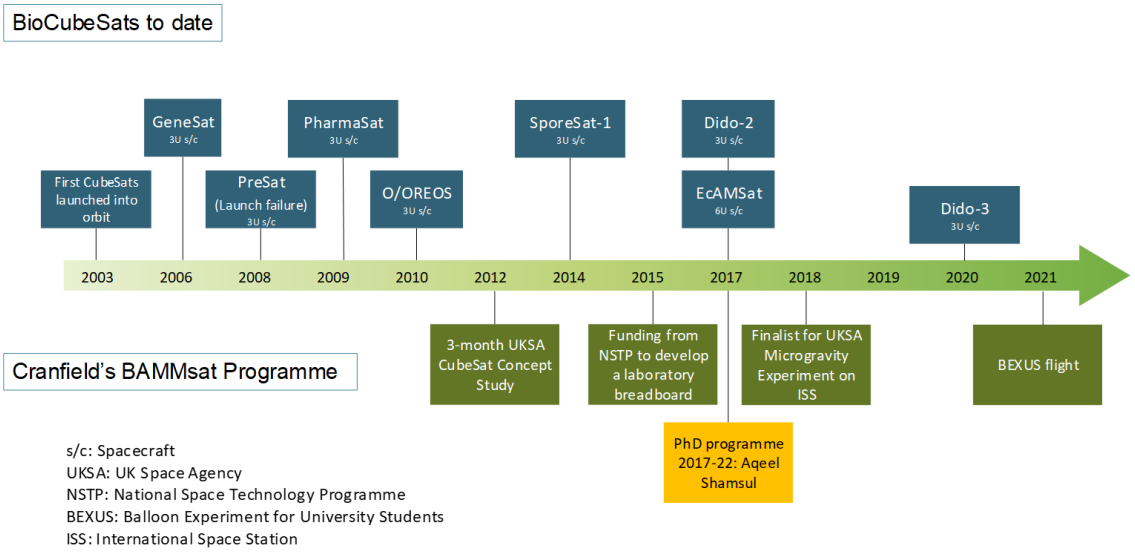

Figure 1-1. Timeline representing the BAMMsat development alongside the successfully launched bioCubeSat to date.

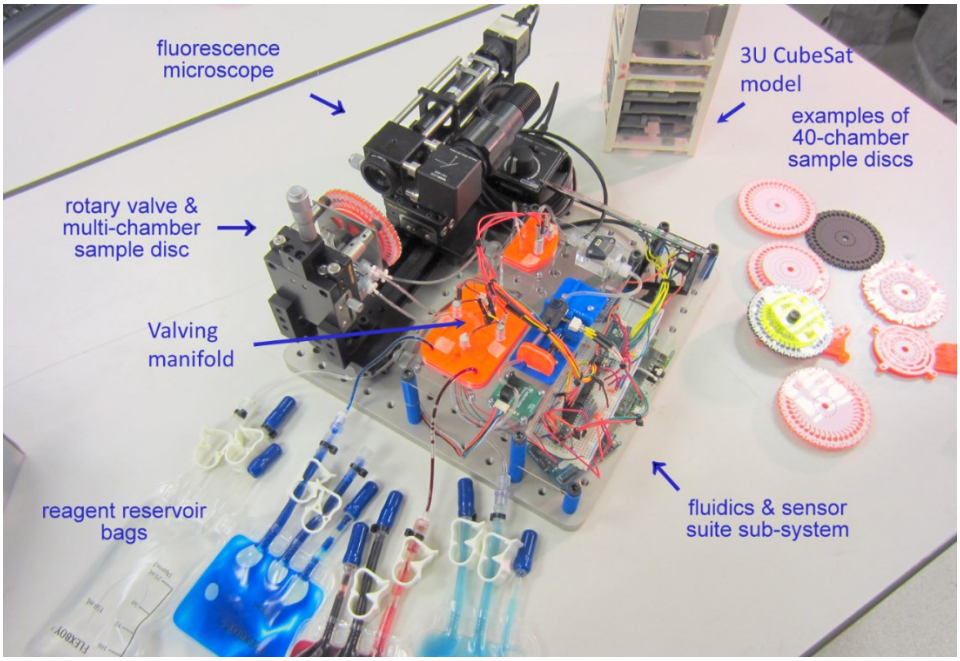

Figure 1-2. BAMMsat NSTP-2 integrated fluidic and microscope breadboard of 1st generation BAMMSat (Image courtesy of Prof Cullen).

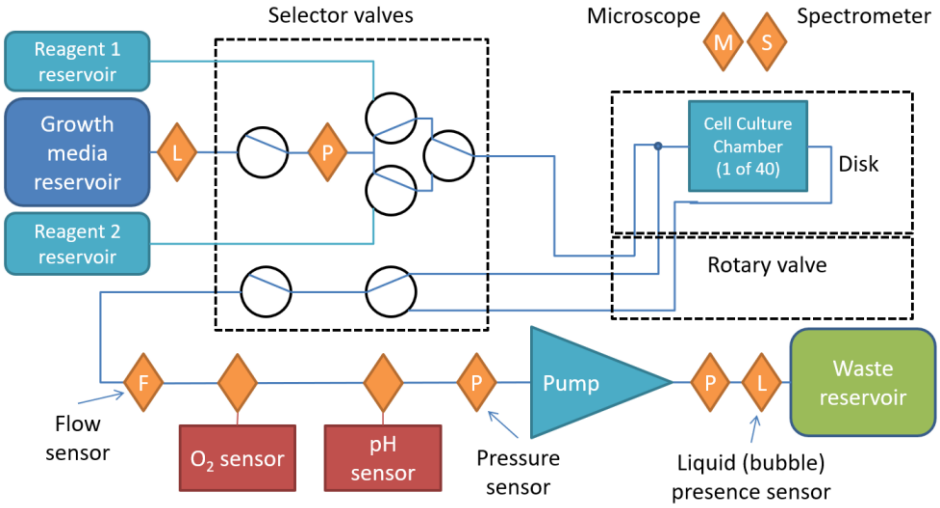

Figure 1-3. BAMMsat NSTP-2 fluidics network, actuators, and sensor subsystem (Image courtesy of Prof Cullen).

The BAMMsat concept is built upon the common experiment needs in the bioscience, astrobiology, material, and medical fields to (i) house and maintain, (ii) expose, (iii) perturb, and (iv) observe biological and related experiments. BAMMsat aims to replicate common laboratory functionality and repackage it into

a miniaturised and autonomous system. The concept uses microfluidics to house and maintain samples in a controlled liquid environment and to perturb the sample by exchanging the bathing liquid. The samples are exposed to the space environment during spaceflight, and any changes are monitored via sensors.

Before the PhD research, the work performed in 2015 highlighted that BAMMsat could provide three new developments within the scientific community, compared to other bioCubeSats, i.e., (i) in the implementation of a variant of BAMMSat to allow the flight of human cell cultures and (ii) implementation of CubeSat compatible optical/fluorescence microscopy (iii) the ability to address each sample chambers independently fluidically enabled by the Rotary Valve (see Figure 1-3). The Rotary Valve concept was influenced by the Rotary Valve design within the Life Marker Chip instrument (Sims et al., 2012).

The following bullet points summarise the technological status of the BAMMsat concept at the start of the PhD research in September 2017 (Cullen et al., 2016). These represent the background knowledge of the BAMMsat system used for the PhD research.

- Demonstrated a multi-chamber sample disc (MCSD) to isolate each sample in an individual fluidic chamber. The initial chamber design was based on 96-well microplate volume and later reduced to 384-well microplate volume to increase the number of samples in the same 8 cm disc. The design change doubled the number of samples from twenty-chambers to forty-chambers, see Figure 1-2.
- Performed an early demonstration of the ability to grow human cell cultures. The result demonstrated that materials inside the MCSD did not significantly affect cell growth in BAMMsat.
- Demonstration of a custom valving manifold to allow selection and mixing of reagents before being drawn to the selected chamber in the MCSD, see Figure 1-2.
- The study established a baseline spacecraft bus using the COTS subsystem with a suitable context within various mission profiles.

- Performed an early space systems study in thermal requirements, power budgets and expected data rates for returning daily microscope imagery.
- The NTSP programmes completed a CAD packing exercise of the BAMMsat hardware components into a 2U format, see Figure 7-1.

1.3 Introduction to the BAMMsat-on-BEXUS (BoB) mission

The objective of this section is to introduce the BAMMsat-on-BEXUS (BoB) mission. BoB is a technology and operation demonstration of a CubeSat compatible bioCubeSat. The PhD research story was heavily influenced by the BoB mission. Throughout the PhD thesis, the BoB mission will be referred to constantly, and it is worth introducing it here to avoid ambiguity. The BoB mission will be described as an overview in section 1.3.2. The BoB mission was enabled by the REXUS/BEXUS programme, a European student experiment programme. Similarly, an overview of the REXUS/BEXUS will be described in section 1.3.1.

To help contextualise the discussion, four terminologies are being used to describe BAMMsat-on-BEXUS throughout the thesis

- BAMMsat-on-BEXUS mission or BoB mission

The term BoB mission refers to activities that encompass a typical space mission. This term represents the activities and processes behind the overall mission aim of performing technology and operational demonstration of the 2nd gen. BAMMsat bioCubeSat payload on a stratospheric balloon flight.

- BAMMsat-on-BEXUS flight campaign or BoB flight campaign

The term BoB flight campaign refers to a series of activities performed during the flight campaign between the 24th of September – the 4th of October 2022 at ESRANGE Space Centre, Kiruna. The activities included pre-flight operations, flight operations and post-flight operations.

- BAMMsat-on-BEXUS system or BoB system

The term BoB system refers to the 3U CubeSat format system encompassing the 1U bus and the 2nd gen. BAMMsat bioCubeSat payload. The 1U bus was the "brain" of the BoB system and acted as the mechanical, electrical and data interface between the 2nd gen. BAMMsat bioCubeSat payload and the BEXUS gondola.

- 2nd gen. BAMMsat bioCubeSat payload

The 2nd gen. BAMMsat bioCubeSat payload is the autonomous miniaturised laboratory at the core of the BAMMsat concept with the subsystems developed during this PhD. It is a 2U bioCubeSat payload system used to house and observe biological samples. It continued from the laboratory breadboard version (1st gen. BAMMsat bioCubeSat payload) into the 2nd gen. BAMMsat bioCubeSat payload, which flew into the stratosphere.

1.3.1 Introduction to the REXUS/BEXUS programme

The REXUS/BEXUS programme allows students from universities and higher education colleges across Europe to develop and launch their experiments on board a sub-orbital sounding rocket or stratospheric balloon. The programme is realised under the bilateral Agency Agreement between the Swedish National Space Agency (SNSA) and German Aerospace Centre (DLR). The Swedish share of the payload is made available to students from other European countries through a collaboration with European Space Agency (ESA).

BEXUS or Balloon Experiments for University Students is a large stratospheric balloon with an onboard gondola to carry four student experiments. The gondola has a volume of 1.16 m x 1.16 m x 0.84 m, able to take a payload between 30 kg and 112 kg in weight

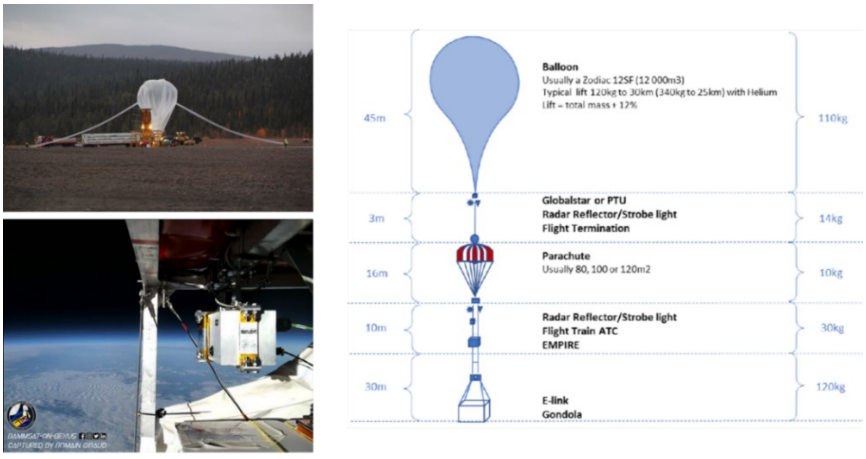

Figure 1-4. Images of BEXUS large stratospheric balloon and BAMMsat-on-BEXUS.

The complete BEXUS flight train is shown in Figure 1-4. (Top right image) BEXUS large stratospheric balloon being inflated with helium before release. (Bottom right) BAMMsat-on-BEXUS system during flight mounted on the BEXUS Gondola. (Left) A BEXUS flight train with a total lift-off mass of approximately 300 kg (Frenea-Schmidt, 2021). The BoB mission was flown on BEXUS

One of the programme's benefits is that experts from DLR, SSC, ZARM and ESA provide technical support to the student teams throughout the project. REXUS and BEXUS are launched from SSC, Esrange Space Center, in northern Sweden. The BEXUS programme was created in 2007, following on from an already ongoing REXUS programme which started in 1995. Each year two REXUS and BEXUS are launched from SSC, Esrange Space Center in northern Sweden (REXUS/BEXUS, 2021).

1.3.2 Brief overview of the BoB mission, system, and payload

1.3.2.1 BoB mission

The BAMMsat-on-BEXUS (BoB) mission was a technological and operational demonstration of a bioCubeSat payload. It performed an automated experiment in a harsh environment in a spaceflight representative context. The BEXUS flight campaign and the platform provide a suitable spaceflight operation and environment analogue, which were (i) pre-flight, (ii) flight, and post-flight.

BoB mission flew *C. elegans*, a nematode/roundworm, as a biological sample. The biological sample was used to demonstrate the hardware’s ability to maintain a viable biological organism during (i) pre-flight operations and platform integration and (ii) during flight via appropriate payload internal pressure and thermal control. The mission revolved around demonstrating the hardware’s fluidic, pressure and thermal functionality. And the sensors' ability to observe the *C. elegans* in extreme environments.

During pre-flight operation, the handling and integration of the biological sample is an analogue to an orbital spaceflight. Compared to an Earth observation experiment, a biological experiment has additional requirements and constraints

on the mission, particularly in biological handling and temperature control. This impacts the pre-flight operations at the launch site, where extra care was taken to address the biological requirements to maintain the viability of *C. elegans*.

During the flight operation, the external air temperature could go down to -80ºC and pressure between 5 and 25 mbar (Frenea-Schmidt, 2021). The extreme environment is another analogue of a free-flying orbital satellite and imparts environmental stressors into the system.

For post-flight operation, the BEXUS platform provides post-flight recovery. The post-flight handling after recovery on BEXUS can be an analogue for spaceflight with return capabilities such as the Space Shuttle, ISS, Bion and future platforms supplied by private companies such as Blue Origin, SpaceX, SierraSpace, Virgin Galactic and Axiom. Understanding post-flight operations and how they impact handling and hardware will be crucial as BAMMsat prepares for future spaceflight.

The knowledge and lessons learnt going through the technology development and flight campaign will be inputted towards a 3rd generation BAMMsat payload intended for in-orbit demonstration inside the ISS.

The BoB team was composed of students from Cranfield University and the University of Exeter. Cranfield University led the development on the technological aspect, while the University of Exeter provided the biological samples and handling expertise. The team applied to the one-year BEXUS programme in October 2019 and was meant to fly in October 2020. However, the flight campaign was delayed in the middle of the programme to October 2021 due to the COVID-19 pandemic

1.3.2.2 BoB system

The 2nd gen. BAMMsat bioCubeSat payload was designed to replicate the features available in a common bioscience laboratory and repackage into a miniaturised 2U (20cm x 10cm x 10cm) CubeSats format. The BAMMsat bioCubeSat is on the left side of the image, with the 1U bus on the other side (see Figure 1-5). The features revolve around the four core features identified for

various experiments during BAMMsat systems-level study and are presented below.

House multiple samples

The ability to house and independently isolate multiple samples in a device increases the number of samples and discrete experiments. The biological samples are housed in the multi-chamber sample disc (MCSD), accommodating 32 sample chambers, see Figure 1-5.

Maintain samples in an appropriate local environment

The biological samples need to be contained in a controlled pressure and thermal environment to maintain their viability. During spaceflight, the vacuum environment will deplete the atmosphere that was carried from the ground. For example, a common aerobic cell culture will require some O_2 for respiration. The samples and the associated hardware will need to be contained in a pressure vessel. The vessel needs to be sealed during pre-flight on the ground to contain the ambient atmosphere with an acceptable leak rate. This will ensure that O_2 and CO_2 are contained and exchanged between the sample and the trapped atmosphere. Note that the vessel has a limited headspace volume, and the experiment can only be performed in a finite timescale due to the limited volume of O_2 and sink volume for CO_2. In addition, the temperature inside the pressure vessel will need to be regulated to meet the sample's thermal requirements. An atmosphere could be an asset in maintaining the temperature convectively.

Perturb sample fluidically

The ability to perturb fluidically enables the ability to change the state of the biological samples. Fluidics can be used to allow for biological maintenance by replenishing new growth media or perturbing the state of biology by pumping reagents such as drugs and fixatives. The fluidic subsystem will combine the pump, solenoid valves, media reservoir bags, liquid flow sensor and fluidic pressure sensor. For BAMMsat, the combination of MCSD and fluidic subsystems provide the unique ability to address independent samples.

Monitor sample

The monitoring features provide the ability to extract valuable experiment data. For the BoB system, the 2nd gen. BAMMsat bioCubeSat payload will include an imaging system to image the status of the biological samples.

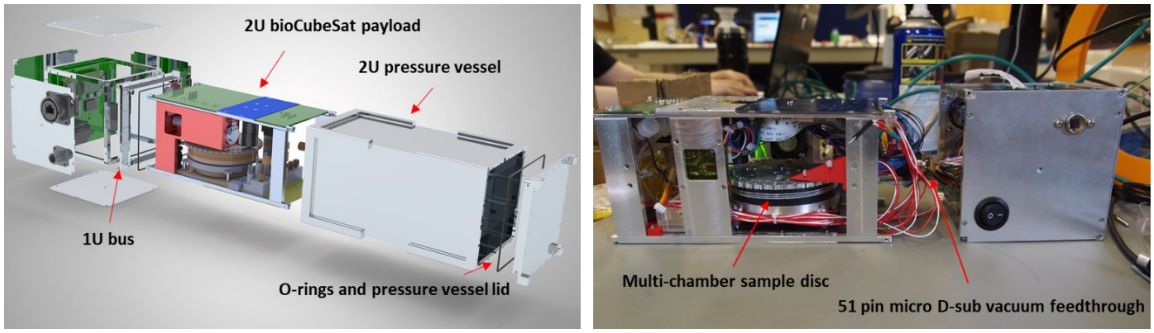

Figure 1-5. (Top) Rendered CAD showing the 3U BoB system. (Bottom) 3U BoB system during the full-system test without the 2U pressure vessel.

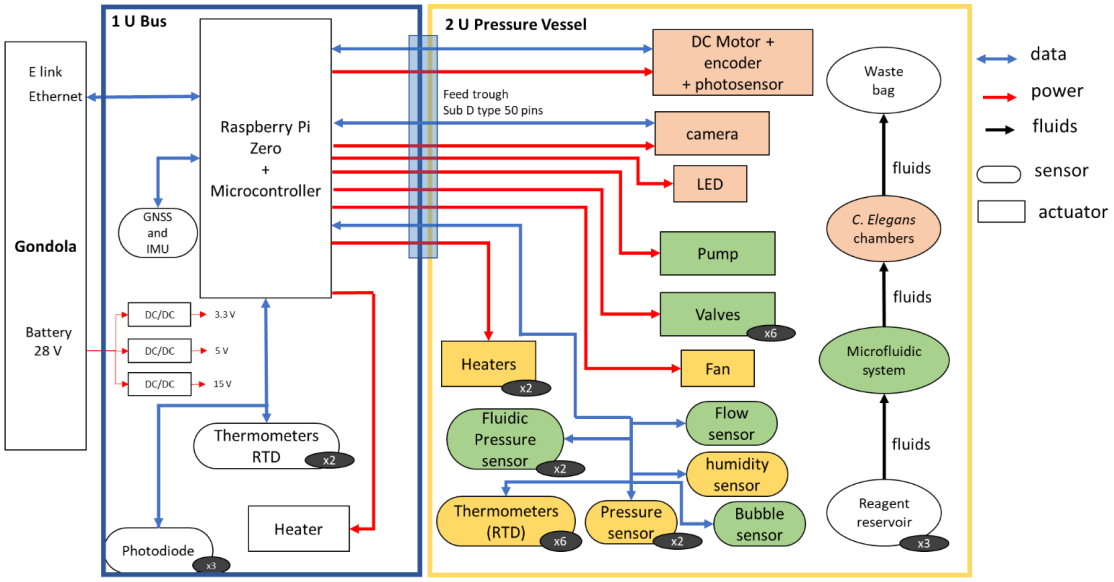

Figure 1-6. Block diagram of the overall BAMMsat-on-BEXUS system. The diagram represents the interface between the sensors and actuators.

1.4 PhD research aim and objectives

1.4.1 Aim

To advance the developmental status of Cranfield's BAMMsat bioCubeSat compatible payload from a 1st gen. implementation into a 2nd gen. able to be demonstrated in a spaceflight relevant environment, e.g., large stratospheric balloon platform and flight and prior to the future 3rd gen. implementation for in-orbit demonstration.

1.4.2 Objectives

The objectives of the PhD research are presented here with the necessary justification for a better context of the research scope.

1) *To summarise the state-of-the-art in the literature to inform the BAMMsat payload design for Bioscience, Astrobiology, Medicine and Material science experiment in space environments and extreme Earth environments.*
   a) To perform a structured literature review on previous bioCubeSat research.
   b) To establish top-level requirements for BAMMsat payload design, which utilise the common features for BAMM (Bioscience, Astrobiology, Medicine and Material science) experiment in space environments and extreme Earth environments.

2) *To rectify design issues, re-design, manufacture and test the BAMMsat Multi-chamber Sample Disc (MCSD) and Rotary Valve (RV) for the 2nd gen. BAMMsat bioCubeSat payload.*

   BAMMsat has two key design propositions that enable it to investigate a wider variety of samples and a higher number of experiments in the same 2U form factor than other bioCubeSat. The two designs are the MCSD and RV. See Figure 1-2 and Figure 1-3. Combining the MCSD and RV, each sample chamber can be individually addressed by intermittently rotating the chamber to access independent fluidic ports and sensors. The MCSD and RV allow

several sample chambers to be designed compactly without the additional valving, wire, and fluidic standard design.

The 1st gen. MCSD and RV had several issues to be solved at the start of the PhD. The first issue was (i) the leaking between the MCSD and RV surfaces. The second issue was (ii) the manufacturability and build quality of the MCSD and Geneva gear which failed during testing. The third issue was (iii) the heritage design of laser cutting layers of polymethyl methacrylate (PMMA) with interlayer lamination of double-sided pressure-sensitive adhesive meant that it was not easy to assemble and disassemble the MCSD for sample exchange during Assembly, Integration and Verification (AIV).

3) *To design, manufacture, and test a compact brightfield microscope for the 2nd gen. BAMMsat bioCubeSat payload.*

A compact brightfield microscope was required for the BAMMsat-on-BEXUS stratospheric balloon flight. The microscope was used to observe the *C. elegans* mobility and motility during the flight to verify the physiological state of the *C. elegans.* BAMMSat 1st generation had an epi-fluorescence breadboard microscope. However, the breadboard microscope had a volume larger than the 2U form factor. A miniaturised flight model design has been produced based on BAMMsat 1st generation. However, the design has never been tested, and the lack of financial and human resources meant that a simpler compact brightfield microscope was required.

4) *To repackage, design, manufacture, and test the sensors, fluidics subsystem, and associated mechanical supports for the 2nd gen. BAMMsat bioCubeSat payload.*

A suite of sensors and actuators is required to perform the necessary functionalities in BAMMsat. BAMMsat also includes a fluidic subsystem with a pump and valves to perturb the biological samples accordingly. The collection of sensors and fluidics subsystems is shown in Figure 1-3. The PhD research involved repackaging the sensors and fluidic subsystem into a 2U form faction with the appropriate mechanical support.

5) *To perform systems integration and testing of the BoB 2U payload in preparation for the BEXUS flight.*

   Objective five built upon objectives one to four and performed assembly, integration and testing (AIV) of the 2U 2nd gen. BAMMsat bioCubeSat payload.

6) *To summarise the BAMMsat-on-BEXUS flight and preliminary analysis of the flight result*

   Objective six summarises the BAMMsat-on-BEXUS flight that occurred on the 30th of September 2021.

1.5 Narrative of the PhD research

The PhD research started in September 2017 to advance the developmental status of the BAMMsat concept from a laboratory breadboard into a real-world application, bringing it closer to spaceflight. The research continued from the last technological development funded by the UKSA National Space Technology Programme (NSTP) grant. A laboratory breadboard has been developed with functions representative of the final CubeSat payload from the grant work. In this thesis, the laboratory breadboard is referred to as 1st generation BAMMsat bioCubeSat payload. The PhD research involves rectifying some design issues with the 1st gen., which will be explored further in the thesis. The research also involved repackaging the breadboard into a CubeSat format for the 2nd gen. BAMMsat bioCubeSat payload. Towards the end of the research, the 2nd gen. BAMMsat bioCubeSat payload was flown as a technology demonstration on board a large stratospheric balloon under the BEXUS programme with *C. elegans* as its biological payload.

The PhD programme started as part of the ongoing development of Cranfield University's BAMMsat concept. It began in 2017 and has evolved with further development and flight opportunities throughout the PhD programme. The research started with the initial focus of advancing the development of the breadboard closer to real-world application, with spaceflight being the end goal. Initial plans involved commissioning the existing breadboard to include a technology demonstration at varying radiation levels, i.e., at sea level (lab environment), low-level radiation (Boulby mine (Wadsworth et al., 2020) – deep salt / potash mine), and high-level radiation in (stratosphere). The rationale behind the experiment design was to develop BAMMsat to support radiation studies for flight beyond LEO. During the PhD, this was not implemented since other opportunities arose, such as a 2018 ISS flight opportunity; see next paragraph. Plus, securing two test facilities, such as the Boulby mine and the stratospheric flight, could be challenging within the PhD timeline.

In 2018, a competitive spaceflight opportunity arose for a flight onboard the ISS inside the KUBIK facility (UK Space Agency, 2021a). Cranfield University, University of Exeter and Kayser Space Ltd developed a full science case proposal to study the therapeutic efficacy of drug compounds against molecular pathways involved in detrimental human response to space radiation and microgravity. For this experiment, a variant of BAMMsat hardware was conceptualised to house and maintain *C. elegans*, a nematode worm, and fluidically deliver nutrient medium and drug compounds. Unfortunately, the proposal was not accepted due to the short turnaround of the programme and that BAMMsat would struggle to meet the required development timeline.

However, the conceptualisation exercise helped highlight an issue with the BAMMsat 1st generation multi-chamber sample disc (MCSD) during assembly, verification, and integration (AIV). The 1st gen. MCSD was permanently assembled with laser-cut acrylic with interlayer adhesive. The adhesive bonding limits the flexibility when handing the samples, which increases complications during pre-flight AIV. The ISS opportunity also put forth the applicability of *C. elegans* into the BAMMsat systems, and it has never flown on a CubeSat platform. Identifying the issues around MCSD meant that the early PhD effort included the development of the second generation MCSD.

In the same year (2018), BEXUS (Balloon Experiment for University Student) programme was identified as a suitable demonstration opportunity for the next step of technological development for BAMMsat. The flight environment and operation were seen as a representative spaceflight context. BAMMsat-on-BEXUS (BoB) was developed to package the BAMMsat laboratory breadboard using *C. elegans* as the biological samples inside a pressure vessel and mount it on the BEXUS gondola platform. Unfortunately, the initial proposal (submitted to the 2018 BEXUS call) was not selected as the original plan was to fly a larger, non-CubeSat version. Therefore, the flight of a non-CubeSat format was not considered justifiable.

Initially, the proposal was intended only as a technological and operational demonstration which could then inform the design of the final CubeSat format. It was thought that repackaging the system into a CubeSat format would be challenging in the one-year programme (2018-19) from proposal to flight.

The first proposed experiment was designed to package the BAMMsat laboratory breadboard with a robust mechanical and electrical interface, fluidic and wire harnessing, and software inside a pressure vessel without miniaturising it into a CubeSat format. The justification was to help simplify project management and technological development. The intended experiment was 13.2 kg with a volume of 36 cm x 31 cm x 26 cm. It's worth noting that the BEXUS counterpart, REXUS (Rocket Experiment for University Student), was considered. However, the additional rocket design requirement would be too challenging in the one-year programme. Even though the proposal was rejected, the feedback provided was used to inform the second proposal.

The following year, a second BAMMsat-on-BEXUS (BoB) proposal was submitted in October 2019 with the rectified feedback from the previous proposal. The proposed experiment was a technology and operation demonstration of the BAMMsat bioCubeSat payload in a spaceflight relevant context.

The operation environment, which includes handling biological samples (*C. elegans*) pre-flight, flight and post-flight, and the harsh flight environment in the stratosphere, can help validate BAMMsat's functionalities. The proposed experiment also repackages BAMMsat into a CubeSat format and simplifies the system's sensor suite. The repackaging exercise into a CubeSat format would provide transferable knowledge to the final CubeSat. Due to the resource constraint, fluorescence microscopy was exchanged with a fixed focus compact brightfield optical microscope. The radiation sensor also had to be removed to simplify the design.

The proposal was accepted for a flight on the BEXUS 30 gondola for the 2019-20 flight campaign. In the middle of the one-year programme, the COVID-19

pandemic impacted Europe, and the programme was extended for another year and flown in October 2021.

In summary, the narrative highlights how the PhD research changed over time due to the emergence of various opportunities, activities, and a global pandemic. The initial plan was to commission the laboratory breadboard that could be tested at varying ionising radiation levels using a range of biological samples, yet to be selected at the initial stage. The final BoB flight did not explore the varying radiation level but emphasised the technology demonstration of the key functionalities and operational handling of the payload and associated biology.

The unexpected flight opportunity call for the ISS has brought forth the issue with the initial MCSD, especially during AIV. It also highlighted the applicability of *C. elegans* as a biological sample and the importance of pre-flight operations. It redirected the PhD effort toward developing the 2nd gen. MCSD and RV. It also put forth the relevance and applicability of *C. elegans* as the primary biological candidate for the BAMMsat-on-BEXUS flight.

There were other key design drivers that influenced the PhD development. These were (i) heritage to BAMMsat 1st generation, (ii) BEXUS flight design and programmatic (timeline and documentation) requirements and constraints, and (iii) requirements in anticipation for spaceflight.

1.6 Contributions to knowledge

This section aims to capture the new contribution to knowledge that was developed through the PhD research. It is introduced here as an early summary to help put the contribution in context.

- The primary contribution during the PhD was to advance the knowledge in the bioCubeSat field to fly a broader range of organisms, such as multicellular organisms.
    - Previous free-flying bioCubeSat have opted for a single-cell organism that can remain in stasis for a long period. Such an option accommodated the need for bioCubeSat to be turned off for a long period as CubeSat is still considered a secondary payload during an orbital launch.
    - Developed a mechanically assembled design of a sample chamber device (named multi-chamber sample disc; MCSD).
        - Some organisms require late-access to the launch vehicle to maintain the organism's viability before integration into the bioCubeSat.
        - A mechanically assembled design overcomes the limitation of sample exchange and retrieval during pre-flight and post-flight.
        - Provide flexibility during assembly, integration, and verification (AIV) for biological handling.
    - The BAMMsat concept contained sensors that are not widely adopted in the bioCubeSat, such as chemical sensors such as O2 CO2, pH, fluorescence microscope and visible spectrometer. These sensors are commonly used on Earth for a wide range of life science studies.
        - Advancing the BAMMsat concept help advance the application of these sensors in space to enable a broader range of organism study.

- During the PhD research, a multicellular organism, C. elegans, was used as an example of a live biological system inside a bioCubeSat.

- Produce a summary of published literature relevant to bioCubeSat
  - A summary of the findings from the literature review has been compiled in this PhD thesis which summarised the different publications that have provided a detailed review of the bioCubeSat concept, the technological status of bioCubeSat (in the context of uncrewed spacecraft) and analysing the advantage and disadvantage of bioCubeSat. The summary could be a source for a new reader interested in the bioCubeSat concept.

- Advance the rotary valve concept for bioCubeSat applications.
  - The rotary valve device is used within the biomedical field for fluidic control. Within BAMMsat, the rotary valve (RV) concept is coupled with the sample chamber device (MCSD), which allows each sample chamber to be individually addressed by intermittently rotating the chamber to access independent fluidic ports and sensors
    - It benefits from efficiently integrating a single microscope and a single spectrometer to cater to each sample chamber by rotating the sample chamber in front of the sensor. Each sample chamber will require its own sensor without the rotary valve, increasing mass and volume.
    - Similarly, the RV reduces the number of valves required for each fluidic port.
  - In a volume constrained bioCubeSat, an RV increases the density of the sample or sample chambers. Hence, increased experiments without the negative impact of increasing mass and volume. Advancing the technology could improve the capability of bioCubeSat

- Demonstration of *C. elegans* in a flight model CubeSat in the stratosphere
    - To the author's best knowledge, the application or flight of *C. elegans* in a CubeSat, either in orbit or extreme environment, has not been performed to date.
    - The PhD research developed a bioCubeSat payload able to house and perturb *C. elegans* in an extreme environment.

1.7 Structure of the thesis documents

The thesis is divided into ten chapters.

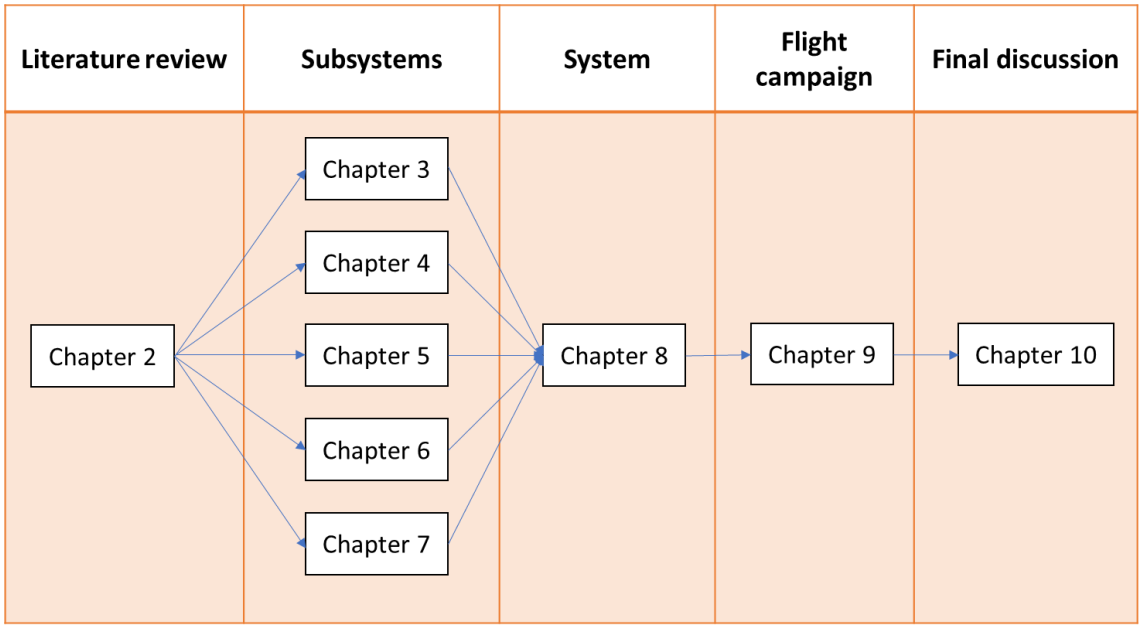

Figure 1-7. Image showing the correlation between the ten chapters and the evolution of the subsystems into a flight model.

1.7.1 Chapter 1

Chapter 1 is the introductory chapter to the thesis, covering the motivation, aims, and objectives behind the PhD research. The chapter sets the scene of the PhD research and describes BAMMsat's history and its technological status at the start of the PhD. It includes a narrative section to discuss how the PhD evolved with further development and flight opportunities. The chapter also introduces the BAMMsat-on-BEXUS (BoB) mission, a stratospheric flight opportunity launched under the BEXUS programme, which became a key driver of the PhD research.

1.7.2 Chapter 2

Chapter 2 presents the review performed on the literature and public domain information related to the scope of the PhD thesis.

1.7.3 Chapter 3

This chapter discusses the research and development performed on the multi-chamber sample disc (MCSD) and rotary valve (RV) during the PhD research. The MCSD and RV are crucial subsystems that provide unique functionalities within the BAMMsat concept.

1.7.4 Chapter 4

This chapter discusses the research and development of a compact brightfield microscope during the PhD research. The compact brightfield microscope was explicitly developed for the BoB mission to capture images and videos of the *C. elegans'* during the BEXUS 30 flight campaign. The captured images will be used to assess the health of *C. elegans* to confirm the functionalities of the 2nd gen. BAMMsat bioCubeSat payload during technological demonstration mission onboard BEXUS 30.

1.7.5 Chapter 5

This chapter discusses the research and development of the 2nd gen. fluidic subsystem. The fluidic subsystem for the BoB system advanced from the concept developed for the 1st gen. BAMMsat bioCubeSat payload. The chapter discusses the tests and characterisation of the lower-level fluidic subsystem, such as actuators and sensors, to verify its functionality and inform the design of the 2nd gen. fluidics subsystems.

1.7.6 Chapter 6

This chapter discusses the research and development of the 2nd gen. Geneva gear mechanism. The mechanism provides intermittent motion to enable discrete independent addresses of each sample chamber for fluidic actuation or data collection. The chapter describes the evolution of the Geneva gear mechanism from the 1st gen. concept into the 2nd gen. subsystem in preparation for the BoB mission.

1.7.7 Chapter 7

This chapter discusses the development of the final subsystem in the PhD research, the mechanical support subsystem. It describes the design and manufacturing process to provide mechanical support. The mechanical support provided the housing for the 2nd gen. BAMMsat bioCubeSat payload, and was designed to fit into a 2U CubeSat format pressure vessel.

1.7.8 Chapter 8

This chapter discusses the assembly, integration, and testing (AIT) of the subsystems and components developed in previous chapters into the 2nd gen. BAMMsat bioCubeSat payload. The 2nd gen. BAMMsat bioCubeSat payload combines the multi-chamber sample disc (MCSD), rotary valve (RV), fluidic subsystem, and Geneva gear mechanism housed in a mechanical housing in a 2U CubeSat format.

1.7.9 Chapter 9

This chapter introduces and presents the BoB flight campaign launched on the 30th of October 2021 and reports a flight campaign summary, preliminary analysis, and lessons learnt.

1.7.10 Chapter 10

This chapter is the final discussion and conclusion that brings together the outputs of all the other previous chapters as a PhD research output.

2 Literature Review

2.1 Introduction

This chapter aims to present the literature review performed on the scope of the thesis during the PhD research. The literature review would help establish the current start of the art within the community to help drive the direction of research and technology development during the PhD. The review could also identify patterns and technologies that can be useful for the PhD and BAMMsat technological roadmap.

The review began by analysing the previous research on the BAMMsat concept before the PhD. The analysis provided the author with an overview of how the BAMMsat concept came into realisation and the background knowledge. This information was later used to collate a list of search strings to search in the indexed database such as Scopus, NASA Technical Reports Server (NTRS), and Google Scholar. The review started at the beginning of the PhD and continued throughout the PhD programme.

It is worth pointing out that during the PhD, there was a plan to publish findings from the review. At the beginning of the PhD in September 2017, no coherent publication was publicly available that consolidated the bioCubeSat launched into orbit. Since a lot more PhD effort was made towards design and laboratory testing, especially during the BoB mission, the publication did not quickly progress.

Towards the end of the PhD (February 2022), other authors published several publications capturing the timeline, mission objectives, and technology of the launched bioCubeSats. The chapter is not aiming to repeat what has been published. It aims to provide context for this PhD research and highlight helpful information and discussion relevant to the BAMMsat concept. These recent articles will be used as a reference to establish the knowledge in the literature in section 2.4.1.

2.2 Aim and objectives

1. *Formulate and perform a review methodology that would return the widest result and most relevant search return within the scope of the PhD.*

This objective was established to set up a survey methodology by collating possible databases and a list of search strings.

2. *Produce background knowledge based on literature review findings*

This objective was introduced to provide an overview of the knowledge that has been published in the literature.

3. *Produce an overview to establish the current state of the art of the technology as a free-flying CubeSat*

This objective was created to provide context for the PhD thesis. For this thesis, a current state of the art will be considered as a flown bioCubeSat.

4. *Produce an overview to establish the current state of the art of the technology as a CubeSat compatible format hosted on a larger platform.*

Similar to objective three, objective four was included as another context for the PhD thesis. CubeSat standardisation meant that they are now hosted on a larger platform such as the International Space Station (ISS). This concept is similar to the BoB mission, where BAMMsat was hosted on a BEXUS stratospheric balloon.

5. *Produce an overview to establish the information in the literature on C. elegans hosted on a CubeSat*

Specific to the BoB mission, this objective was included to review the literature on the application where *C. elegans* is hosted on a CubeSat.

6. *Produce an overview to establish the current public domain knowledge on stratospheric balloon testing on technology demonstration*

This objective was included to review applications of stratospheric balloons for technology demonstration in preparation for spaceflight. It is in a similar context to the BoB mission.

2.3 Literature review research methodology

This section describes the search methodology formulated during the literature review.

2.3.1 List of literature resources

I. Scopus

Scopus is widely known within the academic community and has one of the largest abstract and citation databases.

II. NASA Technical Report Server

NASA's internal server contains access to NASA's records on the research report, presentation slide, conference paper, patents, images, and videos. The content is either created or funded by NASA. The material within this record is often not indexed in Scopus or google scholar.

III. Google Scholar

Google Scholar could be considered to have broader search coverage. It can include non-journal sources such as theses and dissertations, not formally published papers such as preprints and working papers, conferences, and patents.

IV. Company website and press release

In the growing space industry, many innovations and technologies are produced by private companies. These technologies should not be disregarded since they can still be considered state-of-the-art. Private companies are not incentivised to publish their findings in peer-reviewed journals. A website or press release could be viewed as an alternative source.

I. Patents

Patents were used to evaluate the technologies developed by the pre-identified private companies with a track record of spaceflight flown bioCubeSat payload. Patents are publicly accessible and can be used to assess the current state of the art.

2.3.2 List of search strings

The search string was constructed via a combination of text, numbers, and special characters. The search engine is embedded within the database and uses a set of rules derived from the search string to produce a result relevant to the set text, number, and special character.

The list of search strings was compiled using a combination of prior knowledge and field of interest in text format. The text could be written such as successfully launched bioCubeSat as prior knowledge (e.g., GeneSat and PharmaSat) and field of interest (e.g., bacteria, yeast, CubeSat). When producing the search string, the strategy was to compile a list of search strings that combined unique texts, an asterisk (*) as a special character, and a Boolean operator (AND).

The defined search string will then provide the widest search coverage of relevant hits. For instance, the search string (cubesat* AND algae) will produce search results that narrow the search field and combine results under CubeSat and algae. Without having the Boolean operator (AND), the result could produce all relevant hits to CubeSat or algae, and such results will be too many to review. The special character (*) will search for the hit that picks up a variant word ending/spelling, for example, CubeSat* can be written in the publication as CubeSats or CubeSatellite (Beatty, 2022).

In summary, the compiled list of search strings used during the literature survey is listed in bullet points below.

- cubesat* AND algae
- OREOCube
- nanosat* AND yeast
- microfluid* AND cubesat*
- outer space science and nanosat*
- human AND cell* AND nanosat*
- genesat*
- medic* AND nanosat*
- microfluid* AND nanosat*
- biolog* AND cubesat*
- nanosat* AND lunar
- interplanetary AND nanosat*
- ecamsat
- cubesat* AND bacteri*
- cubesat* AND yeast
- pharmasat
- human AND cell* AND nanosat*
- astrobiolog* AND cubesat*
- nanosat* beyond low earth orbit
- deep space science AND nanosat*
- o/oreos
- biolog* AND nanosat*
- cubesat* beyond low earth orbit
- nanosat* AND moon
- nanosat* AND algae
- nanosat* AND bacteri*
- nanosat* AND plant*
- human AND cell* AND cubesat*
- outer space science and nanosat*
- medic* AND cubesat*
- astrobiolog* AND nanosat*
- outer space science and cubesat*
- cubesat* AND plant*
- nanosat* AND mars
- phobos AND life
- deep space science AND cubesat*

- cubesat* AND mars
- interplanetary AND cubesat*
- cubesat* AND moon
- cubesat* AND lunar

Based on those search strings, each of them had an alert on Scopus. This ensures the author (A. Shamsul) is updated with new publications. Alert was also set on prominent authors on Scopus based on the pattern of the search results. Outside of Scopus, an alert was also placed on Zetoc for a new journal publication list.

2.4 Results and analysis from literature review

This section presents the results from the literature review and separates them into three categories.

2.4.1 Establishing the background knowledge for bioCubeSat

This section aims to establish background knowledge based on the findings during the literature review. This section has been written to the author's best knowledge based on results from the literature review.

As a general historical overview, the concept of bioCubeSat started in the early development years of the CubeSat concept. At first sight, it was not apparent that the idea of using CubeSat for biology in space had been discussed at an early stage. GeneSat, the first bioCubeSat, was launched in 2006 (Antonio J Ricco et al., 2007). It was three years after QuakeSat's launch; the first CubeSat launched for a scientific mission (R. Twiggs, 2009). One of the earliest bioCubeSat concepts was developed by Bob Twiggs and Seiji Kuroki in 2002, named BioNano Satellite-1, to study the growth rate of Saccharomyces cerevisiae, a model yeast cell, in microgravity (B. Twiggs & Kuroki, 2002).

In the last 11 years, there has been a steady growth in bioCubeSat research. At the time of writing (February 2022), the Scopus search result for bio* AND cubesat* search string returned 136 documents results. The result is only limited to this search string and does not represent the entire field. The analysis performed here is only evaluating the trendline. The first publication relevant to a bioCubeSat was published on O/OREOS in 2011 (Ehrenfreund et al., 2011). Since then, there has been a steady cumulative increase in publications every year. Robson and Cappelletti mentioned a healthy list of academic bioCubeSats development across the globe, which supported the growing trend behind the bioCubeSats field (D. J. Robson & Cappelletti, 2022).

It is worth noting that the Scopus search result does not reflect the development behind the bioCubeSat. For instance, the first publication that mentioned GeneSat was in 2004 in the context of student development programmes (Kitts

& Quinn, 2004). That was two years before the launch in 2006, and it can be assumed that the concept and development began at least a couple of years before 2004. It is worth mentioning that this paper by Kitts & Quinn was found via Google Scholar and did not appear on the Scopus search result.

Patent search results confirmed that private companies had R&D activities related to bioCubeSats as early as 2015. Most of the patents were filed by SpacePharma, as shown in Table 2-1. The patents made up the technology behind fluidic and reagent actuation within SpacePharma's bioCubeSat payload. The patents were found by searching the name of pre-defined private companies with current bioCubeSat payload presence in space: SpacePharma, Yuri, and Space Tango. Note that Emulate Inc filed one of the patents included in Table 2-1, and it described how Emulate's Brain-on-Chips technology interfaced with Space Tango's CubeLab on board the ISS.

In 2021, Glick and Eyal reviewed uncrewed satellite and vehicle history. The article provided a historical context in developing uncrewed satellites and vehicles from Biosatellite by NASA into the future concept of reusable vehicles such as ESA Space RIDER and Dream Chaser by Sierra Nevada Corporation. The discussion and evolution were described in the context of science questions and technologies, emphasising the technology. The publication made a case on how autonomous or uncrewed spacecraft are growing in utilisation as an alternative to the ISS (Glick & Eyal, 2021). They claimed that the growth is supported by microanalytical systems, microfluidics, and miniaturised instruments, as shown by several successfully launched bioCubeSat missions.

Table 2-1. List of pattern search result.

Patent Number	Title	Filed date	Assignee
US9597686B1	Serviceable Microgravity Fluid-Handling System	31st August 2015	SpacePharma SA
US9808805B2	Liquid reservoir for microgravity system	8th September 2015	SpacePharma SA
US20170355584A1	Multichannel liquid delivery system	9th June 2016	SpacePharma SA
US10150115B2	System and method for rehydrating powder and delivering the rehydrated powder to a reactor	21st July 2016	SpacePharma SA
AU2018283184B2	Effects of space travel on human brain cells	14th June 2018	Emulate, Inc.
US2021300861A1	Drug Crystallization under microgravity conditions	23rd July 2019	SpacePharma R&D Israel LTD.

CubeSat Handbook: From Mission Design to Operations was published in 2021. An extensive review of the NASA bioCubeSat missions was presented In one of the chapters named "CubeSats for microbiology and astrobiological research" (Zea et al., 2021). The book chapter summarised and described the bioCubeSat missions over the years, which covered GeneSat-1, PharmaSat, O/OREOS, SporeSat-1 and EcAMSat. The book chapter also introduced BioSentinel, which is planned to be the first bioCubeSat to travel beyond low earth orbit. One of the key highlights in this book chapter is the relatively in-depth system-level payload design description. The design description for each bioCubeSat even included

materials and instrument choices. The book is meant for CubeSat designers, which explains the level of discussion on the technological aspect.

In 2022, another publication outlined the opportunities and challenges facing a bioCubeSat to support space biomedical research (D. J. Robson & Cappelletti, 2022). The article made a case on how and why an autonomous bioCubeSat and fee-flyer could support space biomedical research complimenting the crewed spacecraft. CubeSat has many advantages, such as lower cost and performing higher-risk missions such as infectious diseases studies that may not be approved for crewed spacecraft. However, it has disadvantages due to its small volume, translating to complicated packaging design and less power. The article also highlighted some technological gaps for future development.

The unique aspect of bioCubeSat is the biological samples compared to other CubeSat, such as an earth observation CubeSat. The addition of biological samples has pre-imposed and additional requirements and constraints. They often have a set temperature range or chemical conditioning, for instance, maintaining a degree of CO_2 level to remain viable. Maintaining environmental control is vital to ensuring a successful mission; however, this can be challenging in a volume constrained CubeSat. Previous NASA bioCubeSats have opted for active thermal control with the heater turned on once the temperature drops below a certain threshold (Diaz-Aguado et al., 2011). As a free-flying bioCubeSat, it is vital to understand orbit-thermal interdependency to design the thermal subsystem. This was one of the lessons learnt from O/OREOS, where the internal temperature exceeded the nominal range for the SESLO organisms (Ehrenfreund et al., 2014).

Maintaining environmental control in orbit is as critical as maintaining it on the ground. CubeSat is still considered a secondary payload and is often powered off once handed to the launch provider (D. J. Robson & Cappelletti, 2022). An example of this issue was highlighted on the PharmaSat mission, where launch vehicle integration was more than six weeks prior to launch (Antonio J. Ricco et al., 2011). This can be challenging, especially when constant temperature

monitoring and subsequent thermal control are required. The challenge also increases if late access to the launch vehicle is required, particularly for samples that could not remain in stasis for long, such as mammalian cell culture. Perhaps, one of the most significant drawbacks of bioCubeSat is logistics with handling biological samples.

In closing, this section hopes to establish the background knowledge based on publications available in the public domain. Some of the articles mentioned in this section have provided a detailed review of the bioCubeSat. The information provided by the publications could help build an understanding of bioCubeSats' technological state and understand more about the advantages and disadvantages of bioCubeSat.

2.4.2 Establishing the current state of the art technology

The PhD is a technology and engineering-focused PhD. The literature review results presented here will focus more on the core technology that enables the bioscience application instead of a review of the CubeSat bus. As mentioned in section 2.4.1, most of the mission and technological aspects of bioCubeSat have been summarised and described elsewhere (Glick & Eyal, 2021; Zea et al., 2021). The section aims to provide a version of the summary as a context for the PhD research. For the purposed of this thesis, state of the art is considered a successfully launched bioCubeSat into orbit.

The section is divided into two categories. One is a free-flying CubeSat, and the second is a CubeSat hosted on a larger platform. As the name entails, a free-flying CubeSat is a standalone CubeSat, often constructed of two elements a bioCubeSat payload and a CubeSat bus. On the other hand, a CubeSat hosted on a larger platform is typically hosted on the ISS. This concept leverages CubeSat standardisation to interface with the ISS and the end-user.

2.4.2.1 Free-flying CubeSat

The concept of biological experiments and CubeSat has been established in LEO by NASA and SpacePharma. To date, seven bioCubeSats have successfully launched into orbit. The seven bioCubeSat are GeneSat, PharmaSat, O/OREOS, SporeSat, Dido-2, EcAMSat, and Dido-3. Five of these bioCubeSats shared a common heritage from NASA Ames, and SpacePharma developed and launched Dido-2 and Dido-3.

2.4.2.1.1 GeneSat by NASA Ames

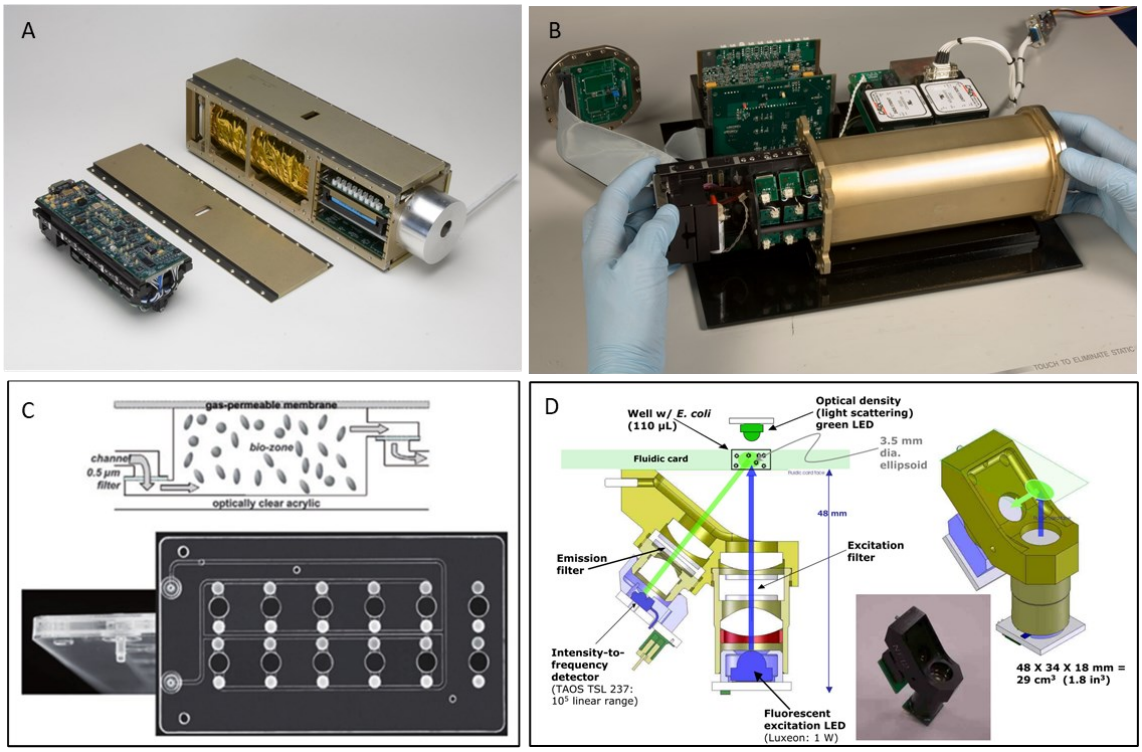

Figure 2-1. Various images of GeneSat[1].

GeneSat was the first bioCubeSat to perform a biological experiment in a CubeSat in orbit. The experiment was performed on the survivability and growth of *E. coli* in space environments by characterising the bacterial growth and

[1] A – Image shows the 3U GeneSat. B – GeneSat 2U bioCubeSat payload. C – Microfluidic card. D – GeneSat optical subsystem. Image A and B were extracted from (NASA, 2006). Image C was extracted from (Antonio J Ricco et al., 2007), and Image D was extracted from (Antonio J. Ricco, n.d.)

metabolic activity of *E. Coli* bacteria. The objective of the mission was to demonstrate the survivability and growth of *E. coli* in space environments demonstrating the feasibility of the technology behind bioCubeSat.

The *E. coli* was housed inside a pressure vessel with an internal volume of 0.9 litres. See images A and B in Figure 2-1. The miniaturised laboratory inside the pressure vessel consists of a fluidic card, microfluidics, optical sensors and environmental sensors (Antonio J Ricco et al., 2007). The miniaturised laboratory was capable of incubating microorganism growth in multiple fluidic microwells and monitored their gene expression via an optical fluorescence system to identify microbe population vs time (Antonio J Ricco et al., 2007).

The fluidic card was able to house multiple *E. coli* during both dried storage phase and a wet growth phase. It consisted of 12 wells where 10 wells were inoculated with *E. coli* culture, which were kept from washing out using filters on the inlet and outlet (A. J. Ricco et al., 2005). The other two were used as solid-state references. Pre-determined nutrient concentration of growth media was pumped through the solenoid valve to replace the statis media inside the well to begin the experiment and initiate growth.

The fluidic card was constructed using interlayers of laser cut acrylic plastic interlayered with pressure-sensitive adhesive (Levine et al., 2007). See image C in Figure 2-1 for reference. The layers included: pressure-sensitive adhesives (PSA) supported on PET (poly(ethylene terephthalate)) carrier films, optical quality cast acrylic (to enable high-quality optical measurements), and optical quality 75μm thick CO_2/O_2 gas permeable polystyrene membrane sealed the device after sample addition as the final layer. The membrane allows gas exchange and minimises evaporation. The gas-permeable membrane was treated with a corona discharge to make it hydrophilic (Antonio J Ricco et al., 2007).

The microfluidic subsystem was used to re-animate the two dormant strains of *E.* coli by replacing the statis medium with a growth medium (Antonio J Ricco et al., 2007). The bacteria were placed in a dormant state; GeneSat had to be powered

off for five weeks prior to launch to be integrated into the launch vehicle. This involves pumping through the nutrient-filled growth medium into the microwell to replace the statis medium via diffusion. It was recorded that ground experiments with coloured dye demonstrated that ~90% of the displacement requires about five minutes, relatively shorter than 1 – 4 days needed for *E. coli* to reach its growth plateau (A. J. Ricco et al., 2005).

Filters were used to contain the *E. coli* during pumping. 0.5 µm-porosity nylon fibre filter membranes were manifold in a pocket formed at the inlet and outlet of each well (Antonio J Ricco et al., 2007), refer to image C in Figure 2-1. The filter membrane kept the bacteria from washing out when pumping the nutrient or reagent through it. The non-cytotoxic individual membranes were glued into each location using a UV cure medical grade adhesive. The membranes were manually glued using a constant volume dispenser through a 24-gauge needle (Levine et al., 2007). The filter also serves as a fluidic impedance-matching network by restricting flow through any single well. This helped ensure that all 10 wells were filled evenly from the single inlet channel (Kitts et al., 2006).

GeneSat had an optical subsystem capable of monitoring gene expression and population size via fluorescence imaging and light scattering. Each one of the 12 microwells had an optical assembly. See images D and B in Figure 2-1 for reference. GeneSat optical subsystems were used to collect two measurements from *E. coli* in orbit.

The first measurement was on the metabolism of *E. coli* via fluorescence. The engineered *E. coli* had plasmid green fluorescent protein (GFP) fused into genes associated with metabolism (Yost et al., 2005). The *E. coli's* GFP excites when the 470 nm 3W blue LED (Luxeon) illuminates the biology. The blue LED illuminated through a ~3 mm spot through an excitation filter (Chroma Technology Corp., VT, USA) and a pair of lenses. The reflected light is then backscattered at 315º to be collected by an intensity-to-frequency detector (TSL 237, Texas Advanced Optoelectronic Solution). The backscattered light travelled through an emission filter (535 nm, Chroma Technology Corp.) and was then focused by a

pair of lenses. The linear digital output can be translated to *E. coli's* metabolic activity.

The second measurement provided information on the size of *E. coli* population. Measurement was achieved by illuminating a 2.3 mW green LED (Osram) (Antonio J Ricco et al., 2007). The reflected light was then forward scattered at 135º, to be detected by the same photodetector. Quantifying the scattered light provided an "optical density". The optical density can be extracted as an indication of the size of the *E. coli* population (Minelli et al., 2008) since the optical density was directly proportional to cell number (Antonio J Ricco et al., 2007). The blue and green LEDs were energised sequentially with one well optically probed at a time to eliminate crosstalk.

Commercial off-the-shelf (COTS) sensors were used to obtain data and monitor the samples inside the ~1 atm pressurised vessel. Data was collected on pressure, humidity, and temperature at multiple locations across the spacecraft, including radiation dose, to monitor the payload's internal environmental parameters and understand its impact on *E. coli* (A. J. Ricco et al., 2005). The spacecraft adapted a cold-biased system with an active thermal control system to heat the fluidic card to 34 ± 0.5ºC to ensure a viable temperature for the biology (Antonio J Ricco et al., 2007). The internal atmosphere was humidified to near saturation to mitigate evaporation from the microwell. The atmosphere also had O_2 and CO_2 to ensure adequate gas exchange into the fluidics card's microwells containing the biology via a gas-permeable membrane (Kitts et al., 2007).

2.4.2.1.2 PharmaSat by NASA Ames

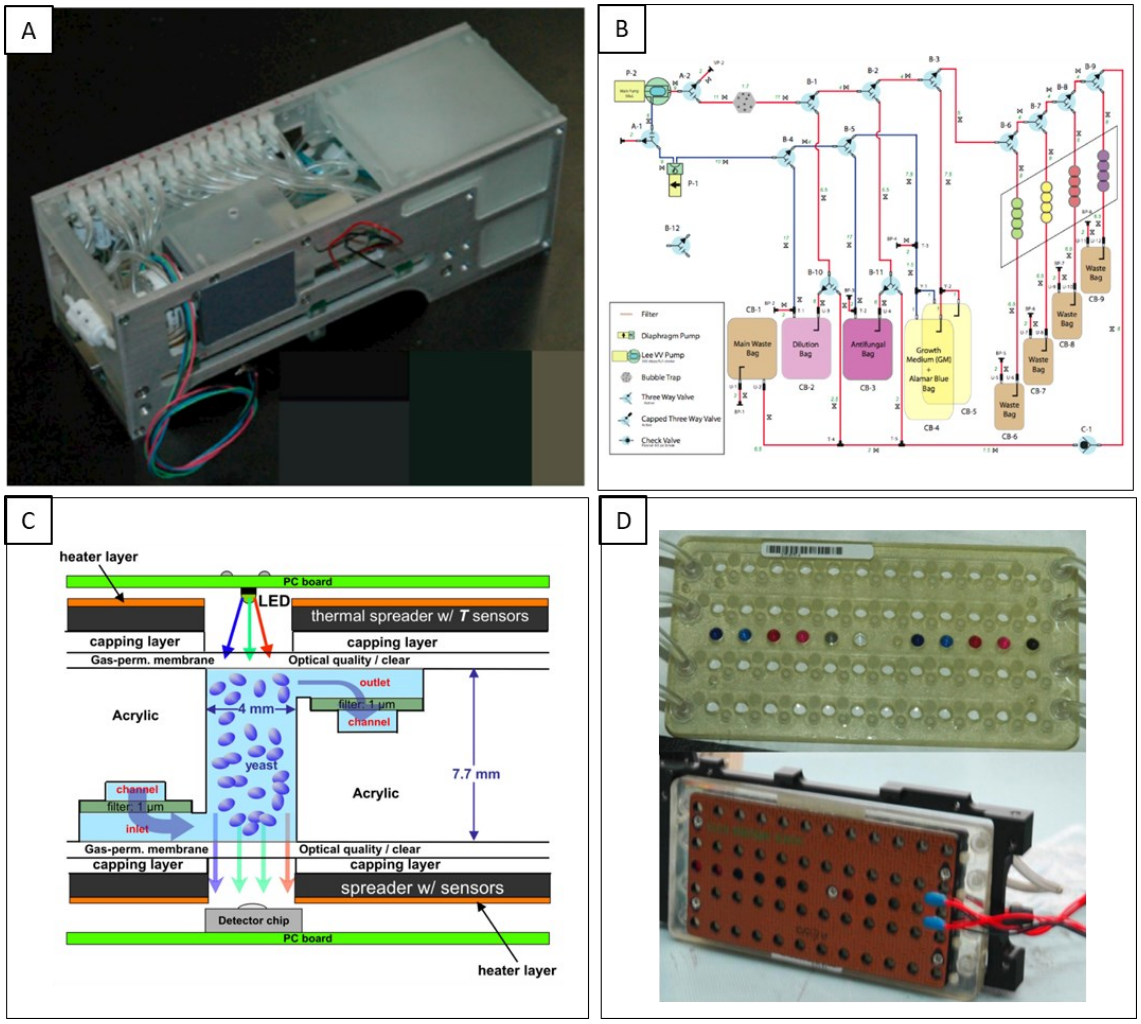

Figure 2-2. Various images of 2U PharmaSat bioCubeSat payload[1].

Three years after GeneSat, PharmaSat was the second 3U bioCubeSat launched into orbit. PharmaSat was launched on May 19, 2009, from the Wallops Flight Facility on board the Minotaur 1 launch vehicle (Kitts, n.d.). It was reported to have been the first fully autonomous pharmaceutical drug dose-response bioanalytical system on a free-flying satellite (Antonio J Ricco et al., 2010).

[1] Image A - 2U PharmaSat bioCubeSat payload. Image B - PharmaSat fluidic network. Image C - PharmaSat fluidic card cross-section. And image D - PharmaSat fluidic card with a thermal heater at the bottom. Images were extracted from (Antonio J. Ricco et al., 2011).

The scientific objective of PharmaSat was to measure and determine the effect of microgravity on *S. cerevisiae* (a well-studied brewer's yeast) on the yeast resistance to the common antifungal drug, Voriconazole. The drug was administrated to the yeast to analyse the efficacy by documenting alteration in antimicrobial resistance when applied to the yeast in microgravity (Antonio J. Ricco et al., 2011).

PharmaSat built upon the knowledge of GeneSat and PRESat with an improved microfluidics capability. PRESat was a precursor bioCubeSat to PharmaSat. Both were developed by NASA Ames to de-risk the new onboard instrumentations. Unfortunately, the PRESat mission was lost on 2nd August 2008 due to the launch failure of the 3rd Falcon 1 launch (Kitts et al., 2009).

The PharmaSat bioCubeSat payload had a similar configuration to GeneSat, i.e., the fluidic card, microfluidics, and optical manifold. It was placed inside a cylindrical 1.2-litre pressure vessel alongside COTS environmental sensors (Antonio J Ricco et al., 2010). The fluidic card was manufactured via laser-cut acrylic layers laminated to one another using pressure-sensitive acrylic adhesive interlayers (Antonio J. Ricco et al., 2011).

There were several differences in the design, such as the microfluidics, the optical subsystem and PharmaSat's biological system. The fluidic card inside PharmaSat's microfluidic subsystem had more samples with 48 microwells. See image D in Figure 2-2. It was a significant increase from 12 microwells on GeneSat, which enhanced the incubation capacity. The additional microwells required additional valves; see image B in Figure 2-2. The change in biological systems from bacteria to yeast meant that the filters in the fluidic card had to be changed to 1.2 µm pore-size nylon fibre membrane filters (Sterlitech) to accommodate the different biological sizes (Antonio J. Ricco et al., 2011).

PharmaSat demonstrated an advancement in the microfluidic subsystem. The subsystem delivered three different concentrations of antifungal drug medium into the microwells (Antonio J. Ricco et al., 2011). This was made possible by combining additional hardware and an integrated fluid network, refer to image B

in Figure 2-2. The network constituted nine medical-grade fluoropolymer bags (American Flouroseal); it was changed from GeneSat, which had a 15 mL medical-grade poly(ethylene) vinyl acetate (PEVA) polymer bag (Antonio J Ricco et al., 2007). The bags, pump and fluidic card, are connected via a medical-grade polymer tube (Sanipure 60 tubing, Saint-Gobain). The 14 solenoid valves (The Lee Co.) were placed at the network junctions to control the fluidic path by opening or closing the channels. A bubble trap (developed in-house by NASA AMES) and a check valve ensure fluid flow in one direction. PharmaSat had two pumps, a diaphragm pump (KNF Neuberger) and a piston metering pump (The Lee Co.). The diaphragm pump provided the higher flow rates required for circulation and mixing, while the piston metering pump enabled precise dilution of the antifungal agent at three different concentrations (Antonio J Ricco et al., 2010). The exact flow rate was not reported to the knowledge of the author.

Regarding the optical subsystem, the difference between the mechanisms in the two varying optical subsystems can be seen in Figure 2-1 and Figure 2-2. The basis of the function is the same for both, where the LED light source illuminates the biological samples, and the light detector collects the emitted light. The LEDs and photodetectors were assembled on a printed circuit board (PCB) matched to the size of the fluidic card. Upon assembly, the PCBs are then mounted to the fluidic card. Each well on all the bioCubeSat had its own dedicated optical subsystem. The design enabled a "sandwiched" configuration and avoided alignment plus reliability issues that could arise with a moving system.

One difference observed is the optical light source and detector configuration. GeneSat had two different LED light sources in the opposite direction, and a detector at a 45º angle adjacent to the fluorescent excitation LED (Antonio J Ricco et al., 2007). PharmaSat utilised an alternative design where one LED light source was placed opposite the photodetector. The design changes reduced the volume envelope of the optical subsystems and arguably simplified the design. However, the design changes also removed the capability to perform fluorescent imaging, which could benefit other studies. For PharmaSat, each of the 48 wells had a dedicated optical subsystem. Each assembly had a three colour LED (Lite-

On) capable of illuminating at 615nm (~red), 525nm (green) and 470nm (blue) with a recorded spectral half-width of 26nm, 35nm and 18nm, respectively (Antonio J. Ricco et al., 2011)

The information gathered from the absorbed light can measure the metabolic activities of the *S. cerevisiae* or yeast cell in PharmaSat. By adding Alamar Blue (AB) or "viability dye" into the growth media, the dye will change colour from oxidised (non-fluorescent, blue) to reduced (fluorescent, pink) upon active cell metabolic activities (John et al., 2000). During development, it was recorded that AB in blue has its absorbance maximum at 600 nm whilst the pink at 570 nm, corresponding to the red and blue band on the three colours LED (Antonio J Ricco et al., 2010). The red LED was sensitive to the disappearance of blue AB. Conversely, the green LED was sensitive to pink AB. All three wavelengths were used to measure the changes in optical density due to light scattering response, where the signals' deconvolution can be measured to represent the cell density. This is similar to GeneSat optical subsystem, where the optical density is proportional to the yeast cell population.

The functionality behind the PharmaSat optical subsystem resembles GeneSat's optical design. One key difference was that PharmaSat did not incorporate the fluorescent imaging capability from GeneSat. The basis of the subsystem remained the same, with LEDs being used to illuminate the biological samples, and the light detectors then collect the emitted light using a photosensor.

PharmaSat used a three colour LED to provide illumination centred at 470, 525 and 615 nm and the sensor utilised 3-colour absorbance measurements to characterise the dose-response. The optical systems can track the organism's growth by detecting the yeast's colour changes the optical density using the three spectrums. The AB colour change represents the metabolic activity, and the optical density represents the yeast cell population. As such, PharmaSat did not require the optical capabilities of GeneSat because it was able to provide similar information with reduced complexity.

2.4.2.1.3 O/OREOS by NASA Ames

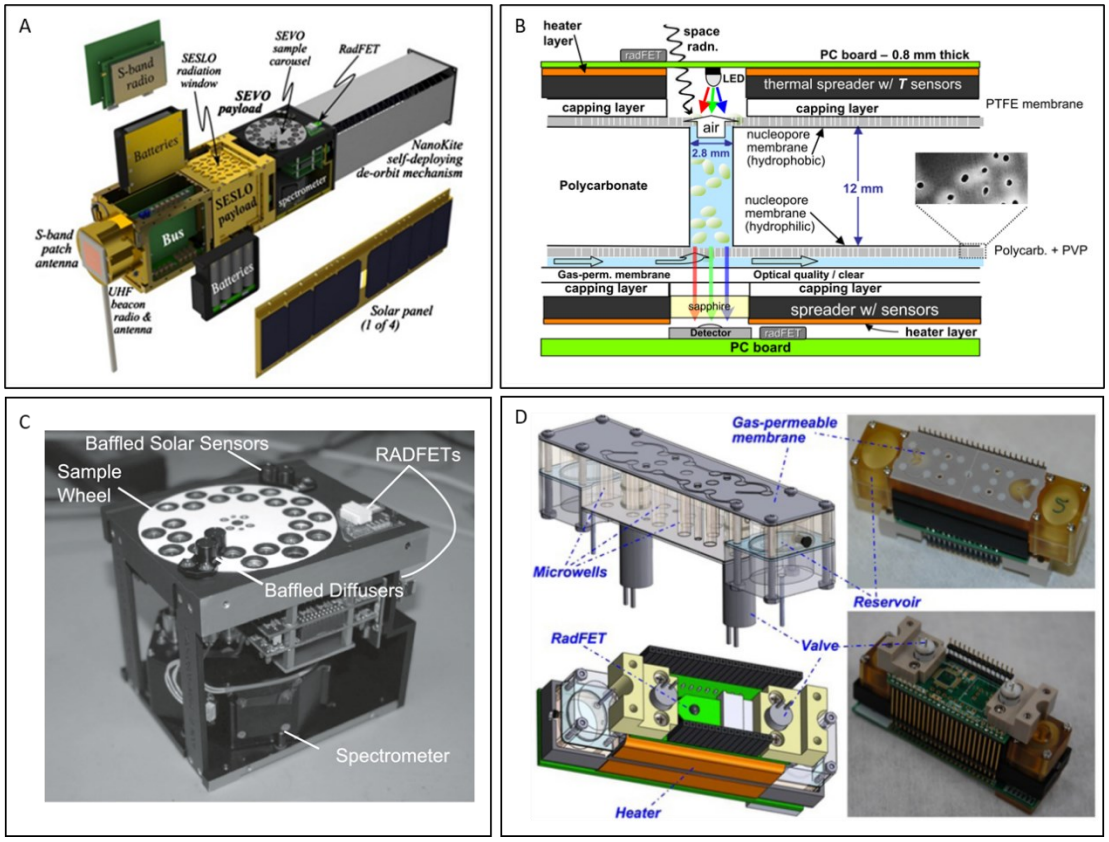

Figure 2-3. Various images of O/OREOS[1].

One year after PharmaSat, O/OREOS was launched on November 19, 2010 on-board the Minotaur IV rocket from Kodiak Launch Complex, Alaska (Ehrenfreund et al., 2014). O/OREOS stands for Organism/Organic Exposure to Orbital Stresses. It has two independent payloads, i.e., SEVO and SESLO (see image A in Figure 2-3. SESLO experimented with the survival of *B. subtilis* against the space environment. At the same time, SEVO experimented with the long-term degradation of organic bio-building blocks.

SESLO (Space Environment Survivability of Living Organisms) and SEVO (Space Environment Viability of Organics) were independent and standalone

[1] A - Image showing the 3U O/OREOS free-flying CubeSat. B – Cross-section view of O/OREOS fluidic card. C – SEVO payload. D SESLO payload. Image in A and D was extracted from (Ehrenfreund et al., 2014). Image B was extracted from (Antonio J. Ricco, 2011), and image C was extracted from (Bramall et al., 2012)

experimental payloads developed by two separate science teams. The SESLO payload can be referred to in image D, and the SEVO payload can be referred to in image C in Figure 2-3. The overall scientific objective of O/OREOS was to analyse the survivability and metabolic activity of microorganisms (SESLO) and photostability of organics and biomarkers (SEVO) to the cumulative nominal 6-month long-term ionising radiation exposure to the space environment. Each SESLO and SEVO experimental payload included its own electronics, microcontroller, and data storage to autonomously execute its respective experiment (Ehrenfreund et al., 2014). The SESLO payload will be discussed first and will later continue with SEVO.

SESLO characterised the health, growth and metabolic activity of *Bacillus subtilis* (*B. subtilis*) and *Halorubrum chaoviatoris* (*H. chaoviatoris*) (Ehrenfreund et al., 2014). It was built upon the heritage of GeneSat and PharmaSat microfluidics systems. The 1U payload consisted of three "bioblocks" with 12 microwells each. The long-duration radiation experiment of SESLO was initiated by inducing growth at three-time points relative to the launch date. These growth points were at 14 days, 97 days, and 6 months. The biological samples were monitored using the 3-colour optical subsystem like PharmaSat.

SESLO fluidic card lamination had some variation compared to previous GeneSat and PharmaSat. It has a layer covering the wells with a "track-etched" or nucleopore polycarbonate membrane; see image B in Figure 2-3. Both polycarbonate membranes trapped *B. subtilis* in the well whilst allowing gas exchange with the trapped headspace in the pressure vessel. The polycarbonate membrane enabled a monolithic design by placing the membrane on the end of the wells. Since it only provides flow in one direction, the biological sample could not escape laterally. The design is beneficial during assembly since a single layer can filter multiple sample microwells.

The microfluidic subsystem for SESLO also had some variation. The SESLO payload was designed to have three independent bioblocks refer to image D in Figure 2-3. Each of the bioblocks had an independent reservoir with one pump

on each side built into a single solid unit. One side of the pump had six wells dedicated to *B. subtilis,* and the other side was for *H. chaoviatoris*. The bioblocks were built as a manifold with the fluidic card instead of reservoir bags. The solid reservoir was made from polycarbonate (Nicholson et al., 2011). SESLO had this configuration to enable each bioblocks to be independent fluidically. This was to initiate the experiment at three mission time points: 14, 97 and 180 days. Another advantage of using polycarbonate was the higher melting point than the previous polymer, PMMA. It enables autoclave sterilisation which benefits pre-flight assembly.

The pumping also differed from PharmaSat and GeneSat. A diaphragm pump (KNF Neuberger) was used to pump air instead of fluid. When pumping, it supplied pressure onto a distensible elastomeric membrane separating the liquid medium from the pressured air in the fluid reservoir (Minelli et al., 2010).

SESLO's optical design was the same as PharmaSat. An additional feature of a sapphire window was included to provide radiation protection to the photodetector without blocking the transmitted light. Refer to image C in Figure 2-3. A sapphire window offers protection from radiation because of its similar radiation attenuation to the aluminium metal (Minelli et al., 2010). O/OREOS flew at a higher altitude and inclination and experienced higher radiation levels.

Regarding SEVO, the experiment was designed to characterise photostability or organics. These were amino acid (*tryptophan*), quinone (*anthrarufin*), polycyclic aromatic hydrocarbon (*isoviolanthrene*) and metalloporphyrin (*iron tetraphenylporphyrin*) (Cook et al., 2014). These organics and biomarkers were chosen for their astrobiological significance.

SEVO has heritage from the EXPOSE research facility on board the ISS, particularly the sample cell of the ORGANIC Experiment on EXPOSE-R (Ehrenfreund et al., 2014). SEVO was constructed of a sample carousel that holds 24 hermetically sealed sample cells covered and attenuated by MgF_2 and sapphire (Al_2O_3) optical windows (Minelli et al., 2010). The four different organics mentioned earlier were placed on the window, and a thin film formed and sealed

it into four microenvironments. These microenvironments represented interplanetary/interstellar space, the lunar surface, wet/salty environment and the Martian atmosphere (Bramall et al., 2012). A novel UV/VIS/NIR spectrometer was developed to measure the changes induced in the molecule during exposure, see image C in Figure 2-3.

2.4.2.1.4 SporeSat-1 by NASA Ames

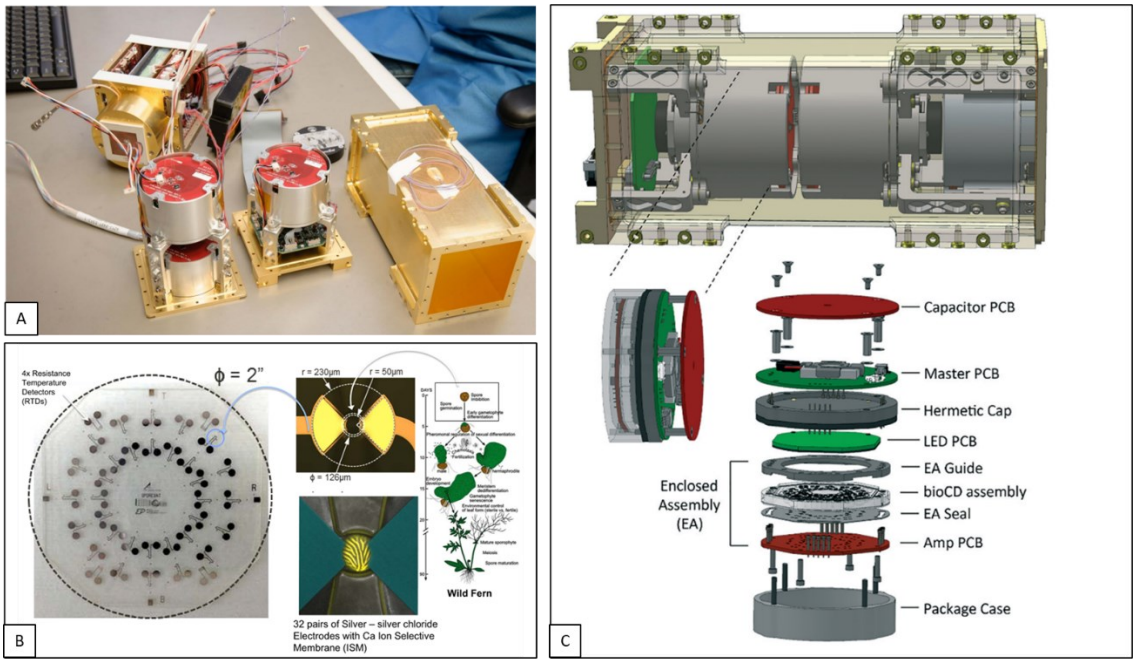

Figure 2-4. Various images of SporeSat[1].

SporeSat was launched into orbit four years after O/OREOS on April 18 2014, from Cape Canaveral, Florida on board the SpaceX-3 Falcon 9 rocket (Martinez, 2014).

The scientific objective of SporeSat was to understand the mechanism of plant cell gravity sensing (Wan Salim et al., 2014). This can be achieved by investigating the gravitational threshold for calcium-ion channel and pump activation in the single-cell spore of fern, *Ceratopteris richardii* (*C. richardii*). It often uses gravity to determine the direction and guide its roots down to Earth, where nutrients are located (Edwards & Roux, 1998). *C. richardii* were subjected to varying artificial gravities to understand the ferns' gravity sensing mechanism by measuring the impact on/off modulation of cellular calcium ion channels (NASA, 2014).

[1] A – The 3U SporeSat is ready to be assembled. B – SporeSat lab-on-chip used to house the fern. C – SporeSat bioCD. Images A and B were extracted from (Martinez, 2014). Image C was extracted from (Park et al., 2017)

The experimental payload inside SporeSat incorporated three bioCD inside a 2U pressure vessel. The bioCD is a lab-on-chip device on top of a miniaturised centrifugal system. It can rotate the ferns and produce varying artificial gravities, made possible by the space microgravity environment, to measure the real-time impact on the cellular calcium ion channels. Two bioCD were rotated to exert an artificial gravitational force, and one remained stationary as a control to the ambient microgravity. Each bioCD contained four rings of eight fern spores, which carried 32 spores per bioCD. The bioCD was built upon the strand of work at Purdue University called CEL-C biochip (ul Haque et al., 2007).

The bioCD has an integrated centrifuge platform developed by NASA Ames. The centrifuge rotates the system and provides varying levels of artificial gravity via centrifugal force (Wan Salim et al., 2014). The gravitational response of the fern spores was monitored by measuring the activity of their calcium ion channels at different gravity levels. In total, there were three bioCDSs on board the SporeSat. Two bioCDs were rotated under pre-determined gravity levels, and one remained stationary as a control in microgravity. All were housed in a pressure vessel with an internal pressure of 1 ATM (Wan Salim et al., 2014).

Each bioCD had 32 ferns distributed over four rings of eight fern spores; refer to image B in Figure 2-4. The four rings were separated at four radii of 18, 15, 12, and 9 mm from the centre axis of rotation (Park et al., 2017). The rotation speed ranges from 80,112,158 and 315 rpm, and each speed corresponded to four different centrifugal gravities from micro-g to hyper-g.

The bioCD was fabricated on a 50mm diameter fused silica substrate bonded with 32 cylindrical SU-8 well that acts as a holding structure (Park et al., 2017). Each well had a diameter of 126 μm and an aspect ratio of 1:1, capable of housing exactly one fern seed, as represented in image B in Figure 2-4. The four Pt RTD provided the closed-loop thermal control (Wan Salim et al., 2014) and were exposed to the same volume of germination medium in the spore wells to accurately indicate the spore temperature (Park et al., 2017).

After loading the spores into the bioCD, a polycarbonate layer was attached to the bioCD using PSA or EA seal (Park et al., 2017), see image C Figure 2-4. The machined polycarbonate layer called EA wall enabled the well to accommodate the agar germination medium to maintain spore viability and good ionic conductivity. The agar used for the flight has not been specified. However, it has been reported that the agar used during the ground test could either be from Sigma-Aldrich (Bacteriological agar) or BD Bioscience (Difco™ Noble) (Park et al., 2017).

A thin layer of polycarbonate called EA cover was attached to the EA wall using PSA to complete the bioCD assembly. It is worth highlighting that this was a similar bonding technique used in other bioCubeSat fluidic cards. The bioCD assembly was then attached to the amplifier PCB and LED PCB on the opposite end (see image C Figure 2-4). The LED PCB contained 32 individual red LEDs (Kingbright APT1608SRCPRV) aligned to each spore well to germinate the spore through the transparent bioCD. The LEDs had a peak wavelength of 655 nm. The entire assembly was housed in black-anodised aluminium to minimise light reflection and capped using a machined hermetic cap made from black PEEK with a fluoropolymer elastomer gasket to provide the sealing.

2.4.2.1.5 EcAMSat by NASA Ames

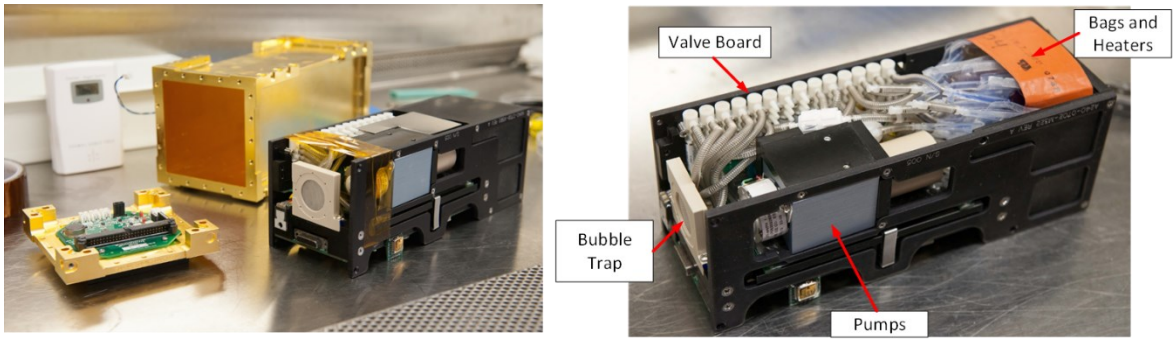

Figure 2-5. EcAMSat 2U bioCubeSat payload with the pressure vessel. Left image (Boone et al., 2014)**.** Right image (M. Padgen, 2017)**.**

EcAMSat was launched on November 12, 2017, on board the Antares rocket inside the Cygnus spacecraft from the Wallop Flight Facility (Spremo, 2018). It

was the first NASA mission with a 6U CubeSat configuration (Spremo, 2018). Although the complete CubeSat was 6U, the bioCubeSat payload remained a 2U form factor, see Figure 2-6.

The science objective of EcAMSat was to investigate the effect of space microgravity on the resistance of *E. coli* to an antibiotic, Gentamicin. Two strains were flown, i.e., the wild type *E. coli* and its σ^s-deficient mutant (M. R. Padgen et al., 2020). The experiment was designed to determine if the sigma factor (σ^s) has a role in any potential increase in Gentamicin resistance.

The experimental payload hardware, in essence, is re-flown hardware of PharmaSat. Both the optical subsystem and microfluidic subsystem was based on PharmaSat. Some modification was made to accommodate *E. coli* instead of *S. cerevisiae.* Changes were made to the filter pore size from 1.2μm to 0.2μm to accommodate the *E. coli* instead of *S. cerevisiae*. The filter contained the bacteria in the fluidic well. The experiment temperature was also increased from 27ºC to 37ºC to meet *E. coli's* thermal requirement (M. Padgen, 2017). It meant that the previous 3U design had to be modified to support additional solar panels to provide more power for the heater (Boone et al., 2014). EcAMSat microfluidic subsystem was built on the knowledge and hardware of PharmaSat (Matin et al., 2017). The microfluidic subsystem was administrated to supply three specific antibiotic concentrations into the 48-well fluidic card; see image B Figure 2-2 for the fluidic pathways.

2.4.2.1.6 Dido-2 and Dido-3 via SpacePharma microgravity lab (SPmg)

Dido-2 and Dido-3 were launched in orbit as a series of bioCubeSat developed by SpacePharma, a company based in Israel (Hovell, 2017). It is a privately owned commercial company and the only other entity that has reported launching a bioCubeSat other than NASA. The results presented here are what was found in the public domain since the private company is not incentivised to publish their findings.

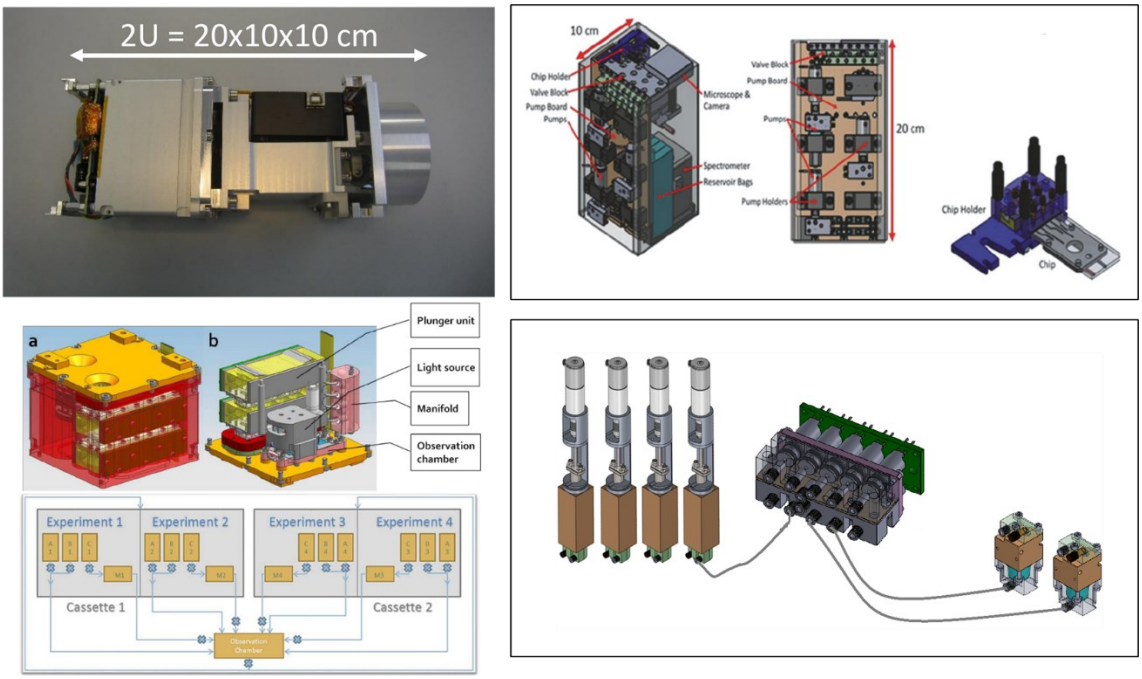

Figure 2-6. Various images of SpacePharma's SPmg lab[1].

SPmg (see Figure 2-6) is one of the microgravity platform services offered by SpacePharma. Other services included platforms on the simulated microgravity on a random positioning machine, parabolic flight and the experimental facility onboard the ISS.

Dido-2 was launched on 15th February 2017 on board the Polar Satellite Launch Vehicle (PSLV) C-37 from Satish Dhawan Space Centre, Sriharikota, into sun-synchronous orbit (Innovative Solutions In Space, n.d.)(Department of Space Indian Space Research Organisation, 2017). Dido-3 was launched on 3rd September 2020 from French Guiana (Glick & Eyal, 2021).

SPmg lab is a miniaturised microgravity laboratory platform developed by SpacePharma for their Dido bioCubeSats. The end-to-end system included lab-on-chip devices, a spectrometer, a microscope and a SpacePharma Microgravity

[1] Top left – Image of SPmg, a 2U bioCubeSat payload, extracted from (Yamin, 2016). Top right – Labelled CAD of SPmg, extracted from (Dhall et al., 2016). Bottom left – Layout of the SPmg sample chambers and fluidic pathways, extracted from (Amselem, 2019). Bottom right – SpacePharma's SPuMP, extracted from (SpacePharma, n.d.)

Miniature Pump (SPuMP) (Samburski, 2018). The SPmg can house four experiments; refer to the bottom left in Figure 2-6. Each experiment contained three reservoirs and a main chamber. Results are viewed using an observation chamber, which was shared between the four experiments.

The SPuMP actuated the microfluidic within SPmg. It is a miniaturised, non-pulsatile pump with integrated reservoir temperature control. The SPuMP was developed under the EU Horizon 2020 grant, and the report can be viewed at (SpacePharma, 2017). They claimed that compared to a peristaltic pump, SPuMP is capable of pulsation-free flow and highly accurate flow control, which enabled a new set of experiments such as direct droplet-based macro-molecular crystallisation. SpacePharma claimed that the SPuMP is capable of a smooth flow between 10µL/min and 500µL/min with temperature control between 4ºC to 40ºC (SpacePharma, n.d.).

2.4.2.2 CubeSat compatible format hosted on a larger platform

This section aims to capture the CubeSat concept hosted on a larger platform. The review was performed to complement the PhD research, which included the BoB mission which was BAMMsat hosted on the BEXUS platform.

The section only covers the core technology of bioCubeSat payload, which can perform scientific research under its own remit. It does not cover CubeSat hosting facilities such as Nanolab by NanoRacks, ICECUBES by SAS and Bartolomeo by Airbus.

This section was included since the technology being developed by these private companies can be considered state of the art. There are included as part of the literature review to evaluate the technology which could help the direction of the PhD and BAMMsat. The result mostly revealed an industrial-led technology. Since most of the information is proprietary, the results presented here are what is available in the public domain.

2.4.2.2.1 CubeLab by Space Tango

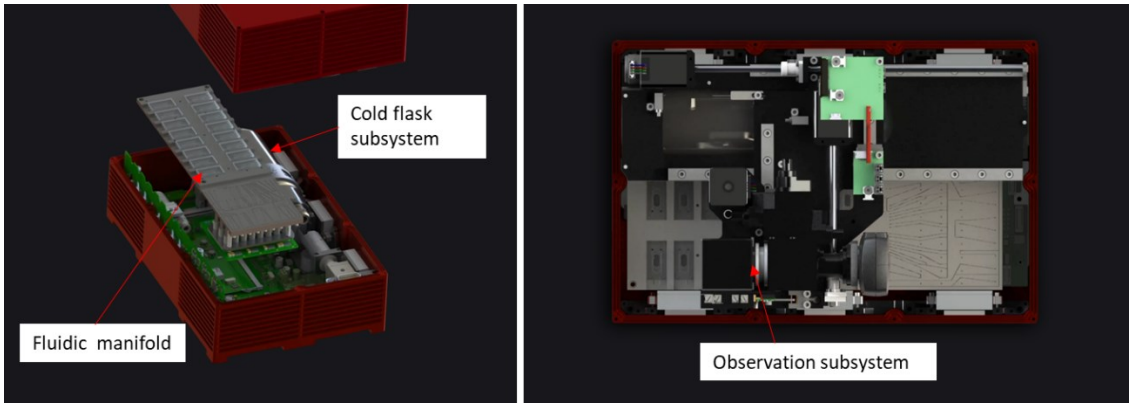

Figure 2-7. Images of CubeLab by Space Tango. Images from their website (Space Tango, 2022).

Cubelabs™ is one of the products offered by a US-based space company named Space Tango. The idea behind Cubelabs™ is to provide a standardised platform based on the CubeSat standard to enable R&D inside the ISS U.S National Laboratory. Based on their website (Space Tango, 2022), the product offering, which includes an end-to-end, is sized at 9U. It has a fluidic manifold that enables the management of multiple fluids, fixation, sampling and media exchange. It can be speculated that it has 16 sample chambers; refer to the left image in Figure 2-7. The company also claimed it has a thermal control that can maintain the low temperature at 4°C using a cold-flask subsystem. The right image in Figure 2-7 shows the observation subsystem. The company claimed to have various imaging capabilities, including advanced lighting cycles and microscopy.

2.4.2.2.2 SPAd-ISS by SpacePharma

SpacePharma Advanced Lab (SPad) is an alternative product offering from SpacePharma. It was primarily developed for application on the ISS (Glick, 2018). Their website claimed that it could also be flown as a free-flying CubeSat. At the time of writing (February 2022), there has not been any launch with SPad as a free-flying CubeSat was ever recorded.

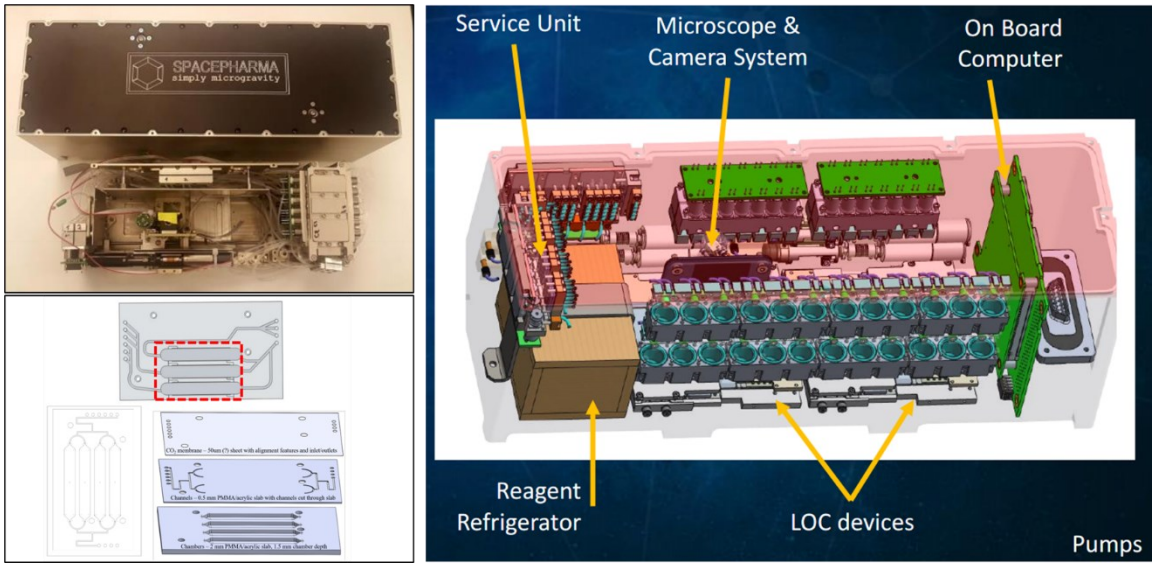

Figure 2-8. Various images of the SpacePharma Advanced Lab (SPad). Images extracted from (Glick, 2018)**.**

SPad has a volume form factor of a 3U CubeSat (Glick, 2018). A larger volume meant that Space Pharma can increase its discrete experiment capacity from four to eight compared to SPmg (see 2.4.2.1.6). The Lab-on-a-Chip (LOC) device (see bottom left of Figure 2-8) used the same technique as NASA Ames's bioCubeSats. It was constructed from a PMMA acrylic slab which provided the channels and chamber depth (Glick, 2018). Another unique trait highlighted in Figure 2-8 is the reagent refrigerator. This capability was not apparent in the SPmg review, and the refrigerator helps maintain the viability of the reagent.

2.4.2.2.3 Experiment shells by Yuri

Yuri is a space company based in Germany. The noticeable key difference between the other bioCubeSats mentioned in this chapter is the volume form factor. The Experiment Shells can be referred to in the bottom right image in Figure 2-9. Three experiment shells are housed in a 1U CubeSat; see top right image. The concept is essentially a petri dish that can be packaged to the International Space Station. Yuri offers six different experiment shells with different configurations. These enabled them to perform experiments ranging from cells, fishes, plants, crystals, flies and custom experiments. The Type-IV and Type-V (bottom left image in Figure 2-9) offer fluidics functionality (Yuri,

2022). One drawback with Yuri's offering is the lack of an observation system which limits the in-situ experiment data.

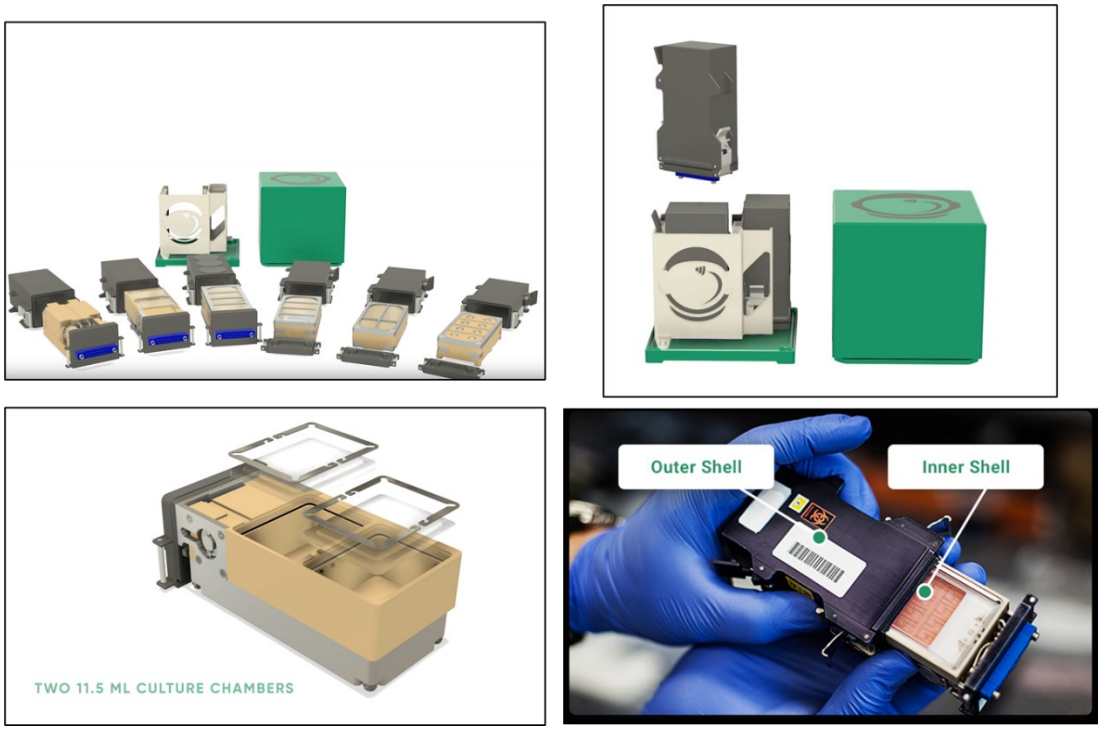

Figure 2-9. Various images of Experiment Shells by Yuri. Images extracted from their website (Yuri, 2022)

2.4.2.3 *C. elegans* hosted on CubeSat

This section aims to briefly review the concept of *C. elegans* hosted in a CubeSat. The reason behind the review is to evaluate the current public domain knowledge of the concept. This was performed in preparation for the BoB mission since the mission was designed with *C. elegans* being hosted in BAMMsat.

The results returned two concepts currently in development. The first is the Microsatellite In-Situ Technologies, or MisST, developed by NASA Ames (Tan et al., 2011). The second concept is the University of Nottingham bio-CubeSat, which is currently in development by the University of Nottingham (D. Robson et al., 2020).

The University of Nottingham Bio-Cubesat is still in development at an early stage. The group mentioned a 3U CubeSat with a 2U payload design utilising off-

the-shelf components. The 2U payload will be based on microfluidics with the ability to house and maintain *C. elegans.* It will have thermal control with a suitable Environmental Control and Life Support System (ECLSS) inside a pressure flask. The health and behavioural of the *C. elegans* will be monitored via a small, low-power microscope with an illumination source.

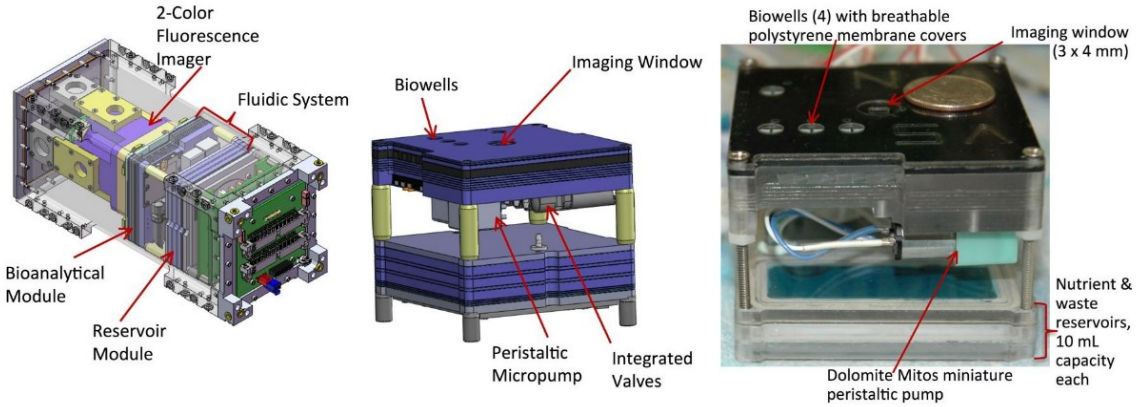

Figure 2-10. Various images of 2U MisST payload[1].

Another concept that has mentioned *C. elegans* is MisST. MisST is a 2U payload aimed at integrating *C. elegans* and recording its health via a two-colour fluorescent microscope. It has been reported that MisST is currently on TRL 6 (Zea et al., 2021). The technology behind MisST is similar to other NASA Ames bioCubeSat except for the fluorescent-based imaging capability. The fluidic card was fabricated using laser cutting, traditional machining and laminated with pressure-sensitive adhesive (PSA) interlayers (Tan et al., 2011). The layers are built by machining polycarbonate bonded with PSA. Like previous NASA Ames bioCubeSats, the track-etched membrane filter was also utilised in the design.

The fluidic subsystem is enabled by an integrated pump and valve manifold; see the right image in Figure 2-10. The experiment was designed to perform two primary functions. The first is to pump liquid to transfer the *C. elegans* from the

[1] Left – Image of a fully assembled 2U MisST payload. Middle – CAD image of fluidic card manifold with integrated pump and valves. Right – Lab image of the MisST fluidic card manifold. Image extracted from (Tan et al., 2011).

storage well to the imaging area. The second is to pump the detection chamber and subsequent injection of the following sample set. Once the *C. elegans* is placed in the detection chamber, the two-colour fluorescence imager will capture images through the 3 × 4 mm window cover, see the middle image in Figure 2-10.

2.4.3 Establishing the current public domain knowledge on stratospheric balloon testing for technology demonstration

This section aims to briefly review the current public domain knowledge on using stratospheric balloon testing for technology demonstration. The review was performed to establish background knowledge for the BoB mission as part of the PhD research.

Using the stratospheric environment for technology demonstration is not a new idea. Based on the literature survey, it was suggested in 1988 to test optical space communication technology on a stratospheric balloon as a technology demonstration (Johann & Reiland, 1988). It was suggested that the test could verify concepts and critical system parameters utilising the near-space condition. It has also been suggested as a testbed for testing new space telescope technologies (Tilley III et al., 1995).

The use of stratospheric balloons as a technology demonstration platform has continued in recent years. Skolkovo Institute of Science and Technology has been using stratospheric balloons as a potential precursor to satellite demonstrator missions alongside a hands-on education programme (Golkar, 2020). Other institution, such as Hasselt University, has utilised stratospheric balloon platform technology demonstration and in-flight investigation of organic-based solar cells for space application (Schreurs et al., 2018).

The harsh dynamic environment in the stratosphere could not easily be replicated in the lab. It could provide essential testing ability to prove technical issues in a space-like environment with near-vacuum and extremely low temperatures.

Similarly, the flight operation mimics a satellite with onboard data handling, power management, telemetry and telecommand, representative of a spaceflight.

Performing a real-world test under harsh stressors could be essential in providing early insight before spaceflight. One key message is that the balloon experiment could overcome waiting for a suitable launch window. Coupled with the possibility of flying on multiple occasions, performing technology demonstrations on stratospheric balloons could enable progress achieved only by multiple space missions (Smith & Sowa, 2017).

2.5 Discussion and conclusion

This chapter presented the results performed during the literature review. The literature review was conducted to establish the current background knowledge in the field. A literature review is a standard practice within academic work and can help build the knowledge for research and potentially find a gap.

The literature review started at the beginning of the PhD (Sep 2017) and surveyed available literature in the public domain. The survey started by formulating a list of the search string that could provide the broadest and targeted result in the field of bioCubeSat. As a reminder, a bioCubeSat is a term used in this thesis to define a CubeSat with a biological payload or experiment onboard. This strategy has been discussed in section 2.3

Analysis of the search result showed that the field of bioCubeSat was still growing. The work performed by NASA trailblazed the bioCubeSat concept to de-risk and prove its applicability. There are records of academic bioCubeSat development throughout the years, and even a private company that launched a bioCubeSat just before the PhD.

One of the gaps identified in the early stage was the lack of coherent literature that consolidates bioCubeSat to explain the historical, technological development, and the current state of the art. Incidentally, towards the end of the PhD research (2022), several pieces of literature have filled this gap. The findings have been discussed in section 2.4.1 of this thesis. The section was written to provide an overview of the background knowledge based on published literature. The overview could be considered a baseline of what is available in the literature at the time of writing, which can be a helpful resource to grasp the historical context, technological development, advantages, and disadvantages of a bioCubeSat.

Further analysis of the literature review was focused on the current state of the art of the technology. The development was to identify technological solutions and design choices that could benefit the PhD research and general BAMMsat

development. These results were categorised into free-flying CubeSat and CubeSat compatible formats hosted on a larger platform.

NASA has led chiefly the free-flying CubeSat. Over the years, they have launched five bioCubeSat as free-flying units. The technology basis behind it was built from the early GeneSat concept and was subsequently improved over the years. However, not all the BioCubeSat were relevant to BAMMsat, which was true for the SporeSat and O/OREOS SEVO payload.

Regarding the CubeSat compatible format hosted on a larger platform, the growth in the CubeSat standardisation meant that they are being adopted as a standard interface on board larger orbital platforms. This was evident on the International Space Station, especially for private space companies. Space Tango, SpacePharma, and Yuri have adopted the CubeSat format to interface the ISS. Considering the nascent space industry and the growth rate, the technology behind them could be regarded as state of the art. The results from the finding have been discussed in section 2.4.2.2.

Later in the PhD, a follow-on literature review was conducted to support the BoB mission. This was presented in the context of *C. elegans* being hosted in a CubeSat and a technological demonstration mission using a stratospheric balloon. The findings show a limited design concept in the literature on *C. elegans* hosted on board a bioCubeSat for spaceflight experiments. It is worth pointing out that the MisST concept has the same objective as the BAMMsat concept. Both concepts are developing behind the idea of an automated, uncrewed biological experiment in space with fluorescent imaging capability.

In conclusion, the literature solidifies the idea of bioCubeSat, where concepts have been de-risked and proven. The space industry is also seeing growth in the bioCubeSat segment since private companies offer a bioCubeSat solution to access the microgravity environment. However, the literature review showed that the field is still developing and growing steadily. Alternative design concepts such as BAMMsat with its MCSD, RV and fluorescent justify that BAMMsat is still relevant and timely as an addition to the research field.

3 Subsystem level – 2nd gen. MCSD and RV subsystems: Design, manufacture, and test

3.1 Introduction to the chapter

This chapter discusses the research and development performed on the multi-chamber sample disc (MCSD) and rotary valve (RV) during the PhD research. The MCSD and RV are key components that provide unique functionalities within the BAMMsat concept. The 1st generation was developed before the PhD but had some legacy issues in the design. At the beginning of the PhD research, the 2nd generation MCSD and RV development has been a critical objective. It was particularly influenced during the development of the ISS spaceflight opportunity in March 2018; see section 1.5 for historical context. The ISS spaceflight opportunity highlighted the issue with the 1st gen. MCSD and RV, particularly in the handling limitation during pre-flight due to lamination by adhesive.

This chapter evaluated and critiqued the 1st generation MCSD and RV to justify the development of 2nd generation MCSD and RV. The outputs from the evaluation were used to inform the design requirements and were used as a basis for the design concept, material choices and manufacturing approaches. The research and development began with initial conceptualisation, iterative CAD reviews, and materials trade-offs before manufacturing the initial design (v1). The initial design immediately highlighted a leaking issue which was investigated and solved for the final design (v2). The final design was a version used for the subsequent testing in the 2nd generation BAMMsat bioCubeSat payload and flew on the BAMMsat-on-BEXUS flight.

3.2 Introduction to the MCSD and RV concept

The multi-chamber sample disc is a custom component developed to house multiple samples inside the BAMMsat bioCubeSat payload. Similarly, the rotary valve is another custom instrument designed to provide unique fluidic functionality for the BAMMsat bioCubeSat payload. The MCSD and RV have interdependent functionality and hence were developed in parallel.

The advantage of the BAMMsat concept is the flexibility to perform a broader range of scientific experiments and biological systems compared to other bioCubeSat. The design combination of the MCSD and RV enables this feature. The 1st gen. MCSD was able to house 40 discrete samples. Each sample can be addressed discretely because the rotary valve (RV) rotates to make or break fluidic valves. The RV allows 120 valves (3 valves per chamber × 40 chambers) in a compact 80 mm disc format. The concept permits a compact valve per volume setup compared to a conventional format where each of the 120 valves will require an individual fluidic port, connector, and tubing.

The rotating functionality also provides the ability to have a single stationary sensor, and each sample can be individually addressed by rotating the chamber to the sensor when required, for example, a microscope or spectrometer. Compared to an alternative where each sample chamber has its sensors, that is equivalent to 40 sensors for 40 samples. The concept reduces the overall system's mass, volume, and cost.

3.3 Aim and objectives

1) *Evaluate and critique the 1st generation MCSD and RV to establish requirements from lessons learnt as an input into the 2nd generation MCSD and RV design.*

The objective originated from the realisation that the first generation MCSD and RV had significant drawbacks, especially during pre-flight operation and biological integration. The heritage design utilised laminated layers of pressure-sensitive adhesive with a laser-cut polymethyl methacrylate (PMMA) sheet. PMMA is also known as an acrylic sheet. As the PMMA sheet was bonded by adhesive, it has limitations during handling, especially when the sample inside the MCSD requires replacement. The 2nd generation MCSD and RV aim to provide a design that offers flexible access to the sample during pre-flight and post-flight. Note that outgassing is not an issue since the MCSD and RV are placed inside a pressure vessel.

2) *Produce an initial design of 2nd generation MCSD and RV for an iterative design process.*

The second objective was built upon the extracted requirements and lessons learnt from objective one. An initial design (v1) was designed, manufactured, and tested to evaluate any immediate issue.

3) *Manufacture, assemble and test a final design of MCSD and RV ready for BoB mission.*

The MCSD and RV were developed throughout the PhD, and the final design was used for the BoB mission.

3.4 Overview of the 1st gen. MCSD and RV

3.4.1 Introduction to the 1st gen. design

This section introduces the design of the 1st gen. MCSD and RV, which are then evaluated and critiqued in the following section. The design of the 1st gen. MCSD and RV were developed as part of the BAMMsat laboratory breadboard. During the NSTP programme in 2015, 1st gen. BAMMsat bioCubeSat payload was completed as a laboratory breadboard; see section 1.2 of the thesis for a historical overview. At the start of the PhD in 2017, the design of the 1st gen. BAMMsat bioCubeSat payload was the baseline of the PhD research.

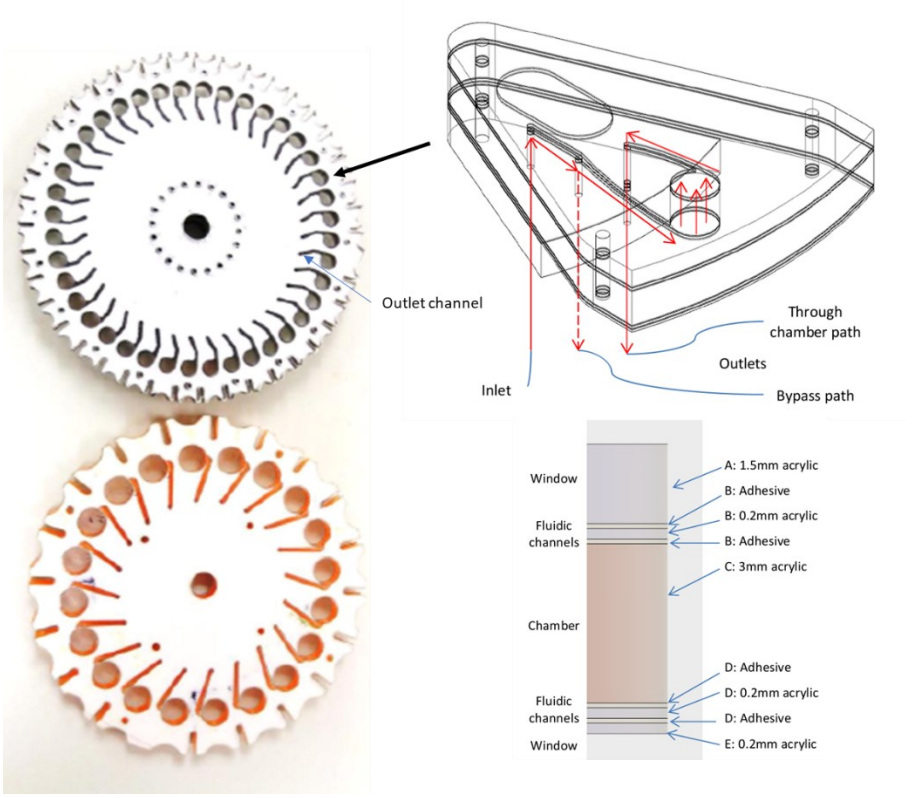

Figure 3-1. Image of 1st gen. MCSD (Image courtesy of Prof Cullen with minor editing).

Two versions were created, with a 20 and 40 chambers version. The volume per chamber in the 20 chamber MCSD was based on the 96-well microtiter plate. While the volume per chamber in the 40 chamber MCSD was based on the 384-well microtiter plate. Microtiter well volume was used as a baseline to make it comparable to a conventional bioscience and R&D laboratory.

The design philosophy behind 1st gen. MCSD and RV were to keep it low-cost and use manufacturing techniques that were easily accessible. The approach helped to de-risk the concept rapidly. The fundamental technology behind the design was to laminate laser-cut acrylic sheets and build a 3D structure with empty internal volume for fluidics channels and sample chamber. The NASA Ames series of bioCubeSats influenced the choice of manufacturing technique. NASA Ames and Aline, Inc. developed a similar process of using laser cut acrylic and adhesive during the GeneSat programme in 2007 (Levine et al., 2007)

Figure 3-1 shows how the 1st gen. MCSD was constructed using laser cut acrylic bonded by double-sided pressure-sensitive adhesive tape. The fluidic channel and sample chambers' 2D profile were laser cut through the double-sided pressure-sensitive adhesive tape.

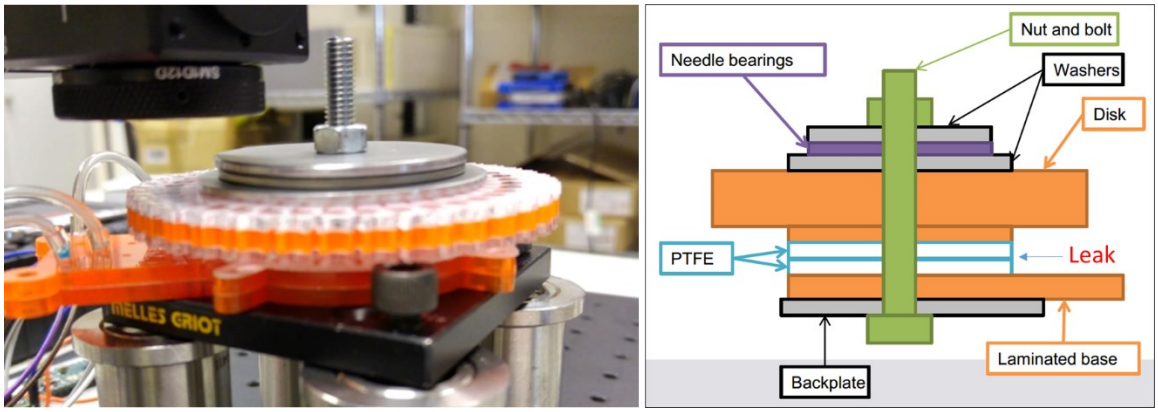

Figure 3-2. Image of the 1st gen. MCSD and RV. (Image courtesy of Prof Cullen with minor editing).

The image in Figure 3-2 shows the 1st gen. MCSD and RV bolted on an optical test bench. The two rotating surfaces were the needle bearings and PTFE. The fluidic ports on the RV were located between the two PTFE layers. The nut and bolt provided the pressure, which pushed the two PTFE layers together.

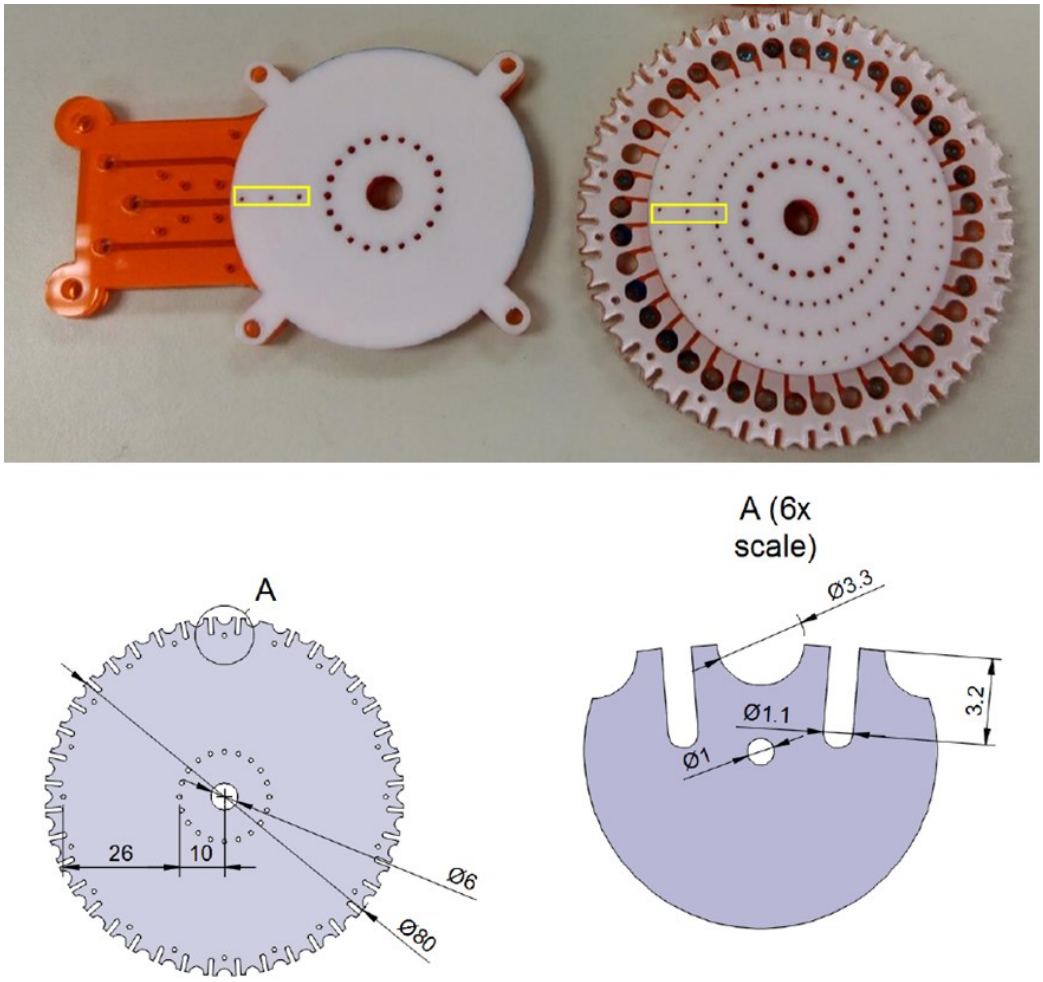

Figure 3-3. (Top) Image of the BAMMsat 1st gen. RV (Image courtesy of Prof Cullen with minor editing).

The laser-cut PTFE surfaces have one surface that remained stationary and another surface rotating around the centre axis. The top left image was the stationary surface with three fluidic ports, and the top right image was the rotating surface with three fluidic ports for each of the 40 chambers. The PTFE was bonded to the MCSD via the pressure-sensitive adhesive. As the MCSD rotates on the sliding surface, the fluidic channel (highlighted inside the yellow box) makes or breaks the fluidic connection. The bottom image is the Geneva gear tooth on the MCSD.

The RV was constructed using laser-cut PTFE surfaces with fluidic ports and Geneva drive. The Geneva drive provided an intermittent rotary motion.

Compared to a continuous rotatory motion, the Geneva gear provided inherent mechanical locking to align the fluidic channels.

3.4.2 Evaluation and critiques on 1st gen. design

In 2018, Cranfield University, University of Exeter and Kayser Space Ltd. developed a complete science case for a spaceflight opportunity on the ISS. The scientific case behind it was to study the therapeutic efficacy of existing approved drug compounds against molecular pathways involved in harmful human responses to space radiation and microgravity. A variant of the BAMMsat hardware platform was designed based on the core functionality to house and maintain C. elegans and fluidically deliver nutrient medium and drug compounds for this spaceflight opportunity. This platform was intended to be integrated into KUBIK and hosted inside the ISS.

During the design process, it became apparent that the 1st gen. MCSD with adhesive bonds could be an issue during pre-flight operations such as assembly, integration, and verification. Similarly, access to the sample will be required for post-flight analysis. The issue was highlighted when developing the flight operation, which involved late-access handling and post-flight analysis.

The 1st gen. design was adequate at the time of development for rapid prototyping, leveraging the knowledge and lessons learnt from previous bioCubeSats and the microfluidics community. It became apparent that design improvement to consider operations during pre-flight AIV, late-access handling at the launch site, and post-flight analysis is required as BAMMsat progresses with science applications and opportunities

The lamination by adhesive has some advantages in a CubeSat flight. CubeSat often flew as a secondary payload or in a rideshare programme. The nature of this flight opportunity meant that the CubeSat had to be powered off and had to be delivered weeks in advance to the launch provider. For bioCubeSat, the system had to remain sterile from bio-loading to the start of the experiment in orbit. It also meant that the biological samples remained viable for an unknown

period. The biological samples placed in the fluidic wells were often *E. coli* or *S. cerevisiae*. They could survive being in stasis for a longer period than a mammalian cell before being reinvigorated in orbit with a nutrient medium (M. R. Padgen et al., 2019; Santa Maria et al., 2020). The stability with lamination by adhesive ensured that the fluidic card remained free of particulate and contamination. The design permits long-term storage of the bioCubeSat.

The drawback of lamination by the adhesive bond is the lack of access to the biological samples. Breaking into the sample is strenuous and could damage the device. The lack of access translates to the limitation of types of biological samples cultured in such a system and complicates the AIV tasks. It also limits the ability to perform late-access handling at the launch site for organisms that must be cultured at the launch site since they can't be desiccated to halt metabolic activity. Adhesive bonding could also restrict sample retrieval post-flight.

The 1st gen. RV had an issue with leaking. The leaking occurred between the two PTFE layers (see Figure 3-2). The two PTFE layers were bolted through the MCSD and RV to compress and seal. PTFE is well known for its low coefficient of friction and can be laser cut. Hence, it was a good solution as the rotating surface layer. However, PTFE tends to cold creep under compression (Chen & Hui, 2005; Rae & Dattelbaum, 2004). After prolonged use, the liquid tends to leak along the PTFE surface. One mitigation is to increase the pressure of the sealing surface by increasing the closure force with the bolt. However, it increased friction and did not solve the underlying issue with cold creep.

The 1st gen. RV was not fully developed at that time, and the build quality was not built for high torque Geneva drive. The Geneva gear mechanism was laser cut into the acrylic and did not have the mechanical strength for the cyclic loading on the gear teeth (see Figure 3-3).

3.5 List of design needs for the 2nd gen.

These design needs were extracted from lessons learnt from the 1st gen. MCSD and RV. In future, the need can be extracted into requirements for a specific spaceflight mission. During the development of the 2nd gen. MCSD and RV, the needs were used as the basis of the design for 2nd gen. MCSD and RV. Requirement based on ECSS-E-ST-10-06C was not defined at this stage of MCSD and RV development since a mission was not yet identified at this stage of research. Other subsystems in subsequent chapters have their requirements defined based on ECSS specifically for the BoB mission for comparison purposes.

MCSDRV -1 **The 2nd generation multi-chamber sample disc needs to allow repeated access to the sample chamber to allow sample exchange**.

As mentioned in section 3.4.2, one of the design limitations of bonding the material by adhesive is the inflexibility during handling. This affects the pre-flight and post-flight operations where access to the sample chamber is strenuous. The need was included to explore a less taxing design for the MCSD and the operator when dissembling and assembling.

MCSDRV – 2 **The rotary valve's rotating surface material needs to minimise the fluidic leak to an acceptable rate.**

Leaking around the PTFE rotating surfaces was a significant issue in the 1st generation. The need was included to explore material that addresses the leaking issue due to PTFE cold creep.

MCSDRV – 3 **The material for the Geneva mechanism, i.e., the gear teeth on the 2nd generation MCSD, need to have the mechanical strength to withstand the cyclic loading from the motor actuation pushing with the Geneva drive shaft.**

The Geneva gear mechanism, which enables the RV in the 1st gen., was not fully developed beyond a functional prototype. The need was

included to increase the mechanical reliability of the Geneve gear mechanism.

MCSDRV – 4 **The diameter of the 2nd generation multi-chamber sample dish could not be larger than 90 mm.**

Since the 2nd gen. MCSD will be used in a CubeSat format; the size should not exceed the width of a 1U CubeSat, i.e., 100 mm. 90 mm was chosen as an upper limit, and the difference was spared for the pressure vessel's wall and insulation. The MCSD will likely be housed inside the pressure vessel during spaceflight, containing the atmosphere for sample use.

MCSDRV – 5 ***The material for the 2nd generation multi-chamber sample disc needs to be biocompatible with most biological samples***

One of the application fields for BAMMsat is bioscience, and the experiment need was added to review the material's biocompatibility.

MCSDRV – 6 ***The material needs to be inert to most chemicals.***

The need was included to review the material's inertness, ensuring that the 2nd gen. MCSD is compatible with most applications.

MCSDRV – 7 ***The material for the MCSD and RV needs to be autoclavable for ease of sterilisation during pre-flight***

A biological experiment requires vigorous sterilisation and cleanliness during pre-flight. Adding the need for material that can be autoclave help ease the pre-flight operation, and PMMA and adhesive layer does not autoclave well.

MCSDRV – 8 ***The design of the fluidic channels needs to minimise bubble formation to an acceptable rate***

The need was added to review the design of the fluidic channels to incorporate standard microfluidics and fluidics design practices to minimise bubbles. Generally, the objective is to limit dead volumes such as microwell and sharp ends or edges to avoid trapped air.

MCSDRV – 9 ***The material needs to include an optically transparent gas permeable membrane.***

A gas-permeable membrane allows the exchange of O_2 and CO_2 for sample use. At the same time, optical transparency allows application for microscopy and spectrometry. The 1st gen. MCSD did not have one fully defined as the final design.

MCSDRV– 10 ***The 2nd generation MCSD needs to include a sample particulate filter or filters to contain the sample within its respective chamber and avoid cross-contamination***

A filter is added to block the samples from escaping or being flushed away from the sample chamber during fluidic actuation. The filter was not fully defined in the 1st gen. design.

3.6 Preliminary design concept and material selection for the 2nd gen.

The design of the 2nd gen. MCSD and RV involved many research and conceptualisation before an initial design (v1) was produced. The initial design was built to test for any immediate issue and addressed in the subsequent prototype. Although the design of the 2nd gen. MCSD and RV differ considerably from the 1st generation. The fundamental concept for the 2nd gen. was influenced by the 1st gen., especially the material layering technique to build fluidic channels and sample chambers.

The driving factor behind the initial concept was MCSDRV1 which stated, "*The 2nd generation multi-chamber sample disc needs to allow repeated access to the sample chamber to allow sample exchange"*. This underlying function is to easily assemble and disassemble access to the sample chambers. Since the 1st gen. was manufactured by layering acrylics and adhesive tape to build the fluidic channels and the sample chambers, the apparent solution was to have the layers mechanically bolted together. The solution allows the top layer to be removed by unbolting it. The challenge was to ensure the layers were sealing the fluidic channels against fluidic leaks and that unbolting the top layer did not affect the rest of the assembly. Several CAD versions were made to visualise the concept and review its feasibility before being manufactured.

3.6.1 Preliminary design - MCSD and RV material selection

In parallel with the CAD design, visualisation, and development, the material selection was performed to assess the material choices and their manufacturability.

3.6.1.1 Material selection for the RV

At the start of the development, research was performed to find a suitable replacement material from the open literature. As mentioned in section 3.4.2, one of the issues with the 1st gen. RV was the leak due to PTFE cold creeping under compression. The challenge with finding a suitable replacement material was the wide range of materials available in the market. Preference was made towards engineering materials that satisfy specific mechanical properties such as compressive strength and inertness. An exhaustive list of the mechanical properties can be viewed in Table 3-1.

The materials list was built by evaluating the current material solution within the commercial Rotary Valves in the market. The search scope was based on the commercial product since it is assumed that the material chosen by these companies is a reasonable starting point as a design solution. Previously, a similar methodology was also used during the 1st gen. design process, resulting in PTFE selection. The search was performed by searching the term "fluidic rotary valve" in the internet search engine. The returned search / product was then evaluated to confirm its design relevance to the BAMMsat RV and if the type of materials were listed within its website or datasheet.

The search result performed in late 2018 and early 2019 identified five companies which supplied Rotary Valve as a product solution that can be translated into BAMMsat RV. An example of a product from each company are Diba Omnifit® Rotary Valve (Diba; WZ-21939-24), Cadent™ 3 Pump Rotary Valve (Norgren Kloehn; 23327), OEM - Rotary valve controller (Elveflow), OEM RVM Microfluidic Electric Rotary Valve (Advanced Microfluidics SA), and SwitchEZ™ Electric Rotary Valves (Precigenome LLC). Some companies, for example, Norgren

Kloehn, have various versions of Rotary Valve with different materials; hence, the presented list is not exhaustive.

Five different types of material were listed as potential solutions from the search results. These were (i) Polychlorotrifluoroethylene (PCTFE) , (ii) – Polyetheretherketone (PEEK), (iii) Polytetrafluoroethylene (PTFE), (iv) Polyphenylene Sulfide (PPS), and (v) Ultra-High Molecular Weight Polyethylene (UHMWPE). The companies mentioned that these materials were used as wetted material, i.e., in contact with the sample. The challenge with this approach was that the part material used in the design was not publicised as it was considered a trade secret.

Further assessment was performed to identify common materials from the list. It became evident that three materials, PCTFE, PEEK, and PTFE, were more common in various rotary valves than PPS and UHMWPE. For this reason, it was decided that the three materials (PTFE, PCTFE and PEEK) will advance into the trade-off analysis. Note that PTFE was previously chosen in the 1st gen. design. The trade-off is being performed to find a replacement material since there was an issue with leaking when using PTFE (see section 3.4.2). PTFE is included in the analysis as a baseline (see Table 3-1 and Table 3-2).

Table 3-1. Material properties and design functions of PTFE, PCTFE, and PEEK.

Material properties*	Design functions	Option 1	Option 2	Option 3	References (PTFE; PTCFE; PEEK)**
		PTFE	PCTFE	PEEK	
Coefficient of friction	To reduce the torque required to rotate the material on its surface	0.03 - 0.05	0.35	0.35-0.45	(Fluorocarbon, 2020a, 2020b)
Glass transition temperature	To allow the material to be autoclaved	116°C	40°C – 70°C	143°C	(Calleja et al., 2013; ERIKS, 2005; Waller et al., 2001)
Compressive strength (% deformation)	To ensure that the material doesn't permanently deform under load	0.7 MPa (2)	11-13 MPa (1)	138 MPa (10)	(FLUOROTHERM, 2022; Poly-Tech Industrial Inc., 2022b, 2022a)
Machinability	To ensure that design feature can be easily machined	Good	Good	Very good	(Fluorocarbon, 2020a, 2020b)
Inertness	To ensure that the material can be used in a wide range of biological experiments	Virtually inert	Excellent	Affected by Sulphuric Acid	(Fluorocarbon, 2020a, 2020b)

* Material properties often vary across different manufacturer

** Where possible, material properties data were taken from a single manufacturer or source.

Table 3-2. Trade-off analysis result for material for MCSD and RV

Material properties (weighting)	Description	Material scores		
		PTFE	PCTFE	PEEK
Coefficient of friction (4)	The coefficient of friction impacts the power needed by the motor to turn the Rotary Valve. A lower coefficient of friction means that the two surfaces will rotate easier at lower torque than a higher coefficient of friction.	5	3	3
Glass transition temperature (2)	The glass transition temperature helps gauge when the "amorphous" polymer change to a softer or rubbery structure from a crystalline structure. Autoclave sterilisation operates typically at 121°C, 132°C, and 135°C.	4	1	5
Compressive strength (5)	The compressive strength helps gauge how much stress can be applied to the material without deformation. The property was selected to mitigate the issue with PTFE in the 1st gen. design.	1	3	5
Machinability (3)	The machinability option gives the flexibility to add design features machined to the material.	4	4	5
Inertness (4)	Being inert to most materials enables a wider range of experiments by ensuring biocompatibility to most biology and compatibility with many reagents.	5	4	4
Total score (weighting × score)		65	57	78

The result from the trade-off analysis showed that PEEK scored the highest among the result. Evaluating the result showed that PEEK is a good compromise. Generally, the three materials have good machinability, providing flexibility in machining the desired design features.

The coefficient of friction is another material property included in the trade-off. Friction plays a role since the material's surface will be rotating against itself or another surface, and the torque required will impact the motor size required to actuate the RV. Based on Table 3-1, the coefficient of friction of PCTFE and PEEK are similar. Although higher than PTFE, the coefficient of friction for PCTFE and PEEK was perceived to be in a manageable range.

The inertness property of these three materials is almost similar. These materials are known within the industry to be compatible with most biology and chemicals.

It can be very challenging to find a specific Material Safety Data Sheet; hence a thorough material compatibility test must be performed before any experiment. PTFE has excellent inertness due to the firm carbon-fluorine bond and is inert to a wider variety of substances than a partially fluorinated polymer such as PCTFE (Ibeh, 2011). PCTFE has a similar bond which also makes it inert to most substances. The difference between PCTFE and PTFE is the chloride element, creating a greater atomic radius and better mechanical properties than PTFE. PEEK does not have the carbon-fluorine bond, but it has a biocompatibility track record earning USP Class VI for medical application (Ibeh, 2011).

Two key material property differences set the PEEK apart: the glass transition temperature and compressive strength. A higher glass transition temperature above 121°C provides the ability for the material to be autoclaved. PEEK has the highest glass transition temperature, which is the least affected during autoclave operation. One of the benefits of autoclaving is streamlining the pre-flight operation to sterilise the sample chamber, which is less taxing than individual sterilisation.

The compressive strength was included to assess how the material will behave under compression since the RV will be bolted to provide the fluidic sealing. PEEK required 138 MPa before experiencing 10% deformation. Both materials are better than the PTFE. In a more subjective assessment, PCTFE has been mentioned to have better creep resistance than PTFE, while PEEK has excellent specific stiffness properties (Ibeh, 2011).

The result from the trade-off analysis showed that PEEK is the best compromise and will be used as the material for the RV.

3.6.1.2 Material selection for the 2nd gen. MCSD

Material selection for the 2nd gen. MCSD was performed in parallel with the CAD development. The previous analysis decided that the PEEK material properties were useful as the core material for the 2nd gen. MCSD. Alongside PEEK, four other vital layers made up the MCSD. 2nd gen. MCSD built upon the technique from the 1st gen., where materials were layered to build a fluidic manifold with

internal fluidic channels and sample chambers to achieve the required fluidic channels and functionalities. The subsequent sub-sections explore the layers required and the chosen material for the initial prototype.

3.6.1.2.1 Material selection for optical transparent window

The optically transparent layer was a layer that closed one end of the sample chamber and allowed light transmission through it. The transparency allows light transmission into the sample chamber and the optical sensors, i.e., optical microscope or visible light spectrometer. The material choices evaluated for this layer were polycarbonate and PMMA, assessing their optical properties, autoclavability and manufacturing techniques.

The applicability of polycarbonate was found during the technological review of NASA's bioCubeSat. O/OREOS SESLO and SporeSat opted for polycarbonate to build their experimental payload (Nicholson et al., 2011; Park et al., 2017). Figure 3-5 shows the O/OREOS SESLO payload for visualisation purposes. The reason behind NASA's selection for polycarbonate was not clear from the literature, but it can be assumed it could be due to its ability to be autoclaved (De Brouwer et al., 2015). In contrast, the PMMA was a heritage material from the 1st gen.

The qualitative trade-off was performed to assess the difference between the two materials (see Table 3-3). Based on this trade-off, polycarbonate was selected as the primary material. The primary driver behind this selection was the autoclavability to make it less taxing to the researcher and pre-flight operations.

Table 3-3. Polycarbonate vs PMMA

Material properties	Polycarbonate	Polymethyl methacrylate (PMMA)	References
Optical transparency (visible light)	89-91% transmission	93-95% transmission	(Brouwer & Bogerd, 2011; Serrano & Moreno, 2020)
Autoclavable	Autoclavable but may be weakened after repeated autoclaving	Not autoclavable	(Antylia Scientific Blog Team, 2015; Princeton University Environmental Health and Safety, n.d.)
Manufacturing techniques	CNC. Laser cutting is possible with poor post-cut quality due to a combination of melt shearing and chemical degradation.	CNC and CO_2 laser cut	Tested in the lab and workshop. (Moradi et al., 2017; Powell, 1998)

Regarding optical transparency, both materials have high optical transmission, and the difference is negligible. The manufacturing techniques do have an impact on lead time for polycarbonate since the CNC machine has a longer lead time than the readily available CO_2 laser cutter. This was manageable within the PhD research. Although, for increased repeated use, degradation can occur in polycarbonate. If excessive repeated use is required, it is worth doing a future cost analysis to assess the machining vs autoclaving cost.

3.6.1.2.2 Material selection for fluidic sealing in between MCSD

During development, an alternative material was considered to remove the "permanent" bonding limitation from the double-sided pressure-sensitive adhesive (PSA) tape. The concept of mechanically bolting the layers together to provide a seal was similar to the application of a head gasket inside an internal combustion engine.

The first material considered was fluoroelastomer (FKM), commonly known as Viton. FKM is well regarded in the industry for application in an aggressive, high-temperature environment. It is chemically inert to most chemicals and is used for

medical devices. FKM can be laser cut using a low power CO_2 laser cutter with a good finish in the heat-affected zone (Banerjee & Bhowmick, 2015). The applicability of laser cutting was necessary since the profile for the fluidic channel will be cut onto the surface. It is worth noting that laser cutting thermally ablates the surface and will change the cut area's chemical composition, potentially off-gassing toxic volatiles. A biological specimen or chemical sample will require future testing to consider this impact on the sample's viability. FKM material properties made it a suitable candidate for adhesive tape replacement.

Unfortunately, the thinnest FKM readily available in the market is 0.5 mm. 0.25 mm was available for a made-to-order batch outside the research budget. Since elastomer will be used as a fluidic channel, the thickness will impact the fluidic flow rate. For comparison purposes, the previous PSA tape had a thickness of 0.05 mm or 50 microns. The difference in thickness will significantly impact the flow rate of the fluidic system.

Market research was performed to search for an alternative elastomer to minimise significant changes in the fluidics system. The search resulted in the thinnest elastomer on the market: a silicone elastomer, specifically 0.1 mm Ultra-thin silicone film (Silex, UK). Silicone elastomer has demonstrated application in medical devices, and manufacturers claim it to be autoclavable, making it a suitable second-generation solution for 2nd gen. MCSD.

3.6.1.2.3 Material selection for the sample filter

A sample filter is required to contain the sample inside the chamber. Without the filter, the sample could be flushed during fluidic actuation. An example of how the sample filter is integrated within the sample chamber can be seen in Figure 3-5. See the two layers of 1µm track-etched filters, which can be seen on the top and bottom fluidic channel to contain the yeast. The filter also avoids "crosstalk" between samples by preventing escape through the inlet or the outlet channels. At the start of the PhD research, the filter type and design placement were not fully defined in the 1st gen. MCSD.

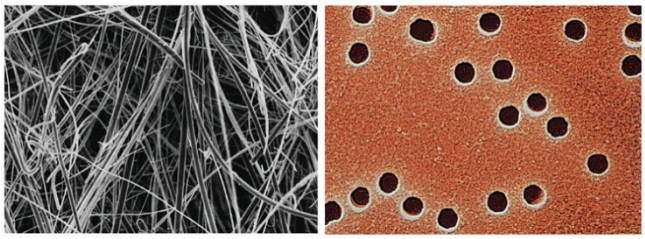

Figure 3-4. (Left) Glass fibre filter vs (Right) Track-etched membrane filter. Credit (Merck)

Two different filters were assessed to evaluate their feasibility within the MCSD design. The two filters were (i) track-etched membrane and (ii) membrane filter. Membrane filters are commonly used in bioscience labs and are made up of polymers or fibres such as cellulose, glass fibre, nylon, etc. On the other hand, the track-etched membrane is a porous filter with thin-channels defined-size pores running in only one direction. The uni-direction nanopores were etched by passing heavy-ion through a polymer (Sartowska et al., 2012). The topography difference between these two pores can be viewed in Figure 3-4. Both filters can be purchased in varying pore sizes to accommodate different sizes of biological samples ranging from micro-animal such as *C. elegans*, bacteria and viruses.

The key difference in the topography of these two materials highlighted that the track-etched membrane is a suitable filter for the 2nd gen. MCSD. The track-etched membrane was found during the literature review of NASA's BioSentinel fluidic μwell design; see Figure 3-5. A. The benefit of using this membrane is its simplicity. A single membrane can be attached to multiple sample wells/chambers, reducing the complexity and assembly. Because the pore only allows flow in a single direction, there are no lateral crossovers between the individual pores compared to a fibrous filter. The biological sample could not move sideways to the next chamber and could only follow the fluidic pathways. Its unique properties and the ability to simplify 2nd gen. MCSD design and assembly meant that the track-etched membrane was chosen as the filter solution. The next step in the PhD research was to manufacture the filter that needed to be cut with the right profile.

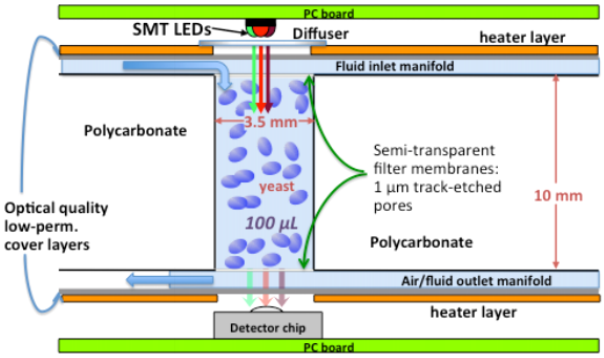

Figure 3-5. Cross-section image of NASA BioSentinel fluidic µwell with the sample filters (A J Ricco et al., 2016).

3.6.1.2.4 Material selection for the gas permeable membrane

The gas-permeable membrane has three required functionalities for the 2nd gen. MCSD. The first functionality was to allow gas exchange from the inside of the sample chamber to the outside atmosphere. This is important for biological specimens where CO_2 build-up can occur inside the sample chamber, and for the specimen to survive, O_2 and CO_2 exchange must occur through the gas-permeable membrane. The second functionality was to provide a top layer to contain the sample within its chamber, located opposite the optically transparent window mentioned in section 3.6.1.2.1. The third functionality was to allow light transmission through it for the optical sensors in the 2nd gen. BAMMsat bioCubeSat payload. At the start of the development, the gas-permeable membrane was not fully defined and was researched during the PhD.

During the research, three possible materials were considered. The first was the FEP – Fluorinated Ethylene Propylene. The second was PMP – Polymethylpentene, and the third was PS - Polystyrene. Kayser Space ltd suggested the FEP during the 2018 ISS flight opportunity based on their flight heritage. At the same time, the PMP was discovered via a patent search for material for humidity and gas control (Marcucci Ribeiro, 2004). PS was found during the literature review when it was used as a solution for NASA GeneSat (Antonio J Ricco et al., 2007). Only FEP and PMP were procured during the PhD research for further testing. Similar to the filter, FEP and PMP were new materials

within the BAMMsat historical development, and further investigation was required into the manufacturing techniques.

3.6.2 Preliminary design - Geneva mechanism sizing and material selection

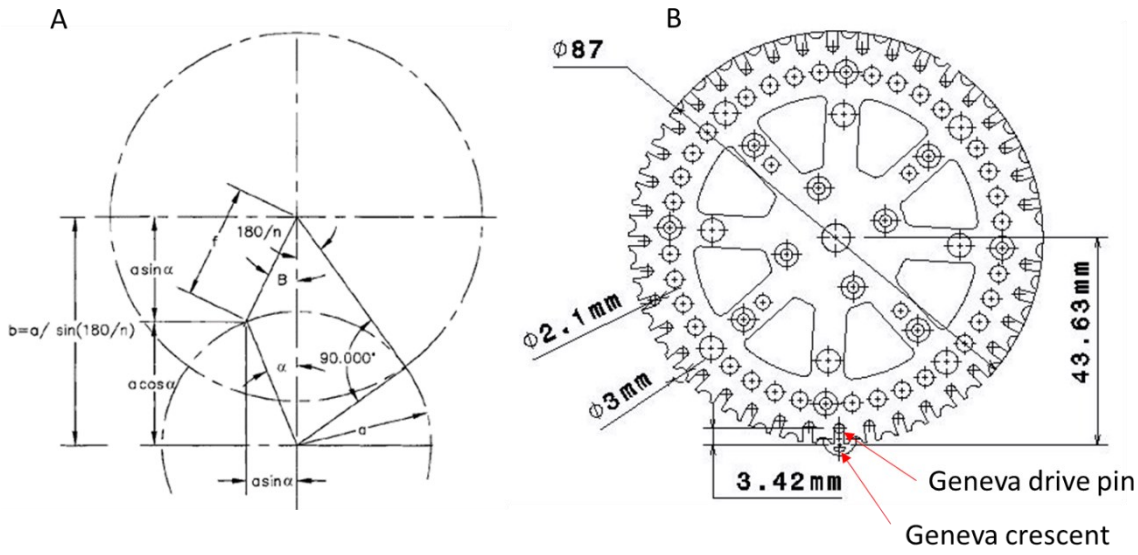

Figure 3-6. Mathematical relationship of Geneva gear size and resulting MCSD dimensions.[1]

The Geneva gear mechanism in the 2nd gen. MCSD had to be resized since the design change in the 2nd gen. impacted the overall size of the MCSD. The 2nd gen. has an outer diameter of 87 mm compared to 80 mm on the 1st generation to accommodate the bolts' volume. The size of the Geneva drive pin was increased to 2 mm from 1 mm to improve its mechanical strength during rotation.

For an 87 mm diameter disc, 40 chambers or 40 gear teeth is the maximum number of teeth before the size of the teeth, and its mechanical strength was compromised. The material chosen for the initial design (v1) was aluminium grade 6082T6 for its versatility and accessibility, making it ideal for prototyping.

[1] Left – Image of the mathematical relationship for a Geneva gear mechanism, used during the sizing of the 2nd gen. MCSD Geneva gear (Walsh, 2001). Right - Image of the 2nd generation MCSD aluminium top layer with a = 3.42 mm and b = 43.63 mm.

Due to the small size of the Geneva pin and Geneva crescent, machining tolerance played an essential factor. A kinematic simulation was performed on CATIA V5 to evaluate the rotation and potential dimensional interference.

3.7 Manufacturing techniques

The section describes the different manufacturing techniques used throughout the PhD research. The choice of manufacturing techniques described here was driven by accessibility, using what is readily available at the university.

3.7.1 CNC machining

Computer Numerical Control (CNC) machining was the primary technique used to machine the required parts throughout the PhD. It is accessible within the Cranfield University Workshop for research purposes. The machining was performed on an XYZ 710 VMC machine. Most of the parts are for 2nd gen. BAMMsat BioCubeSat payload was machined using this machine. The only limitation of this machine was its rotating speed which was limited to 8,000 rpm. The speed meant that the smallest drill or milling bit was constrained at 1 mm. This limitation does impact the design, especially in the holes for the fluidic channels. Some parts were machined externally using a CNC machining company Hubs to overcome the tolerance limits, formerly known as 3D Hubs.

CO_2, UV, and fibre laser cutter

BAMMsat development leverages the standard laboratory tool and materials for accessibility and lower cost. Most parts, mainly for the fluidic subsystem, were laser cut to create geometric profiles and fluidic channels. Most of the laser cutting was performed in-house using a CO_2 laser cutter. However, the limitation with the CO_2 laser cutter became apparent significantly when cutting thin-layer polymers. Collaborative research was conducted with ES Precision Ltd to overcome the restriction, explore UV laser cutter as a solution, and access the fibre laser cutter for metal cutting.

3.7.1.1 CO_2 laser cutter

The in-house manufacturing technique was a relatively low power 40W CO_2 laser cutter to cut the fluidic channel profile and acrylic. The CO_2 laser cutter (King Rabbit; LS3040) emitted infrared radiation at 10.6μm and was used to cut the

material by inducing photothermal ablation. Cutting is achieved when chemical bonds are broken down via thermal energy as the material heats up.

3.7.1.2 UV laser cutter

UV laser cutters have a much shorter wavelength at 355 nm within the Ultraviolet range. UV laser uses high energy photons to break down chemical bonds in photochemical ablation. Breaking down chemical bond avoid the thermal damage associated with photothermal ablation. The UV laser cutter used was Rofin Powerline E UV 5-355 with 3 W laser power with 355 nm wavelength.

3.7.1.3 Fibre laser cutter

The fibre laser cutter was primarily used to cut thin stainless steel used as a washer or load spreader. The laser cutter used was the Powerline F20 20 W laser cutter with a wavelength of 1064 nm.

3.7.1.4 Results and discussion on CO_2 vs UV laser cutter to cut thin layer polymers

One of the least desirable effects of CO_2 laser cutting was the poor edge cut quality from photothermal ablation. This process produced thermal deformation (heat damage) on the inner layers and nearby areas of the target area. It was an issue since the fluidic channels in the 2nd gen. MCSD was located close to each other, separated at 0.1 mm. In some fluidic channel designs, the border between fluidic channels was limited by the CO_2 laser cutting since the boundary between the channels melted post laser-cut, and the channels merged.

The PhD research explored photochemical ablation via UV laser cutting to improve the surface finish. This can be achieved by avoiding photothermal ablation. High surface quality with $Ra<0.2$ µm can be performed using photochemical ablation (Mai & Nguyen, 2002). However, the cut will occur at a slower ablation time. Photochemical ablation occurs when the high photon energy breaks bonds via photodissociation, avoiding charring and discolouration of the material.

A test was performed to compare CO_2 and UV laser cutter. The materials tested were the material under consideration for the 2nd gen. MCSD. The materials were 0.02 mm thick Whatman Nucleopore polycarbonate track-etched membrane (Sigma Aldrich, UK); 0.19 mm thick Double Coated Polyester Diagnostic Tape (3M, US), also known as the double-sided pressure-sensitive adhesive (PSA); 0.02 mm thick Ultra-thin silicone (Silex, UK); 0.05mm TPX® Polymethylpentene (Goodfellow, UK); and 0.05 mm thick Fluorinated Ethylene Propylene, FEP (Goodfellow, UK).

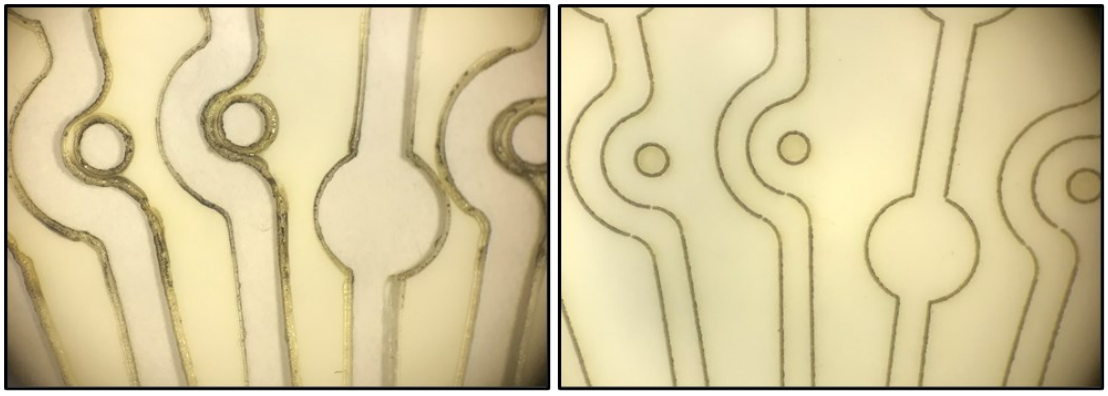

Figure 3-7. Images of PSA material cut using CO_2 and UV laser cutter.[1]

[1] Left - Image of PSA (3M, US) with CO_2 laser cut fluidic channels. Right - Image of PSA with UV laser-cut fluidic channels. The difference in topography can be seen with CO_2 cut had burned edges. The image was taken with Nikon upright microscope with 10X magnification.

Table 3-4. The result from CO_2 laser cutting and UV laser cutting of materials under consideration for the 2nd gen. MCSD.

	CO_2 laser cutter	*UV laser cutter*	*Number of passes*
Polycarbonate	Yes	Yes	2
Polyester	Yes	Partially	2175
Silicone	Yes	No	N/A
PMP	Yes	No	N/A
FEP	Yes	No	N/A

The result showed that the UV laser cutter could only cut polycarbonate and partially the polyester. The silicone, PMP, and FEP remained uncut since they did not absorb the UV wavelength at 355 nm. The UV laser cut the polycarbonate thoroughly. Figure 3-8 demonstrated that the UV laser cutter provided a superior cut quality compared to CO_2 and enabled the use of the track-etched membrane (polycarbonate) as a filter in the 2nd gen. MCSD. Whereas the polyester was cut partially using a UV laser cutter at an excessive number of passes.

The double-sided pressure-sensitive adhesive polyester had three different layers on each side. The first layer was a silicone-coated transparent polyester film which provided the non-stick properties to protect the adhesive layer. The second layer was the acrylic adhesive layer. The final layer was the white polyester film, which provided the adhesive's structural layer. The UV laser thoroughly cut the silicone-coated polyester film and etched the white polyester film during the test. The cut was stopped since the number of passes became excessive.

One possible explanation was that the laser power density was inadequate to penetrate the polyester materials completely. The power output of the laser is approximately 3 W at maximum current settings of 30 A. The laser-cut was running at 27 A; therefore, the power output will be just shy of the 3 W. ES Precision also had a unique setup to enable a larger working cut area. They used a different lens from the manufacturer's setting. They had an F-theta lens with a

longer focal distance of 330mm (f330). Unfortunately, the downside of this setup is that it would lose a fair amount of energy density compared to using a shorter focal length lens.

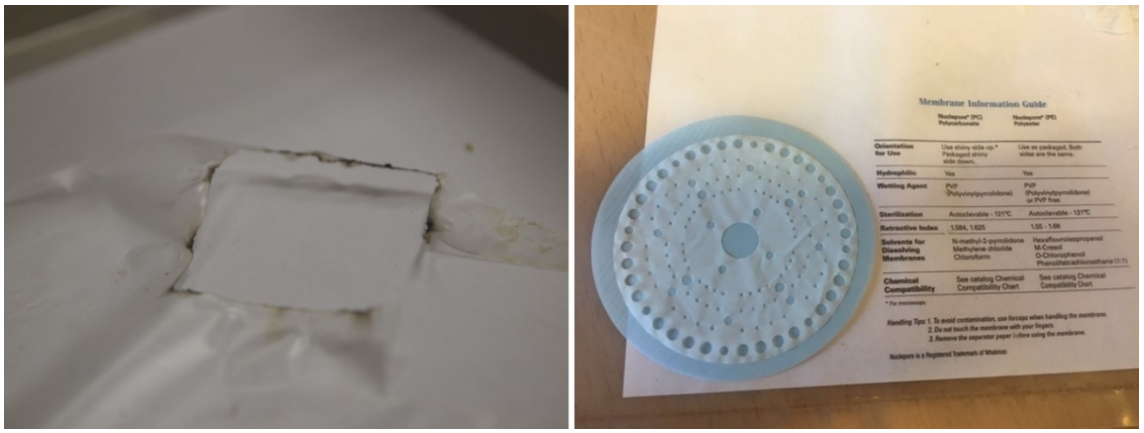

Figure 3-8. Left – CO_2 laser cut polycarbonate. Right – UV laser cut polycarbonate.

An attempt was also made to try and cut the silicone, PMP, and FEP with a 1064 nm wavelength laser. However, these materials still did not absorb the laser at 1064 nm within the infrared range, a significant jump from 355 nm. Future work will include testing to cut the material using a UV laser with a higher power setting and at a different wavelength.

3.8 Initial design (V1) of the 2nd gen. MCSD and RV

3.8.1 Overview of the initial design

This section will discuss the first complete initial design of the 2nd gen. MSCD. The design was completed after several iterations on CAD. It was made using a combination of the researched material and manufacturing techniques previously discussed in sections 3.6.1 and 3.7 of this thesis.

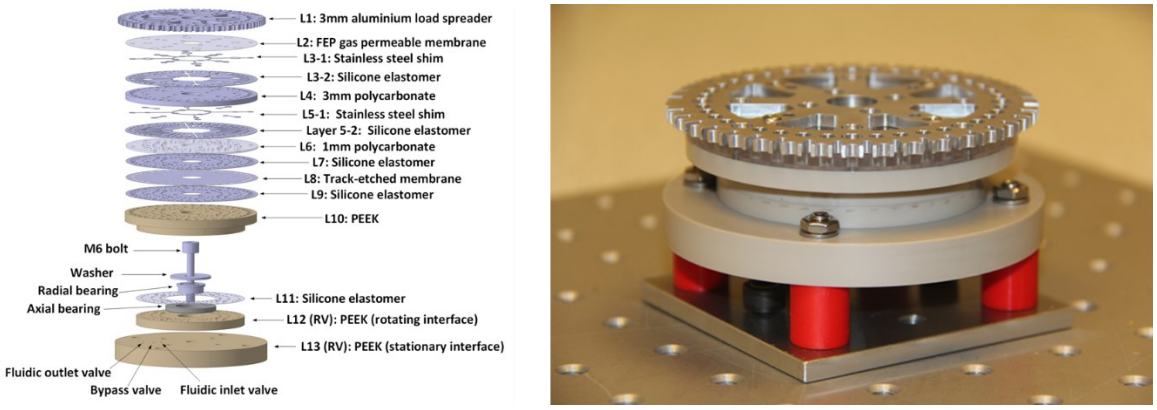

Figure 3-9. Left – Exploded view of the 2nd gen. MCSD, detailing the 13 layers and their respective materials. Right – Fully assembled 2nd gen. MCSD

The initial design was developed to visualise and test the concept in preparation for further biocompatibility, fluidics, and Geneva mechanism testing. The initial design has 13 layers bolted together to create the internal fluidic channel, see Figure 3-9. L1, L4, L6, L10, and L13 were CNC machined. L2, L3-2, L5-2, L7, and L9 were CO_2 laser cut, and L8 was UV laser cut.

The silicone elastomer served two purposes: to compress when bolted to fill the gap between the layers. The second is to provide the lateral fluidic channels inside the MCSD. Finding the balance in finding the correct compression could be challenging without closing the channels and blocking the fluidic flow. Two layers of stainless-steel shims (L3-1 and L5-1) were added to ensure level compression across the surface when bolted using a torque screwdriver.

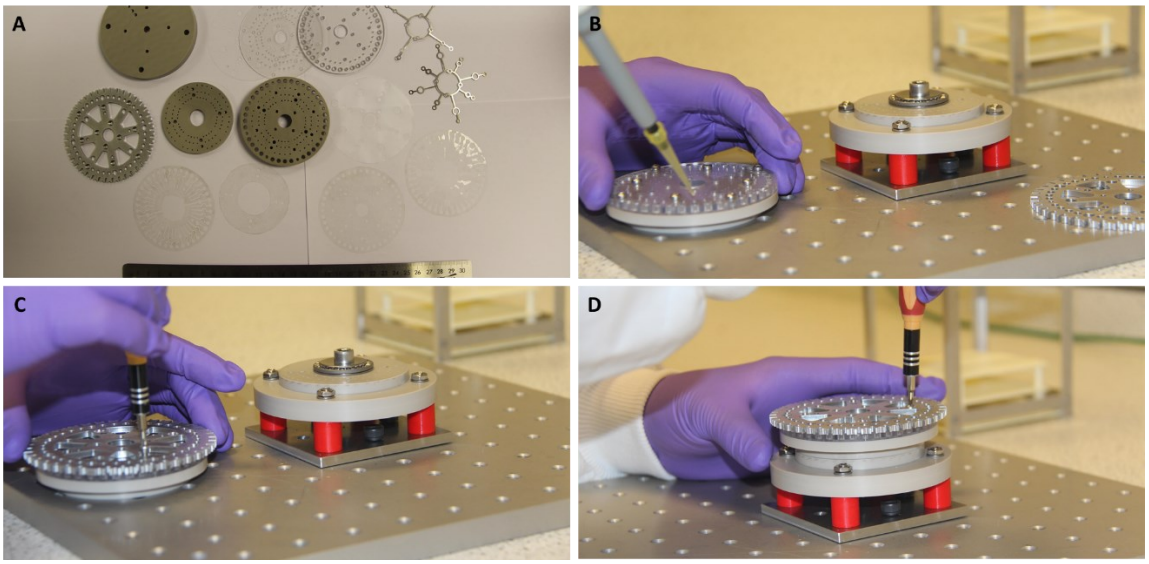

Figure 3-10. Demonstration of the key concept in the 2nd gen. MCSD and RV included the ability to access the sample chamber easily.

In Figure 3-10, Image A showed the manufactured 13 layers before assembly. The MCSD can be configured into three configurations to aid the assembly process. For example, in Configuration 1, the top of the sample chamber was opened for biological loading.

Image B (Configuration 1) was the first step in the assembly process where the L4 to L10 were bolted together. At this stage, the top surface of the sample chambers, L4, was opened, and the sample can be pipetted into their chambers. The rotor (L12) and stator (L13) layers of the rotary valve were assembled separately.

The next step is shown in Image C (Configuration 2), where the top surface of the sample chambers was sealed with the gas-permeable membrane and aluminium load spreader. The process bolted layer L1 to L3-2 to the rest of the MCSD.

The final step is shown in Image D (Configuration 3), which was to bolt the MCSD and the RV together. The prototype demonstrated the concept of mechanically assembled 2nd gen. MCSD and RV were possible by bolting specific layers in the right sequence to build the fluidic channels and sample chambers.

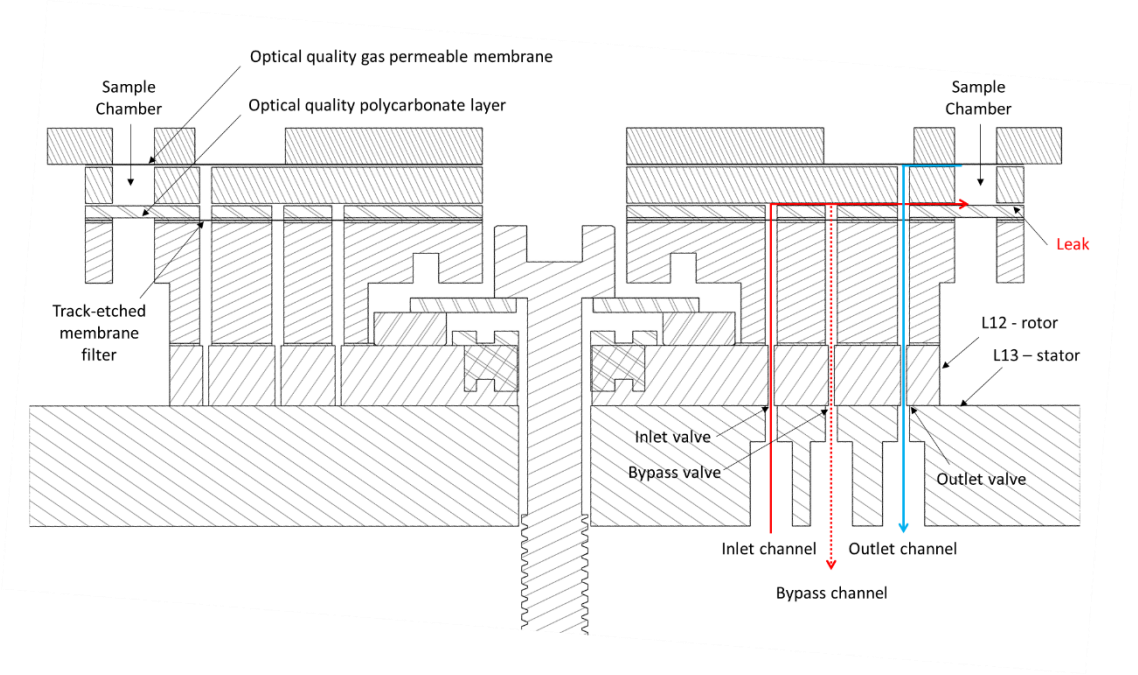

Figure 3-11. Cross-section cut view of the entire assembly of the initial design of the 2nd gen MCSD and RV.

Figure 3-11 demonstrates the fluidic pathway in the MCSD, which began from the inlet channel up the MCSD and flowed laterally into the sample chamber. The bypass channel was included as a flushing pathway to remove previous reagents and minimise cross-contamination. When pumped, the fluid will fill the sample chamber before flowing out through the outlet channel. Although the image showed the inlet and outlet channel crossing, the 3D structure has the channels side-by-side. The sample was contained in its respective chamber as the single unit track-etched membrane filters the inlet, bypass, and outlet channels.

The sample chambers were sealed using an optical quality gas-permeable membrane on the top surface and an optical quality polycarbonate layer on the bottom surface. The design allows a light source and an optical sensor to be placed at the top or bottom.

The L12 and L13 layers enabled the rotary valving capability. The L12 layer makes or breaks 3 out of 96, i.e., inlet, bypass, and outlet valve connections, as

it rotates with the whole assembly above it. The L13 layer remained stationary with three permanent inlet, bypass, and outlet ports.

3.8.2 Discussion on leaking issue in the initial design

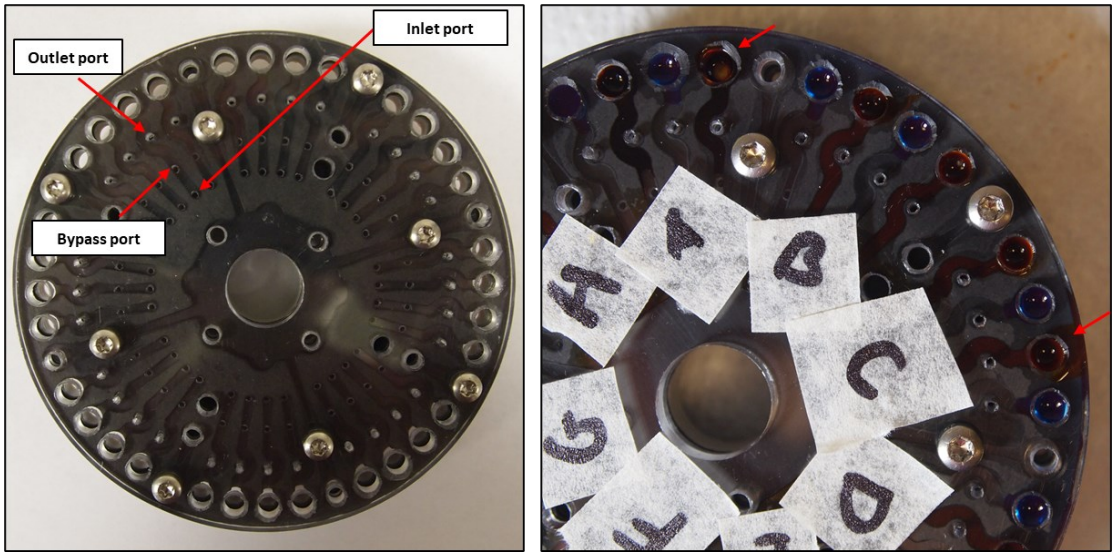

Figure 3-12. Left - Image of the 2nd gen. MCSD in Configuration 1 with the sample chamber opened. Right – Diagnosis test was performed to record the leak (red arrows) from the sample chambers.

During one of the initial biocompatibility tests, leaking was unfortunately observed from the sample chambers. The leak's location between the layers is shown in Figure 3-11. A diagnostic test was performed to assess the leakage. The image on the left of Figure 3-12 was taken before the aqueous food dye solution was pipetted into the sample chamber. The bolts were torqued at 0.5 Nm without the stainless-steel shim to maximise compression. It is also worth noting that the elastomer was changed from Ultra-thin silicone film (Silex, UK) to an FKM elastomer (Viton™). The silicone film was changed due to handling difficulties. The film was highly sticky to the PEEK or polycarbonate surface, making it challenging to align the fluidic ports. The key difference was the Shore A hardness level, where the silicone was 30° while FKM was 75°. It meant that it was harder to compress the FKM elastomer.

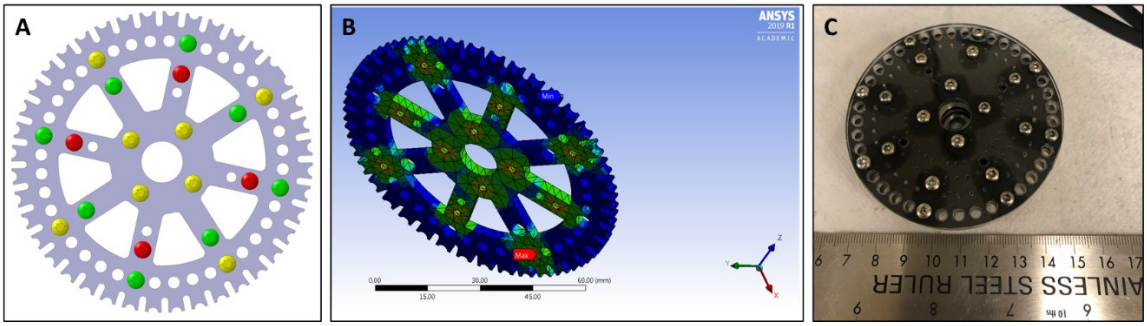

Figure 3-13. Finite element analysis and lab testing on the impact of bolting[1].

$$T = KDF_p \qquad \textbf{Equation 3.1}$$

$\mathrm{T} = \mathrm{Torque}$

$\mathrm{K} = \mathrm{Nut\ factor}$

$\mathrm{D} = \mathrm{Nominal\ bolt\ diameter}$

$\mathrm{F_p} = \mathrm{Bolt\ preload}$

Finite element analysis (FEA) was performed on Ansys 2019 to visualise the compression from the bolt preload. The hypothesis of the initial design was that the elastomer would compress and fill the gaps between the two layers to provide fluidic sealing. Since it was challenging to visualise between layers, FEA was performed to investigate the bolts' pressure on the MCSD. The FEA setup used a programme controlled tetrahedron method with an element size of 3 mm, resulting in a coarse mesh with 14748 nodes and 6534 elements. The bolt preload was calculated at 90% yield stress of M2.5 steel grade A4, giving a theoretical value of 1.4 kN at 0.86 Nm. The relationship between bolt preload and torque can be defined using Equation 3.1 (Bickford, 1998). The FEA result showed that the maximum pressure exerted by the bolt could go up to 9 MPa. The key message behind the FEA result was that the pressure from the bolt head

[1] (A) Bolts placement on the L1 aluminium load spreader. The green (Configuration 1), yellow (Configuration 2), and red (Configuration 3) was in the order bolting sequence, see section 3.8.1 for an explanation on configuration. (B) The result from finite element analysis on the underside of the L1-aluminium load spreader. (C) Post FEA test performed physically, which confirmed the pressure localisation from the bolt head.

was highly localised and did not spread equally across the whole surface since the material did not spread the load.

3.8.3 Design improvement on leaking issue

Three solutions were suggested for the next iteration based on the FEA result. At this stage of the PhD research, there was development time pressure within the BAMMsat-on-BEXUS mission timeline. The philosophy in the design solution was to decrease the likelihood of leaking via risk mitigation analysis and design activities.

3.8.3.1 Increased localised compression of the elastomer

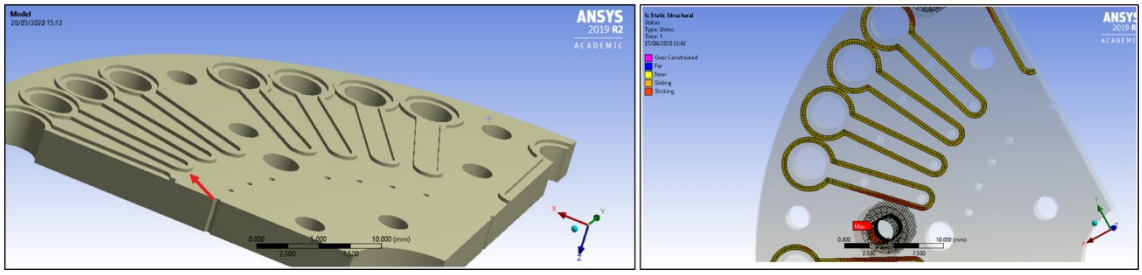

Figure 3-14. FEA was performed on the ¼ of MCSD to evaluate the impact of adding compression ridges.

Armed with the notion that pressure was highly localised, the concept of compression ridges was added to the 2nd gen. MCSD. The idea was to ensure that the elastomer around the fluidic channel will compress. Based on the FEA result, the localised maximum pressure closest to the bolt can reach 457 MPa (see Figure 3-14). The compression ridges were machined to a height of 0.3 mm. FKM elastomer was considered the elastomer of choice, but another silicone elastomer with shore hardness A of 50° was selected as the final version because of optical transparency for visual verification of fluidic alignment and softer properties, providing more compression. The silicone elastomer had a thickness of 0.5 mm, which will be compressed to 0.2 mm at 60% compression.

3.8.3.2 Increased number of bolts

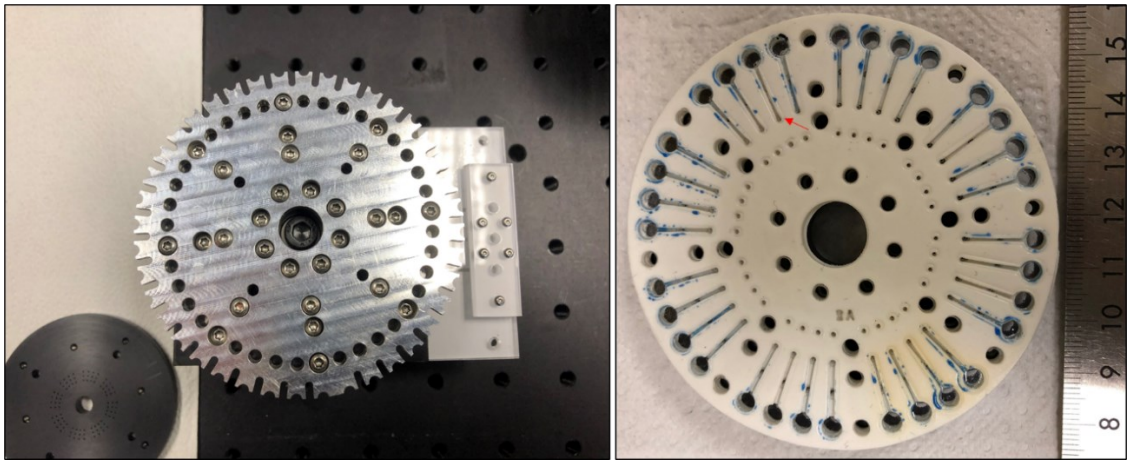

Figure 3-15. Results from testing the compression ridges.

Left – Image of the 2nd gen. MCSD with eight additional bolts added and distributed to ensure level compression. Right – Image showing the compression on silicone elastomer during testing and fluidic containment via the "coffee stain effect" of the aqueous fluidic dye.

3.8.3.3 Modify the pathways of the fluidic channels on the RV to be close to the centre of the M6 bolt.

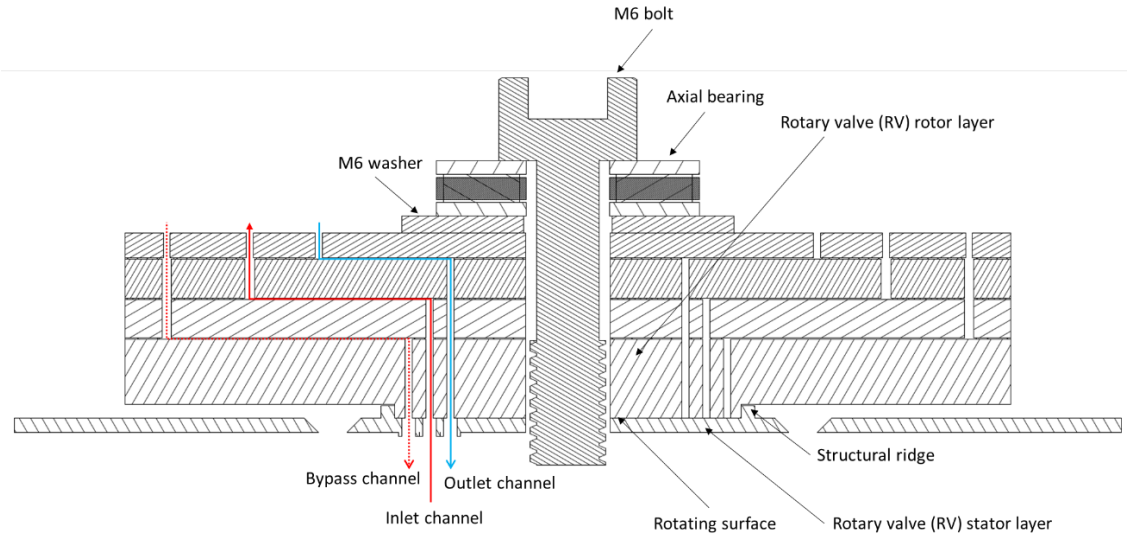

Figure 3-16. Cross-section cut view of the modified 2nd gen. rotary valve without the MCSD.

The rotary valve had modifications to minimise potential failure. The fluidic ports were placed closer to the centre axis. The pressure from the bolt was spread with a larger diameter M6 washer to ensure compression on the fluidic channels underneath it. A structural ridge was placed around the rotating surface to avoid dislocation and material creep under compression.

3.9 Final design (V2) of 2nd gen. MCSD and RV

3.9.1 Overview of the final design (V2)

The following section will discuss the final design, manufacturing, and assembly of the 2nd generation MCSD and RV tested on the 2nd gen. BAMMsat bioCubeSat payload and subsequently flew on the BAMMsat-on-BEXUS flight. The development process involved many iterations, and it is reflected in this chapter. Figure 3-17 shows the final design and assembly that was used for system-level testing. The following text discusses how the final design emerged from a few key design iterations.

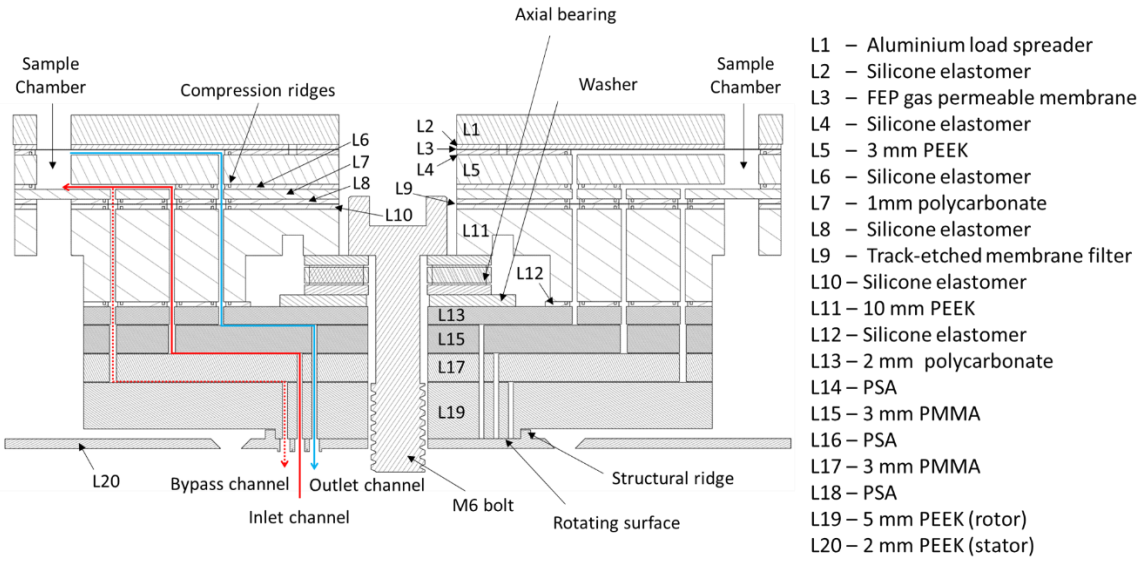

Figure 3-17. Final design and assembly of the 2nd gen. MCSD and RV.

The final L1 - aluminium load spreader material was changed from aluminium 6082T6 to aluminium 2024. The material was changed due to the combination material's availability during machining and realising the benefit of using 2024 as a gearing material. Aluminium 2024 is a counterpart of aluminium bronze, a copper-based alloy. Aluminium bronze alloys are often chosen as a gearing material for reasonable wear and corrosion resistance. In aluminium 2024, the proportion is inverted, and it is an aluminium-based alloy. The copper in 2024 gives this alloy its high strength and wear resistance compared to aluminium 6082T6 and is lighter than copper-based alloy. For the BAMMsat application, due

to its low gearing duty-cycle and volume, the difference between the aluminium may have been minimal. But it may be worth keeping this in consideration during future testing and the next generation.

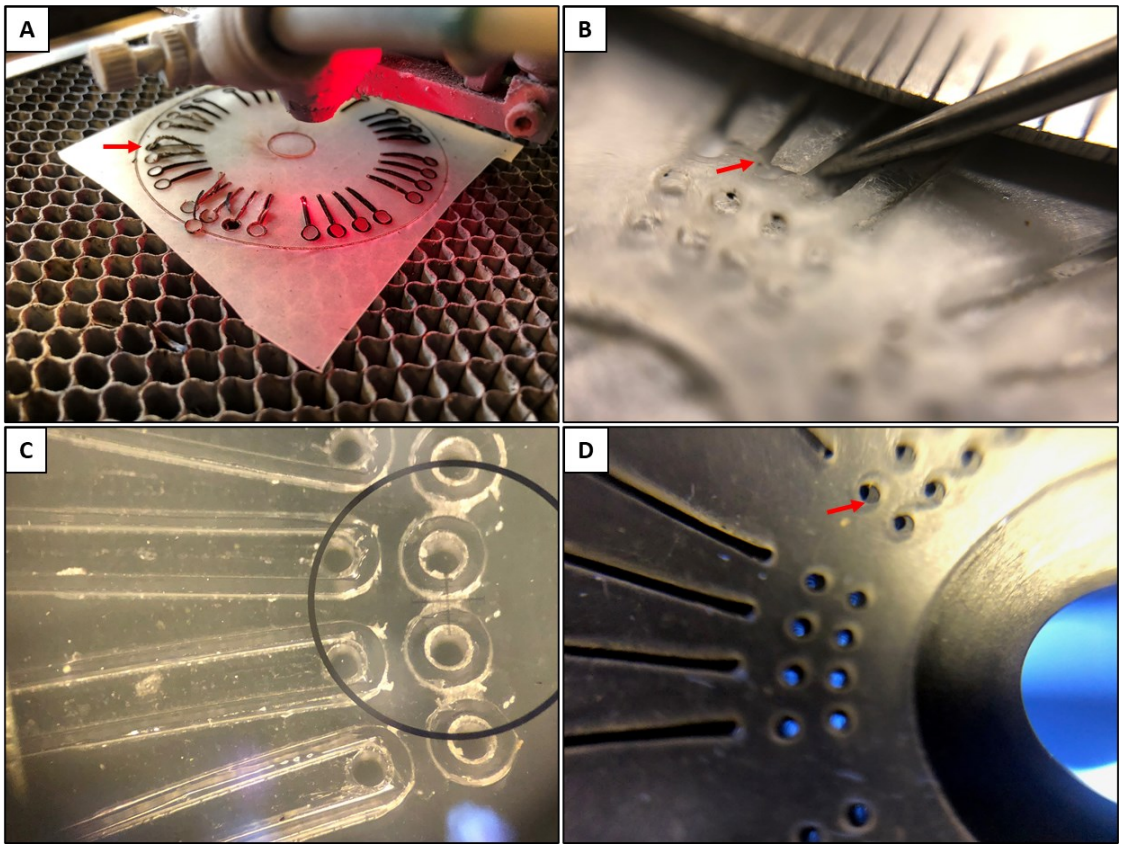

Figure 3-18. Various images of issues associated with CO_2 laser cutting silicone[1].

The final design had 20 layers, an additional 7 layers, compared to the initial design, with only 13 layers. The primary reason was to accommodate the new location of the fluidic ports for the RV to be closer to the centre of the M6 bolt. This design choice was selected to ensure the bolt head exerted enough pressure to provide fluidic sealing, see section 3.8.3.3. In hindsight, it would have been better to bolt the M6 bolt from the top L1 layer rather than the middle, reducing

[1] (A) Silicone elastomer buckling during photothermal ablation from CO_2 laser cutting. (B) The effect of buckling causes cross-cutting of the fluidic channels. (C) Image of L16 with a 0.1 mm division microscopic target slide demonstrated the sub-millimetre tolerance required. The space between the compression ridges was around 0.2 mm. (D) The effect of heat buckling affected the final cut position of the fluidic channel and caused fluidic channel misalignment and blockage.

the layer number. These lessons learnt will be optimised in the design of the next generation.

The additional layers were being used to re-direct the fluidics pathway. A similar design principle was initially applied with compression ridges and silicone elastomer. However, the issue with CO_2 laser cutting meant that these layers between L13 and L19 reverted to the older design using pressure-sensitive adhesive (PSA). The problem can be seen in Figure 3-18, where the buckling due to heat caused fluidic channel misalignment. Many attempts have been made to minimise buckling by optimising the laser speed, laser power, corner power and the number of passes. Unfortunately, due to tight tolerances, even a slight buckling will cause misalignment, merging the channel and causing leakage (Figure 3-19).

The misalignment was challenging since a manual visual inspection was required for each fluidic port and channel alignment, which was strenuous during assembly. The buckling also changed the fluidic channel profile, which removed the curve edges and avoided them being close to one another. Figure 3-12 shows the fluidic channel profile on the initial design. The fluidic channels were straightened and impacted the outlet channel pathway (marked blue in the image), as seen in Figure 3-17 compared to the initial design, Figure 3-11.

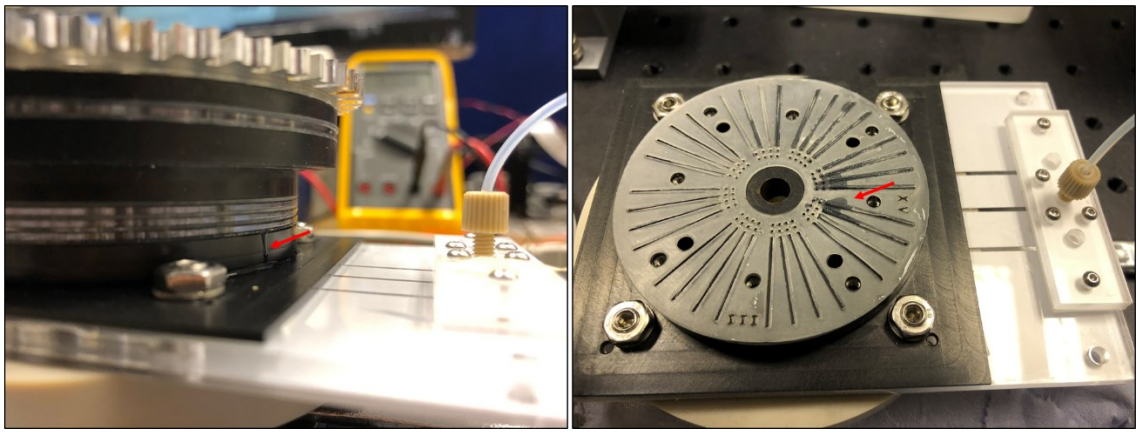

Figure 3-19. Images of leaking on the side of the MCSD due to the misalignment of the fluidic channels.

The final material chosen for all the silicone elastomers was a silicone rubber sheet with 50° Shore A hardness (Silex, UK). The silicone was still relatively soft to ensure compression, and it was translucent to allow manual fluidic visual inspection during assembly. It also performed better under laser cutting than the 40° Shore version but lesser than the FKM elastomer, where the FKM had no visible buckling during cutting. Further investigation will be required to understand this phenomenon.

3.9.2 Testing performed on the 2nd gen. MCSD and RV (V2)

3.9.2.1 Water retention test

After the final design modification on the 2nd generation MCSD, 7-day water retention tests were performed to evaluate the design modification to confirm if the 2nd gen. MCSD was able to contain the water with minimal leakage.

Two sets of experiments were performed, one in (i) an ambient humidity environment and another in (ii) a high humidity environment. In each set of experiments, two configurations of MCSD were tested. The first configuration was with (a) an opened MCSD, and the second configuration was with (b) a sealed MCSD. The test setup can be viewed in Figure 3-20.

The objectives of the test are:

1. To assess the design modification to confirm if the 2nd gen. MCSD was able to contain the water with minimal leakage.
2. To assess the impact of sealing the sample chamber with FEP gas-permeable membrane on water retention. In the flight configuration, the sample chamber will be sealed using L1 to L3 (see Figure 3-17).

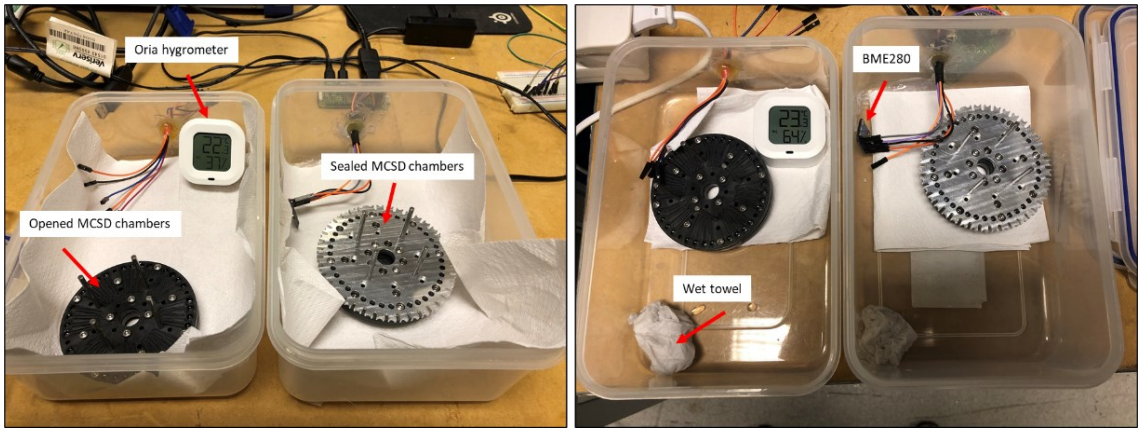

Figure 3-20. Experiment setup for 7-day water retention testing.

In Figure 3-20, the image on the left was set up for the ambient environment, while the image on the right was set up for a high humidity environment. In each experiment setup, one MCSD was left with opened chambers, and another MCSD was sealed in the complete flight configuration. The MCSD was then placed inside the 1.5-litre plastic container to control the headspace where liquid can evaporate, which was then sealed with the plastic container lid with a blue silicone O-ring along the ridges.

Table 3-5. Observational results from the 7-days liquid retention test.

	Opened MCSD	***Sealed MSD***
Ambient	• No observable leakage between layers. • All chambers dried up.	• No observable leakage between layers. • Six chambers had water loss beyond the original meniscus, approximately 5% -10 % reduction (closed to the top surface). • Fourteen chambers had condensation on the underside of the L3 – FEP gas permeable membrane. • One chamber nearly dried up.
High-humidity environment	• No observable leakage between layers. • All chambers had the liquid reduced to halve.	• No observable leakage between layers. • 31/32 chambers had a slight reduction under the original meniscus, approximately 1% - 5% reduction. • One chamber had 1/4 liquid loss.

The results recorded via visual observation demonstrated a significant impact on water retention between ambient and high humidity environments. In the ambient environment, the low humidity headspace significantly impacted the MCSD. The water in the opened MCSD completely dried up, while 7 out of 32 chambers in the sealed MCSD had 5% - 10% water losses. Comparatively, in the high-humidity environment, the condition improved significantly for both opened and sealed MCSD. The sealed MCSD performed much better where the water loss was minimal except for one chamber.

The evaporation was evident and recorded by the humidity sensors. The sensors recorded that the sealed MCSD in ambient humidity took 7 hours to reach saturation in the ambient environment, and opened MCSD took one hour to reach 99% relative humidity. Humidity reading was measured via Oria hygrometer and BME 280 (see Figure 3-20).

Figure 3-21. Example of images with bubble and condensation formation on the MCSD.

The sealed MCSD in a high humidity environment had a slower consistent rise and took six days and nine hours to reach 85% relative humidity, followed by a steady climb to 88% by the end of the seventh day. The opened MCSD took one hour to reach 99% relative humidity.

A calculation was made to estimate the amount of water loss. In a trapped headspace of 1.5 litres (plastic container), the mass of water that could evaporate from the sample chambers to reach water vapour saturation from 50% relative humidity was 13.4 µl. This amounted to 1.4% of the total volume of water in 32 sample chambers (928 µl).

Two interesting observations were evident during testing (see Figure 3-21). The first was the bubble formation, which appeared after 24 hours (observed without opening the sealed container). This is most likely due to trapped air in the fluidic channels that dispersed to the top of the sample chamber.

The second observation was the condensation in the underside of the FEP membrane. When sealing the top layer of the MCSD, there was a small, trapped air space above the water surface and below the FEP membrane due to the curvature of the meniscus. The condensation could appear due to trapped water vapour, which evaporated from the water surface and then condensed once it reached the FEP.

Both bubble and condensation effects could be detrimental to the captured microscope's image since both could block the line of sight to the object in the sample chamber. The experiment provides some insight that extra care should be placed during MCSD AIV to ensure that trapped air space is minimised either via priming the fluidic channels with liquid / growth media or fully filling the sample chamber.

In summary, the result demonstrated that the test successfully demonstrated no observable leakage between the layers. It meant that the 2nd gen. MCSD with compression ridges was able to contain the water compared to the initial design. The results also demonstrated that the FEP could limit water evaporation in full flight configuration. The water retention improves significantly in a high humidity environment since the water vapour could not escape into the trapped headspace. Unfortunately, a repeat test was not performed due to urgency in the BoB mission timeline.

3.9.2.2 Fluidic test

Based on the overall timeline of the PhD, a major part of the fluidic testing took part with a wider fluidic subsystem in the 2nd gen. BAMMsat bioCubeSat payload. The discussion will continue in Chapter 5. The idea is to have a coherent story as an overall fluidic subsystem testing.

3.9.2.3 Geneva gear mechanism test

The Geneva gear mechanism was developed as its own subsystem. It required considerable effort during a PhD for development. Hence, the discussion will continue further in Chapter 6.

3.10 Discussion, conclusion, and future work

3.10.1 Discussion and conclusion

Chapter 3 discussed the research and development of the multi-chamber sample disc (MCSD) and rotary valve (RV) performed during the PhD. The MCSD and RV were key components that provide functionalities unique to the BAMMsat concept.

At the start of the PhD, the 1st generation MCSD was developed to a point where it could house biological samples and perform fluidic functionalities. The design was based on established microfluidics techniques of laminating laser cut polymer with pressure-sensitive adhesive. The technique also has spaceflight heritage with bioCubeSat launched by NASA over the years. Likewise, the 1st generation RV was developed as a basic demonstration of the concept. However, it could be argued that it was not as advanced as the MCSD.

The PhD research continued the development of the MCSD and RV while addressing the critical issue with the legacy design and development. These were (i)The previous design had leakage at the rotating and stationary surfaces of the RV due to material choices and build quality. (ii) The Geneva gear mechanism for the rotary valve was not fully developed. (iii)The gas-permeable membrane was not fully defined as a material or design. (iv)The sample filter design was not fully defined as a material or design.

The PhD research also addressed the issue that was discovered during the research, which was the drawback with lamination by adhesive. The adhesive limits the access to the sample chambers or wells, essentially giving the operator a single shot of assembling the biological sample and the system.

More importantly, it also limits the type of biology that can be flown. Some biological samples, such as mammalian cells, may require late access at the launch site during pre-flight. A similar argument is also valid during post-flight when access to the samples is necessary for post-flight analysis.

During the PhD, the 2nd gen. MCSD and RV were developed to tackle the issues previously mentioned. The 2nd gen. RV used PEEK as a replacement material for the rotating and stationary surfaces of the rotary valve. PEEK addressed the issue with material creeping from the previous PTFE material while having good biocompatibility, inertness, autoclavability and machinability properties.

In comparison to the 1st generation, the 2nd gen. MCSD is mechanically assembled, meaning access to the sample chamber can be accomplished by bolting and unbolting the covering layers. However, there was an issue with fluidic leaking. The leaking was improved with compression ridges to provide localised pressure to compress the elastomer along the fluidic channels. It is worth noting that the new design increased the volume and increased the complexity of the MCSD and RV compared to the 1st gen. However, the lessons learnt from the 2nd gen. highlighted how to repackage it into a compacter version for the 3rd gen.

Fluidic retention testing was performed to evaluate if the leaking issue has improved with compression ridges. The test confirmed no observable leakage and confirmed the ability to retain liquid in the sample chamber for seven days. Further fluidic performance tests on the MCSD will be discussed in Chapter 5 alongside the development of the fluidic subsystem for the 2nd gen. BAMMsat bioCubeSat payload. It was not included in this chapter since the testing was performed with the wider fluidic subsystem for the 2nd generation BAMMsat bioCubeSat payload.

The Geneva gear mechanism actuates the rotary valve enabling each chamber to have an independent fluidic pathway. The chapter briefly discussed the gear dimensioning that was completed to accommodate changes to the 2nd generation MCSD. Further development and testing of the mechanism will be discussed in Chapter 6 and will cover the torque sizing and design of the associated mechanical support for the Geneva gear mechanism.

The research identified the gas permeable membrane that will be used to seal the sample chamber while allowing O_2 and CO_2 gas exchange for sample use. The research procured the FEP and PMP film (Goodfellow, UK). The FEP

membrane was integrated into 2nd generation MCSD, and its sealing ability was tested in a 7-day water retention test, demonstrating its ability to contain water inside the chamber. Due to the timeline of this PhD, driven by the BoB mission, the PMP did not undertake similar testing for fluidic retention. The only test performed was manufacturing the PMP via CO_2 laser cutting.

Table 3-6. Permeability properties of FEP and PMP film.

	FEP (Goodfellow, 2022a)	**PMP (Goodfellow, 2022b)**
Permeability to CO_2 $(\times \mathbf{10^{-13}} cm^3.cm.cm^{-2}s^{-1}Pa^{-1})$	10	70
Permeability to Hydrogen @25°C $(\times \mathbf{10^{-13}} cm^3.cm.cm^{-2}s^{-1}Pa^{-1})$	10	N/A
Permeability to Nitrogen @25°C $(\times \mathbf{10^{-13}} cm^3.cm.cm^{-2}s^{-1}Pa^{-1})$	1	5
Permeability to O_2 @25°C $(\times \mathbf{10^{-13}} cm^3.cm.cm^{-2}s^{-1}Pa^{-1})$	3	20
Permeability to water @25°C $(\times \mathbf{10^{-13}} cm^3.cm.cm^{-2}s^{-1}Pa^{-1})$	13	N/A
Permeability to water @38°C $(\times \mathbf{10^{-13}} cm^3.cm.cm^{-2}s^{-1}Pa^{-1})$	40	700

During the FEP membrane testing, the issue with evaporation was evident. The FEP and PMP are gas permeable, which includes water vapour, see Table 3-6. Against a larger headspace, the water will evaporate from the sample chamber into the open atmosphere. The addition of an FEP membrane did significantly reduce the rate of evaporation. However, the future design will need to consider if the evaporation rate is an issue. GeneSat, the first NASA bioCubeSat, experienced a similar problem, Ricco et al. mentioned evaporation was mitigated when sealed inside the pressure vessel. It was pointed out that the waste bag

was filled with several mL of saline solution to maintain backpressure on all bio-wells to replace water loss (Antonio J Ricco et al., 2007).

The 7-day test also highlighted fluidic application issues: bubble formation and water droplet formation due to condensation. The significant impact is the obstruction during imaging, and the effect was evident during the BoB flight, where the captured image was obstructed. See Figure 9-23 for images during the flight.

Bubbles within the sample chamber also limit the amount of food that affects the sample's viability. Bubble formation is a common issue in microfluidics. There are a few examples of why bubbles could form from dead volume in the channels, contact angle, and temperature cycle. A study has reviewed bubble formation and is a good initial source to understand the mechanics of bubble formation (Pereiro et al., 2019). NASA GeneSat opted to dissolve the CO_2 bubbles in a helium-sparged saline solution (Antonio J Ricco et al., 2007). For BAMMsat, bubble formation will require further investigation, and fluidic channels are optimised to minimise bubble formation.

Regarding the gas-permeable membrane, the research identified polycarbonate track-etched membrane as an elegant solution to have a single unit filter built into the layer of the 2nd gen. MCSD. The research explored UV laser cutting which enabled the filter to be used in the 2nd gen. MCSD. However, a fluidic performance test to evaluate the impact of the filter was never completed during the PhD and did not fly on the BAMMsat-on-BEXUS flight for fear of creating high backpressure to the fluidic system.

In conclusion, the PhD research has investigated the legacy issues from the 1st gen. MCSD and addressed the majority of the issue in the 2nd gen. MCSD. The research developed the concept into a version that was integrated into the 2nd gen. BAMMsat bioCubeSat payload. Due to the time pressure from the BoB mission, many testing were pending for the 2nd gen. MCSD to be fully understood and be considered reliable. The summary can be viewed in Table 3-7.

Table 3-7. Summary of research performed against MCSD and RV design drivers.

Design drivers		Remarks
MCSDRV -1	The 2nd generation multi-chamber sample disc needs to allow repeated access to the sample chamber to allow sample exchange.	A mechanically assembled MCSD and RV were designed, manufactured, and tested, which satisfied the design driver. Combining machined parts and laser cutting (see Table 3-4) allows the layer to be manifolded into sample chambers and fluidic channels.
MCSDRV – 2	The rotary valve's rotating surface material needs to minimise the fluidic leak to an acceptable rate.	PEEK was selected as a replacement material to replace PTFE with better compressive strength.
MCSDRV – 3	The material for the Geneva mechanism, i.e., the gear teeth on the 2nd generation MCSD, need to have the mechanical strength to withstand the cyclic loading from the motor actuation pushing with the Geneva drive shaft.	Material research resulted in aluminium 2024 being chosen as layer 1 of the MCSD with the Geneva gear tooth. Aluminium 2024 is a counterpart of aluminium bronze, a copper-based alloy. Aluminium bronze alloys are often chosen as a gearing material for reasonable wear and corrosion resistance.
.MCSDRV – 4	The diameter of the 2nd generation multi-chamber sample dish could not be larger than 90 mm.	The diameter of the MCSD was set at 87 mm.
MCSDRV – 5	The material for the 2nd generation multi-chamber sample disc needs to be biocompatible with most biological samples.	The materials chosen for the MCSD and RV have a track record of being biocompatible. However, each experiment will require a verification test.
MCSDRV – 6	The material needs to be inert to most chemicals.	The materials chosen for the MCSD and RV have a track record of being inert to most chemicals. However, each experiment will require a verification test.
MCSDRV – 7	The material for the MCSD and RV needs to be autoclavable for ease of sterilisation during pre-flight.	The material selected for the MCSD can be autoclaved.
MCSDRV – 8	The design of the fluidic channels needs to minimise bubble formation to an acceptable rate.	Dead volumes such as microwell and sharp ends or edges were designed to be minimised.
MCSDRV – 9	The material needs to include an optically transparent gas permeable membrane.	The top and bottom layers of the sample chamber polycarbonate and FEP are both optically transparent.
MCSDRV – 10	The 2nd generation MCSD needs to include a sample particulate filter or filters to contain the sample within its respective chamber and avoid cross-contamination.	Track-etched membrane filter has been identified as a suitable filter and integrated into the 2nd gen. design.

3.10.2 Future work

Immediate future works would include further testing on the 2nd generation MCSD and RV performance.

- Repeat the liquid retention test on the 2nd gen. MCSD in full flight configuration using the FEP gas permeable membrane.
    - The 7-day liquid retention testing was beneficial in highlighting any immediate issue with the design, especially with leakage and evaporation. Unfortunately, the test was only performed once due to time constraints and lacked repeatability data. The test should be repeated using the same setup and record the bubble formation over time. Similarly, the test should observe condensation over time. And observe the membrane behaviour to see if there was an increased concavity over time and assess its impact on water contact angle. FEP is hydrophobic, and the concavity could help determine water droplet formation due to condensation.
- Perform flow rate testing against various track-etched membranes with varying pore sizes.
    - Three different track-etched membrane filters were procured and UV laser-cut during the research. The filter varies in its pore sizes of 5 µm, 3 µm, and 0.2 µm. The variation was selected to accommodate *C. elegans* while allowing food (bacteria) to pass through the pore for the BoB flight. The pore size chosen was 3 µm as it should still contain the *C. elegans*. The 0.2 µm was selected to contain bacteria for bacterial experimentation. At the same time, the 5 µm was an upper boundary for flow rate comparison. The test was not performed due to time constraints. The future test should test the filter with varying pores to investigate its respective flow rate. The test can be performed in a setup using laser cut acrylic and laminated adhesive to avoid pressure discrepancy in a larger system. The test should measure flow rate before and after the filter and pressure difference across the filter.

Long-term future work would include the tasks below.

- Test the viability of using FKM elastomer to retain fluids and its fluidic performance as a replacement to the current silicone elastomer, which has issues from heat buckling during CO_2 laser cutting.
- Repeat the liquid retention test on the 2nd gen. MCSD with the PMP gas permeable membrane to understand the difference against the FEP membrane.

4 Subsystem level – Compact brightfield microscope: Design, manufacture, and test

4.1 Introduction

Chapter four discusses the research and development of a compact brightfield microscope during the PhD. The compact brightfield microscope was explicitly developed for the BoB mission to capture images and videos of the *C.*. The captured data would be used to assess the behavioural and health of the *C. elegans*. It also confirms the functionalities of the 2nd gen. BAMMsat bioCubeSat payload, demonstrating the technology and the BAMMsat concept to the community.

As a brief historical context, at the beginning of the PhD, the 1st gen. BAMMsat microscope has been developed into a working optomechanical laboratory breadboard. The BAMMsat 1st gen. microscope was developed as a breadboard version to test the concept and its functionalities.

However, the design and functionality of 1st gen. microscope were beyond the BoB mission scope. The 1st gen. breadboard version was too bulky for a 2U CubeSat design. Note that a 2U flight model (FM) concept was developed as part of the 1st gen. development. The BoB mission could have been built from this concept, but it was concluded that it would have required more financial and development resources than a simpler imaging system. A more straightforward and cost-effective alternative was explored, resulting in the compact brightfield microscope.

The compact brightfield microscope was an optical subsystem developed specifically for BAMMsat-on-BEXUS (BoB) mission. The compact brightfield microscope was used as an optical sensor to observe the health of *C. elegans* by recording its mobility and motility during pre-flight and flight.

4.2 Aim and objectives

1) *Evaluate and critique the 1st generation microscope to establish lessons learnt as an input into the design of the compact brightfield microscope.*

The objective was added to assess BAMMsat 1st generation microscope to incorporate lessons learnt and design guidelines for the compact brightfield microscope.

2) *Produce a list of requirements extracted from BAMMsat-on-BEXUS mission requirements*

This objective was added to produce a list of requirements from the BAMMsat-on-BEXUS mission.

3) *Produce an initial design (V1) of the compact brightfield microscope for initial testing.*

The objective builds from the requirements to produce an initial design concept. The initial design was tested, evaluated and used to resolve immediate issues in preparation for the final design.

4) *Manufacture, assemble, and test a final design (V2) of compact brightfield microscope ready for BAMMsat-on-BEXUS flight.*

The fourth objective was to complete the manufacturing, assembly and testing of a compact brightfield microscope ready for the full system test inside the 2nd gen. BAMMsat bioCubeSat payload.

4.3 Overview of the 1st gen. BAMMsat microscope

4.3.1 Introduction to the 1st gen. design

BAMMsat 1st gen. microscope was developed during the NSTP-funded project in 2015; see section 1.2 for historical context. The microscope was an essential sensory tool to extract valuable information during an experiment in orbit. The development of the 1st gen. microscope was devised to de-risk the concept and produced an initial laboratory breadboard. The design philosophy was to have a modular optical microscope for flexibility during testing and use COTS parts to reduce the cost and lead time of custom optical components. It was assembled using a CCD camera, telecentric lens, collimation lens, filters, and LED light source. The modular optical design allowed the flexibility for the microscope to be set up as white light, epifluorescence, or trans-fluorescence microscope.

In reference to Figure 4-1, Image A was the optomechanical laboratory breadboard version used during laboratory testing during the NSTP programme. The microscope was primarily set up as an epifluorescence microscope during laboratory testing. The main issue with the setup was the large volume envelope it required. Image C shows the size of the 1st gen. microscope with the volume envelope nearly filling the whole 2U pressure vessel. The volume leaves little space for the MCSD fluidic interface and Geneva gear mechanism.

A miniature volume envelope microscope was developed for a flight model version; see Image B in Figure 4-1. However, the conceptual design was never tested. The design would have required custom optical components such as a filter, filter mount, beam splitter, and a smaller collimation lens housed in a custom housing. The concept requires considerable financial and human capital resources for further development beyond the resources available in the BoB mission

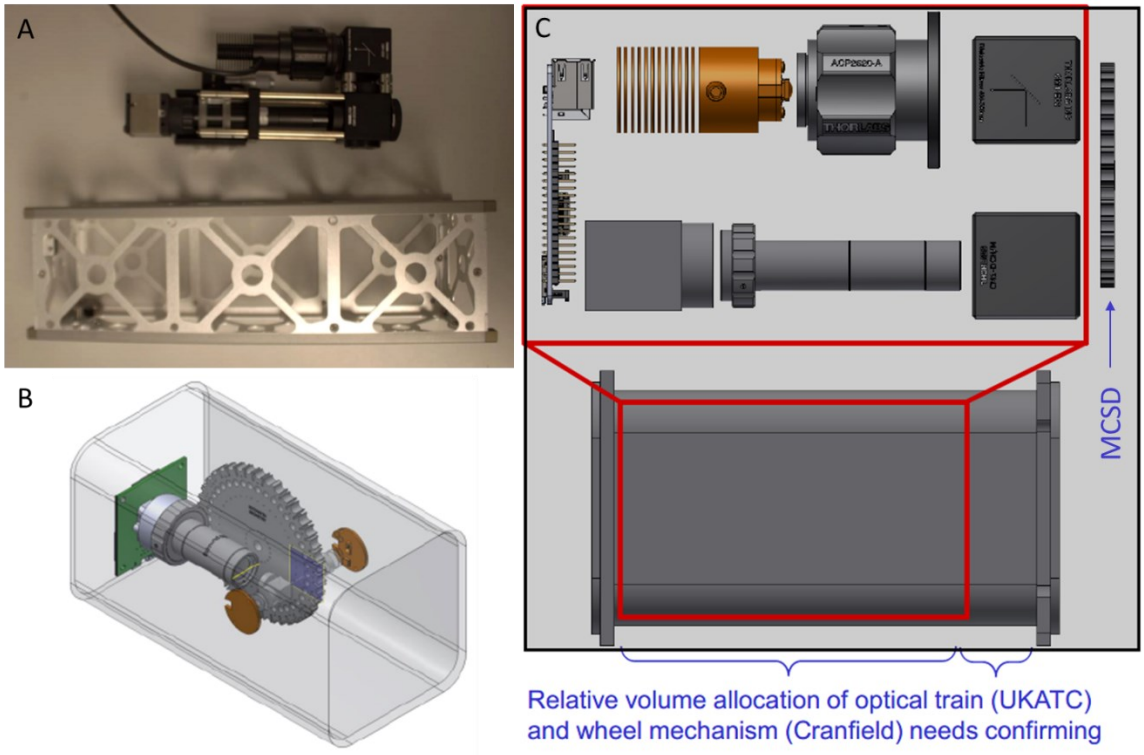

Figure 4-1. Various images of 1st gen. microscope[1].

The 1st gen. microscope was suited for a laboratory testing operation. The microscope was interfaced using freely available IDS software (IDS Imaging Development Systems GmbH) running on Windows 7 to operate the IDS UI-2280SE-C-HQ CCD camera. The general-purpose LED light source has variable brightness control. The design was based on a fixed-focus lens, and the image was focused via a manual micrometre translation stage. The features fit laboratory testing since the operator can easily set up the microscope and change parameters quickly during testing.

However, these features may not be as beneficial for a flight model. For instance, the software is not optimised to run on a single board computer, resulting in heavy software application, if flown, and potential data and control interface issues. The variable LED source was bulky with a large heat sink and was not optimised for

[1] A – Image of the 1st gen. microscope. B – Image of a 2U FM microscope. C – CAD image for a microscope volume comparison against a 2U pressure vessel (images courtesy of Prof Cullen with minor editing).

specific brightness and peak wavelength. Similarly, the manual micrometre translation stage added volume and mass to the system.

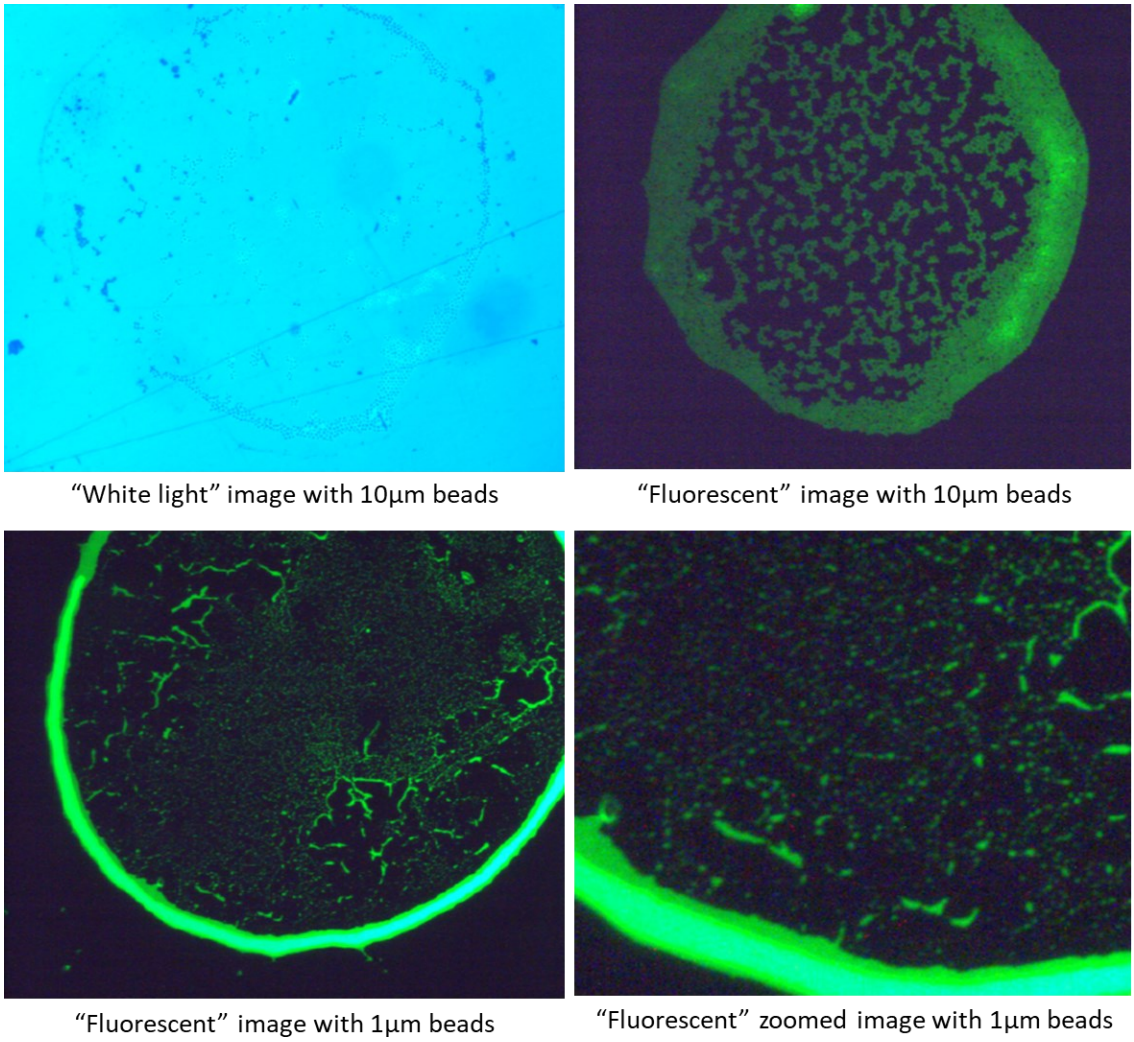

Figure 4-2. Example of white light fluorescent images taken using BAMMsat 1st gen. epi-fluorescent microscope during NSTP project (images courtesy of Prof Cullen with minor editing).

Figure 4-2 demonstrated the capability of the 1st gen. microscope to capture fluorescent images. The fluorescent object was made up of fluorescent beads. The 10µm was quickly resolved from the images, while the 1µm was the lower resolution limit. Fluorescent imaging is useful for studying cell culture to visualise biological processes, and it was developed during the 1st gen. microscope since the fluorescent capability is critical for future spaceflight experiments.

However, the BoB mission had a more straightforward optical requirement than the 1st gen. microscope. The BoB mission requirement was to observe the motility and mobility movement of the *C. elegans*. Therefore, a brightfield of a darkfield microscope with image contrast between the *C. elegans* and background image was deemed sufficient to observe its behaviours.

4.3.2 Evaluation and critique on 1st gen. design

Based on the evaluation and critique in section 4.3, it was concluded that a simpler microscope was required. Both options require further development, but the 1st gen. with the fluorescence capability would have required considerable financial and human capital resources for further development. Since the BoB mission was a student-led development, limited resources were readily available.

In addition, the fluorescent capability of the 1st gen. was not required to meet the BoB mission objective. A simpler microscope, such as a brightfield microscope, was sufficient to observe the *C. elegans'* behaviour. Removing the fluorescent requirement also reduces the complexity of using stained *C. elegans* during testing and flight operations.

After some evaluation, a brightfield microscope was chosen as a design solution. The 2U microscope will be mounted on the 2nd gen. BAMMsat bioCubeSat payload inside a 2U pressure vessel. Therefore, a brightfield microscope was required since the inside of the pressure vessel will not have access to scattered photons for a darkfield microscope.

This section summarised the lessons learnt that influenced the design choices for the compact brightfield microscope.

- The compact brightfield microscope needs to consider a simpler optomechanical mount design since it could have a considerable volume envelope. The volume can be reduced by using a board camera, compact LED, and a shorter lens.

- The compact brightfield microscope should assess the software interface between the camera sensor and operating system to reduce the development effort for the BoB mission.
- A light source will be required in the design of a brightfield microscope.

4.4 List of requirements for the compact brightfield microscope for the BoB mission

The compact brightfield microscope was explicitly designed for the BoB mission. Hence, the requirements were established during the Preliminary Design Review (PDR) of the BoB mission. These requirements were used as the basis of the compact brightfield microscope design and were based on ECSS Space Engineering Technical Requirements Specification or ECSS-E-ST-10-06C standard. This ECSS standard distinguishes the type of requirement in space systems. The BoB requirements were categorised into Functional, Performance and Design requirements.

The requirements relevant to the compact brightfield were extracted from the BoB requirement list available in the appendix of this thesis (see Appendix A).

Functional requirements:

FC-03 100c **The system shall take and log static images and video of the C. elegans inside the MCSD via an imaging system during pre-flight operation and experiment operation to evaluate the health status of the C. elegans.**

The health status of C. elegans can be defined by imaging its population density, mobility, motility, behaviour and size. The imaging system consists of a camera, imaging lenses, and an illumination source. The pre-flight imaging is to confirm the viability of the C. elegans before starting the experiment and confirm the pre-flight experiment procedure

FC-03 200c **The system shall be able to take and log videos of a chamber while the last media is being replaced.**
This will enable us to see the impact of the drug in near real-time when pumped into the chamber. The drug is an anaesthetic; therefore, it is expected to see C. elegans slowing their movement.

Performance requirements:

PR-07 100 **The system shall take and log static images of the C. elegans with a resolution of 0.025 mm over C. elegans with at least 3280 x 2464 pixels.**

The number of pixels was based on the Raspberry Pi camera capabilities

PR-07 200 **The system shall capture and log video with a minimum resolution of 0.075 mm over C. elegans with at least 1080 x 1920 pixels.**

Numbers based on the Raspberry Pi camera capabilities

PR-07 210 **The system shall capture and log video with a minimum of 30 images per second.**

Shall be enough to identify C. elegans type of motility/mobility

Design requirement:

DG-03 201 **The imaging plane on the MCSD should be parallel to the direction of gravity.**

In this orientation, the sedimentation due to gravity doesn't obstruct the imaging system

DG-04 100 **The dimension of the pressure vessel shall not exceed a 2U CubeSat format.**

A 2U CubeSat format is defined as 20cm×10cm×10cm. The 2nd gen. BAMMsat bioCubeSat payload will be housed within the 2U pressure vessel

4.5 Preliminary design for the compact brightfield microscope

4.5.1 Preliminary design concept

A conventional laboratory microscope was the baseline when designing the compact brightfield microscope. The drawback with a traditional microscope was the large system, typically longer than 200 mm, the length of a 2U CubeSat. The benchtop laboratory microscope has an objective lens, an extension tube, a tube lens, and a sensor within its optical system, which makes up the length. Because of the large volume, a standard microscope layout is not compatible with the BoB requirement to house it inside a 2U pressure vessel. See requirement DG-04 100 in section 4.4. The design of the compact brightfield microscope was based on imaging techniques applied in industrial imaging and machine vision. This field involves high-performance microscopy imaging without using a long optical setup. During the technological review, COTS lens or imaging system design was not readily identifiable as a design solution.

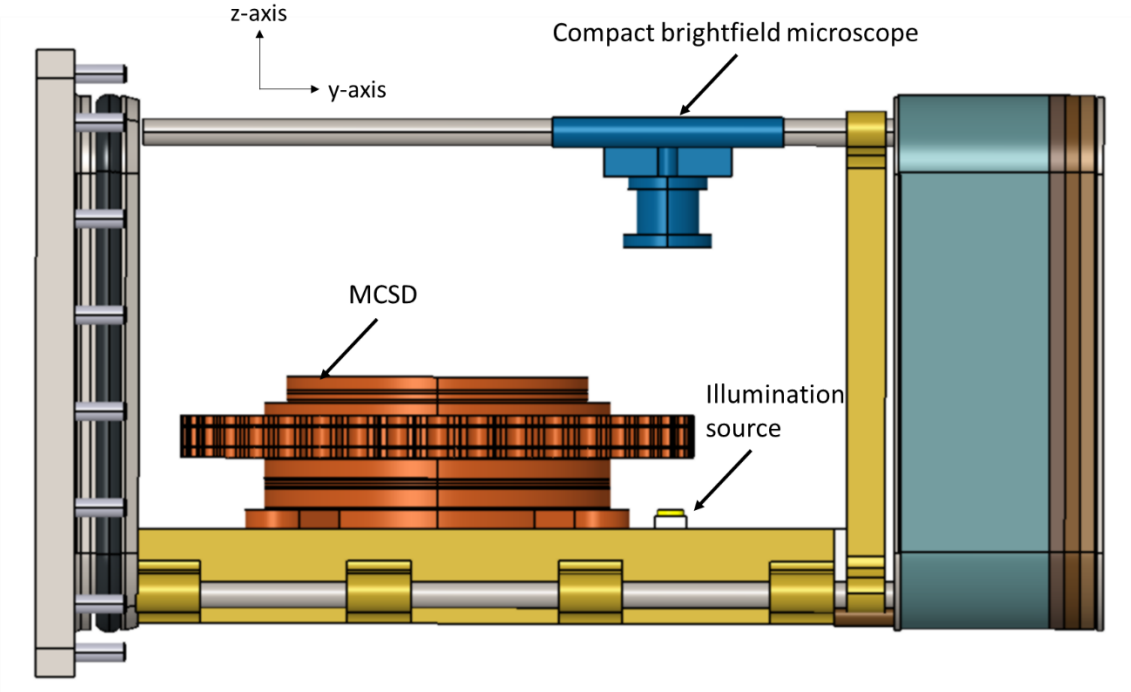

Figure 4-3. Earliest conceptualisation of the compact brightfield microscope for BoB inside a 2U pressure vessel (note the axes).

Figure 4-3 shows the earliest conceptualisation of the compact brightfield microscope. The design philosophy was to have a simple and flexible design to reduce development effort. Brightfield microscopy is the simplest microscope illumination technique. The sample will be observed via a lens and a camera sensor from above the object plane, and the sample chamber will be illuminated by an LED below. The white light from the LED illuminates the biological sample and creates a white background against a "darker" contrast of *C. elegans* due to the change in refractive index. The high contrast happened since the transmitted photon will be scattered when passing through the *C. elegans.* Since *C. elegans* are not coloured, it does not absorb the illumination. The "darkness" comes from losing photons via scattering rather than absorption.

The simple and flexible design was chosen to manage the unknown with optical housing and mounting. Having only three components (sensor, lens, and LED) would reserve housing volume to perform iteration without impacting the other subsystems.

4.5.2 Justification for using Raspberry Pi (RPi) V2.1 camera

Since the beginning of the BoB mission, a small single-board computer (Raspberry Pi Zero W) has been the primary choice as the flight computer for onboard data handling (OBDH). Similar to a satellite architecture, the flight computer is the "brain" of the system and will handle tasks and operations sequences, data handling, data management and telecommunication.

Raspberry Pi Zero W was chosen because it is a small and affordable single-board computer that can fit into a CubeSat format. It also has enough processing power to run as a flight computer. More importantly, the large open-source community meant that many resources were publicly and widely available to shorten the development timeline.

RPi camera is designed explicitly for RPi computers (Rasperry Pi Foundation, 2015). It has readily available software libraries and a specialised camera cable that directly interfaces to the RPi computer. Image processing is also optimised

for the RPi hardware. The RPi computer and RPi camera module also have spaceflight heritage on board the ISS during the Astro Pi project (Honess & Quinlan, 2017).

RPi cameras are commonly used within the scientific community. A comprehensive radiometric characterisation of the image performance has been performed on the RPi V2.1 camera module as a baseline for scientific and engineering purposes (Pagnutti et al., 2017). Raspberry Pi V2.1 camera module has also been demonstrated to monitor *C. elegans* in an automated visual monitoring system (Puchalt et al., 2019).

4.5.3 Sizing the *C. elegans* against the IMX219 RPi camera sensor

It was helpful to visualise what will be imaged on the sensor to assist with the lens selection. The RPi v2.1 camera has a 3.67 mm x 2.76 mm IMX219 CMOS camera sensor (Raspberry Pi Foundation, 2022). Each pixel is sized at 1.12 µm in a full sensor resolution of 3280 x 2464 pixels, capable of imaging still image at 8 Megapixels.

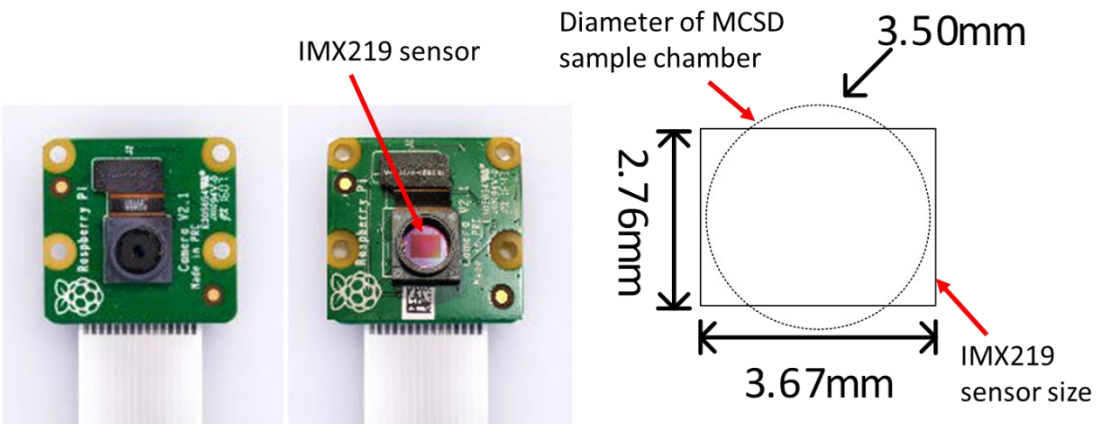

Figure 4-4. Image of RPi v2.1 camera with original lens removed to expose the IMX219 sensor[1].

[1] The image on the right is the diameter of the individual MCSD sample chamber imposed on the IMX 219 sensor.

Comparing the size of the MCSD sample chamber against the IMX219 sensor shows that a 1:1 image can be captured directly on the camera sensor. The far-right of Figure 4-4 shows the comparison between the size of the MCSD sample chamber against the IMX219 sensor. The MCSD sample chamber will house the *C. elegans,* and in a 1:1 image on the sensor, the horizontal field of view (FOV) can capture the full width of the sample chamber with C. elegans inside it. One limitation would be the sample chamber's top and bottom width (vertical FOV) since a 1:1 image is beyond the sensor's size. One mitigation strategy could be reducing the magnification and bringing the sample chamber's vertical and horizontal FOV inside the sensor.

An adult *C. elegans* has an average length of 1000 µm and 100 µm in diameter (Altun & Hall, 2009). A simplistic argument shows that a 1:1 image of a *C. elegans* with a length of 1000 µm on the sensor can be captured directly. 1000 µm can contain approximately 893 pixels (1000 µm divided by 1.12 µm pixels). This is a considerable pixel count and should be sufficient to resolve the *C. elegans.*

4.5.4 Lens selection

There are many lenses in the market, making selecting them not a straightforward task. To begin with the selection, the 4x magnification telecentric lens from BAMMsat 1st gen. flight model (FM) microscope was reviewed. The overall length of the lens was 51.06 mm and had a working distance of 40 mm, making the distance of the optical system, i.e., the distance between the camera sensor and the object greater than 90 mm.

The 1st gen. optical performance was chosen to resolve a single mammalian cell in culture and required high magnification. For BoB flight, the optical performance is excessive to image *C. elegans*. It also has a large working distance, limiting the flexibility to configure the other subsystems. The magnification also meant that the captured images would not image the sample chambers' entire FOV, reducing the number of *C. elegans* being imaged. The telecentric lens was discarded as a viable option considering these factors.

The second lens option considered was a 1:1 image relay lens. A simple assessment in section 4.5.3 shows that a 1:1 image is possible since the FOV size of the object in focus can be mostly captured within the IMX219 sensor size. A relay lens extends the imaging system by relaying the image from the object onto the sensor.

$$FOV = 2 \times WD \times tan\left(\frac{AFOV}{2}\right) \quad \textbf{Equation 4.1}$$

$$m = \frac{H}{FOV} \quad \textbf{Equation 4.2}$$

$\mathrm{FOV} = \mathrm{Field\ of\ view}$

$\mathrm{WD} = \mathrm{Working\ distance}$

$\mathrm{AFOV} = \mathrm{Angular\ field\ of\ view}$

$\mathrm{H} = \mathrm{Image\ height}$

$\mathrm{m} = \mathrm{magnification}$

It is possible to overcome the limitation of the 1:1 image and capture the sample chamber's entire vertical and horizontal FOV. This can be achieved by shortening the distance of the back focal length, which increases the working distance. The resultant changes increase the field of view, focusing on the whole sample chamber. This relationship is described in Equation 4.1 and can be visualised in Figure 4-5. Changing the FOV also impacts the magnification, as shown in Equation 4.2. The key message from understanding this relationship was that it is possible to have a fixed focus lens providing enough clearance on both sides of the lens in the z-direction, see Figure 4-3.

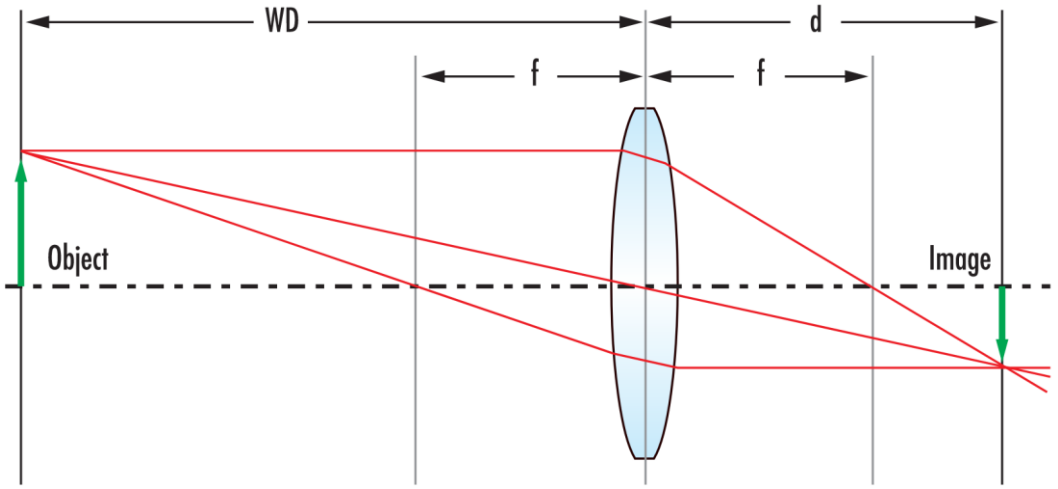

Figure 4-5. Image showing the relationship between working distance (WD) or object distance, focal length, and image distance (Edmund Optics, 2022b).

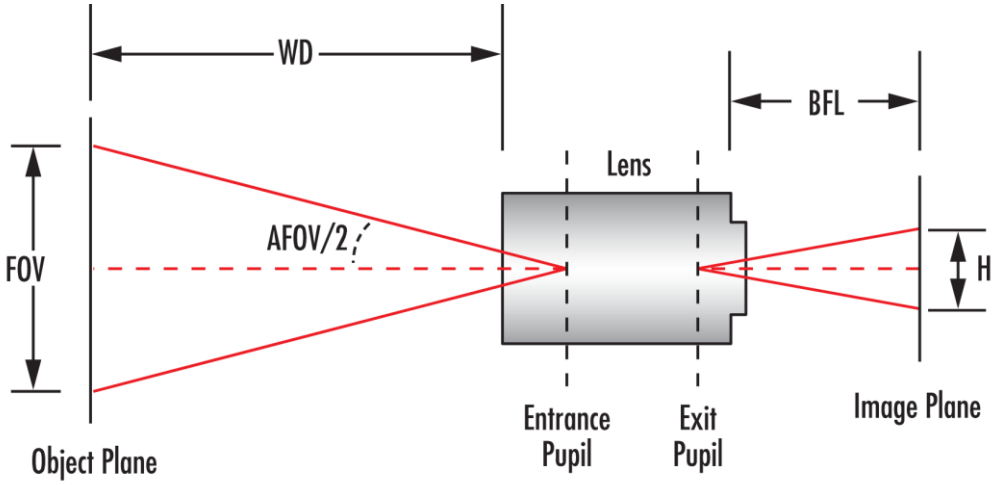

Figure 4-6. The illustration describes an extension of the relationship shown in Figure 4-5 (Hollows & James, 2022).

This relationship is commonly used since the WD (working distance), and BFL (back focal length) are stated at the lens housing for pragmatism during testing. The rest of this chapter will use the terminology from this image to describe WD.

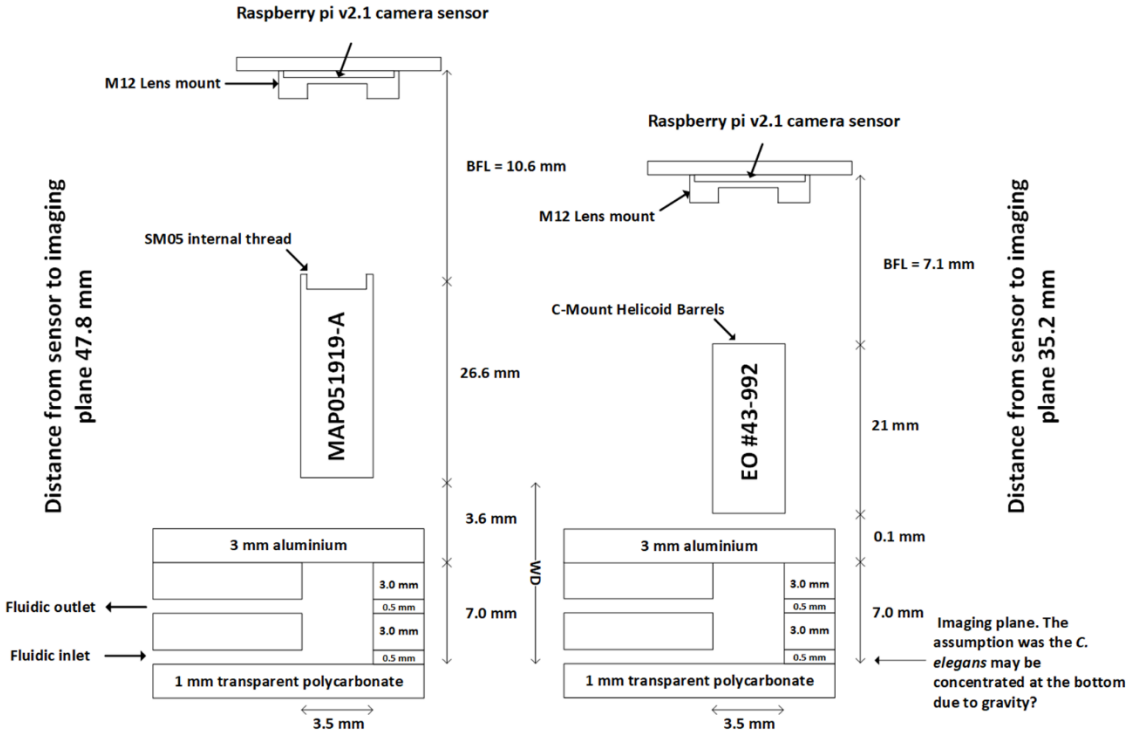

Figure 4-7. Illustration made to visualise the distance between two 1:1 image relay lenses for comparison.

Two major optical component suppliers were used to find the 1:1 image relay lens to simplify the search for lenses. The two suppliers were Edmund Optics and Thorlabs. The investigation identified the two most miniature 1:1 image relay lenses: MAP051919-A (Thorlabs) and EO #43-992 (Edmund Optics).

Illustrations were made to size the distance between the object and the sensor to help visualise the optical system (see Figure 4-7). The image showed that the Thorlabs lens resulted in a lengthier optical system than Edmund Optics. However, the Thorlabs lens provides flexibility in the design. In contrast, the Edmund Optics lens could not increase magnification since it will hit the top aluminium layer of the MCSD with only 0.1 mm clearance.

Table 4-1. Summary of key parameters to compare the two 1:1 image relay lens.

	Thorlabs MAP051919-A	EO #42-992
Lens housing	26.6 mm	21.0 mm
WD	10.6 mm	7.1 mm
BFL	10.6 mm	7.1 mm
RMS spot size	16.5 µm	281.7 µm
Focal length (f)	19.0 mm	14.0 mm

Another significant difference in the optical performance is the RMS spot size in Table 4-1. Since RMS spot size measures expected resolution and includes all aberration, it can be used as a gauge for final resolution. In this case, the Thorlabs lens can be expected to have significantly better resolution. In conclusion, the Thorlabs lens was decided as the primary lens for further testing.

4.6 Initial design and test (V1)

4.6.1 Initial design (V1)

This section discusses the initial design of the compact brightfield microscope (V1). The initial design was completed by selecting and integrating the Thorlabs MAP051919-A lens into the CAD design of the 2nd gen. BAMMsat bioCubeSat payload (see the left image of Figure 4-8). During the BoB mission, the development of various subsystems was pursued in parallel to ensure that the mechanical and electrical design fit within the allocated clearances and tolerances.

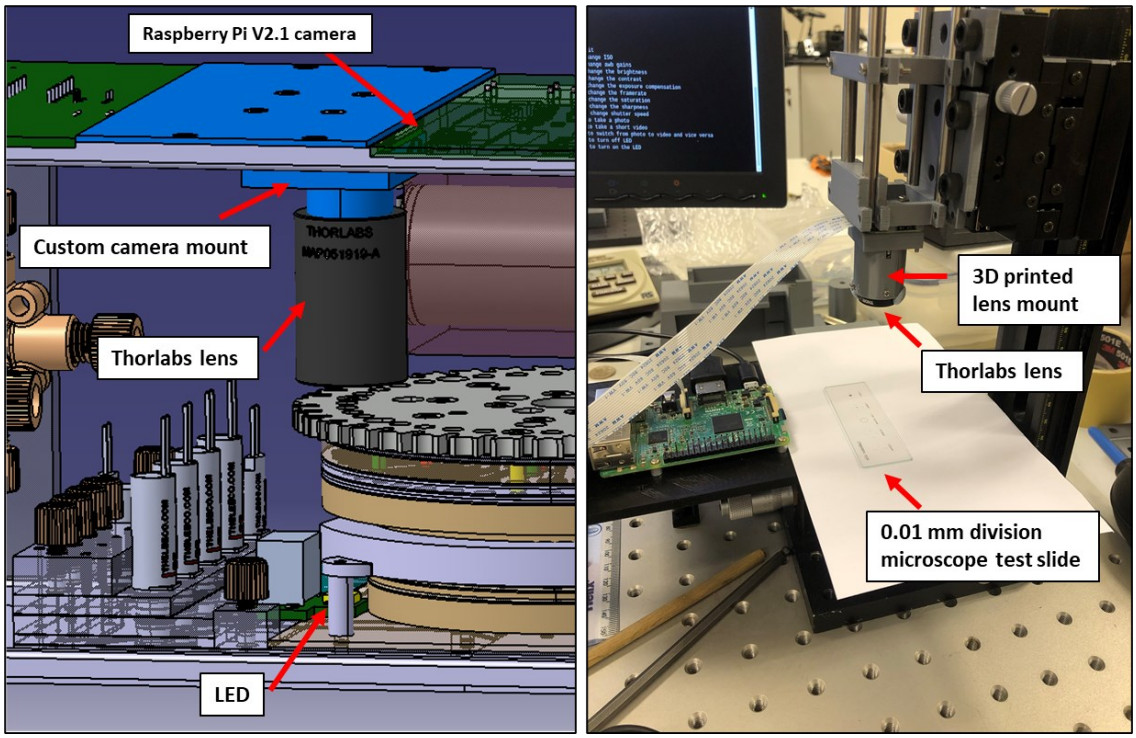

Figure 4-8. Left – CAD image of the initial design of the compact brightfield microscope (v1) inside the 2nd gen. BAMMsat bioCubeSat payload. Right – Optical test bench setup.

The initial design of the compact brightfield microscope consisted of an (i) RPi v2.1 camera, (ii) custom camera mount, (iii) Thorlabs MAP051919-A lens and (iv) white-light LED (CLN6A-WKW-CJ0L0153; CREE). The Rpi v2.1 camera had its original lens removed to expose the sensor; see Figure 4-4 for reference. A custom camera mount was designed to interface the lens with the sensor.

Although it is possible to procure a Rpi v2.1 camera with a standard M12 mount, a compact interface between the internal M12 thread and to internal SM05 thread was not available off the shelves. See Figure 4-7 on the illustration to visualise the interface required within a 10.6 mm length. A custom camera mount was designed and machined from aluminium to provide the flexibility to change the BFL distance. The external SM05 thread will be cut / formed using an SM05 thread die on the camera mount. The BFL distance could then be adjusted by screwing and unscrewing the Thorlabs lens. Note that, during breadboard testing, the camera mount was 3D printed; see the right image of Figure 4-8.

The 5V white LED was selected based on the brightness and packaging format. The baseline for brightness was a luminous flux of 80 lumens; it was based on one of the microscopes in the University of Exeter's biological laboratory. The brightness of the cool white LED can be controlled by varying the forward voltage between 2.2 V to 4.4 V, which corresponds to 60.5 to 101.8 lumens, respectively, as stated on its datasheet.

Adjusting the brightness is useful during testing to avoid oversaturation on the image sensor. The LED was a single surface-mounted LED with a packaging format of 5050 (5 mm × 5 mm in size). The size ensured that the entire width of the 3.5 mm sample chamber would be fully illuminated.

4.6.2 Initial test – Resolving *C. elegans*

An initial test was performed on an optical test bench to evaluate the optical performance of the initial design. The test objective was to ensure that *C. elegans* could be imaged. The sensor's centre was aligned with the centre of the target sample chamber, and the lens's entrance pupil was mounted perpendicular to the imaging plane; see left image Figure 4-8 for the experiment setup. The first variable during the test was the BFL distance which impacted the FOV and magnification. The second variable was the WD which changes with the BFL distance

4.6.2.1 Results and discussion on initial testing (V1)

Figure 4-9 shows the results from the first optical performance test with the initial design (v1); see the left image of Figure 4-8. The initial design was conducted to identify any immediate issue and verify if the design was functional, i.e., can the lens and the sensor image the *C. elegans*. The experiment was set up using an optical breadboard, micrometre translation stage, 3D printed camera mount, Thorlabs lens, and a micrometre test slide (MH-SM05; MUHWA). The experiment setup can be referred to in the right image of Figure 4-8.

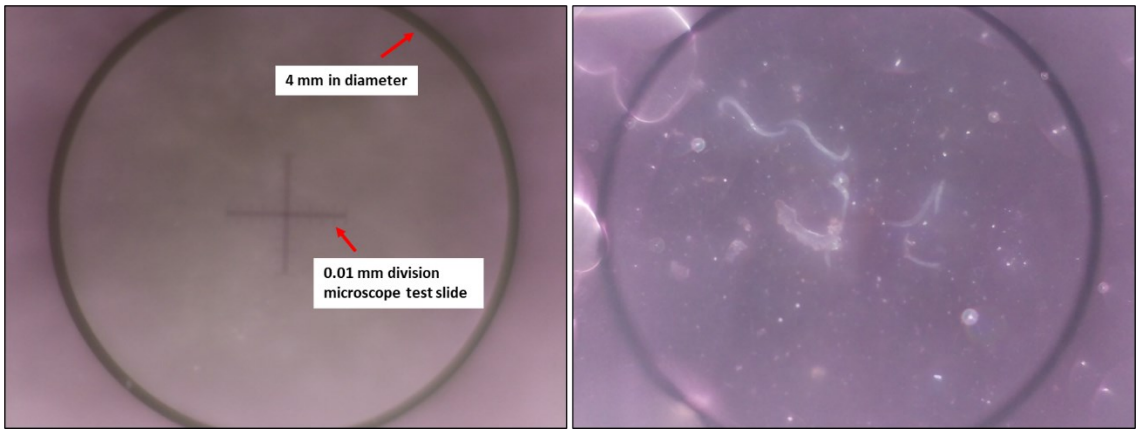

Figure 4-9. Images of result from capturing micrometre test slide and *C. elegans*[1].

Based on the left image of Figure 4-9, the results showed that the design was able to capture the 4 mm diameter circle feature of the micrometre test slide. This means that for an MCSD sample chamber with a 3.5 mm diameter circle, the initial design (v1) should have the FOV with the entire sample chamber within the image since the 3.5 mm circle will sit within the 4 mm circle.

The image on the right continued the test in the same experimental setup. The only difference was that a microscopic slide with dried down *C. elegans* was placed underneath the micrometre test slide. The image showed what could be expected as the final result, i.e., *C. elegans* inside a 3.5 mm sample chamber

[1] Left - Image of the micrometre test slide from the initial test. The cross in the middle has a length of 1 mm in both directions, with a 4 mm circle being a feature of the test slide. Right – Image of micrometre test slide on top of a dried down *C. elegans* microscopic slide, using the same experimental setup. Note that a typical length of an adult *C. elegans* is 1 mm.

(note that the darker circle was the 4 mm feature of the micrometre test slide). The right image showed a dark field microscopy effect since the photon came from a standard overhead laboratory ceiling fluorescence strip light instead of a light source directly underneath the microscopic slide.

The result shown in Figure 4-9 from the initial test was promising since it was possible to quickly image the dried down adult C. elegans. Note that the initial test was performed to verify the functionality of the initial design rapidly; hence the BFL and WD were not recorded. The subsequent tests were performed with distances representing the flight model configuration with a white light LED underneath the target sample. See the right image in Figure 4-10.

4.6.2.1.1 Issue with focusing distance

Subsequent tests highlighted a limitation with the initial design. The initial design was not flexible to modify the FOV, and magnification inside the flight model constrained volume. During the test performed by varying the BFL and WD, adjusting the FOV and magnification will involve moving the Thorlabs lens up and down in z-direction, i.e., changing the BFL distances and finding the required WD by changing the spacers.

After a series of tests varying the WD and BFL distances, the test identified a limitation with the design. The issue was in the total length of the optical system, i.e., the distance between the sensor and the imaging plane. The test showed that the length required to focus the image with a smaller FOV (higher magnification) meant that the mechanical mounting was beyond the top of the 2U pressure vessel; see the right image in Figure 4-10. The total length of the optical system was constrained by the volume envelope of the 2U pressure vessel. The solution was to find an extra 5 mm of length, i.e., adding the 5 mm to the length of the total optical system to provide the flexibility of changing the FOV and magnification. The challenge was adding the 5 mm without going beyond the 2U volume envelope.

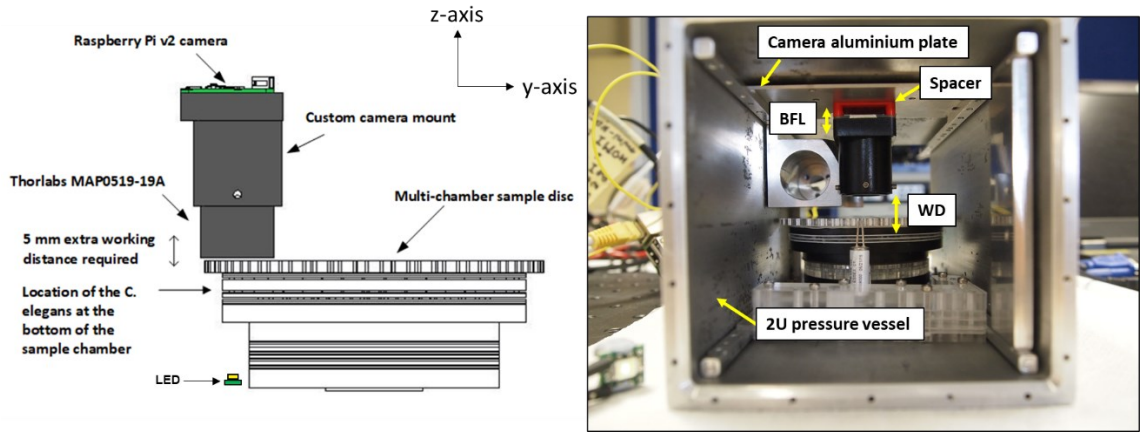

Figure 4-10. Images highlighting the issue with focusing distance[1].

The initial design fits within the 2U pressure vessel with a fixed FOV and magnification. However, at this stage of the development of v1, a test using a live *C. elegans* was not yet conducted because the source of *C. elegans* came from the University of Exeter and was not readily available. After some discussion, it was believed that the flexibility of changing the optical parameters was justifiable since a full system test was never performed, and constricted design could cause an issue in future testing in finding the optimum distances to resolve the *C. elegans*. The modification made to the optical system is discussed further in section 4.6.2.2.

[1] Left – Initial design (v1) test highlighted that the setup required an extra 5 mm working distance (WD) to focus the object, i.e., adding 5 mm to the length of the total optical system. Right – Image of the compact brightfield microscope (v2) during the mechanical fit check representing the WD and the BFL to help the reader visualise the flight model.

4.6.2.2 Modification on the lens housing to increase the optical system length

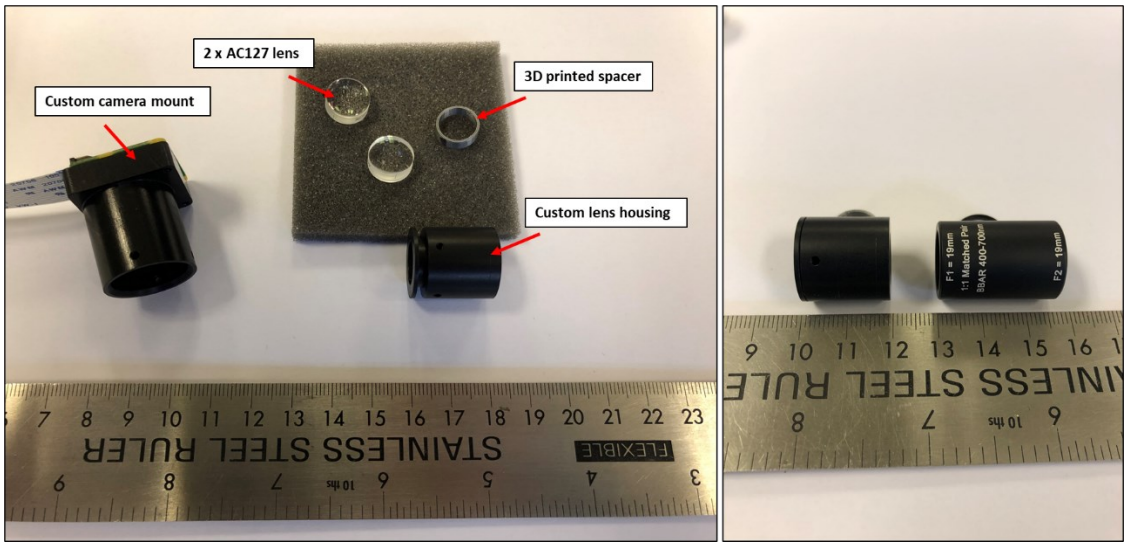

Figure 4-11. Images of custom compact brightfield microscope housing[1].

The challenge in increasing the optical system length was to modify an already constricted design. At this stage of the project, changing the optical system has the least impact on the rest of the 2nd gen. BAMMsat bioCubeSat payload.

After analysing the CAD and reviewing the Thorlabs datasheet, it was apparent that there was a 4 mm space between the two lenses inside the Thorlabs lens. The Thorlabs lens comprised two AC127 lenses in a Thorlabs' custom lens housing; see Appendix C for the datasheet. It was assumed that the optical function of the 4 mm gap was to collimate the photons.

It was suggested that the length of the optical system could be increased by reducing the length of the lens housing. In doing so, the distance between the lens housing to the imaging plane can be shortened without the lens housing hitting the top aluminium layer of the MCSD; see the left image of Figure 4-10. Regarding the photon collimation from the 4 mm gap, it was hypothesised that

[1] Left – Image of the dissembled lenses from the Thorlabs MAP051919-A lens with custom camera mount and the lens housing. Right – Comparison between the custom lens housing against the original Thorlabs lens with a 7 mm difference.

providing the lenses were parallel, it should still be functional. A test with a 3D printed lens housing was performed, and the result verified that shortening the 4 mm gap did not produce a noticeable effect in the image. See Figure 4-13 and Figure 4-15 for the modified lens results.

The design modification was made by manufacturing a custom lens housing (based on the 3D printed prototype) that shortens the 4 mm gap and the ends of the Thorlabs housing; see the left image of Figure 4-11 for lens housing. The AC127 lenses were removed from the Thorlabs housing and placed inside the new housing. A 3D printed spacer was added to avoid the two lens surfaces coming in contact and becoming scratched. The polylactic acid 3D printed spacer was fabricated using fused-deposition modelling via Prusa i3 MK3S and tested iteratively before settling for a 3.2 mm spacer; see the left image of Figure 4-11 for the spacer.

A custom camera mount was designed and manufactured for a more robust mechanical interface between the new lens housing, the camera sensor, and the rest of the system. The camera mount and the lens housing were manufactured from Aluminium 6061T6, and black anodised to absorb stray photons. See Appendix E and Appendix F for the specifications of the custom mount and lens housing.

4.7 Final design and test (V2)

4.7.1 Summary of the final design

The following section summarises the final design of the compact brightfield microscope (V2), ready to be tested with the 2nd gen. BAMMsat bioCubeSat payload.

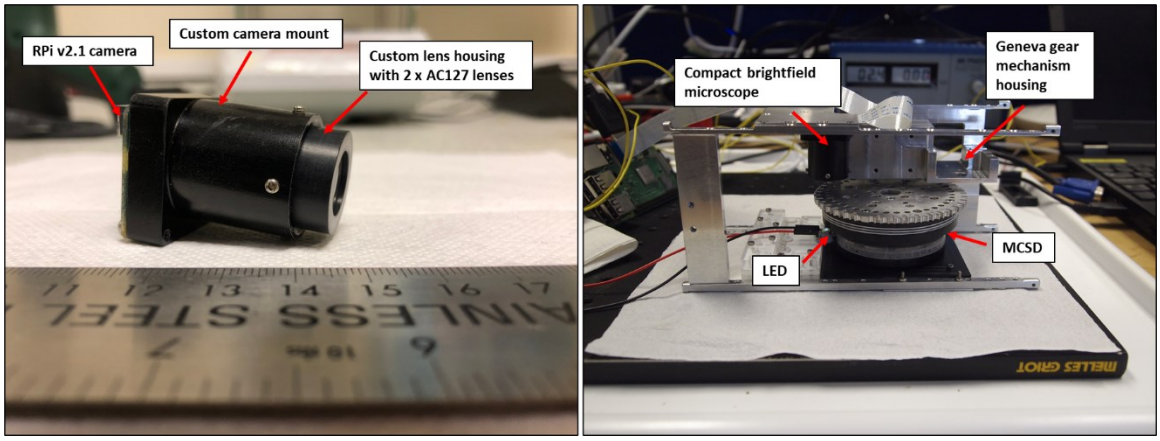

Figure 4-12. Left – Image of the fully assembled compact brightfield microscope. Right - Mechanical fit check and image capture test assembled in the 2nd gen. BAMMSat bioCubeSat payload.

The compact brightfield microscope was manufactured using a combination of RPi v2.1 camera, a custom camera mount, 2 x AC127 lenses inside a custom lens housing, and a 5V white LED as the illumination source. The fully assembled compact brightfield microscope can be seen in the left image of Figure 4-12.

The custom camera mount provided the mechanical interface between the RPi v2.1 IMX219 camera sensor and the custom lens housing. Both camera mount and lens housing were manufactured using aluminium 6061T6, and the aluminium was black anodised to absorb stray photons during imaging. The lens housing can be inserted into the camera mount with a sliding fit tolerance. Grub screws were used to secure the lens in place with the required BFL distance; see the left image of Figure 4-12.

4.7.2 Characterising the optical performance

Two tests were performed on the optical test bench to help characterise the optical performance. The information gathered from these tests helped gauge the final optical performance during the full system test performed in Chapter 8.

4.7.2.1 Results from brightness test on (V2)

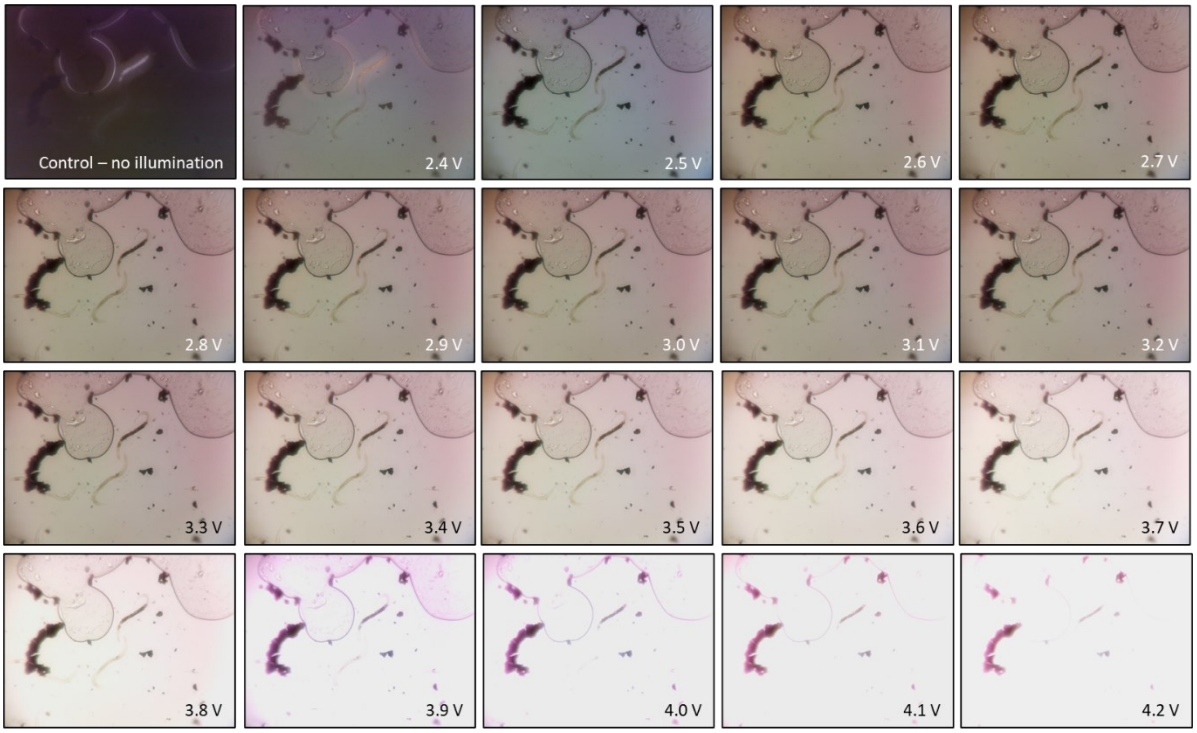

Figure 4-13. Brightness test captured with flight model LED (CREE) at an LED supply voltage ranging from 2.4 V to 4.2 V.

A brightness test was performed to inform the voltage supply required for the LED PCB electrical design. The test was captured at a set working distance (WD) and back-focal length (BFL); see Figure 4-14 for the optical setup used. The results showed that the optical system was sensitive to varying brightness with a tolerance. The voltage tolerance where the optical system was still able to image the *C. elegans* was between 2.5 V to 3.8 V, as shown in Figure 4-13. At 3.9 V, the image was oversaturated by the white light intensity. Interestingly, the control image (no illumination with the LED off) and 2.4 V showed results similar to a darkfield microscopy effect. The test setup was not performed in a dark room,

which meant that scattered light from a standard overhead laboratory fluorescence light caused such an effect.

4.7.2.2 Results from the depth of field test on (V2)

The depth of field test was performed with two objectives. The first objective was to confirm the optical system length of the final design would fit within the 2U volume envelope of the 2nd gen. BAMMsat bioCubeSat payload. The second objective was to measure the total depth of field of the compact brightfield microscope. Understanding the depth of field informs the tolerances required in mechanical mounting, especially on the z-axis.

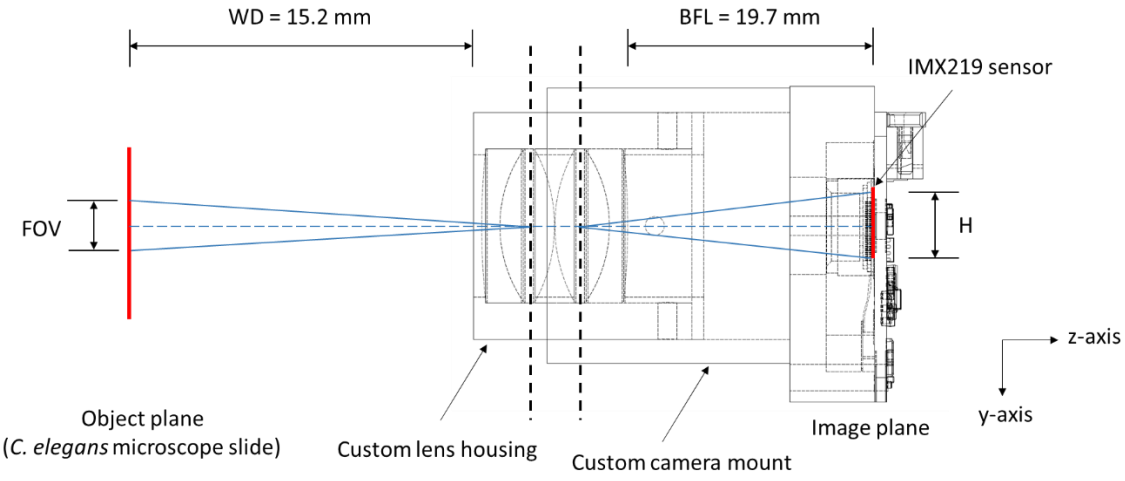

Figure 4-14. Optimised optical setup to focus the object with the required FOV.

The test confirmed that the optical setup could focus the object within the 2U envelope. The modification made to increase the optical system length provided the flexibility for the custom lens to get closer to the object without the lens colliding with the MCSD, see section 4.6.2.2. The ability to adjust the custom lens provided the flexibility to change FOV and hence magnification of the object.

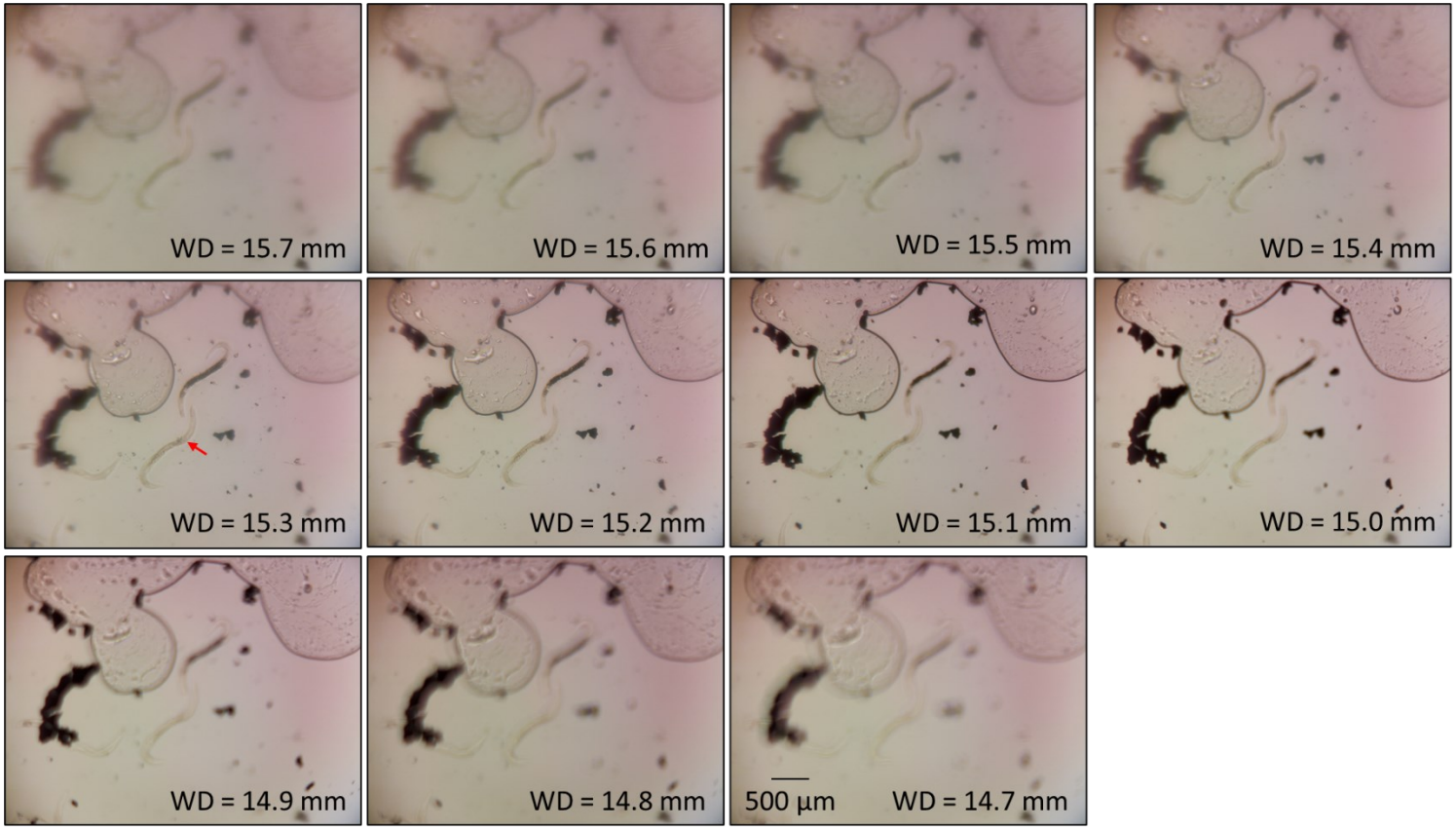

Figure 4-15. Depth of field test with an image taken at an increment of 0.01 mm.

Referring to Figure 4-15, LED illumination was set at 3.3 V. The scale is representative in the last image (bottom right). The C. elegans is marked by the yellow arrow in WD 15.3 mm. The focus quality was confirmed via visual observation.

The depth of field test was performed by varying the WD incrementally at 0.1 mm steps to image the dried down *C. elegans* microscopic slide. The setup fixed the BFL distance to have the FOV inside the 3.5 mm sample chamber. The edge of the sample chamber is indicated by slight blurry darkening in the lower left and upper left of the images in Figure 4-15. The results showed that the depth of field is approximately 0.7 mm, as indicated between the WD 15.7 mm to 15.0 mm; see Figure 4-15. The focus quality was determined by visual observation and judged by the ability to resolve the *C. elegans'* movement. From the results, the compact brightfield microscope has a tolerance of 0.7 mm to variation in the z-direction.

4.8 Verification matrix

This section is added to assess the requirements set for the compact brightfield microscope. Generally, the tests performed demonstrated that most of the requirements were verified except for two partially verified requirements (see Table 4-2. The requirements were partially verified since there was an issue with focusing the *C. elegans* during the full-system test. Detailed discussion and results can be referred to in section 4.9.1, section 9.4.1, and section 8.7.2.2.3

Table 4-2. Verification matrix for compact brightfield microscope.

Functional requirements		**Status**
FC-03 100c	The system shall take and log static images and video of the C. elegans inside the MCSD via an imaging system during pre-flight operation and experiment operation to evaluate the health status of the C. elegans.	**Verified**
FC-03 200c	The system shall be able to take and log videos of a chamber while the last media is being replaced.	**Verified**
Performance requirements		
PR-07 100	The system shall take and log static images of the C. elegans with a resolution of 0.025 mm over C. elegans with at least 3280 x 2464 pixels.	**Partially verified** The microscope can capture the image with the required performance; however, there is an issue with focusing in full system configuration, see Figure 8-13
PR-07 200	The system shall capture and log video with a minimum resolution of 0.075 mm over C. elegans with at least 1080 x 1920 pixels.	**Partially verified** Similar issues occured as mentioned above.
PR-07 210	The system shall capture and log video with a minimum of 30 images per second.	**Verified**
Design requirements		
DG-03 201	The imaging plane on the MCSD should be parallel to the direction of gravity.	**Verified**
DG-04 100	The dimension of the pressure vessel shall not exceed a 2U CubeSat format.	**Verified**

4.9 Discussion, conclusion, and future work

4.9.1 Discussion and conclusion

Chapter 4 discussed the research and technological development of the compact brightfield microscope during the PhD. The compact brightfield microscope was explicitly developed for the BAMMsat-on-BEXUS (BoB) mission to capture images and video of the *C. elegans'* mobility and motility during the BEXUS 30 flight campaign. The captured data will be used to assess the health of *C. elegans* to confirm the functionalities and demonstrate the technology of the 2nd gen. BAMMsat bioCubeSat payload during technological demonstration mission onboard BEXUS 30.

After evaluating the previous 1st gen. microscope to assess its feasibility and extract lessons learned. The concept of simpler brightfield microscopy was selected since the 1st gen. microscope was too large to fit within the 2U volume envelope, and the fluorescent capability was not required. A simpler optical system based on brightfield microscopy was selected as the leading concept.

The Thorlabs MAP051919-A lens was selected as an initial lens solution; see section 4.5.4. However, testing showed that the initial design lacked flexibility in adjusting the FOV and magnification. Increasing the magnification (reducing the FOV) meant that the total length of the optical system was beyond the 2U volume envelope. A modification was made to the Thorlabs lens by extracting the two AC127 lenses and shortening the distance between the two lenses. The resultant test showed no observable difference between the two lenses. However, further rigorous testing, such as the Modular Transfer Function (MTF) test, will be required to confirm the hypothesis. There is a series of standardised tests within the optical field to evaluate an optical design's performance. However, it was not possible to perform them within the time constraint of the PhD research and the BoB mission.

After the PhD, a more rigorous test will be required to characterise the optical performance. The testing performed during the PhD was based on pragmatism and practicality. The tests were conducted primarily to test the optical distances required to ensure that the compact brightfield microscope fit into the 2U volume envelope and optimise the FOV and magnification. The lack of standardised testing limits the ability to quantify these optical parameters.

As an example, it was challenging to grasp the optical resolution performance. The depth of field test provided some insight based on visual observations, but it was not enough to quantify the resolution. It was challenging to compare the performance of the optical system with other lenses. It was also challenging to quantify the difference between the initial Thorlabs MAP051919-A lens against the modified custom lens.

In this case, the Modular Transfer Function (MTF) test will be helpful. A Modular MTF is a measure of true and effective resolution since it accounts for blur and contrast over a range of spatial frequencies. The information can help predict how various object magnifications affect resolution, and it can also quantify resolution for an object with different sizes and opacity. For a reader who would like to read more on this topic, Edmund Optics has an introductory resource to MTF (Edmund Optics, 2022a).

Another test on the impact of brightness on the image was performed to evaluate the flight model LED illumination. The aim was to find an optimum brightness that allows the compact brightfield microscope to image without oversaturating the image. The test can be referred to in section 4.7.2.1. In addition, evaluating the voltage (brightness) informs the electrical design for the LED PCB.

Figure 4-16. Cropped and zoomed-in image of dried down *C. elegans* microscopic slide.

The LED is rated at 5V. The result from the test indicated that the image can still be resolved between the voltage of 2.5 V to 3.8 V before oversaturation; see Figure 4-13. The result provided the brightness tolerance for the flight model, which was between 2.5 V and 3.8 V. It also highlighted that beyond 3.8 V, the sensor became oversaturated. Using visual observation, it was decided that the ideal illumination was at 3.4 V; see Figure 4-16. The image was captured at WD 15.2 mm and BFL=19.7 mm at 3.4V. Illumination was provided by flight model LED, which was CLN6A-WKW-CJ0L0153 from CREE.

Based on this result, the flight model illumination for the BoB system was set at 3.3V. The reason for this selected voltage was to interface with the BoB system's electrical design. The BoB system was built with COTS sensors and actuators, which required typical voltages of 12 V, 5 V and 3.3 V, stepped down from 28 V

using a DC-DC converter. For this reason, the 3.3 V was selected since it was within the voltage tolerance based on the brightness test.

The second optical performance test, the depth of field test, showed that the compact brightfield microscope has a relatively short depth of field at 0.7 mm; see section 4.7.2.2. A depth of field of 0.7 mm could be challenging for a fixed focus lens system. It means that a tight mechanical tolerance (increased manufacturing cost) is required to ensure that the optical system object plane is at the targeted object plane.

In the final configuration, there is variation in thickness of the optical system and the MCSD due to machining, manufacturer tolerance in the material, the thickness of the optical window, variation in the thickness of the *C. elegans*, and behaviour of the *C. elegans* (i.e., *C. elegans* either lie flat or loop away from the surface). The list highlights potential optical system issues that require tighter control during manufacturing and assembly.

The compact brightfield microscope captured *C. elegans* in detail with an optimum setting, revealing its inner anatomical structure, as shown in Figure 4-16. The image was captured after optimising the WD, BFL distance, FOV, and illumination. The image showed a promising optical setup. However, it may be more challenging to achieve such image quality in the flight system for reasons mentioned in the previous paragraph. The flight system will not only have issues with mechanical tolerance. The chamber will also be filled with growth media, which will change the refractive index. In this test, the image was captured using a dried down *C. elegans* microscopic slide, i.e., fixed and immobile. In the flight model, the live *C. elegans* will be moving either along or across the object plane.

In conclusion, the research during the PhD has resulted in a compact brightfield microscope ready for the BoB mission. The optical system fits within a 2U volume envelope, and initial testing showed a promising optical performance with a concerning depth of field of 0.7 mm. It is also worth highlighting that the test was performed on a dried down *C. elegans* microscopic slide that does not represent the flight model.

In the flight model, the optimum object plane is located inside the sample chamber on the top side of the 1 mm polycarbonate layer of the MCSD (see L7 in Figure 3-17). The object plane here was selected, assuming that the *C. elegans* would sink to the bottom of the sample chamber due to gravity. This assumption will be determined during the full system testing in Chapter 8. The sample chamber will also be filled with live and mobile C. elegans and growth media, further changing the optical parameters.

The ideal design solution would be to have an optical design with the depth of field equating to the depth of the chamber. This design would allow the *C. elegans* to be imaged generally through the chamber. However, this design was much more challenging and not considered for the 2nd gen system. Unfortunately, further iteration was not feasible due to time constraints within the BoB mission. This design consideration should be an input for the next generation. The choices are also dependent on the biological system and the science questions.

The compact brightfield microscope development will be continued in the full system testing discussed in Chapter 8.

4.9.2 Future work

Immediate future works would include further testing and quantification of the optical performance of the compact brightfield microscope.

- Perform Modular Transfer Function (MTF) testing to quantify the optical resolution performance of the compact brightfield microscope.
    - MTF is a standard test used in describing a performance of an optical system and can be used to compare optical design. This will be useful to optimise the 2nd gen. compact brightfield microscope. MTF can be performed by capturing a series of sine-wave targets with increasing spatial frequency ($\frac{lp}{mm}$). A typical sine-wave target is the 1951 USAF target. The measured contrast is plotted against spatial frequency to produce the MTF curve. A high value of MTF, >50%, indicates high contrast and the image is well resolved to

evaluate the result. A low MTF, <20%, shows poor contrast and the image is blurred, resulting in a loss of resolution

- Perform ray-tracing simulation for comparing the Thorlabs MAP051919-A lens against the modified custom lens.
    - The optical simulation could have helped predict the light rays' behaviour when changing the parameters during the development. This test aims to evaluate the impact of reducing the Thorlabs lens length into a custom lens. For instance, if it introduced light aberration into the system. The simulation can be performed using optical design software and the optical ray trace diagram of the AC127 lenses from the manufacturers. This is often provided in a Zemax "black box" format. The simulation can vary the distance between the AC127 lenses to evaluate the rays.

Long-term future work would include the tasks below.

- Perform ray tracing simulation and test in varying the size of the aperture to evaluate its impact on the image depth of field.
    - One of the immediate issues with the design is the shallow depth of field of < 1mm. This result in challenging optical tolerance control. Theoretically, it is possible to increase the depth of field by reducing the aperture size. The optical simulation could provide information if changing the aperture will have a larger depth of field for the next generation.
- Perform dept of focus testing to measure the sensitivity of the compact, bright field microscope.
    - Depth of focus could help explain how the quality of focus changes on the sensor side of the lens is moved while the object remains in the same position.
- Develop a fluorescence capability for a future spaceflight model, building from the 1st gen fluorescence microscope.

5 Subsystem level – 2nd gen. fluidics subsystem: Design, manufacture, and test

5.1 Introduction

This section discusses the research and development work on the 2nd gen. fluidics subsystems in preparation for assembly, integration, and testing (AIT). The AIT will be performed as part of the 2nd gen. BAMMSat bioCubeSat payload. Most of the test conducted in the section was built from a lower-level fluidic subsystem, such as actuators and sensor, to verify their functionality and inform the design of the 2nd gen. fluidics subsystems.

The research conducted in Chapter 5 was challenging since the development was performed at intervals and mixed with fixing issues associated with the MCSD (see Chapter 3) and compact brightfield microscope (see Chapter 4). Due to this reason, it was challenging to implement a thorough testing plan, and the strategy was to test rapidly and iteratively to meet the BoB mission milestones.

Chapter 5 captures the development of the fluidic subsystem and how testing influenced its final design in preparation for the BoB mission. The fluidic subsystem is a critical component of the BAMMsat concept and was constructed of actuators and sensors, which enable the ability to perturb the samples to change the state of the biology by pumping reagents. For example, a drug reagent could be pumped into a cell culture to monitor the responses in microgravity. The fluidic subsystem for the BoB system built upon the concept developed for the 1st gen. BAMMsat bioCubeSat payload; see section 1.2 for historical context. The work performed during the PhD was to critique the 1st gen., review and select the actuators (i.e., pump, valves) and sensors and repackage them into a design that fits a 2U volume form factor.

5.2 Aim and objectives

1) *Evaluate and critique the 1st gen. design of the fluidic subsystem as an input into the 2nd gen. design*.

The objective was created to leverage the previous development work during the 1st gen. to extract any lessons learnt that will be valuable for the 2nd gen.

2) *Produce a list of requirements extracted from BAMMsat-on-BEXUS mission requirements*

This objective was added to produce a list of requirements from the BAMMsat-on-BEXUS mission

3) *To design, manufacture, and test the fluidic subsystem for the BAMMsat-on-BEXUS system*.

The fluidic subsystem is a key component of the BAMMsat concept. A version of the fluidic subsystem was required for the BoB system to supply growth media and reagents into the sample chamber.

5.3 Overview of 1st gen. fluidic subsystem

5.3.1 Introduction to the 1st gen. design

The 1st gen. fluidic subsystem was developed as part of the NSTP programme (see section 1.2 for historical context). The 1st gen. fluidic subsystem was composed of a pump, solenoid valves, multi-chamber sample disc (MCSD), rotary valve (RV), pressure sensor, liquid photosensor (bubble sensor), flow sensor, and media reservoirs. Along the fluidics pathways, chemical sensors (O_2 or pH sensor) were placed towards the end of the fluidic network to monitor the cell culture environment.

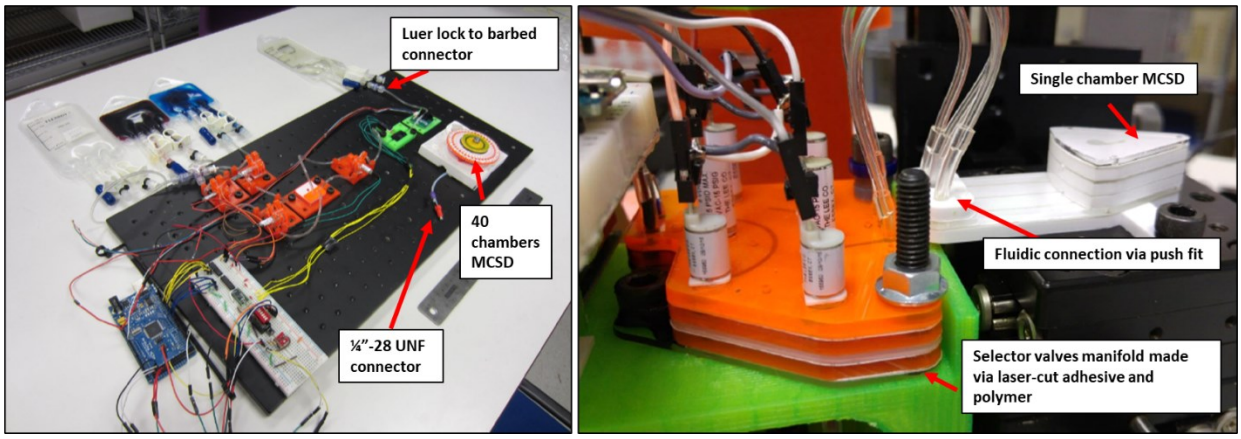

Figure 5-1. (Left) Image of 1st fluidic subsystems flatsat breadboard. (Right) Image of 1st generation selector valves manifold. Images courtesy of Prof Cullen with minor editing.

The image of the fluidic block diagram can be viewed in Figure 1-3 to visualise the entire subsystem. The following bullet points were added to contextualise the components within the fluidic subsystem.

- Fluidic pump (mp6; Bartels Mikrotechnick)

The mp6 fluidic pump is a miniaturised pump that was used to move fluids, either liquids or gasses, around the fluidic channels. For the BoB system, the pump was placed at the end of the fluidic network to minimise cross-contamination (see Figure 1-3 for the 1st gen. fluidic pathway). The pump will also be pulling liquids such as growth media and reagents.

- Solenoid valves (LHD series; The Lee Company)

The solenoid valves provided the ability to open and close fluidic pathways. Combining a 2-way or 3-way solenoid valve in a manifold enables advanced fluidic pathways to access various reagents and fluidic mixing in the fluidic subsystem.

- Multi-chamber sample disc (MCSD)

The MCSD is a custom component developed for BAMMsat to house the samples in separate chambers. See Chapter 3 for a detailed discussion and design.

- Rotary valve (RV)

The RV is another custom instrument developed for BAMMSat. Its design provided the unique functionality to address the sample inside the sample chamber independently. The RV is designed to be coupled with the MCSD and remove the need for individual tubing, valve, and electrical harnessing of each sample chamber. See Chapter 3 for a detailed discussion and design on MCSD and RV.

- Pressure sensors (HSC and ABP pressure sensor; Honeywell)

Pressure sensors provided information on the pressure across the fluidic system (see Figure 1-3) for visualisation. The 1st gen. BAMMsat bioCubeSat payload was a breadboard version used to provide detailed information on the fluidic system during lab testing. The design in the first generation had many pressure sensors across different locations in the fluidic pathways. The Honeywell pressure sensor was the selected component for the pressure reading. It is a miniaturised board-level liquid pressure sensor, ideal for miniaturised systems such as BAMMsat.

- Liquid photosensor (OPN350; TT electronics)

The liquid photosensor is a phototransistor sensor that can mount fluidic tubing. In the 1st gen., the liquid photosensors (bubble sensors) were placed at the beginning and the end of fluidic pathways to detect bubble formation, which could occur from the start of the fluidic pathways and travel across to the end of the

fluidic path. The aim was to understand how the system behaves or react with bubbles.

- Flow sensor (LPG10; Sensirion)

The flow in a fluidic network is vital information for any fluidic system. LPG10 is a planar microfluidic glass package and is one of the most miniaturised flow sensors. The 1st gen. was tested using the evaluation kit (EK-LPG10-1000), which came with a machined polycarbonate block that provided the fluidic interface and standard fluidic ports to the rest of the system (see Figure 1-2).

- O_2 sensor (EOM-02-mini; Presens)

The chemical sensor provides information on the cell culture environment. As the cells live in the sample chamber, they will experience metabolic activities and change the local environment. The selected chemical sensor in the 1st gen. is an in-line electro-optical sensor that measures dissolved O_2 gas. The sensor is placed at the end of the fluidic network to measure the dissolved gas once the liquid is pumped out of the chamber.

- CO_2 sensor (EOM-pH-mini; Presens)

Similar to the O_2 sensor, the sensor measures the dissolved CO_2 gas in the fluidic pathways. One of the critical drawbacks of the CO_2 and O_2 sensor is the volume (40 mm × 100 mm × 22 mm). The length equates to a total length of a 1U CubeSat. See Figure 1.3 for visualisation of the sensor inside a 2U pressure vessel.

The 1st gen. fluidic subsystem was developed into a breadboard version based on the 1st generation fluidic network design. The images of the breadboard and fluidic block of the 1st gen. can be viewed in Figure 1-2 and Figure 1-3, respectively. The breadboard helped de-risked the functionalities and the components of the fluidic system design.

Several fluidic tests were conducted during the NSTP programme. The results from the testing were used to inform the flight model design. Some examples of testing performed during the NSTP programme are listed below

i. Test to characterise the mp6 pump performance
ii. Test to characterise the LPG10-1000 flow sensor performance.
iii. Test to measure the pressure across the fluidic system.
iv. Test to characterise the mixing inside the sample chamber by performing a fluidic dispersion test.
v. Test the mixing capability and accuracy of the fluidic system.

The results from the test were helpful as an input to the 2nd gen. fluidic subsystem. The first two tests have direct input since the same pump, and flow sensor were used in the 2nd gen. design. The remaining test gave some insight into the fluidic performance. A direct comparison could not be made since there were significant design and material changes in the MCSD, RV, and selector valve manifold.

5.3.2 Evaluation and critiques on the 1st gen. design

During the NSTP programme, the design philosophy was to have the key components functionally representative of the flight model. Evaluating the design and component choices, most of the components were translatable to the flight model version onboard the BoB mission. In general, the main critique was the need to miniaturise the design. The complete evaluations, critiques and suggested solutions for the sensor, actuator and components are shown in Table 5-1.

Table 5-1. Summary of the evaluation and critique with a suggested solution for the 2nd gen. fluidic subsystem

Components	Evaluation & Critique	Remarks for the 2nd gen.
Mp6 pump	• The result from 1st gen. testing showed that the current pump is suitable for further testing.	• Further testing on the pump performance in the 2nd gen. MCSD and fluidic pathways will be required.
LPG10-1000 flow sensor	• The evaluation kit with the Sensirion software was suitable for rapid testing without a significant learning curve. • The volume of the polycarbonate manifold is too large for the 2U format. • The software interface is not suitable / optimised for the flight model.	• The 2nd gen. will require a custom manifold to house the sensor along the fluidic pathways.
Pressure sensor (HSC & ABP;	• The number of pressure sensors in the system was too many for a flight model (see Figure 1-3)	• In the flight model, the pressure sensor is primarily used to inform on the health of the fluidic system. The number of sensors can be reduced to a minimal quantity.
Chemical sensor (O_2, CO_2, pH)	• The sensor volume was relatively large compared to the volume of the 2U pressure vessel.	• Due to the large volume, the flight model can only house one type of chemical sensor. • For the BoB mission, a chemical sensor was not required since it was beyond the scope of mission objectives.
Liquid photosensor (OPB350)	• The 1st gen. used a self-calibrating circuit board with a larger volume than a version with only the sensor. • Testing for bubble presence is useful during bench testing. In the	• For the 2nd gen. during the BoB mission, the liquid photosensor could be used as a sensor to confirm the fluidic pumping of different reagents.

	flight model, detecting bubble presence won't be as useful as removing the bubble using a bubble trap.	• The sensor can output a ratiometric analogue reading. Further testing will be required to see if the different media have large voltage reading variations between the growth media and reagents.
LHD solenoid valves	• The 2-way solenoid valves and 3-way solenoid valves are both non-latching. A constant supply of power will be required to keep the port open. • Depending on the fluidic network design and flow rate. The cumulative power consumption could be significant.	• The non-latching solenoid valves were selected to avoid leaving them open in case of power failure, and it is a valid risk. However, the viscous force becomes dominant in a microfluidic system, and fluidic won't flow unless pumped. • For the 2nd gen., latching valves were chosen since there were many unknowns regarding the power consumption of the entire BoB system.
1st gen. selector valve manifold	• The selector valve manifold was constructed from the laser-cut pressure-sensitive adhesive (PSA) and polymer (PMMA). As discussed in section 3.4.2, there are drawbacks to using adhesive, with it being permanently assembled and reducing flexibility during AIT.	• The second gen. selector valves manifold will require repackaging the whole design into a 2U format, integrating the latching valves, and interfacing with the MCSD. Due to the lack of resources for the BoB mission to explore other manufacturing capabilities, it was decided that the manufacturing technique would follow the 1st gen.
Fluidic connector	• Conventional fluidic connectors have not been fully defined. Without a conventional fluidic connector, the seal integrity is compromised and can cause a	• Perform market research on the type of fluidic connector with the smallest volume footprint.

	leak. In the 1st gen., some of the fluidic sealing was achieved by push fitting (see Figure 5-1). • The two fluidic connectors used were the Luer lock to barbed and ¼" -28 UNF.	
Fluidic tubing	• The interface between various sensors and pumps has various internal diameters (ID) and outer diameters (OD).	• Catalogue the interfaces between the sensors, pump and reservoir. The key driver is the internal diameter since most components have a barbed connection.
Fluidic reservoir bag (Flexboy)	• Flexbox reservoir bag does provide flexibility in housing the growth media. • The volume used in 1st gen. was 100 ml (205 mm × 85 mm without tube), and 50 ml (134 mm ×95 mm without tube) bags might be challenging to it fit in the full system (see Figure 5-1).	• Perform market research on the smallest COTS volume bag available.

5.4 List of requirements for the 2nd gen. fluidic subsystem for the BoB mission

A list of requirements produced in this section was extracted from the BAMMsat-on-BEXUS (BoB) mission requirements (see Appendix A for the requirements). The requirements were designed to be relaxed, ensuring that the design can meet the requirement with flexibility. The requirements were primarily used to capture the functionalities of the fluidic subsystem and as a management tool to ensure every team member fully understood the concept. As mentioned in the introduction, the BoB system was designed alongside other team members. The space systems requirements can be used as a management tool to ensure that all team members record and understand the functionality, performance, and design. The requirements could ensure alignment in the design effort, and the suitable interfaces are being developed.

Functional requirements

FC-05 300c	**The system shall pump different types of media out of the MCSD into a fluidic waste reservoir.**
FC-05 200c	**The system shall pump different types of media inside the MCSD.**
	To feed and pump reagents into the C. elegans. Dye solutions are being considered to help distinguish the media.

Performance requirements

PR-08 200	**The system shall measure the fluidic pressure between the inlet and outlet of the pump between 0 and 20 000 Pa.**
	The pressure sensors are placed to measure the pressure difference across the pump for any sudden pressure lost
PR-08 210	**The system shall measure and log the fluidic pressure between the inlet and outlet of the pump at least every second.**
	Every second - to detect a failure.
PR-08 220	**The system shall measure the fluidic pressure between the inlet and outlet of the pump with a ±200 Pa accuracy for each chamber pumped.**

PR-08 300 **The system shall measure and log the fluidic mass flow rate passing through the multi-chamber sample disc between 0 µL/min and 1000 µL/min.**

This allows us to fill the chamber with the right quantity of media

PR-08 310 **The system shall measure and log the fluidic mass flow rate passing through the multi-chamber sample disc at least every second.**

Every second - to detect a failure.

PR-08 320 **The system shall measure and log the fluidic mass flow rate passing through the multi-chamber sample disc with a ± 50 µL/min accuracy.**

PR-10 100 **The system shall carry on-board a minimum of 10 ml of media. ~ 6 ml of growth media + ~1 ml of fixative + margin.**

This is sufficient to validate all mission objectives.

5.5 Description of the design process

This section aims to describe the decision and evolution of the design process during the PhD research. It is hoped that the description can guide the reader on the process and set the tone for the subsequent sections. The initial design process started with finalising the BAMMsat-on-BEXUS (BoB) mission requirements and cascaded to the top-level design of the fluidic subsystems. Both were developed in parallel since they influenced each other and were driven by the BoB mission timeline. The list of fluidic subsystem requirements for the BoB mission is included in section 5.4. On the other hand, the top-level design of the fluidic subsystem can be viewed in Figure 5-2.

The top-level design of the 2nd gen. fluidic subsystem is an evolution of the BAMMsat 1st gen. fluidic subsystem, taking on board the evaluation and critique of the 1st gen. (discussed in section 5.3.2). The general design philosophy was to reduce and optimise the number of sensors and sensor placement. This decision was made to minimise the development scope and ensure that the design can be delivered to meet the BoB mission timeline.

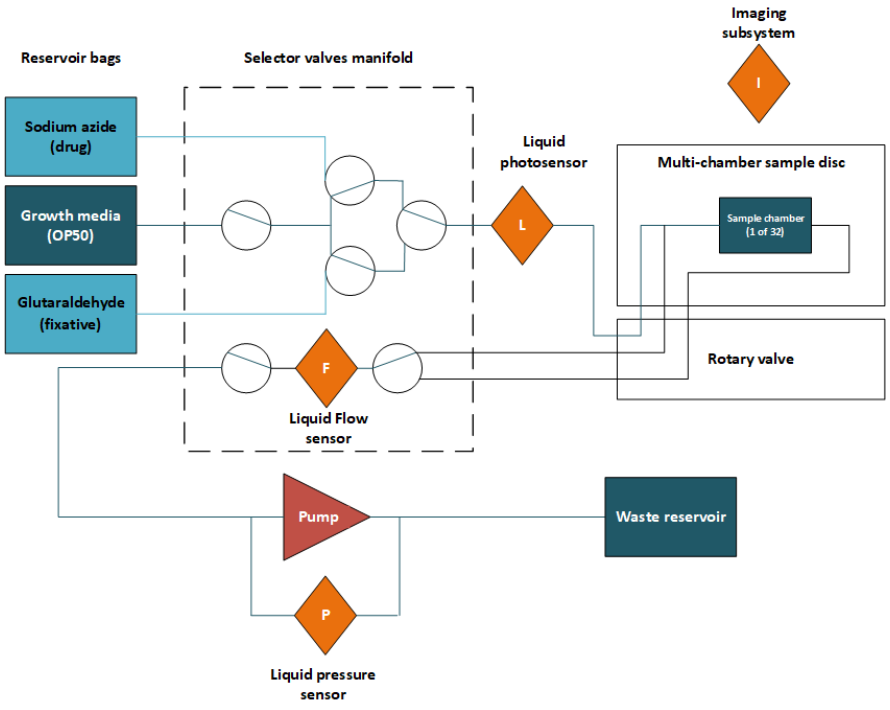

Figure 5-2. Initial fluidic network design for the 2nd gen. fluidic subsystem**.**

The following texts will discuss individual sensors and actuators on the changes made and their justification. Readers who would like to view 1st gen. fluidic network can refer to Figure 1-3 for comparison with Figure 5-2.

In the initial fluidic network design, the pump was still placed at the end of the fluidic network. The pump was placed to avoid cross-contamination since pulling the liquid after the reaction chamber (MCSD) meant that any media flowing across the pump no longer mattered. In the same image, a differential pressure sensor was placed across the pump to measure the pressure difference across the pump. During the flight, it could also indicate whether the pump is functioning nominally or non-nominal such as a pressure loss. The pressure sensors were reduced from three to one in the 2nd gen. design.

The pump pulls the fluidic medium from the reservoir bags across the whole fluidic network. The direction is controlled by selector valves manifold with 2-way and 3-way valves actuated in a pre-set sequence to direct the fluids. For example, the valve's position in Figure 5-2 is set in an initial position where the valve is not opened to any reservoir; hence no fluid will be pulled when the pump is actuated. The design for the 2nd gen. uses a latching valve instead of a non-latching due to the unknown power consumption. The design of the selector valve manifold will be discussed further in section 5.8.

The fluidic flow sensor measures and records the fluidic flow and indicates that the fluidic flow is performing nominally. Like the pump, the flow sensor is placed towards the end of the fluidic network to avoid cross-contamination. Compared to the 1st gen., the flow sensor was integrated as part of the selector valves manifold instead of a standalone sensor. The integration reduced the volume footprint of the flow sensor within the system. Figure 1-1 shows the flow sensor in the 1st gen. design, and Figure 5-12 shows the location flow sensor (LPG10) in the 2nd gen. design.

A liquid photosensor was used as a non-invasive sensor to detect changes in photo transmission along with the fluidic tubing. The change in photo transmission could be used as an indicator of types of reagent or bubbles going

into the MCSD (see Figure 5-2). For the 2nd gen., this could indicate the type of reagents being pumped.

In the 2nd gen. design, the chemical sensor was removed from the fluidic subsystem design. The reason for the decision was the sensor's application was beyond the scope of the BoB mission's objective. The sensor also occupied a large volume which constrained the design of the other subsystem. The combination of stated reasons and the additional resources required to interface the sensor to the rest of the system meant that the chemical sensor was removed from this mission. For the 3rd gen., a spaceflight version would require a chemical sensor to increase its scientific return since it can provide in-situ information on biological activities.

After the initial top-level design, trade-off, and requirements set, the next step was to test and characterise the sensors and actuators during development. The tests were divided into two, with some components such as pump, flow sensor, and solenoid valve manifold having a more rigorous test due to their complexity. The other sensors, such as liquid pressure and liquid photosensor, were seen as low risk and primarily tested to confirm their functionality and inform the electrical design.

5.6 Characterising the mp6 pump performance with the MCSD and RV

This section discusses the test performed using the mp6 pump. The test was performed to verify the pump performance, de-risking the design, and use the result to inform the design of the fluidic subsystem.

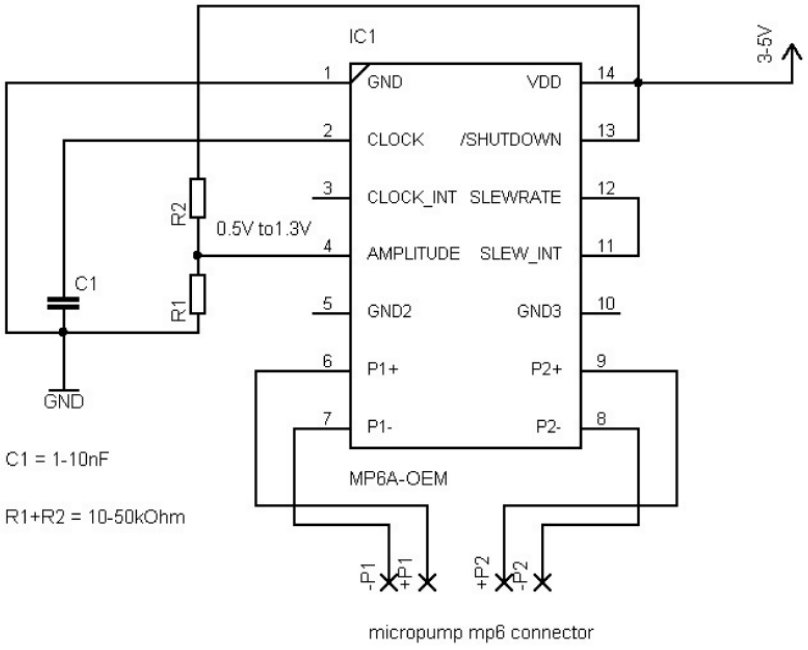

Figure 5-3. mp6 pump electrical schematic in the mp6 datasheet[1].

The mp6 pump (Bartels Mikrotechnik) is one of the most miniature piezoelectric diaphragm pumps available. It utilises the inverse piezoelectric effect to convert electrical energy into mechanical energy to actuate the diaphragms. Electrical energy is used as an input to mechanical energy by changing the electrical characteristic. The volume of deflection of the diaphragms and the rate of deflection can be controlled by varying the voltage and frequency input into the pump.

[1] This electrical schematic is adopted on the 2nd gen. BAMMsat bioCubeSat payload since it provides the most flexibility to change the flow rate parameters.

The mp6 pump is actuated by the mp6-OEM driver, which can be used to configure the mp6 pump flow rate. The electrical schematic for the mp6 pump-OEM driver can be seen in Figure 5-3, and a copy of the datasheet is available in Appendix H. The flow rate can be configured by changing three parameters. These parameters are the Voltage drain to drain (V_{dd}), Amplitude (V_{pump}), and Clock (Frequency). The V_{dd} is the supply of voltage into the mp6-OEM driver ranging from 2.5V to 5.5V. The voltage range is within the typical voltage range of a micro-system. For the BoB system, it could be configured with a supply voltage of either 3.3V or 5V.

The Amplitude or Vpump corresponds to the deflection of the diaphragm of the mp6 pump (see Figure 5-3). The larger the deflection volume, the larger the volume of liquid pushed across the pump resulting in a higher flow rate. The voltage input range at V_{pump} can be set at 0.5 V up to 1.3V. The V_{pump} is proportional to V_{pp} (voltage peak to peak), which corresponds to the diaphragm's deflection.

The last input parameter is the CLOCK (see Figure 5-3). The CLOCK is the frequency at which the pump's diaphragm deflects, hence the pumping frequency. The higher the frequency of deflection, the more volume of liquid is shifted across the pump, resulting in a higher flow rate. The frequency range of the mp6-OEM driver is between 25 Hz to 226 Hz (see Appendix H). The frequency is configurable by changing the capacitance in the system. The suggested range is between 1 nF and 10 nF. The higher the capacitance, the lower the frequency of the mp6 pumping.

5.6.1 Results from initial characterisation testing of the mp6 pump

The initial test performed for the mp6 pump was to check the pump's performance in the laboratory against the flow rate stated in its datasheet. This test aims to confirm that the pump is functioning nominally and detect any issue with the pump.

Figure 5-4 (left) shows the test result performed in the lab by varying the CLOCK input. The frequency was set by the PWM signal (Arduino Uno) going into the CLOCK input. The results demonstrated that the pump behaved nominally when pumping water within the linear region up to 30 Hz. It was challenging to directly compare the upper range since the graph scale with the lower resolution was not provided in the mp6 datasheet (right image of Figure 5-4). The lab test demonstrated that the pump could not pump at 7 ml/min at 100 Hz, despite the claim by Bartels Mikrotechnik. It could be speculated that the difference could be due to experiment variation or manufacturing variation.

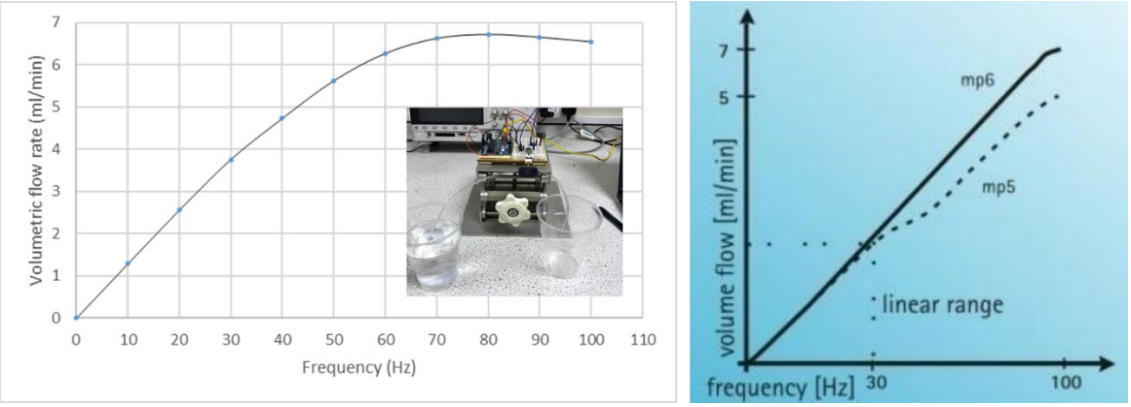

Figure 5-4. Images of mp6 pump initial test result[1].

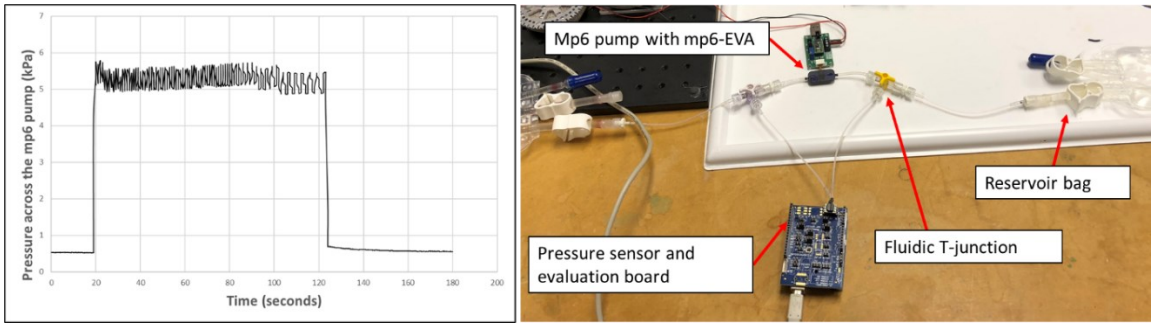

Figure 5-5. Graph and image of the pressure difference across mp6 pump[2].

[1] (Left) Initial test result confirming the nominal flow rate of the pump. The overlay image on the graph was the experiment setup. The result is an average of three repeats and varying frequencies. (Right) Nominal flow rate pump based on the mp6 datasheet.
[2] Left – Graph showing the measured pressure of 5.3 kPa across the mp6 pump during pumping. The pump was turned on at 20 seconds and off at 125 seconds. Right – Test setup on measuring the pressure across the mp6 pump.

The characterisation test of the mp6 pump continued by measuring the pressure difference of the pump at a maximum flow rate. The primary aim of this test was to gauge the pressure range of the pump and hence the fluidic subsystem. The test was set up with both ends of the pump connected to the reservoir bags and the differential pressure sensor measuring the pressure across the pump; see Figure 5-5.

The test helped gauge the pump's pressure range and hence the fluidic subsystem. The test was set up using the mp6-OEM fixed setting. For some context, the mp6-OEM have an internal electrical setting designed to optimise the maximum flow rate. The fixed setting can be configurable by connecting the CLOCK_INT to CLOCK, which provides 100 Hz, and connecting the Vdd to AMPLITUDE, which provides a Vpp of 270 V. At the fixed setting, the expected flow rate, when pumping distilled water is 7 ml/min.

In the pressure test, the setup was performed using mp6-EVA (Bartels Mikrotechnik) attached to an mp6 pump with a 5 V supply. The pressure measurement was achieved using a differential pressure sensor across the pump (ABPDRRT005PG2A5; Honeywell) connected to the Honeywell sensor evaluation board (SEK002). The use of the evaluation kit was to enable rapid testing and avoid any electrical breadboarding variation in the experiment setup. The result showed that the average pressure across the pump was around 5.3 kPa. Note that this pressure will vary in the full fluidic subsystem with the introduction of backpressure across the fluidic tubing, valves manifold, MCSD and RV.

5.6.2 Results from initial pumping into the MCSD and RV

After characterising the pump's performance, the following test assesses the fluidic pumping into the MCSD and RV (see the right image of Figure 5-6 for the setup). The test was performed to evaluate whether liquid (water) could flow into the MCSD sample chamber by connecting the mp6 pumps and RV into the MCSD and RV. The MCSD was configured with an open sample chamber for visualisation. The fluid was pumped through each of the 32 chambers using the mp6-OEM fixed setting, hence the maximum flow rate of the pump

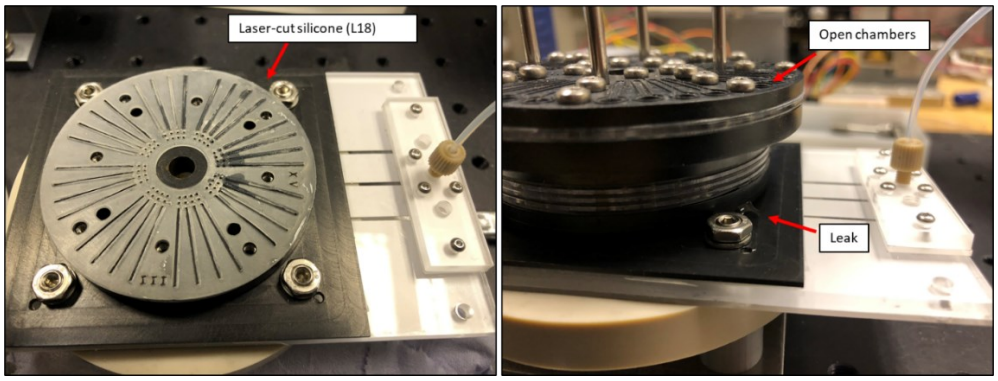

Figure 5-6. Left – Disassemble RV layer showing liquid dispersion across the layer. Right – Test setup and the resulting leak occurred during pumping.

Each chamber was accessed by rotating the RV manually to align the fluidic port. From the test, it was possible to evaluate the time to fill across the 32 chambers measured via the volume of the chamber and stopwatch. The test also showed a leak presence around the RV; see left of Figure 5-6. The result from the test showed that the flow rate to fill the chamber was 430 µl/min and the flow rate to leak away from the chamber was 10 µl/min. For reference to the fluidic pathways of the MCSD, the reader can refer to Figure 3-17.

The initial testing highlighted that the flow rate from the mp6 pump was too high. The flow rate to fill the chamber was recorded at 430 µl/min. At such a high flow rate, the liquid seeps through the leak during pumping due to the backpressure from the flow, see Figure 5-6. The testing highlighted that the MCSD design was not leak-proof and required further iteration. The high flow rate could also adversely affect the biology by agitating the sample.

The subsequent tests in the following sections on the fluidic subsystem were performed to reduce the flow rate for a gentler flow. The result from the test also influenced the final design of MCSD and RV, which changed the RV layer from silicone membrane to pressure-sensitive adhesive. See section 3.9.1 for reference.

5.6.3 Results from testing to find the lowest possible flow rate

This section discusses the testing performed to characterise the fluidic flow of the fluidic subsystem to achieve the lowest possible flow rate. The testing continues from the previous section, emphasising varying the mp6 pump electrical parameters to find the setting that provides the lowest flow rate. As a reminder, the pump can be configurable by adjusting the V_{dd}, AMPLITUDE, and CLOCK (see Figure 5-3).

Figure 5-7 shows the measured pump flow rate varying only the voltage supply (V_{dd}). The test evaluated the impact of varying the V_{dd} between 5 V and 3.3 V into the mp6 pump on the fluidic (water) flow rate. The clock was set with a capacitor value of 1 nF and the AMPLITUDE of 1 V. The flow rate was measured by the LPG10 evaluation kit (Sensirion). Note that the pump was not pumping into the MCSD and RV. The reason was to remove the variability of the leaking MCSD and RV. In addition, the design of MCSD and RV was under iteration during this period.

The two choices of 5 V against 3.3 V were chosen because of the BoB system design. The BoB system was built with COTS sensors and actuators, which required typical voltages of 12V, 5V and 3.3V. 3.3V was the ideal voltage without introducing another step-down converter into the electrical system.

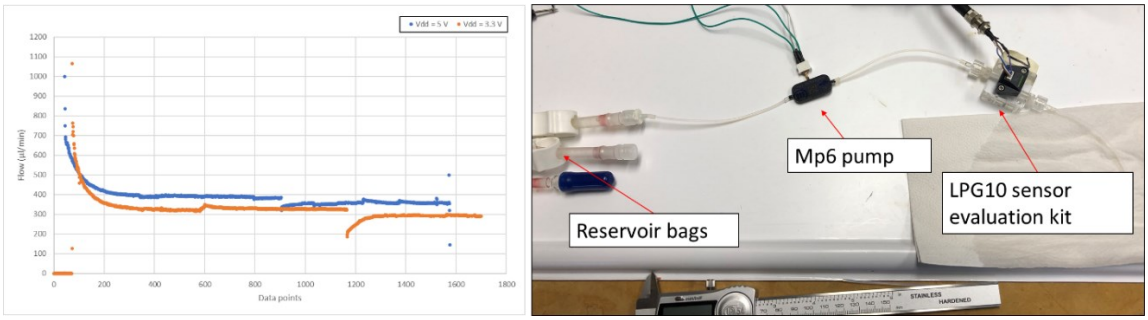

Figure 5-7. Left - Graph of the measured flow rate with V_{dd} at 5 V and 3.3 V to evaluate the flow rate difference. Right – Test setup with mp6 pulling liquid from the reservoir to the flow sensor, which is opened to the atmosphere[1].

Figure 5-7 (left) showed that supplying 3.3 V into the mp6 pump resulted in a lower flow rate than supplying 5V. The difference in flow rate is approximately 70 µl/min. In a microfluidic system, 70 µl/min can be significant. The discrepancy between the start of the pumping sequence was because the power supply was turned on and off manually.

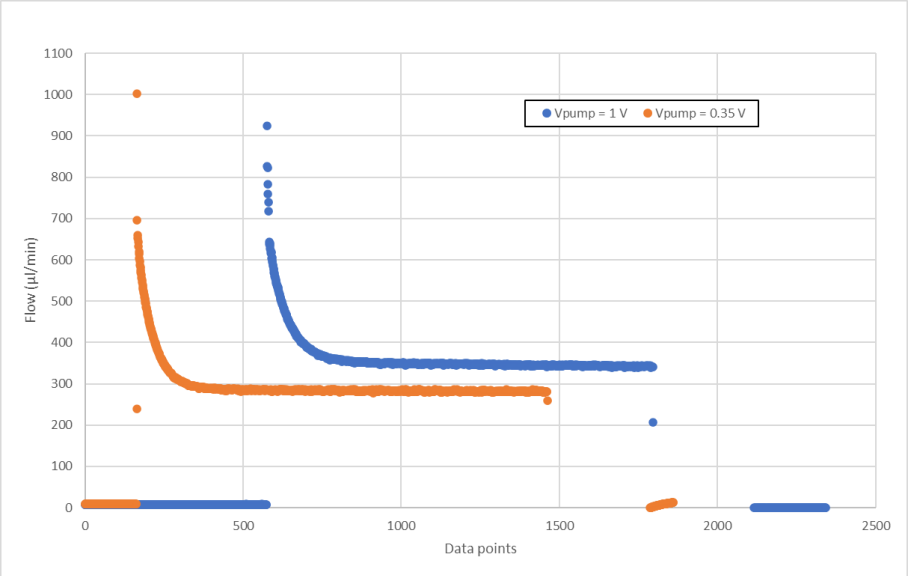

Figure 5-8. Graph of the measured flow rate with varying the AMPLITUDE (Vpump) of the mp6 pump[2].

[1] Measurement was taken over 1800 data points which are approximately 2 minutes, and the data points were used to normalise the two readings.
[2] Note that 1800 data points are approximately 2 minutes

Figure 5-8 shows the measured pump flow rate varying only the pump AMPLITUDE (V_{pump}). The test evaluated the impact of varying the V_{pump} between 1 V and 0.35 V into the mp6 pump on the fluidic (water) flow rate. The CLOCK was set at a capacitor value of 1 nF and V_{dd} at 3.3V, similar to the previous test.

The result showed that supplying 0.35 V into the mp6 pump resulted in a lower flow rate than supplying 1 V. The difference in flow rate is approximately 65 µl/min. The difference is close to the difference in changing V_{dd} in the previous test, which was 70 µl/min.

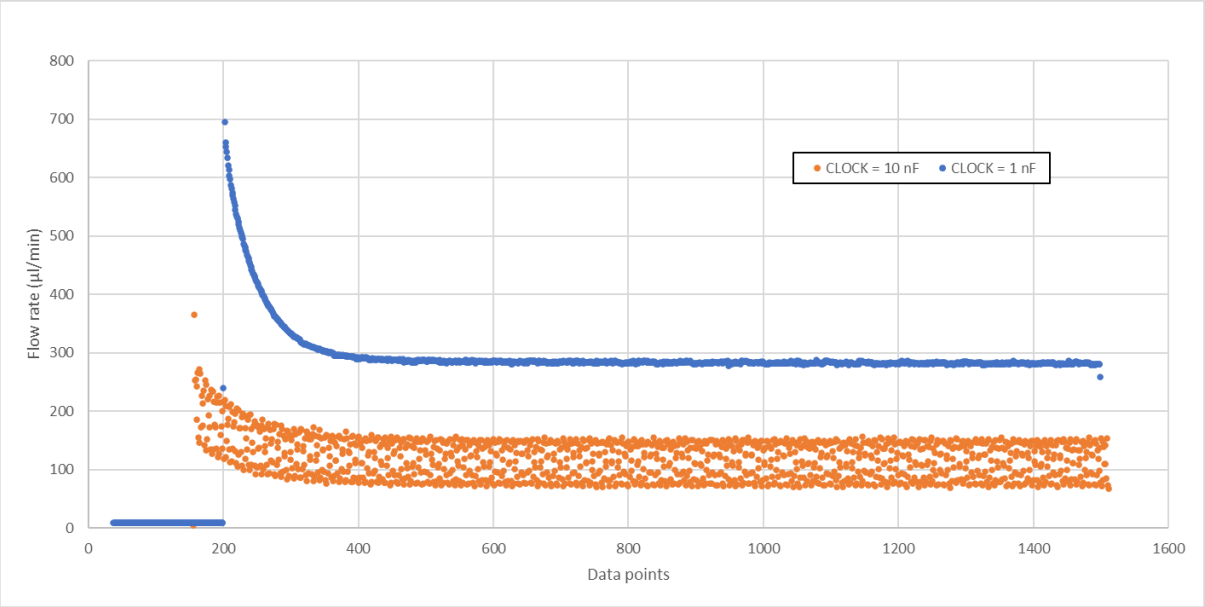

Figure 5-9. Graph of the measured flow rate with varying the CLOCK of the mp6 pump.

Figure 5-9 shows the recorded pump flow rate varying only the mp6-OEM CLOCK. The test aimed to evaluate the impact of varying the CLOCK in the two extreme frequencies. The frequency is configured by varying the capacitance value between 1nF and 10 nF. Based on the datasheet (see Appendix H), at 1 nF, the pump frequency is 226 Hz, and at 10 nF, the frequency is 25 Hz. The V_{pump} was set at 0.35 V, with the V_{dd} at 3.3 V.

The result in Figure 5-9 showed that setting the CLOCK with 10 nF resulted in a significantly lower flow rate than 1 nF. The flow also revealed an interesting flow pattern, resembling a resonance. One hypothesis is due to the resonance of

electronic noise. Note that one audio observation during testing was a slower pumping noise rate. At a lower frequency, the piezo diaphragm was deflecting at a lower rate, shifting a volume of liquid at larger intervals. As such, the pumping rate became slower, hence the pumping noise rate. Further testing will be required to understand this phenomenon. In the context of the BoB mission, this phenomenon is not an immediate issue.

From this test, the difference in flow rate is approximately 160 µl/min. Similar to the previous test, the discrepancy between the start of the pumping sequence was because the power supply was being turned on and off manually. Compared to changing the V_{dd} and V_{pump}, lowering the CLOCK gave the highest difference in flow rate.

In summary, the test performed in this section helped characterise the pump performance by varying its parameter, i.e., voltage supply, frequency, and amplitude. The three tests highlighted that the pump's electrical design should be powered at Vdd = 3.3V, Vpump = 0.35 V, and CLOCK = 25 Hz (10 nF) to achieve the lowest flow rate. Note that this is suggested in the datasheet to achieve the lowest possible flow rate. It was useful to perform these tests within the 2nd gen. fluidic subsystem and record the results to understand the fluidic performance.

5.6.4 Results from testing on pulling vs pushing the liquids

The test in Figure 5-10 was performed to test the initial design of the pump placement within the fluidic network (see Figure 5-2 for the initial fluidic network). The initial design had the mp6 pump located towards the end of the fluidic network. In this configuration, the pump is "pulling" the water from the fluidic reservoir across the fluidic network. The benefit of placing the pump at the end of the fluidic network is to avoid cross-contamination since the fluid and surface contact after the sample chamber no longer impacts the samples. Based on the test setup in Figure 5-10 (left), it means that the pump was connected to the outlet port.

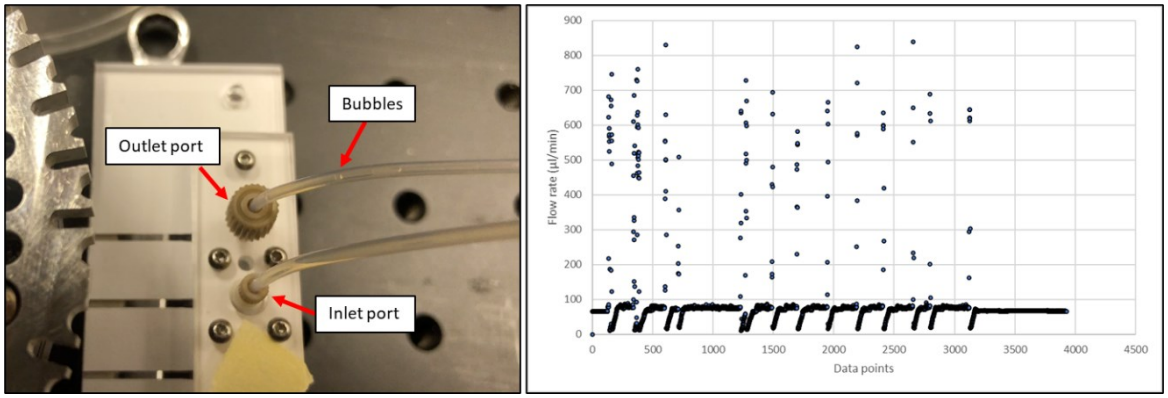

Figure 5-10. Test result showing bubble formation when pulling the liquid[1].

The test highlighted two issues: a persistent leakage problem and the inconsistent flow when pulling the liquid. The leakage can be seen in Figure 5-10 (left) and Figure 5-6. The MCSD was designed to be mechanically assembled, and the sealing was provided by compressing the laser-cut silicone layer. However, the issue with manufacturing tolerance meant that aligning the compression ridges to seal the channel was challenging, resulting in leakage in the system. See Figure 3-18 for reference.

[1] Left – Test setup performed with mp6 pump connected to the outlet channel to pull the liquid (water) across the MCSD and RV. The result showed bubble appearance in intervals. Right – Flow rate measurement during the test. Note that 1800 data points is approximately 2 minutes.

The leak and the resulting bubble caused the second problem, which was the irregular flow. The irregular flow can be viewed in Figure 5-10 (right image). The mp6 pump can pump fluids, both liquid and gas; in this case, when the bubble is pumped through the LPG10 sensor, there is a sudden drop-in flow rate. The bubble could have appeared when the ambient atmosphere was also pulled into the system during pumping through the leak.

Compared with pushing the liquid, the pump is connected to the inlet and pushes the liquid into the MCSD and RV; see Figure 5-10 (right image for the inlet connection). The result from pushing showed that there was no observable bubble in the fluidic tubing coming out the outlet port, based on visual observation. This was because the pump pushes the liquid through the channels filling the air gaps as the fluid travels along the channel. Unfortunately, due to poor planning by the author, the flow rate when pushing the liquid test was not recorded.

The impact of these findings resulted in two design changes. The first was on the MCSD design, which was reverted from back to bonding using laser-cut adhesive in the RV layers. This design change has been discussed in section 3.9.1 of this thesis for reference.

The second design change is on the placement of the pump. For the 2nd gen. fluidic subsystem for the BoB mission, the pump will be placed at the inlet of the MSDC and push the reagents into the sample chamber. This is not ideal since cross-contamination can occur. However, design iteration would not have been feasible due to the BoB mission timeline, and pushing the liquid was seen as a compromise. The fluidic subsystem would still be able to meet the BoB mission objective providing the fluidic subsystem was functional during the flight.

5.7 Characterising the LPG10 flow sensor performance

5.7.1 Result from the flow sensor verification test

The test in this section was performed to characterise the LPG10 sensor. This test aims to verify that the LPG10 was functioning nominally and detect any issue with the flow sensor.

The test evaluated the sensor's digital reading, confirming its digital output if it was representative of the actual physical flow. The test measured the flow rate using the LPG10 sensor (digital output from the sensor) and compared it to the weighted measurement (physical measurement via mass scale and stopwatch). The weighted measurement was collected after the liquid passed through the flow sensor.

The test setup connected the fluidic reservoir bag to the mp6 pump, and the other end of the mp6 was then connected to the LPG10 evaluation kit. After passing through the flow sensor, the liquid was collected on a centrifuge tube and weighted using a precision analytical balance / mass scale (Ohaus). The flow rate measurement was recorded with Sensirion's software. The test was performed at four different times, and the result is presented in Table 5-1.

The results shown in Table 5-2 demonstrated that the LPG10 sensor behaved unpredictably. The test was performed at four different times without any change in variables.

The results showed that the digital reading was not equal to the weighted flow rate. For instance, in Test 1, the sensor was recorded at 302 µl/min, while the weighted measurement was recorded at 924.45 µl/min. This was a 65% difference between the two readings. In the following Test 2, the sensor was recorded at 54 µl/min, while the weighted reading was recorded at 927 µl/min. In this case, it was a 94% difference between the two readings. The sensor reading also had a significant variation between Test 1 (302 µl/min) and Test 2 (54 µl/min), with a difference of 248 µl/min. Note that there was no significant variation between Test 2 and Test 3; see Table 5-1.

The result showed that the flow sensor reading could be unpredictable. One possible explanation was that Test 1 was an outlier, and Test 2 and Test 3 were representatives of the flow reading. However, based on the LPG10 datasheet, the LPG10 sensor can measure up to 1000 µl/min with a 5% error (see Appendix I). The variation between the Test 1 and Test 2 was too significant. More importantly, the % error was beyond the 5 % mentioned in the datasheet.

Another possible explanation was that the flow sensor might have been damaged during laboratory tests. Further testing will be required with increased repeatability on the number of tests and increased data collection to assess if the sensor was indeed damaged.

Table 5-2. The LPG10 flow sensor verification test was taken at four different times[1].

	Attempt	Flowrate digital reading from LPG10 sensor (µl/min)	Weighted Flowrate measurement (µl/min)
Test 1 (9th June 2021)	1st	334	943
	2nd	267	932
	3rd	302	924
Test 2 (9th June 2021)	1st	54	927
	2nd	58	928
	3rd	48	911
Test 3 (9th June 2021)	1st	48	911
	2nd	48	906
	3rd	54	923

The unpredictability of the flow sensor was an issue since it would be challenging to have an accurate flow rate in the complete fluidic subsystem. This impacts the design of the rest of the 2nd gen. fluidic subsystem. For instance, the flow rate was supposed to inform the reservoir bags' size and the fluidic operation timeline.

Sensirion was contacted to provide input on the reading and has provided a Basic Performance Check document to test the sensor. The general procedure for the check is listed below.

1. Verify the sensor reading for an (approximately) constant forward flow.
2. Verify the sensor reading for an (approximately) constant backward flow.
3. Measure the sensor's offset (zero-flow reading).

[1] Difference was evaluated by comparing between the recorded measurement (digital output from the sensor) and the weighted reading (physical measurement via mass scale and stopwatch).

However, due to the time pressure with the BoB mission development, it was not possible to perform the check of the LPG10. The author had to develop other subsystems, which were going ahead in parallel to meet the BoB mission milestones.

In the context of the 2nd gen. fluidic subsystem, the flow sensor still has an added value in the BoB mission. Despite the inaccurate reading, the sensor is placed at the end of the fluidic network and can be used to confirm that fluid is flowing through the sample chamber instead of a failed fluidic flow.

5.8 Design and manufacture of the 2nd gen. selector valve manifold

This section discusses the development of the selector valve manifold. The selector valves manifold was manufactured to construct the fluidic network designed in Figure 5-2. The design and technique used to manufacture the selector valve manifold continued from the development during the 1st gen. (see Figure 5-1). The technique utilised a CO_2 laser cutter to laser-cut polymer (PMMA) and double-sided pressure-sensitive adhesive (3M 9965). The fluidic channels were laser-cut through the adhesive layer and then sandwiched between two layers of laser-cut polymer. These three layers create a 3D structure with a hollow fluidic channel inside of it (see the right image in Figure 5-11). The selector valve manifold builds upon this technique and uses multiple layers to construct the network.

The 2nd gen. selector valve manifold was redesigned to fit within the 2U volume profile. This was achieved by redirecting the fluidic pathways inside the manifold to fit within the volume envelope. See the right image of both Figure 5-11 Figure 5-12 to view the internal fluidic network. The manifold was also designed to interface with the mechanical mounting, layer 20 (L20) of the rotary valve, and the fluidic tubing via a miniaturised fluidic connector (Diba; UNF 6-40). The complete assembly of the manifold can be seen in the left image of Figure 5-12.

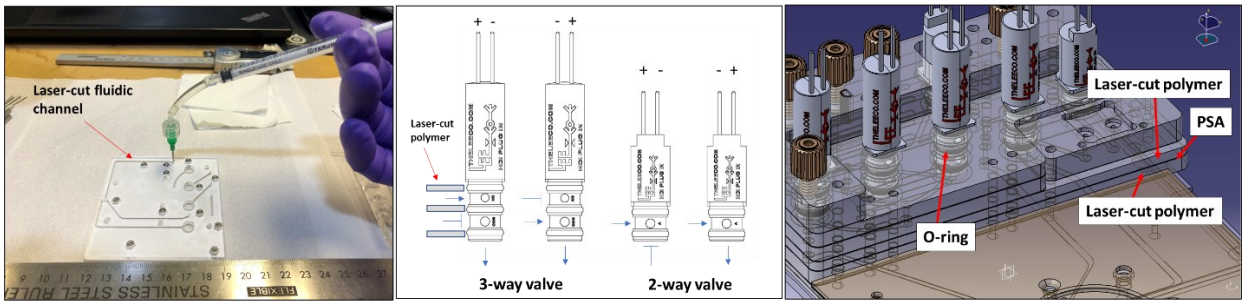

Figure 5-11. Various images of 2nd gen. selector valve manifold[1].

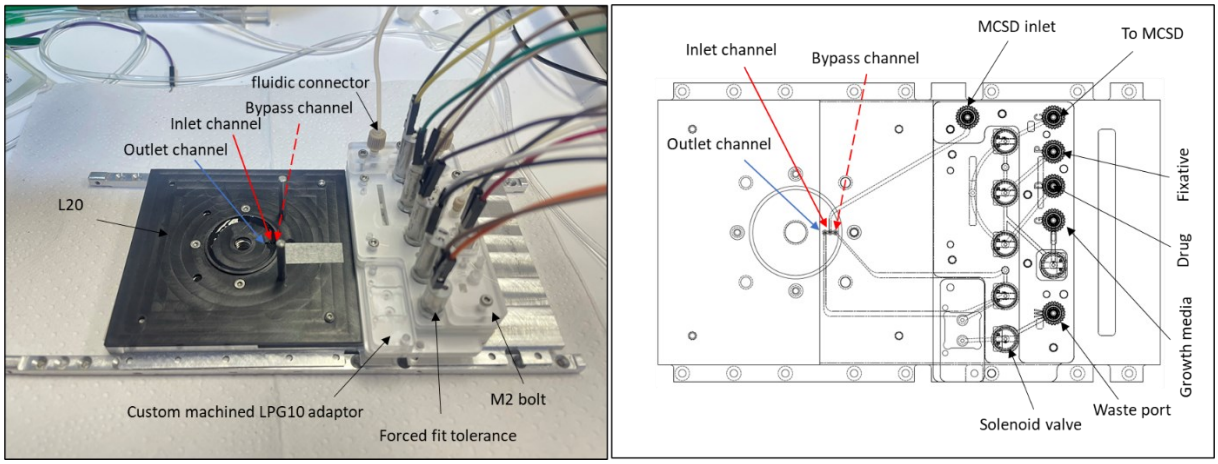

Figure 5-12. Left – Image of fully assembled selector valves manifold. Right – Top view of the manifold with viewable hidden fluidic network.

One key difference between the two gen. of the manifolds was the type of valve used in the design. The 2nd gen. used a latching valve to mitigate the unknown in the system, i.e., total pumping time. With a non-latching valve, the valve must be constantly energised to keep it open, which drains the power from the BoB system's battery. Since the 2nd gen. was the first prototype with a re-designed fluidic network and the MCSD, the performance of the complete fluidic subsystem was not yet characterised. The total time to energise the valve was unknown, and this was perceived as a risk to the total power consumption of the BoB system.

[1] Left – Image of the bottom 3D layer of selector valve manifold during flow verification. Centre - Image of solenoid valves and two different pathways for each type of valves. Right. Transparent 3D CAD showing the internal fluidic network.

The non-latching valve was selected in the 1st gen. to minimise the risk of the fluidic port being left open after a power loss. This could be an issue when mixing fluidic when the port is left open, and diffusion can occur over time. However, for the BoB mission, the fluids are pre-mixed in their own reservoir bags. Additionally, the liquid does not move in a microchannel unless actuated because surface tension becomes dominant. For this reason, mitigating the risk of power consumption was more pertinent.

The valve selected for the design was a 3-port / 2-way solenoid valve (LHLA051111H; The Lee Company) and a 2-port / 2-way solenoid valve (LHLA0542311H; The Lee Company). The valves were integrated via forced fit into a pre-laser-cut hole and sealed with O-rings. The image of the valve and the corresponding open/closed port are shown in the middle image in Figure 5-11. The valve was energised by changing the (+) and (-) polarity on the valve terminal. For the 2-way valve, changing polarity opens and closes the port.

In contrast, the 3-way valve has three ports and closes one port at a time, and changing the polarity opens two unique fluidic pathways at one time. Combining the valves' functionality and intricate fluidic network within the selector valves manifold allows the author to create the fluidic network to meet the design requirement.

At this stage, the 2nd gen. selector valve manifold was ready to be assembled into the 2nd gen. BAMMsat bioCubeSat payload. The testing will continue in Chapter 8 in the full system context.

5.9 Verification matrix

This section assesses the requirements set for the 2nd gen. fluidic subsystem. The tests performed demonstrated five out of nine requirements were verified, see Table 5-3. The requirements PR-08 220 and PR-08 310 were not verified since there was an issue with housing the pressure sensor due to the large volume of fluidic T-junction, see section 8.7.2.2.1. The other two requirements PR-08 300 and PR-08 320 were not verified since the flow sensor may have been damaged, see section 5.7.1.

Table 5-3. Verification matrix for 2nd gen. fluidic subsystem.

Functional requirements		**Status**
FC-05 300c	The system shall pump different types of media out of the MCSD into a fluidic waste reservoir.	**Verified**
FC-05 200c	The system shall pump different types of media inside the MCSD.	**Verified**
Performance requirements		
PR-08 200	The system shall measure the fluidic pressure between the inlet and outlet of the pump between 0 and 20 000 Pa.	**Verified**
PR-08 210	The system shall measure and log the fluidic pressure between the inlet and outlet of the pump at least every second.	**Verified**
PR-08 220	The system shall measure the fluidic pressure between the inlet and outlet of the pump with a ±200 Pa accuracy for each chamber pumped.	**Not verified** Unable to assemble the pressure sensor since the fluidic T-junction has a large volume
PR-08 300	The system shall measure and log the fluidic mass flow rate passing through the multi-chamber sample disc between 0 µL/min and 1000 µL/min.	**Not verified** Possibly damaged LPG10 sensor
PR-08 310	The system shall measure and log the fluidic pressure between the inlet and outlet of the pump at least every second.	**Not verified** Unable to assemble the pressure sensor since the fluidic T-junction has a large volume
PR-08 320	The system shall measure and log the fluidic mass flow rate passing through the multi-chamber sample disc with a ± 50 µL/min accuracy	**Not verified** Possibly damaged LPG10 sensor
PR-10 100	The system shall carry on-board a minimum of 10 ml of media. ~ 6 ml of growth media + ~1 ml of fixative + margin.	**Verified**

5.10 Discussion, conclusion, and future work

5.10.1 Discussion and conclusion

The 2nd gen. fluidic subsystem was developed to perform the fluidic functionalities designed for the 2nd gen. BAMMsat bioCubeSat payload (see section 5). The fluidic functions were part of the technology demonstrated during the BoB mission and are a key subsystem for future BAMMsat spaceflight generation.

In the 2nd gen., the fluidic subsystem included actuators (pump and solenoid valves) and sensors (liquid flow sensor and photosensor). The design advanced 1st gen. design and was simplified since the BoB mission was designed for a technology demonstration mission instead of a scientific mission. A similar fluidic pump, flow sensor, and liquid photosensor were brought forward to the 2nd gen. The chemical sensor was removed to reduce the development scope. The solenoid valves were also changed to a latching valve version to mitigate the unknown time to power the valve open during pumping.

Regarding the fluidic pump, the testing results demonstrated that the pump is suitable as the final design with some modifications. In summary, the pump will need to be reconfigured to push the fluids at the lowest possible flow. The first test confirmed the performance of the pump against its datasheet. Further tests showed that the pump must be configured with the lowest possible flow rate to reduce the risk of leaking and agitating the biological sample inside the sample chambers. To achieve the lowest possible flow rate, the pump must be set with Vdd = 3.3V, AMPLITUDE = 0.35 V, and Frequency = 25 Hz. Connecting the reservoir-pump-flow sensor-MCSD showed that the recorded flow rate was below 100 µl/min at this pump setting. In a full fluidic subsystem assembly with the selector valves manifold, the flow rate will reduce significantly due to additional backpressure.

During the pump test, one of the key findings was the consistent leaking of the MCSD, especially near the rotary valve. The leaking occurred since the silicone layer was not compressed according to the fluidic channel and the effect of poor

laser cutting caused fluidic channel misalignment and blockage. The result of this testing feed back into 2nd gen. MCSD final design. A detailed discussion on this issue can be referred to in section 3.9.1. In summary, the impact of this testing led to some of the layers near the RV reverting to the 1st gen. design of using pressure-sensitive adhesive.

Regarding the LPG10 sensor, the reading recorded showed that the sensor was unpredictable. During the testing performed in section 5.7, the flow rate sensor reading showed the expected pattern. For instance, if the flow were expected to decrease because of the set pump setting, the reading would decrease accordingly.

The unpredictability of the sensor was found during testing when the sensor reading was compared with a weighted flow rate reading. Unfortunately, due to time constraints, the sensor was never fully diagnosed to understand the root cause of the problem. Further testing will be required to diagnose the issues. For the BoB mission, the flow reading will primarily be used to confirm pumping.

The 2nd gen. selector valves manifold utilises the same manufacturing technique as the 1st gen. Nonetheless, the fluidic network had a major re-design, and the structure was repackaged into a version that fits into the 2U CubeSat format. The key differences between the two generations were the build quality, which included miniaturised fluidic connectors and M2 bolts to maintain the sealing integrity.

A drawback during the testing was the lack of testing for the pressure sensor and liquid photosensor. The pressure sensor and liquid photosensor could have been tested more rigorously to characterise their performance in an ideal situation. Due to time constraints, the testing effort was focused on the fluidic pump and flow sensor. The fluidic pump test was performed to ensure expected pumping behaviour, while the flow sensor informs the pumping speed and liquid volume.

At this stage of the project, the 2nd gen. fluidic subsystem had advanced significantly and was ready for full-system integration and testing. The discussion will continue in Chapter 8.

5.10.2 Future work

Immediate future work would include further testing to diagnose the issue encountered during the testing.

- Further testing to perform diagnostic on the LPG10 sensor
    - The LP10 sensor was not behaving nominally based on its datasheet. The manufacturer stated that the sensor would remain accurate within 5% of the measured value. However, the result showed that the reading could be at 94% difference between the two readings during testing. Further testing will repeat the similar test to remove any potential variables. The testing would then continue by performing the manufacturer's application note for the Basic Performance Check (see Appendix J). The test will help confirm if the variables caused the issue or if the sensor was damaged during testing.
- Perform a fluidic dispersion / mixing inside the MCSD sample chamber.
    - Understanding the impact of fluidic mixing within the BAMMsat fluidic subsystem and inside the MCSD sample chamber is key for future spaceflight. In microgravity, mixing fluid could be a risk to the experiment without gravity-driven convection. Primarily in microgravity, diffusion will be the driving force for fluidic mixing. Therefore, it is critical to understand the how fluidic system performs, especially in the dispersion and mixing inside the sample chamber.
    - Although the testing was planned, the test was never performed due to an issue with MCSD leaking, and it was not solved before the BoB mission. Immediate future work is to record pumping different coloured solutions into the sample chamber and observe

the fluidic dispersion. The dispersion's efficiency could be measured via an optical system to record video and assess the luminescence / brightness extracted from the images.

- Perform a full fluidic response test on the complete 2nd gen. fluidic subsystem
    - Although the testing was planned, a complete full fluidic response test was never performed due to an issue with MCSD leaking, and it was not solved before the BoB mission. The aim of this test is to record the fluidic performance across the complete fluidic system. The testing will record pressure and flow rate across different points in the fluidic system to understand fluids behaviour as it travels across components such as the fluidic tubing, selector valves manifold, MCSD and RV.

Long-term future work would include design optimisation on the fluidic subsystem.

- Perform a test to characterise the pressure sensor.
    - During the scope of the PhD and BoB mission, the pressure sensor was only tested to confirm its functionality and inform the electrical design. It is worth characterising its performance for future applications, such as verifying its reading against a known pressure head.
- Perform a test to characterise the liquid photosensor.
    - Like the pressure sensor, the liquid photosensor was tested only to confirm its functionality and inform the electrical design. A further test would help evaluate if the sensor is applicable to the design for future applications. A further test should perform a baseline test to assess the impact of different tubing on the sensor's readability. For the BoB mission, a 1/16" PEEK tubing was the primary choice, and it is translucent. The test should then continue with the different reagents to evaluate its reading.

6 Subsystem level – 2nd gen. Geneva gear mechanism: Design, manufacture, and test

6.1 Introduction

This section discusses the PhD research and development work on the 2nd gen. Geneva gear mechanism in preparation for assembly, integration, and testing (AIT). The AIT will be performed as part of the 2nd gen. BAMMSat bioCubeSat payload in Chapter 8. The Geneva gear mechanism is often used in mechanical watches and provides an intermittent and locking / indexing rotary motion that is inherently built into its mechanical design. For BAMMsat, the intermittent motion is a valuable trait since the multi-chamber sample disc (MCSD) can be rotated intermittently and enables discrete independent addresses of each sample chamber for fluidic actuation or data collection.

Similar to the other subsystems, the Geneva gear mechanism continued from the 1st gen. concept. The work performed during the PhD was to critique the 1st gen. design, trading off the motor selection, manufacture, and assemble them into the Geneva gear mechanism's mechanical housing that fits into the 2U volume. The chapter ends by presenting the result gathered from testing the subsystem assembly of the Geneva gear mechanism.

The research conducted in Chapter 5 was challenging since the development was performed at intervals and mixed with solving issues associated with the MCSD and RV (see Chapter 3) and compact brightfield microscope (see Chapter 4). The development was particularly affected by the MCSD and RV since a completely functional prototype was required before the mechanism could be tested. Due to this reason, it was challenging to implement a thorough testing plan, and the strategy was to test rapidly and iteratively to meet the BoB mission milestones.

6.2 Aim and objectives

1) *Evaluate and critique the 1st gen. design of the Geneva gear mechanism as an input into the 2nd gen. design*.

The objective was created to leverage the previous development work during the 1st gen. to extract any lessons learnt that will be valuable for the 2nd gen.

2) *Produce a list of requirements extracted from BAMMsat-on-BEXUS mission requirements*

This objective was added to produce a list of requirements from the BAMMsat-on-BEXUS mission

3) *To design, manufacture and test the Geneva gear mechanism for the BAMMsat-on-BEXUS system*.

The Geneva gear mechanism was a critical component in the BAMMsat concept, and it provides the unique ability to address individual sample chamber independently. The objective originated to advance the design from the 1st gen. into the 2nd gen., ready for the BoB mission.

6.3 Overview of the 1st gen. Geneva gear mechanism

6.3.1 Introduction to the 1st gen. design

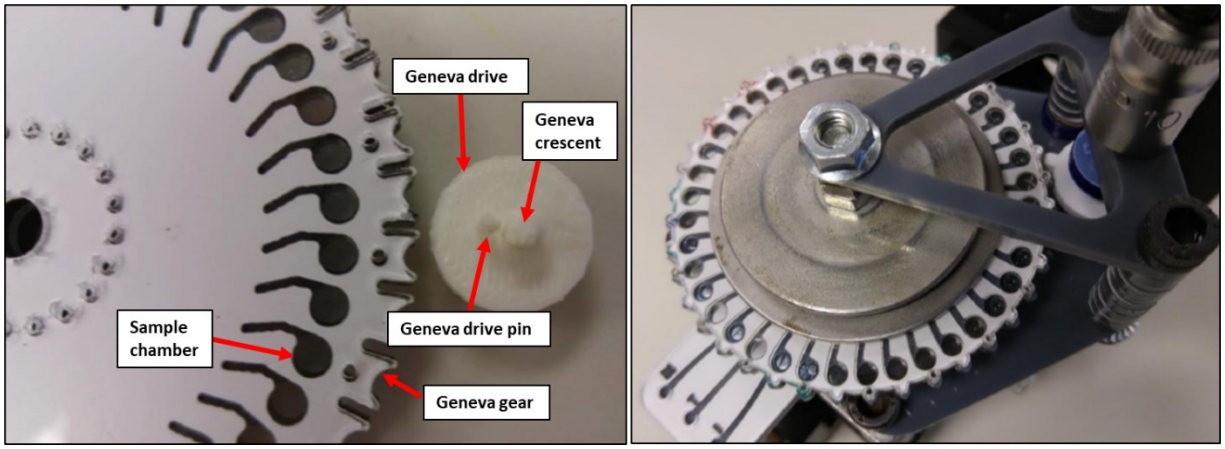

Figure 6-1. (Left) Image of 1st gen. Geneva gear mechanism. (Right) Alternative gear system explored during the NSTP programme. Images courtesy of Prof Cullen with minor editing.

The Geneva gear mechanism is a unique design solution for the BAMMsat concept. The mechanism provides the ability to move between discreet sample chambers and lock the MCSD when it is in position. The Geneva gear mechanism is inherently linked to the rotary valve design as the intermittent rotation makes or breaks the fluidic ports. See Figure 3-3 for the image of the fluidic port on the 1st gen. rotary valve and MCSD.

Before the PhD, during the NSTP programme, the key development in the design was the increased number of sample chambers from 20 chambers to 40 chambers. The increased number of sample chambers means more samples and experiments can be included within the same volume. In return, this provides more scientific output. See Figure 3-1 to compare the MCSD design with 20 chambers and 40 chambers.

The increasing number of samples does have a shortcoming to the Geneva gear tooth design. The diameter of the sample chamber is directly proportional to the size of the Geneva gear teeth (see Figure 6-1). Increasing the number of samples in a constrained volume meant that each sample chamber's size, i.e., diameter,

needed to be reduced. The reduction of the sample chamber diameter reduces the size of the Geneva gear and directly reduces the size of the Geneva drive (Figure 6-1).

The impact of reducing the Geneva drive size was the reduction in the mechanical strength. As shown in Figure 6-1, the Geneva drive has two gear profiles specific to a Geneva gear: the Geneva drive pin and Geneva drive crescent. The Geneva drive pin pushes the MCSD with the gear tooth, and the Geneva drive crescent locks it in position. The image showed a poor build quality part since the part was 3D printed using fused-deposition modelling (FDM). The resolution and tolerance required by a Geneva gear at this level could not be achieved with a 3D printed part or CO_2 laser cutter. It was recorded during the NSTP programme that the Geneva drive pin often fails at the point of contact. An alternative gear mechanism was explored with a design that induced less stress in the Geneva drive (see right of Figure 6-1). However, a similar issue occurred with the size and tolerance, and it diminished the locking effectiveness below the practical level.

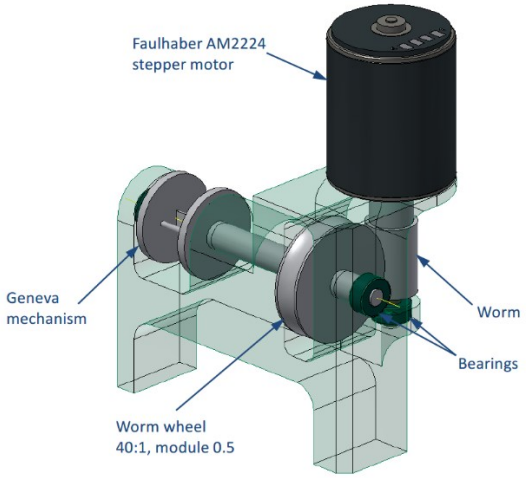

Figure 6-2. The Geneva gear mechanism was designed during the packaging exercise for a fit check.

At the end of the NSTP programme, a version of the Geneva gear mechanism was designed to fit into a 2U CubeSat. The full assembly of the CAD for the packaging exercise is shown in Figure 6-2. The design suggested the use of

Faulhaber AM2224 motor in conjunction with a worm gearbox (G50B40R1 and W50SUR1B; Reliance Precision) to actuate the mechanism.

6.3.2 Evaluation and critiques of the 1st gen. design

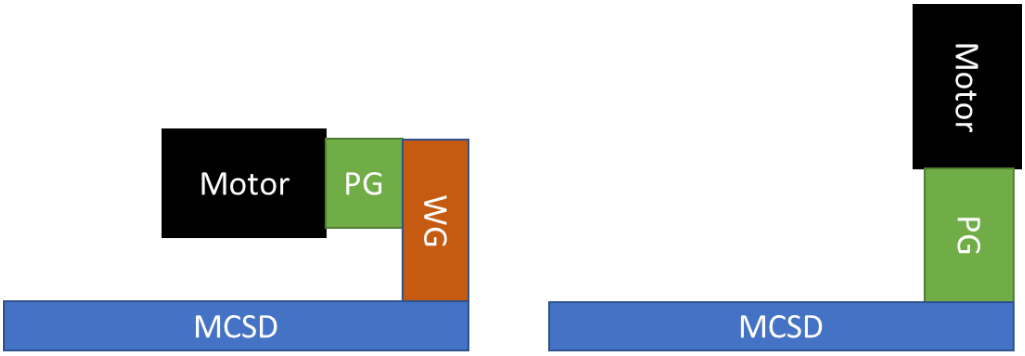

Figure 6-3. A simple sketch of the gearing mechanism**.**

Evaluating the CAD developed during the NTSP packaging exercise highlighted the functional design aspect. The worm gear was a compact mechanism to increase the gear ratio without increasing the volume above the MCSD. Figure 6-3 showed two possible gear mechanisms to actuate the MCSD. The image on the left showed that the gear setup took less volume above the MCSD than the image on the right.

The key difference between the two setups is an additional worm gear (WG) to have the perpendicular motion translation. A direct drive setup on the right took more volume above the MCSD. Without the WG, the design might require a longer planetary gearhead to have a similar gear ratio. However, one drawback in the design on the left is that the worm gear is also known to be inefficient. The worm gear has the gear meshing dominated by sliding friction which produces more heat. This inefficiency will need to be considered during the motor sizing. Fortunately for BAMMsat, the design does not require high rotation speed and has a low duty cycle.

At the end of the NSTP programme, there was a significant design issue with the Geneva gear mechanism. The size reduction of the gear profile reduced its mechanical integrity and deemed it to be unusable. There were two issues with

the design which caused such an outcome. The first is the material choice, and the second is the build quality. The material choice during this development was polylactic acid (PLA), widely used in FDM 3D printing. Using 3D printing also made getting the tolerance required challenging, especially with the Geneva drive pin, which was 1 mm in diameter. The Geneve drive pin has a clearance inside the Geneva gear slot, which was 0.1 mm. For initial prototyping and de-risking, the kinematic of the Geneva gear, the material and the manufacturing choices were sufficient. However, better build quality was needed as the Geneva gear became more intricate and under actual loading.

For completeness, it is worth evaluating any other alternative to Geneva gear. During the NSTP programme, an alternative “mutilated” gear was explored (see right of Figure 6-1). Nonetheless, the issue remained with such a small tooth that the locking became ineffective. Comparing it with a Geneva gear, a Geneva gear has a more intricate tooth profile and better controls of the fluidic alignment. Inherently the Geneva gear is a better design to have intermittent rotation.

Another alternative design is to use a standard gear with the rotation controlled programmatically. This design can be achieved using a stepper motor that steps from one chamber to another. The challenge with this design is that the stepper motor is known to slip and could lose its position. Two high-resolution encoders may be required on the motor and the MCSD to support such a design. The design adds complexity to the electrical subsystem and software subsystem.

The evaluation demonstrated that the Geneva gear is still a relevant design solution for the BAMMsat concept. It also highlights the 2nd gen. Geneva gear mechanism will require some development in the material choices and build quality.

6.4 List of requirements for the 2nd gen. Geneva gear mechanism for the BoB mission

A list of requirements produced in this section was extracted from the BoB mission requirements, see Appendix A. The requirements were designed to be relaxed, ensuring that the design can meet the requirement with flexibility. The requirements were primarily used to capture the functionalities of the Geneva gear mechanism and as a management tool to ensure every team member fully understood the concept. As mentioned in the introduction, the BoB system was designed alongside other team members.

Functional requirements

FC-05 400c **The system shall measure and log the angular position of the MCSD in reference to the imaging system.**

FC-07 100c **The system shall rotate the MCSD via a Geneva drive to address independent chamber for fluidic and imaging.**

Design requirements

DG-02 100 **The electric motor shall use an encoder.**

This combined with the abutment of the MCSD will allow the system to know which chamber is being analysed by the imaging system and connected to the fluidic system.

6.5 Description on the design process

This section aims to describe the decision and evolution of the design process during the PhD research. It is hoped that the description can guide the reader and set the tone for the subsequent sections. The development began by analysing and breaking down the mechanism into parts of the actuation system, and this encompasses the motor, planetary gearhead, worm gear, Geneva gear, and bearings.

The research and development started with experimenting with the torque required to turn the MCSD. The torque required to turn the MCSD varies with the torque required to attach the MCSD with the RV. The experiment evaluated the impact of increasing the torque to clamp the MCSD with the RV on the torque required to turn the MCSD and RV ensemble.

The result from the torque experiment informs the motor selection. The torque value can be used to theoretically calculate the torque seen at the motor after the reduction from the gear ratio. Based on this information, a selection of motors can be trade-off to find the most optimal design.

After selecting the motor, the design process continued with designing the whole assembly in CAD. The CAD was designed to house the entire parts associated with the Geneva gear mechanism and interface with the MCSD and the mechanical support of the 2U BAMMsat bioCubeSat payload.

6.6 Motor selection for the Geneva gear mechanism

6.6.1 Characterising the estimated torque to rotate the MCSD once bolted

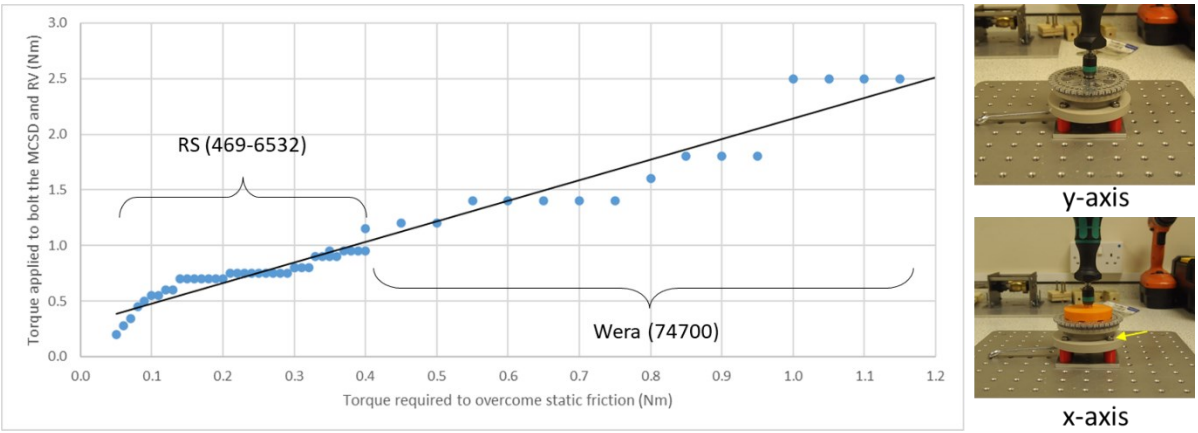

Figure 6-4. Images of torque determination test and result [1]

The graph and images in Figure 6-4 showed the result from the laboratory testing to estimate the torque required to turn the MCSD. The test was set up by bolting the MCSD and RV together using a predefined torque. Two torque screwdrivers (RS and Wera) were used to provide a range of torque from 0.05 Nm to 1.2 Nm. Once bolted, a 3D printed orange adapter was connected to either the RS or the Wera torque screwdriver to turn the MCSD (see the bottom right image in Figure t). The torque was increased gradually until the MCSD started to turn, overcoming the static friction on the rotating surface.

The torque results can gauge the range of torque in the system and directly input the motor selection. In general, the result showed that the torque required to turn the MCSD by overcoming the static friction increases with the increasing compressive force once the MCSD and RV were bolted together.

[1] Left – Results from torque testing to turn the MCSD and RV. The y-axis was the torque applied to seal the MCSD and RV. The x-axis was the torque measured to start sliding the RV surfaces. The arrow (yellow) points to the sliding surface of the rotary valve (RV). Right – Image of test setup representing the action for x and y axes.

The test was not ideal and had too many variables. It was a makeshift test setup using the resources readily available in the laboratory. The test also used the initial design of the 2nd gen. MCSD instead of the final design. Some of the issues with the setup were that the applied torque to overcome the static friction was applied to the centre of the MCSD instead of at the gear. The 3D printed part was malleable. Finally, two different torque screwdrivers were used, which have not been calibrated since the beginning of the PhD research. Each torque screwdriver also had a different resolution. For instance, the RS torque screwdriver has a resolution of 0.01 Nm, while the Wera has a resolution of 0.05 Nm. The difference in resolution can be seen in Figure 6-4. Each of these points added variables to the test result, which meant that huge margins of 3.5 times the measured values were used during the motor's sizing.

6.6.2 Estimating the torque translated at the motor from the MCSD

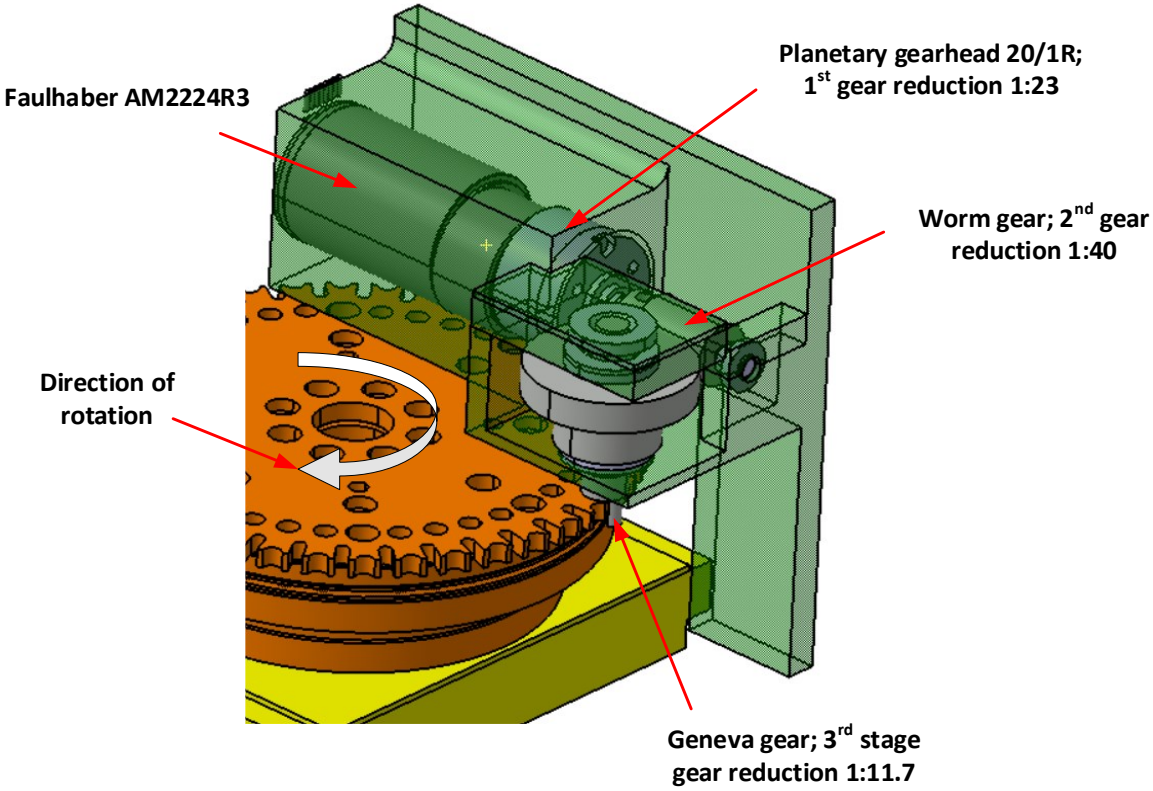

Figure 6-5. Image of the initial Geneva gear mechanism design highlighting the three gear reductions.

The rated torque of the motor primarily drives the motor selection. To begin with the selection, the torque baseline chosen as the turning torque of the MCSD was 3.5 Nm. This torque significantly increases from the highest torque value during the testing in section 6.6.1. The value was chosen to provide a considerable margin to mitigate the variables in the experiment and the unknown with the first prototype of the Geneva gear mechanism. At this stage of the development, the torque to bolt the MCSD and RV was not fully defined and unknown, linked with the pending iteration in the design and the material of the 2nd gen. MCSD and RV. The challenge with the torque value was that no motor with suitable power and volume could be found during the market research to the author's best knowledge.

The torque required at the motor can be calculated using the 3.5 Nm as a torque baseline. The calculation considered the gear efficiencies and gear reduction across the three gears stages. The first evaluation was performed on the NSTP design choice with the Faulhaber AM2224R3 and 1:40 worm gear ratio. In the worst-efficiency scenario, the motor will be required to provide a torque of 165 mNm. The AM2224R3 was rated at 22 mNm. A rated torque is the continuous torque that the motor can produce at its rated speed. In general, a higher-rated torque often translates to a bigger volume motor.

The initial evaluation demonstrated that another gear stage would be required to significantly increase the motor's torque. The finding resulted in two design changes with a planetary gearhead (1:23 gear ratio) added, and the worm gear ratio increased to 1:50. The resulting modifications showed that in the worst efficiency case, the torque required by the motor was 7 mNm, which was significantly lower than the rated torque of 22 mNm.

After the changes made to the gears, the design was promising and should be able to rotate the MCSD. Nonetheless, a trade-off was performed to optimise the system to evaluate if a much more compact drive system could be achieved.

6.6.3 Motor selection trade-off analysis

A trade-off analysis was performed to compare several motors to find a compact design solution. There are many options for miniature electronics motors in the market, and reviewing every option was not possible within the PhD and the BoB mission timeline. The same manufacturer suggested in the previous NSTP work (Faulhaber) was used to simplify the search parameters.

The parameters for the trade-off are listed below in Table 5.3, and each is weighted from 1 – to 5, with 5 being the highest-ranking score.

Table 6-1. Weighted parameter used during trade-off analysis.

Parameters	Description	Weighting
Volume envelope	The volume envelope of the motor plus associated hardware such as the planetary gearhead and encoder.	5
Encoders	An encoder enables the detection of angular motion, which helps with providing feedback on the motor's position, speed of rotation and direction.	4
Motor drivers	Faulhaber's motor often can be interfaced with its proprietary motor driver. In this trade-off, the higher score is given to a higher number of motor driver option available that is compatible with the motor. The choice was included for design flexibility in the case of design iteration.	3
Number of electrical pinouts	The number of electrical pinouts will impact the wire harnessing of the electrical system.	3

The motor with the smallest volume was selected and coupled with the appropriate planetary gearhead during the motor selection. Using the same method in section 6.6.3, the motor's rated torque from all the options was confirmed to be higher than the required torque, ensuring compatibility with the MSCD torque requirement.

The rated torque was not Included in the trade-off since it was viewed that if the rated torque is higher than the required torque, the motor will turn the MCSD. The

trade-off was performed to evaluate the other motor parameters, as shown in Table 6-1.

Based on Faulhaber's catalogue, four different motors with the appropriate planetary gearhead and encoder were selected. Both the planetary gearhead and encoders can be chosen from a pre-defined selection based on compatibility manufactured by Faulhaber. Once ordered, these options will be manufactured and assembled into a single motor unit. These four options are stated below.

Option 1: AM224 + 20-1R (1:14) + PE22-120

AM224 (22 mNm) is a stepper motor previously selected during the NSTP programme. It was included as a baseline. Compared to the discussion in section 5.5.2.2, the 20-1R planetary gearhead with a 1:14 gear ratio was chosen to reduce the cost while still being higher than the required torque. It was assumed that a lower gear reduction would translate to a lower price. The P222-120 is an incremental optical encoder. The combined total length of the motor unit is 62.1 mm, with an outer diameter of 22 mm.

Option 2: 2232BX4 + 22GPT + AES-4096

2232BX4 (18 mNm) is a servomotor and was selected as an alternative motor type. It was coupled with a 22GPT planetary gearhead with a (1:16 gear ratio) and AES-4096 magnetic absolute encoder. One of the benefits of an absolute encoder is that it provides information when the power is lost. In comparison, an incremental encoder provides only velocity and direction information. The combined total length of the unit is 71.2 mm, with an outer diameter of 22 mm.

Option 3: AM1524 + 15/10 + AE23B8

AM1524 (6 mNm) is a stepper motor. It was chosen as a smaller volume stepper motor compared to the AM224. It can be coupled with the 15/10 planetary gearhead with a 1:37 gear ratio and AE23B8 incremental encoder. The combined total length of the units is 53.4 mm, with an outer diameter of 16 mm.

Option 4: 2232 SR + 20-1R +1EH3-256

2232SR (10 mNm) is a brushed DC motor. A brushed DC motor is a classic electric motor and was added to complete the different types of motor for a full evaluation. It can be coupled with a 20-1R planetary gearhead with a gear ratio of 1:23. The gearhead is similar to the model in option 1, with a higher gear ratio. It can also be coupled with a 1EH3-256 incremental encoder.

Table 6-2. Result from trade-off analysis

	Volume envelope (5)	**Encoder (4)**	**Motor driver (3)**	**Number of electrical pinouts (3)**	**Total score**
Option 1	3	3	3	4	48
Option 2	2	5	4	4	54
Option 3	5	2	3	4	54
Option 4	4	4	4	4	60

The results in Table 6-2 showed that option 4 scored the highest during the trade-off analysis. Evaluating the result from the trade-off analysis showed that option 4 was a good compromise. In general, all the options had the same number of electrical pinouts with eight pins because of the encoders. Option 1 had 10 pins, but two of the pins are not connected and can be discarded. It was not scored as five since the simplest motor will online require two pins.

Option 3 was the smallest volume motor unit, and option 4 was the second smallest. The difference was minimal, but option 4 provided a better range of motor driver choices and a higher resolution encoder. It would have been a plus to have an absolute encoder since, in any event of power loss, the absolute position of the MCSD can be recovered. However, the volume penalty from option 2 was too significant to ignore. Based on the result, it was decided that option 4 was a good motor unit for further testing.

6.7 Final design and manufacture of Geneva gear and motor housing

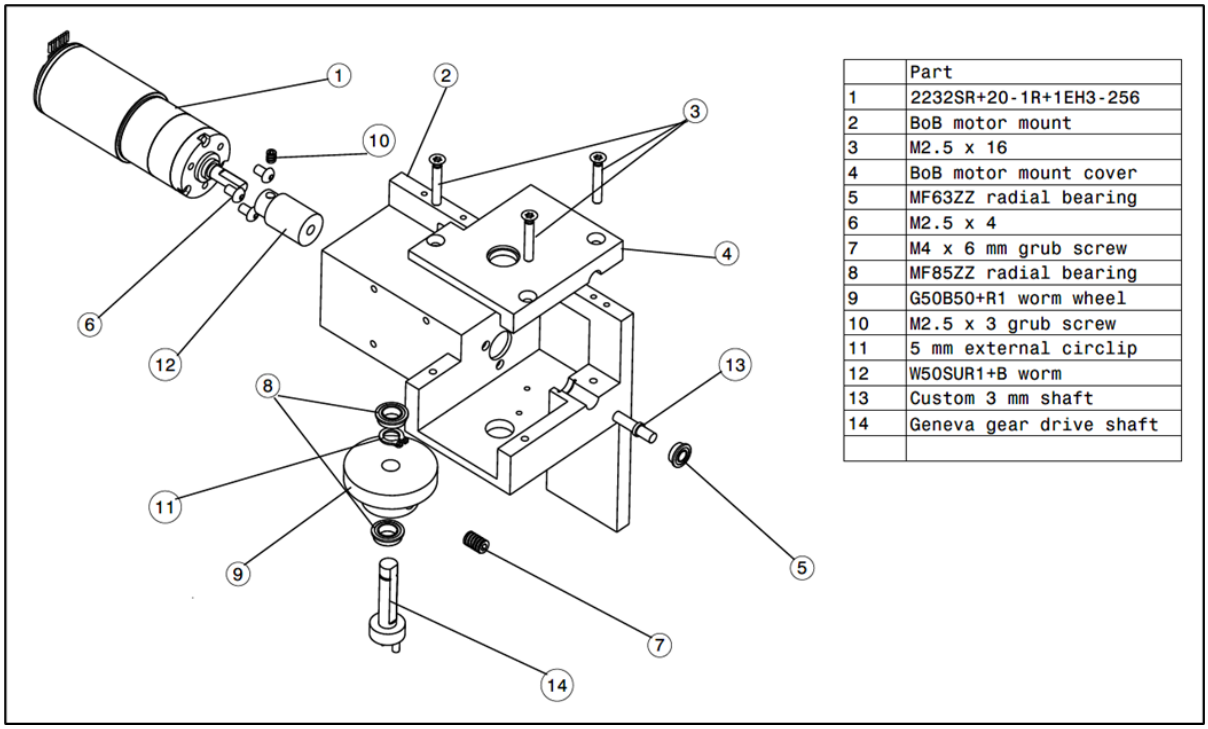

	Part
1	2232SR+20-1R+1EH3-256
2	BoB motor mount
3	M2.5 x 16
4	BoB motor mount cover
5	MF63ZZ radial bearing
6	M2.5 x 4
7	M4 x 6 mm grub screw
8	MF85ZZ radial bearing
9	G50B50+R1 worm wheel
10	M2.5 x 3 grub screw
11	5 mm external circlip
12	W50SUR1+B worm
13	Custom 3 mm shaft
14	Geneva gear drive shaft

Figure 6-6. An exploded view of the Geneva gear mechanism**.**

The Geneva gear mechanism was constructed of a motor with a planetary gearhead and encoder as a single unit, worm gear, bearings, and custom parts such as the 3 mm shaft. The entire components are then housed in a custom motor housing. The complete list of the Geneva gear mechanism is shown in Figure 6-6.

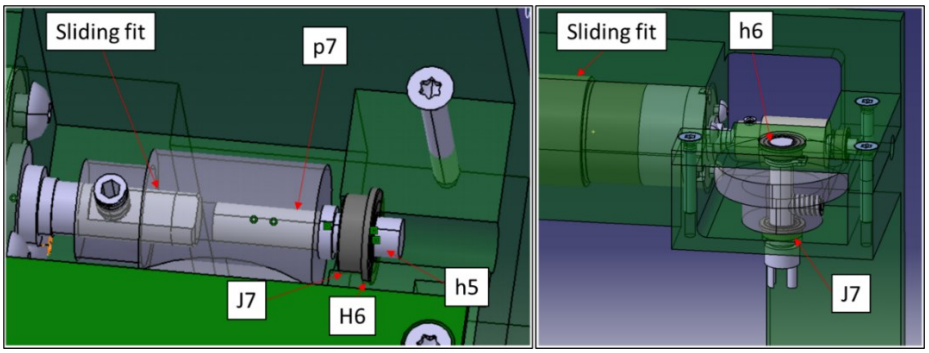

Figure 6-7. Image showing alpha-numeric code based on the ISO system of limits and fits for the tolerance fitting required by various components.

One of the challenges with designing the Geneva gear mechanism was finding the most optimum design to fit the different parts with the right tolerances. They were many different tolerances across the motor body, different sized shafts, bearings, and worm gear. It was essential to define each fitting to avoid backlash or loose parts during rotation which could have an adverse to the Geneva gear, such as loss of torque, damaged tooth or damaged motor.

The motor housing was manufactured in-house by the Cranfield Workshop to ensure the defined engineering fit could be met (see Figure 5.6). Similarly, the modification of the gears was also performed in-house. The motor housing was manufactured using aluminium 6082T6, and the Geneva drive was machined from stainless steel 303.

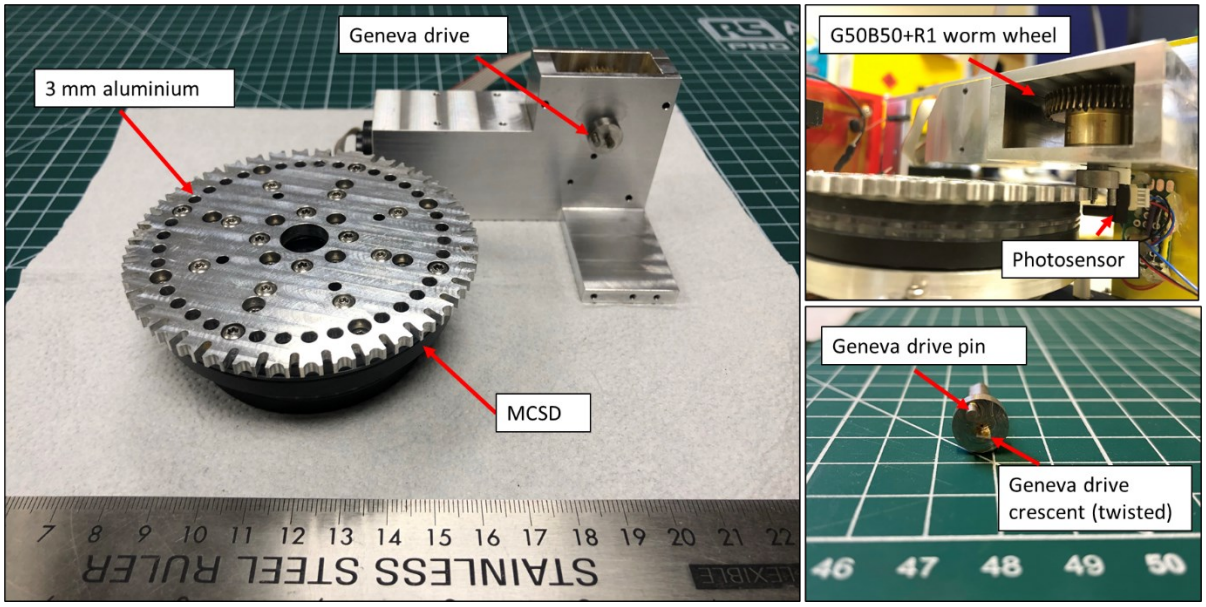

Figure 6-8. Left and top-right images show the complete assembly of the Geneva gear mechanism, and the bottom-right image shows a twisted Geneva drive crescent due to misalignment.

The final and manufactured design of the Geneva gear mechanism can be seen in Figure 6-8 alongside the MCSD. The final design also included a 5V photosensor (EE-SX3162-P2; Omron Electronics). The sensor was included in the system as an addition to the 1EH3-256 encoder. The photosensor outputs higher voltage when the gear tooth passes through it (blocking the emitter). The

sensor has a side mounting that can be attached to the motor housing and a clearance of 5 mm, which was enough for the MCSD 3 mm aluminium. The photosensor provides additional information that the encoder did not offer, such as confirming the rotation of the Geneva gear.

6.8 2nd gen. Geneva gear mechanism test

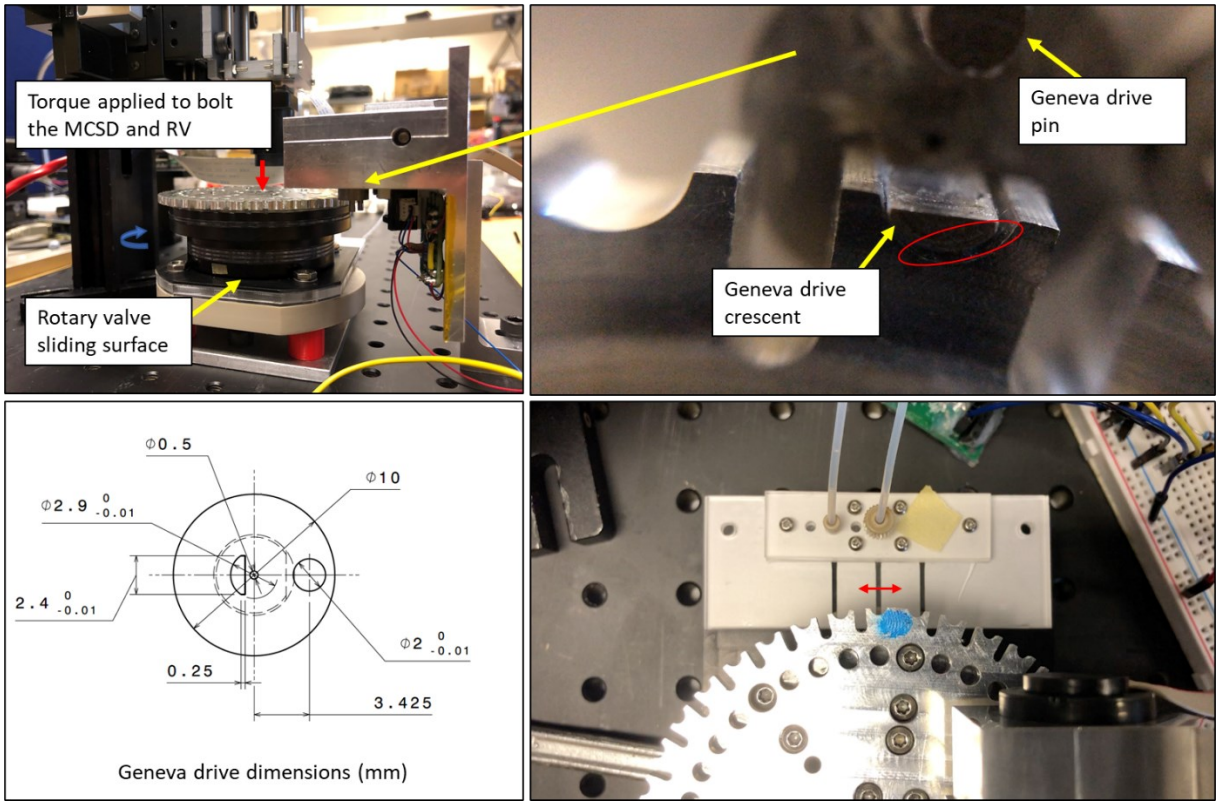

Figure 6-9. Various images of 2nd gen. Geneva gear mechanism bench test[1].

The test bench was set up to test and evaluate the Geneva gear mechanism to rotate the MCSD with the RV. The test was attached to the breadboard using custom adapters (see the top left image of Figure 6-9). Compared to the final assembly, the Geneva gear was aligned visually instead of mechanically by the housing in the full system assembly.

The test measured the current pulled from the power supply by the motor. The current can be used as a pseudo measurement of the torque applied by the Geneva drive to turn the MCSD. The power supply was connected through the current sensor (INA260; Adafruit) to the motor driver (S 1801 P; Faulhaber). The

[1] Top left – Test bench setup to evaluate the Geneva gear mechanism. Top right – Image showing the backlash in the Geneva gear. Bottom left – Geneve drive dimension used during machining. Bottom right – The impact of the backlash with the red arrow showing the backlash kinematics.

setup provided variation in the current reading once the Geneva drive pin pushes against the Geneva gear tooth on the 3 mm aluminium.

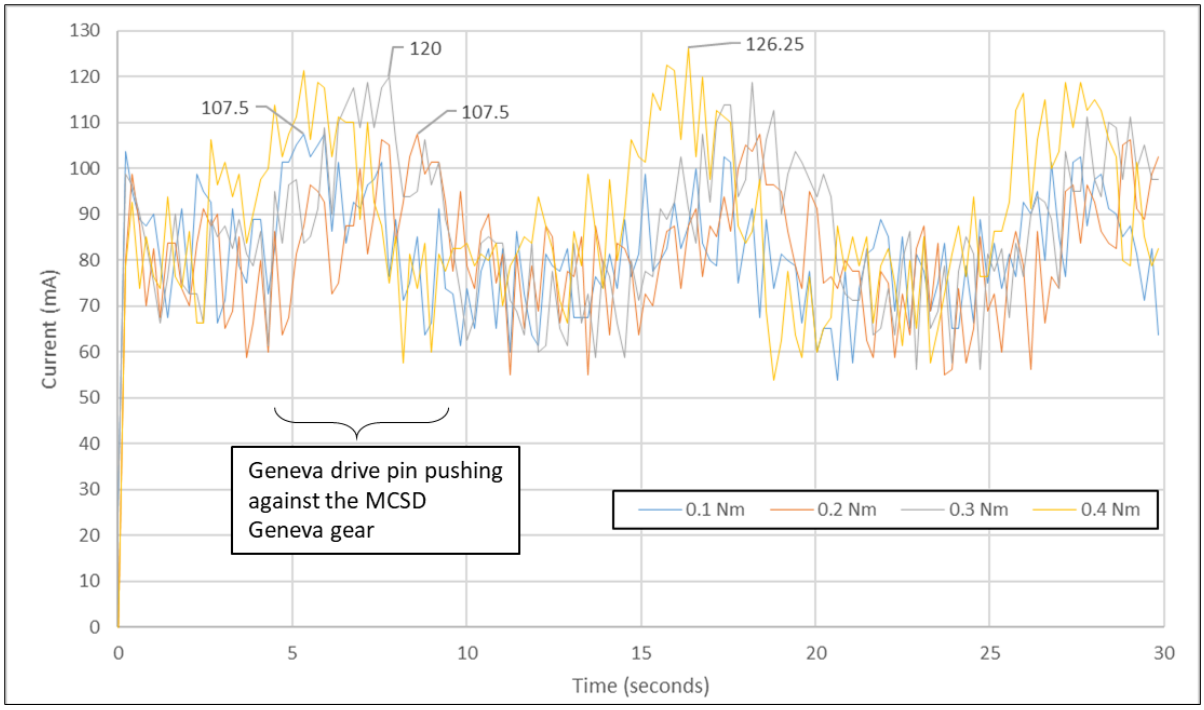

Figure 6-10. Graph of the current measurement for an increasing torque (0.1 Nm to 0.4 Nm) applied to bolt the MCSD and RV.

Figure 6-10 showed a pattern representative of the Geneva gear movement. The peak current occurred when the motor was under load when driving / turning the MCSD, and it then falls when the Geneva drive crescent is locking the MCSD in position, i.e., not under any load. The peak current (mA) difference between torque to clamp the MCSD and RV at its lowest torque of 0.1 Nm and the highest torque of 0.4 Nm was 19 mA.

The result from the test demonstrated a successful Geneva gear rotation with a minor backlash. One interesting observation during the testing was a minor backlash in the system. The backlash caused the MCSD to overshoot during rotation and return to the intended position as the Geneva drive completed its full rotation. See the red arrow bottom right image in Figure 6-9 to visualise the overshoot movement. The misalignment that caused the backlash can be seen in the top right image of Figure 6-9. The misalignment was evident when the

Geneva drive crescent was locking the MCSD. One immediate explanation could be due to manufacturing imperfection. Unfortunately, at this stage of the project, another design iteration was not possible to evaluate the backlash and provide the necessary repair. The backlash was deemed acceptable since the liquid was still pumped into the MCSD. Further testing will be required to evaluate the backlash for the next generation.

6.9 Verification matrix

This section is added to assess the requirements set for the 2nd gen. fluidic subsystem. The tests performed demonstrated that all requirements were verified, see Table 6-3. Note that there was an acceptable slight backlash with the system due to mechanical tolerance from machining and misalignment of the reference point, see section 6.8.

Table 6-3. Verification matrix for 2nd gen. Geneva gear mechanism.

Functional requirements		**Status**
FC-05 400c	The system shall measure and log the angular position of the MCSD in reference to the imaging system.	**Verified**
FC-07 100c	The system shall rotate the MCSD via a Geneva drive to address independent chamber for fluidic and imaging.	**Verified**
Design requirements		
DG-02 100	The electric motor shall use an encoder.	**Verified**

6.10 Discussion, conclusion, and future work

6.10.1 Discussion and conclusion

The Geneva gear mechanism was developed to rotate the 2nd gen. MCSD and enabling the design functionality of the rotary valve. Without the Geneva gear mechanism, the unique design feature of BAMMsat's ability to have 32 - 40 independent and discrete sample chambers will not be possible.

When evaluating the 1st gen. Geneva mechanism feasibility, the result showed that it was not ready for flight. A significant development was required to size the mechanism from motor selection, gear selection, and encoder selection. Also, the build quality needed to be improved significantly to operate the Geneva gear, especially at the lower end of the gear dimension.

A trade-off was performed to compare the motor selected during the 1st gen. with other appropriate motors from Faulhaber to ensure that an optimum motor was selected. Once selected, the motor with the planetary gearhead and encoder came as a single unit. It was then coupled with the worm gear to provide increased torque transmission and the right-angle transmission required to turn the MCSD. The trade-off resulted in the 2232SR DC motor with a 20-1R planetary gearhead with a 23:1 gear ratio and IEH3-256 optical encoder. Another photosensor, EE-SX3162-P2, was also included in the design to provide information on the MCSD rotation.

Regarding build quality, the millimetre range dimension of the Geneva gear teeth and drive meant that tolerance was a key factor during design and manufacturing. Similarly, the tolerance for housing of the motor, shaft and bearings had to be defined to avoid any loose parts and misalignment. Despite the attempt to control the dimension, there was still backlash in the Geneva drive. The backlash resulted in the MCSD overshot when turning to the next chamber and returning to the required alignment.

It was impossible to observe any potential misalignment within the design to see if the fluidic port was blocked and at what level since it was located between many

obscure layers. Immediate pumping showed that liquid can still flow after moving to the next chamber. After this test, further iteration was not possible due to the BoB mission timeline. The backlash was deemed acceptable since the fluid was still flowing during pump actuation.

The initial attempt to characterise the motor was performed by measuring the current pulled against the increasing friction to rotate the rotary valve. Current measurement is often proportional to torque value and can be helpful during operation to provide information on motor performance. The result showed that the current was behaving as expected with increasing peak current as the friction increased.

Further testing on motor characterisation must be performed to translate the current reading into a physical torque value. The first test will repeat the test performed to record more data on the current value at a much more extensive range of friction. It is also worth performing a rotary torque sensor test to have a precise and accurate shaft output torque measurement and compare it with the current consumption for the complete motor plus gearing characterisation.

One criticism of the design was the oversized motor. The reason behind the oversized motor was the high margin allocated to turn the MCSD and RV. The torque required to turn the MCSD and RV was set at 3.5 Nm to mitigate the unknown risk associated with the design. At 3.5 Nm, any motor of choice required a planetary gearhead to increase its torque transmission.

The trade-off resulted in a smaller motor with 7.1 mm in diameter and 4.1 mm in length less than if the 1st gen. motor was selected. The next iteration design can be sized at the lower-rated torque with or without the planetary gearhead. Either way, it is envisioned that the volume envelope of the next generation Geneva gear mechanism will have a smaller volume envelope and, subsequently a smaller housing envelope.

After the design, manufacture and test, the Geneva gear mechanism was ready to be integrated into the full-system test and further evaluation.

6.10.2 Future work

Immediate future work would include further testing to diagnose the issue encountered during the testing.

- Further testing to diagnose the backlash from the Geneva gear.
    - During the Geneva gear mechanism test, there was an apparent backlash in the system. It is hypothesised that the backlash could be due to misalignment during assembly or imperfection in the Geneva gear geometry. Further testing will repeat the test while mitigating any possible misalignment. In parallel, an in-depth evaluation will be performed on the machined Geneva gear geometry against the theoretical design to evaluate manufacturing imperfections or mistakes during the design.

Long-term future work would include design optimisation on the Geneva gear mechanism.

- Perform design optimisation for the Geneva gear mechanism.
    - As mentioned in the discussion in section 5.7.3, the motor for the subsystem was oversized. It is worth optimising the motor and the gearing unit since it will reduce the Geneva gear mechanism's total volume envelope and mass. The optimisation can begin with incorporating lessons learnt on the realistic torque required to bolt the MCSD and RV. The input will evaluate the resulting impact on the coefficient of friction and the torque needed to turn the MCSD. The torque required to turn MCSD will be used as the motor and gear sizing baseline.
- Perform a test using a rotary torque sensor to characterise the Geneva gear mechanism (motor plus gears) to measure the torque to turn the MCSD for direct comparison with the current consumption.
    - Based on the current industry design practice, measuring the torque using a calibrated rotary torque sensor is possible. The benefit of performing this test via a calibrated rotary torque sensor

is the value of the physical torque imparted on the MCSD. The torque value can then be coupled with the current reading as another source of information. The current reading can be valuable information on motor performance in spaceflight since direct access is not possible.

7 Subsystem level – Mechanical support: Design, manufacture and test

7.1 Introduction

Chapter 7 discusses the development of the final subsystem in the PhD research. The chapter aims to capture the process behind the design and manufacturing to provide the mechanical support BoB mission. The mechanical support provided the housing for the 2nd gen. BAMMsat bioCubeSat payload. It was designed to fit into a 2U CubeSat format pressure vessel. The payload encompassed the subsystems discussed in this chapter and previous chapters, such as the MCSD and RV, compact brightfield microscope, fluidic subsystems, Geneva gear mechanisms and fluidic reservoir bags. The mechanical support also housed other components such as PCBs, thermal heaters, and thermal sensors developed by the other team members. See section 9.3 for more detail on the different work packages and associated team members.

The mechanical support for the BoB system is built upon the concept developed for the 1st gen. BAMMsat bioCubeSat payload; see section 1.2 for historical context. At the start of the PhD, 1st gen. BAMMsat bioCubeSat payload design was advanced to an initial CAD concept for a volume fit check. The work performed during PhD took the lessons learnt from 1st gen. CAD design to design, manufacture, and assemble a functional mechanical housing for the BoB mission. This chapter will end the discussion at the subsystem level before the assembly, integration, and verification (AIT) in Chapter 8.

7.2 Aim and objectives

1) *Evaluate and critique the 1st gen. design of the mechanical support as an input into the 2nd gen. design*

The objective was created to leverage the previous development work during the 1st gen. to extract any lessons learnt that will be valuable for the 2nd gen.

2) *Produce a list of requirements extracted from BAMMsat-on-BEXUS mission requirements*

This objective was added to produce a list of requirements from the BAMMsat-on-BEXUS mission

3) *To design, manufacture and assemble mechanical support to house the MCSD and RV, the imaging subsystem, Geneva gear mechanism, and fluidic subsystem inside the BAMMsat-on-BEXUS 2U pressure vessel*.

The objective originated from the need to repackage the subsystems and components that construct the 2nd gen. BAMMsat bioCubeSat payload into a 2U format ready for the BoB mission.

7.3 Overview of the 1st gen. mechanical support

7.3.1 Introduction to the 1st gen. design

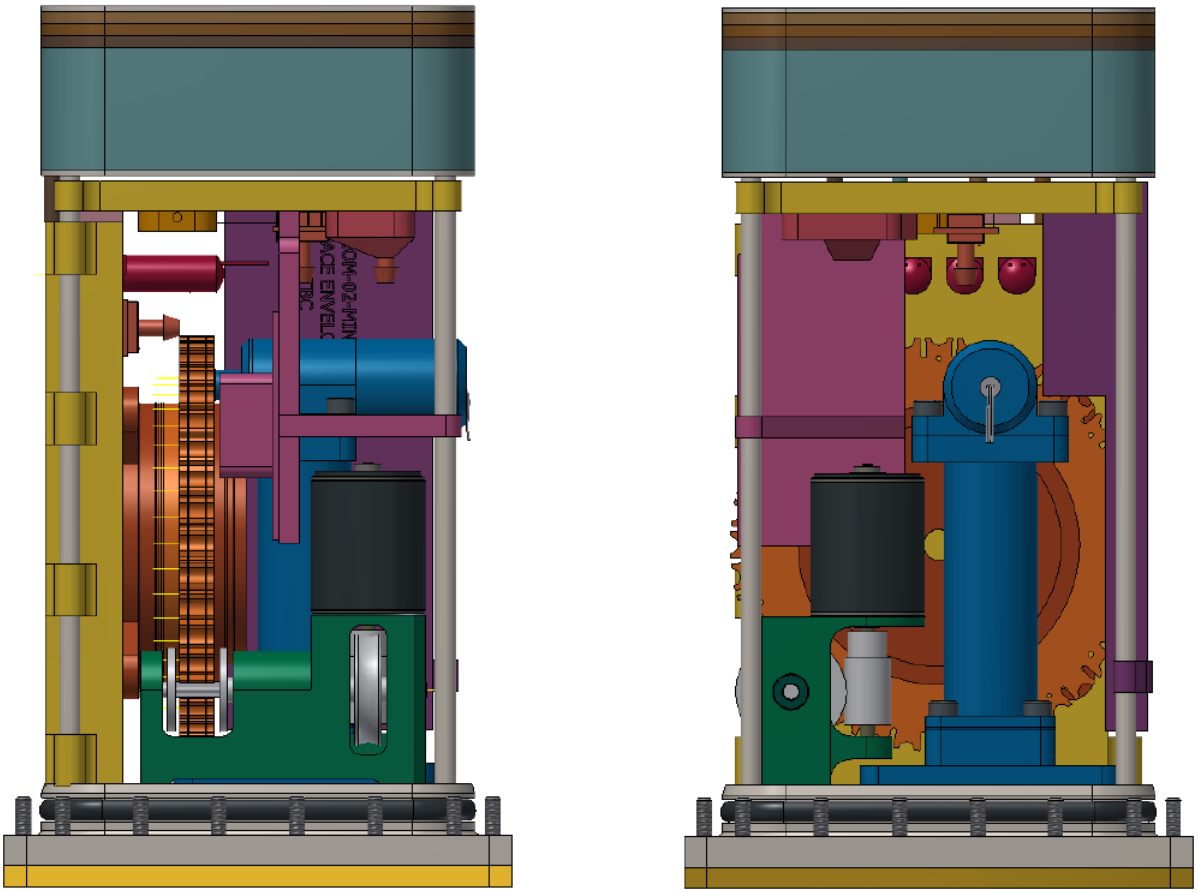

Figure 7-1. Two projections of the CubeSat payload assembly with vessel cover removed**.** Images courtesy of Prof Cullen.

The first-generation mechanical support has been designed and manufactured into a laboratory breadboard version. It was first developed as a flat sat breadboard (see Figure 5-1) for fluidic testing and later integrated with the BAMMsat 1st gen. microscope (see Figure 1-2). In both designs, the mechanical support was optimised for laboratory breadboard versions.

As part of the NSTP programme, a small work package was included to package the components of the 1st gen BAMMsat bioCubeSat payload for a fit check inside a 2U pressure vessel (see Figure 7-1). The CAD packaging exercise was performed to evaluate any showstopper in the design. The CAD demonstrated

the various components and subsystems which were designed for 1st gen. BAMMsat bioCubeSat payload fits into the 2U pressure vessel. It also highlighted the limited spare volume available and the importance of assembly and integration procedures. There was also limited mechanical mounting volume and the complexity of including wire and fluidic harnessing.

7.3.2 Evaluation and critiques of the 1st gen. design

At the start of the PhD research, the further mechanical support of the BAMMsat concept was developed into an initial CAD design of the 1st gen. with the flight volume form factor. The design was helpful to conceptualise what will be required in the 2nd generation design and understanding the parts to be manufactured. The design was still early stage and required significant development from the 1st gen. BAMMsat bioCubeSat payload into the 2nd gen. BAMMsat bioCubeSat payload ready for BoB mission.

The NSTP CAD was also missing some key designs. One of them was the PCBs that needed to be inside the 2U pressure. At this stage of the project, the PCB has not been designed. The dimension and volume of the PCB will affect the mechanical mounting it requires and the structure inside the 2U pressure vessel. Similarly, the 2nd gen. mechanical support will require integration of the 2nd gen. MCSD and RV (see Chapter 3) and compact brightfield microscope (see Chapter 4).

7.4 List of requirements for the 2nd gen. mechanical support

The requirement in the section was extracted from the BoB requirements. A reader interested in the complete list of the requirements can see Appendix A. As mentioned previously, the requirements BoB mission were designed to be relaxed, ensuring that the design can meet the requirement with maximum flexibility. The only requirement for the mechanical support subsystem is to ensure that the volume and size are below 2U.

Design requirements

DG-04 100	**The dimension of the pressure vessel shall not exceed a 2U CubeSat format.**

7.5 Discussion on the design and manufacturing process

The mechanical housing design was driven by a design philosophy and a few design drivers. The design philosophy was to have an open space concept to provide flexibility so any structure could be added, removed, and modified without an adverse effect. The philosophy came from managing the unknown risk associated with being the first complete prototype in a flight representative format. The design philosophy resulted in the design of the rails and supporting columns (see Figure 7-2).

The rails were used as a reference point during the design, where the subsystem was aligned and assembled along the rails. The square ends of the rails were designed with H6/h6 location fit, which has close clearance and can be assembled without force. The pressure vessel and the pressure vessel lid were designed by A. Chabi, one of the BAMMsat-on-BEXUS team members. The mechanical interface to the 2U pressure vessel was developed in collaboration with A. Chabi.

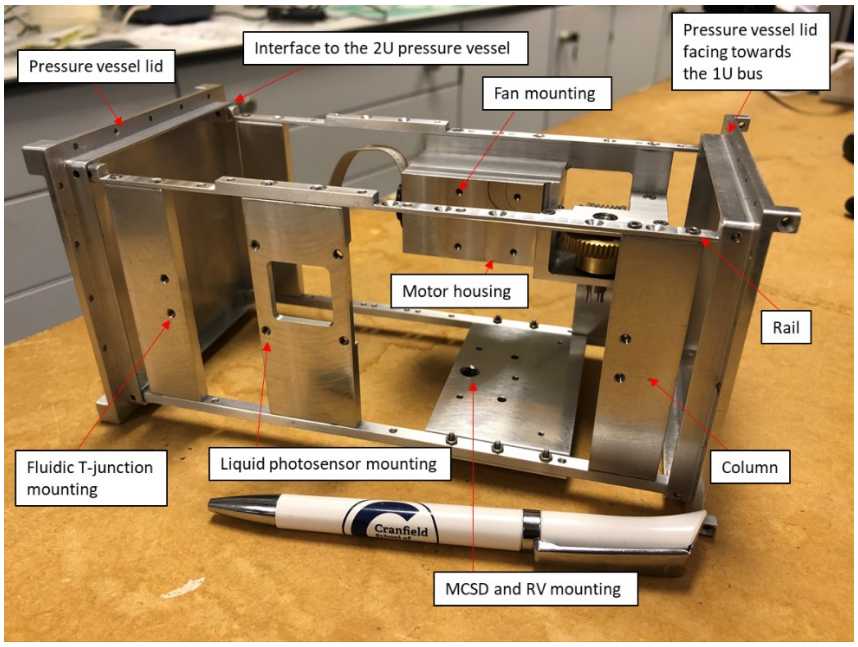

Figure 7-2. The mechanical support for the 2nd gen. BAMMsat bioCubeSat payload was manufactured and assembled during a mechanical fit check.

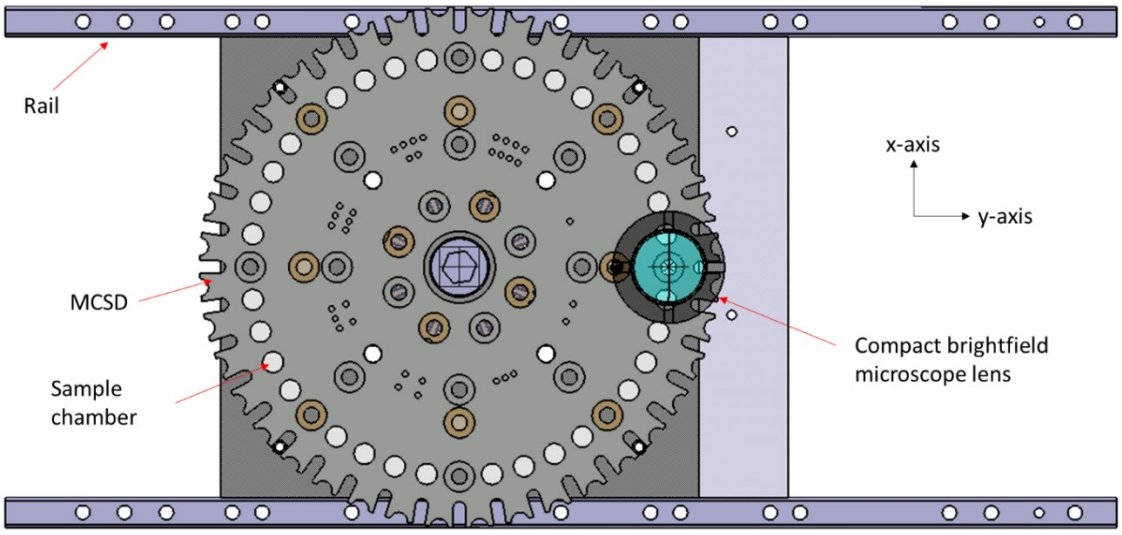

Figure 7-3. Top view CAD image showing the MCSD and the compact brightfield microscope lens.

There were two design drivers identified during the development. The first design driver was aligning the MCSD with the mechanical structure. The diameter of the MCSD was 87mm. In a CubeSat format, the short axis (x-axis) of the 2U CubeSat is 100 mm. The MCSD was mounted in the middle of the x-axis between the two rails (see Figure 7-3). By aligning the MCSD in the middle, the MCSD was used as a reference point for positioning the rest of the subsystem.

The second driver was the alignment of the compact brightfield microscope to the imaging plane. The challenge with a circular MCSD design was ensuring that the centre of the circular lens matched the centre of the sample chamber. Geometrically, if the lens was placed at an angle to the centre of the MCSD, the mounting points for the compact brightfield microscope would also be at an angle.

The impact will be on the dimensioning of the parts for machining, which will be more challenging to machine to the correct dimensions. At this stage of the project, the compact brightfield microscope was developed in parallel, and the FOV and sensitivity of the compact brightfield microscope were not thoroughly tested. Similarly to the MCSD, the lens was placed in the middle of the x-axis to simplify the dimensioning. By having the position of the MCSD and compact

brightfield microscope fixed on one axis, the MCSD and the compact brightfield microscope can be adjusted by moving along the y-axis (see Figure 5-11).

7.6 Issue during the initial mechanical assembly test

After all the parts were machined, an initial assembly test was performed to ensure that parts were machined accordingly and could be assembled. During the test, it was identified that the interface between the rails and the pressure vessel lid did not fit and had to be forced in. The impact of forcing the fit caused the rail to bend at its weakest point (see Figure 7-4).

After the diagnostic, two design issues were found to have caused the problem. It was found that bending happened because the length of the rails was the same length as the pressure vessel. During assembly, the surface of the rail facing the pressure vessel lid was pushing against the wall of the pressure vessel lid, putting an inward pressure on the rails.

The second design issue was the fitting issue. This was because the square end of the rail did not fit into the square hole of the pressure vessel lid (see Figure 7-5). The issue occurred during machining due to the small diameter drill bit and the depth of the drill. The milling bit was defined by the square corner radius of 1 mm (see Figure 7-5), and the depth of the drill was 7 mm. The small milling bit and relatively deep drilling caused the bit to wobble during machining. The impact of wobbling meant that each square surface was not perpendicular to one another.

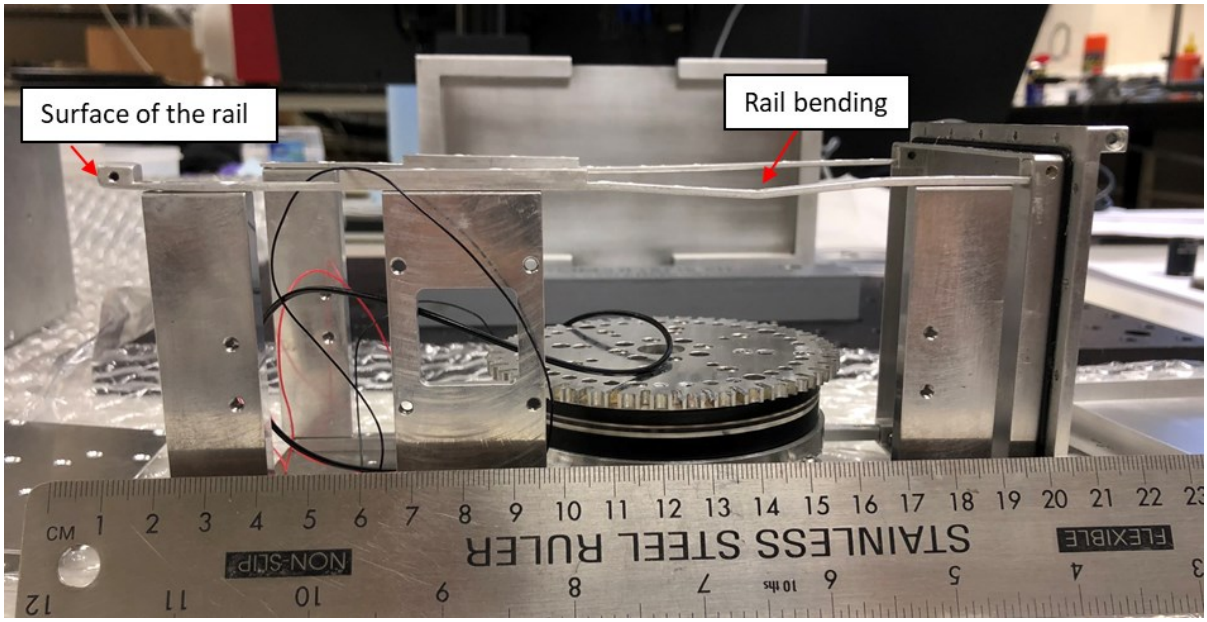

Figure 7-4. Damage was incurred on one of the rails during a mechanical fit check.

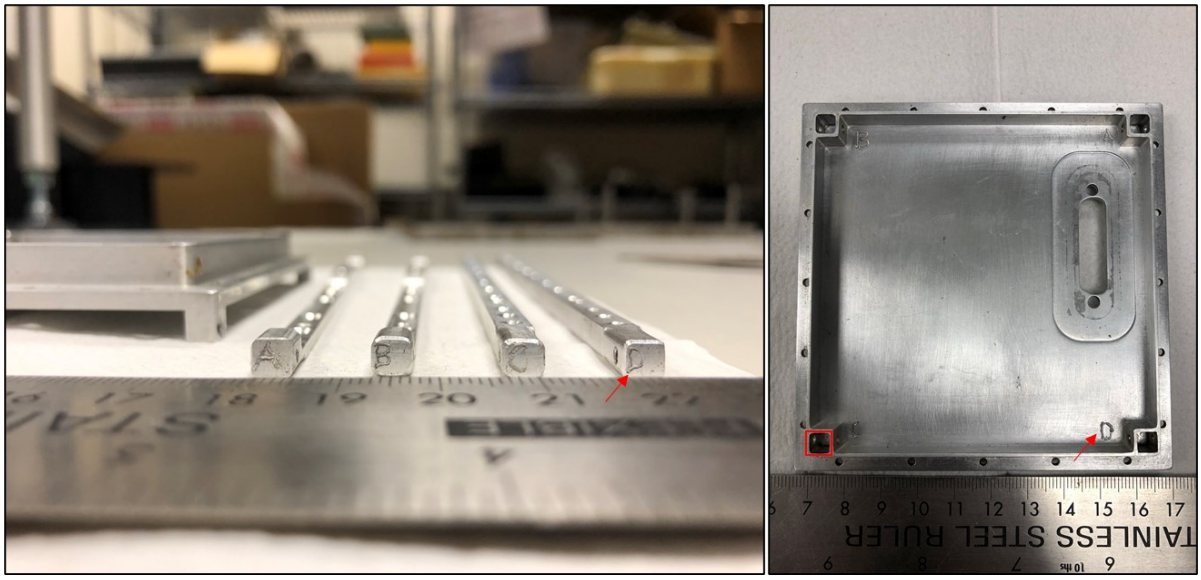

Figure 7-5. The modified rails are custom-fitted to each square hole on the pressure vessel lid to accommodate the design issue with each square end of the rail.

The rails were modified since a replacement was required after the damage. Redesigning a new mechanical interface was not feasible within the project timeline, and machining a new pressure vessel lid will incur additional costs and pressure vessel re-verification.

The rail was redesigned with three changes to accommodate the design issue. The rail material was changed from aluminium 6060 to aluminium 7075T6, with a higher tensile strength. Every square end was custom-fitted to the rail slot, with each face of the square sanded down until the right fit was achieved. Each rail was then labelled to ensure correct fitting during assembly. The final design change also shortened the rail's total length to avoid the rail pushing against the lid.

7.7 Verification matrix

This section is added to assess the requirements set for the mechanical support subsystem. The tests performed demonstrated that all requirements were verified, see Table 7-1.

Table 7-1. Verification matrix for mechanical support subsystem.

Design requirements		
DG-04 100	The dimension of the pressure vessel shall not exceed a 2U CubeSat format.	**Verified**

7.8 Discussion, conclusion, and future work

Chapter 5 discusses the research and development of the remaining subsystems and components that formed the 2nd gen. BAMMsat bioCubeSat payload. These subsystems and components were developed in parallel alongside the 2nd gen. MCSD and RV (see Chapter 3) and the compact brightfield microscope (see Chapter 4). The activities around design, manufacture and test were completed during the BAMMsat-on-BEXUS (BoB) mission before the flight in October 2021.

7.8.1 Discussion and conclusion

The mechanical support provided the housing and mechanical interfaces for all the subsystems and components within the 2nd gen. BAMMsat bioCubeSat payload. This range from the subsystems and components developed as part of this PhD research, such as the MCSD and RV, compact brightfield microscope, fluidic subsystems, Geneva gear mechanisms and fluidic reservoir bags. It also housed other subsystems and components such as PCBs, thermal heater, and thermal sensors developed by the other team member of the BAMMsat-on-BEXUS team.

During the 2nd gen. mechanical support research and development, one of the biggest challenges was managing the interfaces between the entire subsystems and components since the design was often incomplete or not thoroughly tested when the decision was made. For this reason, open space design was the primary design philosophy. The design resulted in a cuboid frame constructed from machined aluminium rails with columns and a base plate for support. The frame then allows the various parts to be mounted where necessary or possible.

However, the design is not optimum since the electrical and fluidic interface requires wires and fluidic tubing. Without optimising the location, in a volume restricted CubeSat, the impact of many wirings and tubing can be significant. Nonetheless, the design decision was fruitful in some cases since some design iteration was required with the selector valves manifold and motor housing. The

open space design allowed both subsystems to be dissembled and changed without adversely affecting the rest of the system.

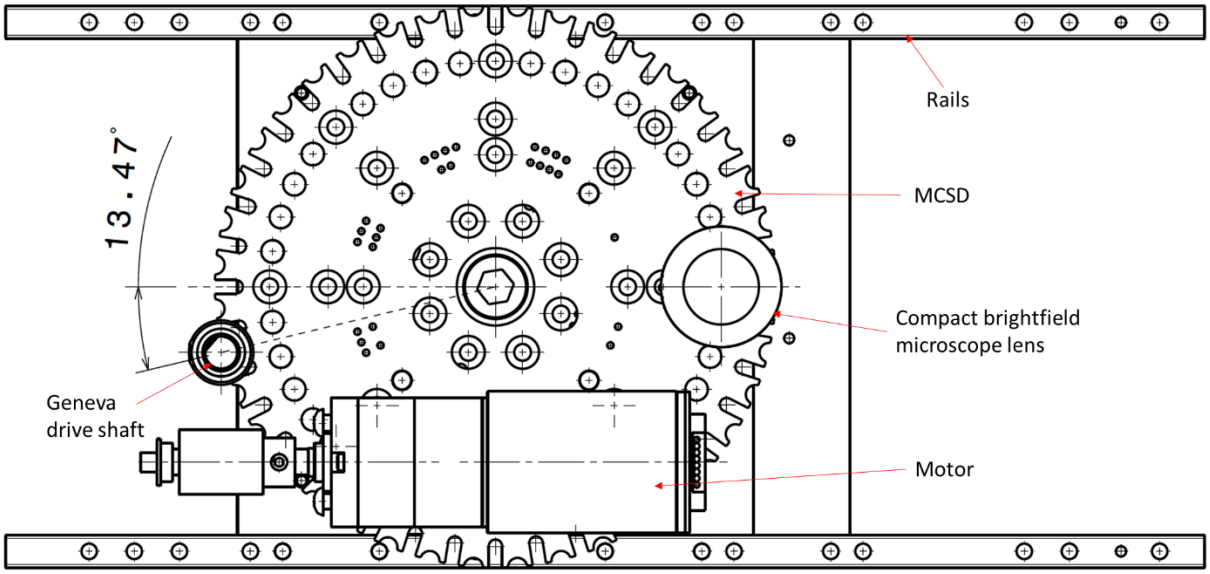

Figure 7-6. Top view image of the MCSD bolted to the RV and the compact brightfield microscope and Geneva drive shaft[1].

One criticism of the design of the mechanical support was the motor housing. During the design phase, the Geneva drive shaft will be placed at an angle to the centre of MCSD. It was proven to be challenging during manufacturing since the mechanical drawing resulted in an unfriendly dimension for the machinist. It meant that more care had to be placed during machining to ensure the correct tolerance could be met.

Although this design issue was identified since it was very similar to the argument for aligning the compact brightfield microscope, the decision was made to reduce the mass of the aluminium since the motor housing required a much more mechanical structure. For the next iteration, to reduce complexity during manufacturing, it is suggested that the centre of the Geneva drive is along the centreline of the MSDC, similar to the compact brightfield microscope.

[1] The motor housing and part of worm gear were removed for illustration purposes.

The biggest issue with the design was the rails. Relative to the rest of the structure, the rails were small in volume and had many structural weak points. On top of that, the square shape hole mechanical interface to the 2U pressure lid was the wrong design choice. A circular-shaped hole and shaft would be more effective if a similar design were required since a larger milling bit can be used for tighter tolerance control. For the BoB mission, it was adequate. However, for a spaceflight version, a significant redesign will be required on the entirety of the mechanical structure to optimise the location, housing and mechanical load path.

7.8.2 Future work

Future work would include design optimisation on the fluidic subsystem, Geneva gear mechanism and mechanical support.

- Perform design optimisation on the mechanical support.
    - The design optimisation should consider the lesson learnt during the development to optimise the location of the subsystems and components to reduce mechanical support, wire and wire harnessing, and fluidic tubing.
- Redesign the mechanical interface with the 2U pressure vessel.
    - The mechanical interface in the current design (rails) is not suitable for spaceflight, considering the stress and loading during launch vibration. A complete redesign will be required taking into account spaceflight requirements.

8 System level – 2nd gen. BAMMsat bioCubeSat payload: Assembly, Integration, and Testing (AIT)

8.1 Introduction

This chapter discusses the full system integration of the subsystems and components developed in previous chapters into the 2nd gen. BAMMsat bioCubeSat payload. The 2nd gen. BAMMsat bioCubeSat payload combines multi-chamber sample disc (MCSD), rotary valve (RV), fluidic subsystem, and Geneva gear mechanism housed in mechanical housing in a 2U CubeSat format in preparation for the BoB flight campaign.

As a reference, four terminologies are re-introduced here as a reminder to help contextualise the discussion. The four terminologies will be referred to regularly throughout the chapter.

- BAMMsat-on-BEXUS mission or BoB mission

The term BoB mission refers to activities that encompass a typical space mission. This term represents the activities and processes behind the overall mission aim of performing technology and operational demonstration of the 2nd gen. BAMMsat bioCubeSat payload on a stratospheric balloon flight.

- BAMMsat-on-BEXUS flight campaign or BoB flight campaign

The term BoB flight campaign refers to a series of activities performed during the flight campaign between 24th September – 4th October 2022 at ESRANGE Space Centre, Kiruna. The activities included pre-flight operations, flight operations and post-flight operations.

- BAMMsat-on-BEXUS system or BoB system

The term BoB system refers to the 3U CubeSat format system encompassing the 1U bus and the 2nd gen. BAMMsat bioCubeSat payload. The 1U bus was the "brain" of the BoB system and acted as the mechanical, electrical and data interface between the 2nd gen. BAMMsat bioCubeSat payload and the BEXUS gondola.

- 2nd gen. BAMMsat bioCubeSat payload

The 2nd gen. BAMMsat bioCubeSat payload is the autonomous miniaturised laboratory at the core of the BAMMsat concept with the subsystems developed during this PhD. It is a 2U bioCubeSat payload system used to house and observe the biological samples and a subsequent generation development from the laboratory breadboard version (1st gen. BAMMsat bioCubeSat payload) flown into the stratosphere.

Chapter 6 aims to bring together the various subsystems developed and construct them into a full system. In a space engineering development workflow, this will fall under assembly, integration, and testing (AIT). The discussion will begin with an overview of the planned BoB system at the CDR stage (May 2020) and end with a version of the BoB system ready to be shipped to Esrange Space Center (August 2021). Within the BoB mission timeline, a formal from the BEXUS programme was required for participants. At this stage of the BoB mission, a full system conceptualised design has been developed.

It is essential to acknowledge that a student team developed the BoB systems. The subsystems and components that sit within the 2nd gen. BAMMsat bioCubeSat payload also included the 2U pressure vessel (Chabi, 2020), an active thermal subsystem (Bolliand, 2020), printed circuit board (PCBs) from the electrical subsystem (Sinclair, 2020), biological system (M. Cooke), and software (M. Zalasiewicz). Some team members had their work package as their MSc thesis output, and some opted not to do it. The author worked closely with these team members to ensure that the design outputs from the author's work package interface correctly with their respective work packages and vice versa. A more detailed breakdown of each team member's responsibilities can be read in section 9.3 of this thesis.

During the development, due to time constraints and results from testing, the design was changed from the version that was initially intended for AIT (June 2021) to a version that was ready to be shipped to Esrange Space Centre. This chapter aims to capture the design changes.

With regards to the 2nd gen. BAMMsat bioCubeSat payload. The activities performed during AIT, discussed within this chapter, helped verify and validate the design. The discussion will describe the assembly and integration process. It then continues with testing, highlighting the issue and modifications to the design in preparation for the BoB flight campaign.

8.2 Aim and objectives

1. *Provide an overview of the BoB system and its evolution from the initial design into a version ready to be shipped to the Esrange Space Centre for the BoB flight campaign.*

The objective was included to capture how the planned initial design of the BoB system evolved into a version ready to be shipped to the Esrange Space Centre due to results throughout the development.

2. *Perform assembly, integration, and testing of the 2nd gen. BAMMsat bioCubeSat payload into the BoB system.*

The objective was to build toward a complete BoB system incorporating the subsystem and components developed throughout the PhD research. The multi-chamber sample disc (MCSD), rotary valve (RV), compact brightfield microscope, fluidic subsystems, Geneva gear mechanisms, and fluidic reservoir bags. These subsystems and components were assembled, integrated, and tested into a 2nd gen. BAMMsat bioCubeSat payload and then into the BoB system.

8.3 Overview of BoB system (3U) initial design

This section aims to provide an overview of the BoB system. BoB system is a 3U CubeSat format consisting of a 1U bus and a 2U 2nd gen. BAMMsat bioCubeSat payload (see Figure 8-1 and Figure 8-2). The 2U payload was housed inside a custom 2U pressure vessel which maintained the ambient atmosphere against a near-vacuum environment in the stratosphere. The 1U bus was the "brain" of the BoB system. It housed the onboard data and the electrical power system (EPS), which step-down the 28 V power supply to power the primary computer, microcontroller, sensors and actuators. The 1U bus was the bridge or interface between the BEXUS gondola and the 2nd gen. BAMMsat bioCubeSat payload.

It must be made clear that the BoB system was developed by the BoB team members and not just by the author of this document. The author of this document researched and developed the core BAMMsat concept of the 2nd gen. BAMMsat bioCubeSat payload inside the 2U pressure vessel. The list of the worked technology is the multi-chamber sample disc (MCSD), rotary valve (RV), compact brightfield microscope, fluidic subsystems, Geneva gear mechanisms, and mechanical housing. The other subsystem is mechanical (Chabi, 2020), thermal subsystem (Bolliand, 2020), electrical (Sinclair, 2020), biological system (M. Cooke), and software (M. Zalasiewicz). The corresponding team members led the design, manufacturing, and testing of these subsystems.

The author worked closely with these team members to ensure that the design outputs from the author's work package interface correctly with their respective work packages and vice versa. A more detailed breakdown of each team member's responsibilities can be read in section 9.3 of this thesis.

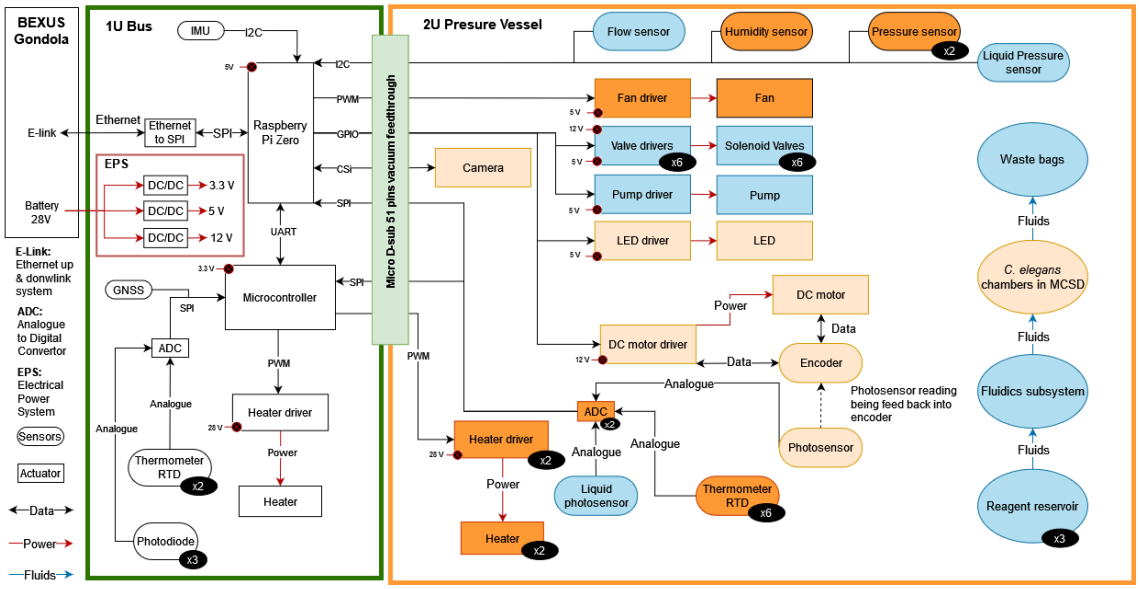

Figure 8-1. Block diagram of the BoB system during CDR stage with the associated interfaces for electrical, communication protocol and power.

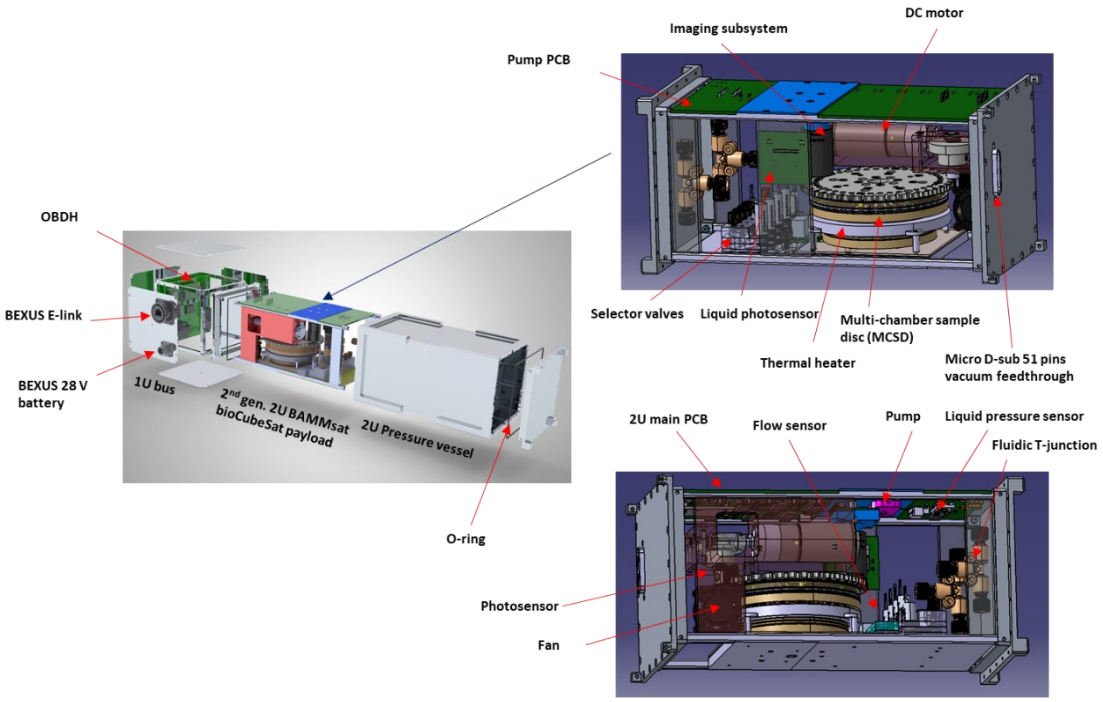

Figure 8-2. (Left) Labelled exploded CAD overview of the 3U BoB system with a 1U bus and 2U BAMMsat bioCubeSat payload. (Right – top and bottom) Labelled 2U BAMMsat bioCubeSat payload.

As a reference point, this section presents the BoB system that was designed during the CDR stage of the BoB missions. The design is captured in Figure 8-1 and Figure 8-2. As the project progressed, the design that was shipped to the flight campaign evolved into a design with reduced functionality. The reduction was due to assembly, integration, testing and time constraint.

The 1U bus can be considered a standalone "satellite" unit. The 1U bus housed the primary flight computer (Raspberry Pi Zero W) and microcontroller (Adafruit ItsyBitsy M4 Express with ATSAMD51 processor). The flight computer and microcontroller provide the processing functionality for the autonomous operations, power, data, telemetry and telecommand handling of the system. It also housed the electrical power system (EPS). The EPS converts 28 V to 3.3 V, 5 V, and 12 V for the computer, microcontroller, sensors, and actuators. The 1U also has thermal sensors and a heater to ensure that the computer's temperature does not go below its minimum operating temperature due to the cold temperature in the stratosphere.

In the initial 1U bus design, it was intended that the design replicates the complete functionalities of a 1U free-flying bioCubeSat. The justification was to use BEXUS opportunity and technological development to learn the design as broadly as possible in preparation for spaceflight. For this reason, positioning sensors such as IMU and GNSS were included since going through the design process will inform future design. However, the BoB mission was not a direct comparison to a free-flying CubeSat. The power and communication were supplied by a host satellite (BEXUS gondola) instead of having a solar panel and antenna.

The block diagram in Figure 8-1 shows three primary units: the BEXUS Gondola, 1U bus, and 2nd gen. BAMMsat bioCubeSat payload inside a 2U pressure vessel. Each of these units has a mechanical and electrical (power and data) interface between them. Mechanically, the 2U pressure vessel was bolted to the 1U as a single unit BoB system. The BoB system was mounted to the BEXUS gondola using a custom-made mounting frame.

The power to the BoB system was provided by the BEXUS gondola. Eight SAFT LSH 20 batteries (lithium-thionyl chloride) supplied the 28 V/1 mA through the Amphenol PT02E8-4P connector (Frenea-Schmidt, 2021). Bidirectional data was provided by the BEXUS E-Link, which can transmit and receive data from the Esrange ground station. The data interface was connected via an Amphenol RJF21B connector. See Figure 8-2 for the connection points on the 1U bus.

8.4 Overview of the 2nd gen. BAMMsat bioCubeSat payload (2U) initial design

The section provides an overview of the complete initial design of the 2nd gen. BAMMsat bioCubeSat payload as a continuation of the previous section 8.3. As an overview, the BAMMsat bioCubeSat payload can be defined as an autonomous miniaturised laboratory. The BAMMsat concept aims to replicate the functionalities frequently found in the laboratory and repackage that into a space system. The diagram in Figure 8-3 shows the initial design of the fluidic network with the associated sensors and actuators within the payload. The image captures the elements within the payload and also its functionalities. The development elements, i.e., the subsystem and components, have been discussed in previous subsystem level chapters of this thesis.

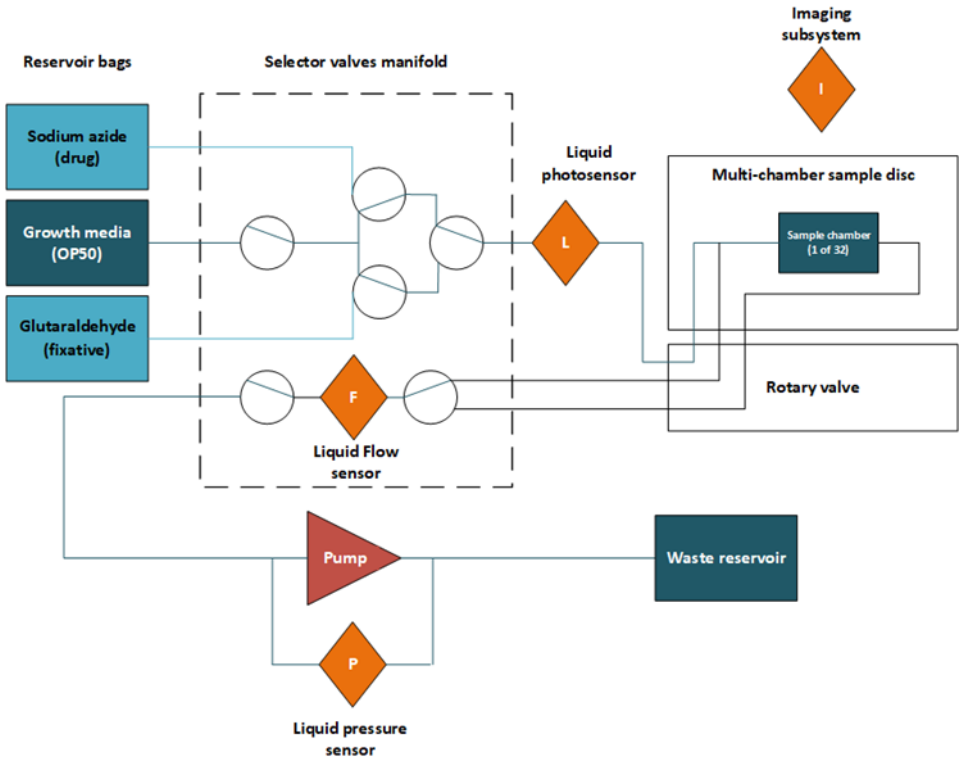

Figure 8-3. An initial fluidic network designed for the BoB fluidics subsystem at the CDR stage of the BoB mission.

One of the biggest challenges during development is to go from the 1st to 2nd gen. BAMMsat bioCubeSat payload was to repackage the laboratory breadboard into

a miniaturised 2U (20 cm x 10 cm x 10cm) CubeSat format. The 2nd gen. BAMMsat contained many elements, including sensors, actuators, mechanical support, wiring and wiring harness, and fluidic tubing and fluidic harnessing. Packaging them in a small volume required several iterations on CAD to ensure that the element fit and had the necessary interface.

As an overview, it is worth comparing the 1st and the 2nd gen. design to see the evolution and justify the design choices. As a context, the 2nd gen. was explicitly designed for the BoB mission. The BoB mission's objective was to perform a technology demonstration instead of a science mission. For this reason, some of the sensors, such as the chemical sensors (O_2 and pH), were removed from the design. The design of the 1st gen. can be referred to in Figure 1-3. Within a similar context, the visible light spectrometer was also removed from the design since the reading would not provide valuable input into the mission objective. It has to be said that including these sensors during development would have been helpful from a technological development perspective; however, the lack of resources within the mission meant that these sensors had to be decommissioned.

The lack of resources was also a factor in the 2nd gen. imaging subsystem. The previous 1st gen. had a fluorescence microscope, which was replaced with a simpler compact brightfield microscope. It was assumed that recorded images and video of the biological sample being mobile or motile could be captured with a simpler microscope. In the BoB mission, the biological sample under the microscope was *C. elegans*. The fluorescence microscope required significant resources to purchase the components and miniaturise the design.

Another difference between the two generations was the fluidic sensor's quantity and placement. The number of pressure sensors, liquid photosensors, and liquid flow sensors was reduced to one each. For reference, the design of the 1st gen. can be referred to in Figure 1-3. The quantity was reduced to a minimal amount without sacrificing the information to minimise the total cost of the sensor and wire harness.

The fluidic sensors were placed to extract the most valuable information in terms of placement. For example, the differential liquid pressure sensor has two ports, and each port is connected to each end of the pump. This was achieved using a fluidic T-junction that allows observation of the pump functionality confirmed via nominal or non-nominal pressure difference. The liquid photosensor was placed before the fluids entered the MCSD to observe the difference between the three media and any potential bubble formation, see the image in Figure 8-3 and Table 8-1. The liquid flow sensor was placed on the selector valve manifold to avoid extra manifold body and fluidic harnessing. The flow sensor confirms if the fluids are being pumped across the MCSD and measure the flow rate during pumping. Both pump and flow sensors were placed after the MCSD since the state of the liquid no longer has an impact on the biological samples.

8.5 Core functionalities of the 2nd gen. BAMMsat bioCubeSat payload for BoB mission

This section describes the core functionalities of the 2nd gen. BAMMsat bioCubeSat payload designed for the BoB mission. This section aims to capture the payload's core functionalities, which build upon the previous BAMMsat system-level studies. The studies identified that a typical experiment requires four core functions of the hardware, which are to (i) house multiple samples, (ii) maintain samples in an appropriate local environment, (iii) perturb samples fluidically, and (iv) monitor samples. The following text describes how the core functionalities were implemented into the BoB system.

i. *House multiple samples*

The BoB mission was designed to have five strains of *C. elegans* incubated in 15 cylindrical sample chambers, 3.5mm (diameter) x 3mm (depth). The selection of the *C. elegans* phenotype, biological design and biological handling was performed by M. Cooke, a biologist, and a member of the BoB team.

Each of the mutant five strains had three replicates, and the wild-type (WT) had four replicates to increase the baseline data. The MCSD can house 32 samples. For the BoB mission, it was foreseen that the combination of three replicates of five mutant strains was sufficient to meet the BoB mission objectives. Refer to section 9.2 for the list of objectives. The number of sample chambers was reduced to decrease the total experiment time and volume of media. Having more chambers meant that additional time was required to operate the MCSD.

Similarly, additional chambers will require extra media for running the experiment. Before the flight, there was uncertainty about the total float time during the BEXUS flight. Depending on the weather and flight path during the flight, the total float time could range between 1 to 5 hours (Frenea-Schmidt, 2021).

Table 8-1. *C. elegans* strain on-board BAMMsat-on-BEXUS flight

Type of C. elegans strain	***Remarks***
Wild type (WT)	Phenotype representative of *C. elegans* species naturally occurring in the wild. WT will provide the baseline data for the experiment where the other phenotype behavioural will compare to WT.
Cha-1 Heat sensitive	The phenotype will react to the temperature changes. Observing the behaviour of *Cha-1* will provide observational data on the thermal environment.
Dpy-13 Dumpy	The phenotype will grow shorter than WT, and this will prove that the BAMMsat imaging subsystem can show changes in body size, mobility and motility movement
Unc-54 Slow-moving	The phenotype will be used as a control to show that the WT is moving at the expected rate
Unc-43 Fast-moving	The phenotype will be used as a control to show that the WT is moving at the expected rate

ii. Maintain samples in an appropriate local environment

The BoB system was designed with controlled pressure and thermal environment inside the 2U pressure vessel. When sealed on the ground, the pressure vessel contained the ambient atmosphere with an acceptable leak rate. This will ensure O_2 and CO_2 are contained and can be exchanged via a gas-permeable membrane between the sample chambers and the trapped atmosphere for the *C. elegans* to utilise. The temperature will be regulated within the acceptable range to ensure it does not get too hot or cold during the pre-flight and flight experiment phases. Extreme thermal fluctuation can be harmful to *C. elegans*. For the BoB mission, it was expected that *C. elegans* during the flight would be maintained at a temperature of +20^{o}C ± 2^{o}C and kept at a low metabolic rate at a lower temperature during pre-flight at +12^{o}C ± 2^{o}C (the temperature control will be provided by a combination of active and passive thermal control).

iii. Perturb sample fluidically

Having a fluidic handling capability enables the maintenance of biological samples. In the BoB mission, the growth media inside the *C. elegans'* sample chamber can be replenished via pumping new growth media. The fluidic actuation and direction are controlled by pump and solenoid valves. The ability to perturb the fluids also enables the ability to change the state of *C. elegans* by pumping in new reagents such as drugs and fixatives to perform various aspects of a science experiment. In the BoB mission, three different types of reagents were selected to maintain the *C. elegans* by replenishing the growth media and demonstrating the capability of the BoB fluidic subsystem to pump different types of media, see Table 8-2.

Table 8-2. Different media used in BoB mission

Type of media	***Comments***
Growth media (OP50)	A liquid solution designed to support/feed the growth of *C. elegans*
Drugs (Sodium Azide)	Administration of a low concentration of anaesthetic will stop *C. elegans* movement. Observing the movement after drug administration during the flight validates the technology demonstration of the BAMMsat fluidic subsystem.
Fixative (Glutaraldehyde)	A chemical substance used to preserve or stabilise *C. elegans*. One of the few that do not contain any flammable substances

iv. Monitor sample

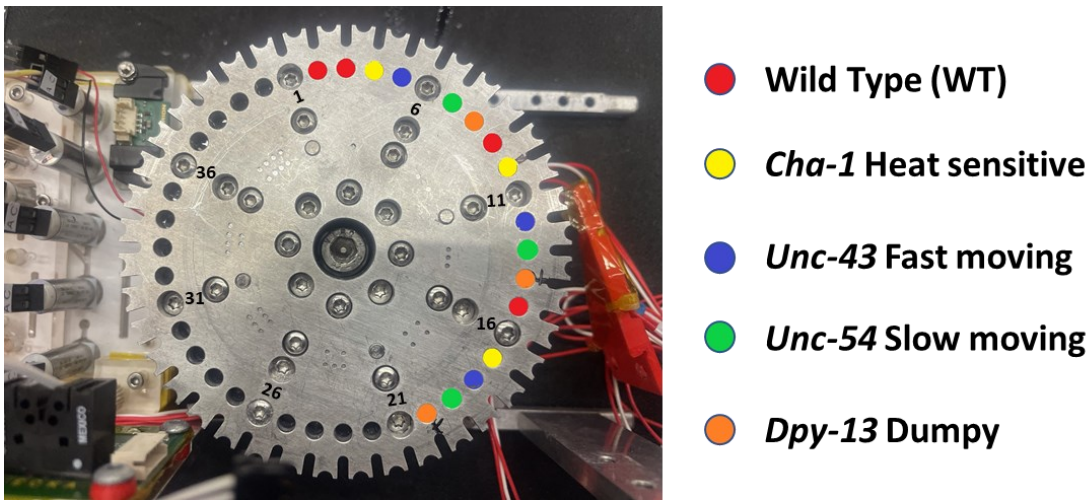

Figure 8-4. The location of the five different *C. elegans* phenotypes and their replicates.

The monitoring functionality provides the ability to extract experiment data. A common sensor to monitor a sample in a laboratory is a microscope. Three sensors are included within the BAMMsat concept: the fluorescence microscope, a visible spectrometer, and chemical sensors.

Specifically for the BoB mission, the 2nd gen. BAMMsat bioCubeSat payload was designed to include only a compact brightfield microscope as part of its imaging subsystem. The compact brightfield microscope was used to capture still images and videos of *C. elegans*. The wild-type strain will be used as a baseline for comparison with the other strains to observe the difference in behaviour. The image of the *C. elegans* phenotype being monitored inside the MCSD can be viewed in Figure 8-4.

8.6 List of requirements for the BoB system

A complete list of requirements for the BoB system can be referred to in Appendix A

8.7 AIT of the 2nd gen. BAMMsat bioCubeSat payload (2U) into the BoB system (3U)

This section aims to bring together the development from the previous chapters into one coherent system, the 2nd gen BAMMsat bioCubeSat payload. The process will be described in an assembly, integration, and testing (AIT) workflow. The section will discuss the planned AIT process and how some design issues arose and were modified.

8.7.1 Description of the planned AIT process

The list in Table 8-3 is an attempt at capturing the assembly and integration process, and it is not an exhaustive list and more of an overview of the process, which will be referred to during the discussion. For reference on all the subsystems and components within the assembly, the reader can refer to Figure 8-2.

Table 8-3. List of AIT processes for the BoB system.

Step 1 –	Assemble the bottom rails, aluminium base, and selector valves manifold
Step 2 –	Connect the fluidic tubings and reservoirs
Step 3 –	Mechanically assemble the rotary valve (RV)
Step 4 –	Mechanically assemble the column and liquid photosensor
Step 5 –	Connect the valve wiring, mechanically assemble the flow sensor
Step 6 –	Mechanically assemble the MCSD thermal heater
Step 7 –	Mechanically assemble the MCSD
Step 8 –	Mechanically assemble the Geneva gear mechanism
Step 9 –	Mechanically assemble the top rails
Step 10 –	Mechanically assemble the LED PCB for the compact brightfield microscope
Step 11 –	Connect and place the RTDs to the required position
Step 12 –	Connect the electrical wiring and wiring harness
Step 13 –	Mechanically mount the 2U main PCB
Step 14 –	Mechanically mount the pump PCB
Step 15 –	Mechanically mount the compact brightfield microscope
Step 16 –	Mechanically assemble the rails to the pressure vessel lid (on the 1U side).
Step 17 –	Slide the assembly into the 2U pressure vessel
Step 18 –	Fit the rails into the slot on the pressure vessel lid (opposite lid to step 13)
Step 19 –	Bolt both sides of the pressure vessel lid with O-rings

8.7.2 Implementation of AIT process

This section captures and discusses the implementation of the AIT process. It is separated into two sub-sections, with the first section capturing the nominal AIT process. The second sub-section highlights and addresses the issues that arose during AIT and the modification to accommodate the issues.

8.7.2.1 Nominal AIT process

The following images and text capture the nominal AIT process regarding the steps described in section 8.7.1. Unfortunately, images of the planned AIT's step-by-step process were never formally documented due to time constraints during the BoB mission. During the BoB flight campaign, the assembly was performed with a text-based checklist. The images presented below are a collection of images organised in the planned AIT process.

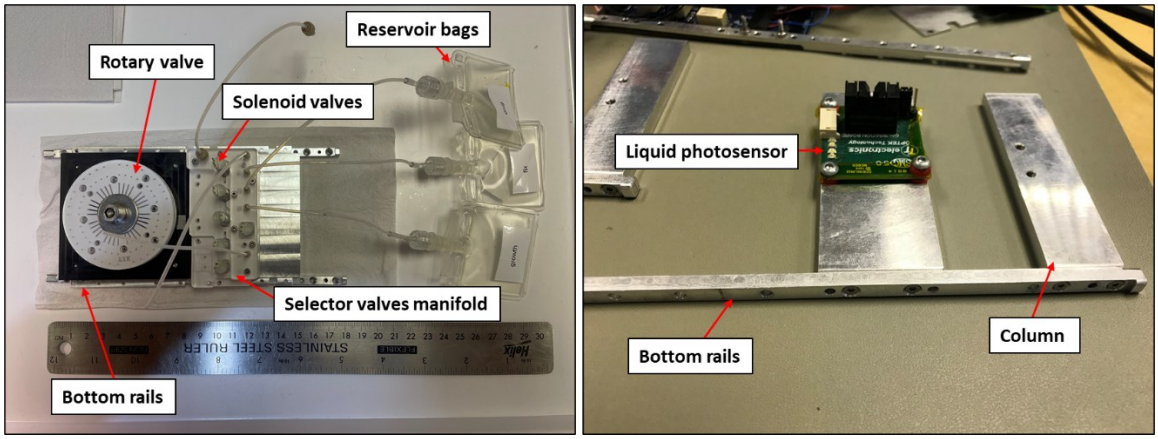

Figure 8-5. Images illustrating Step 1 to Step 4 of the assembly process.

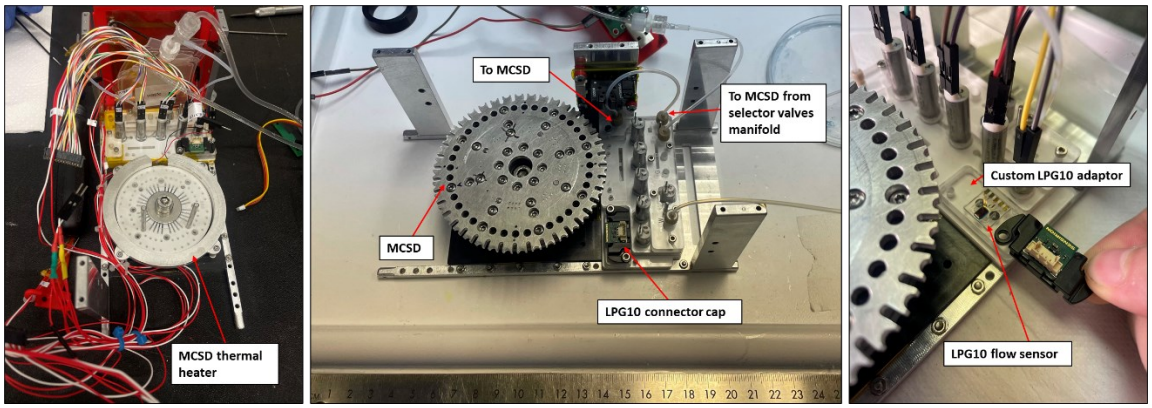

Figure 8-6. Images illustrating Step 5 to step 7 of the assembly process.

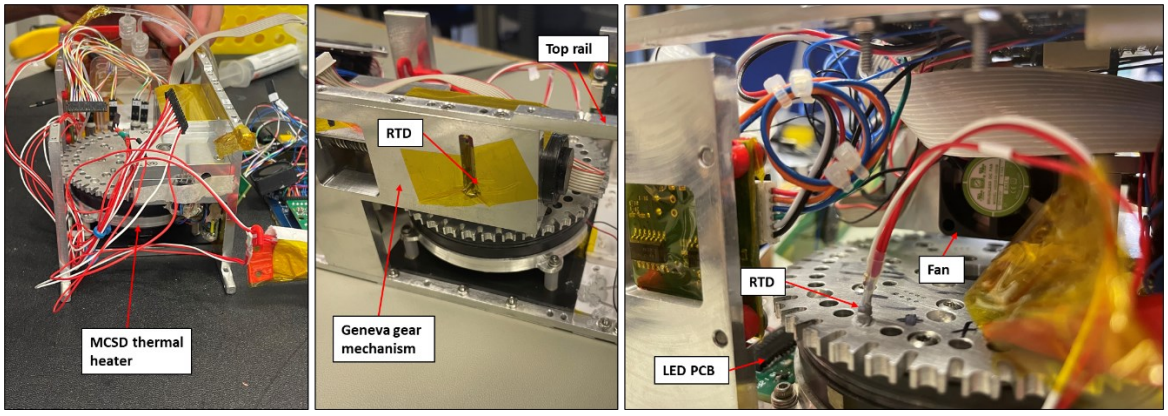

Figure 8-7. Images illustrating Step 8 to Step 12 of the assembly process.

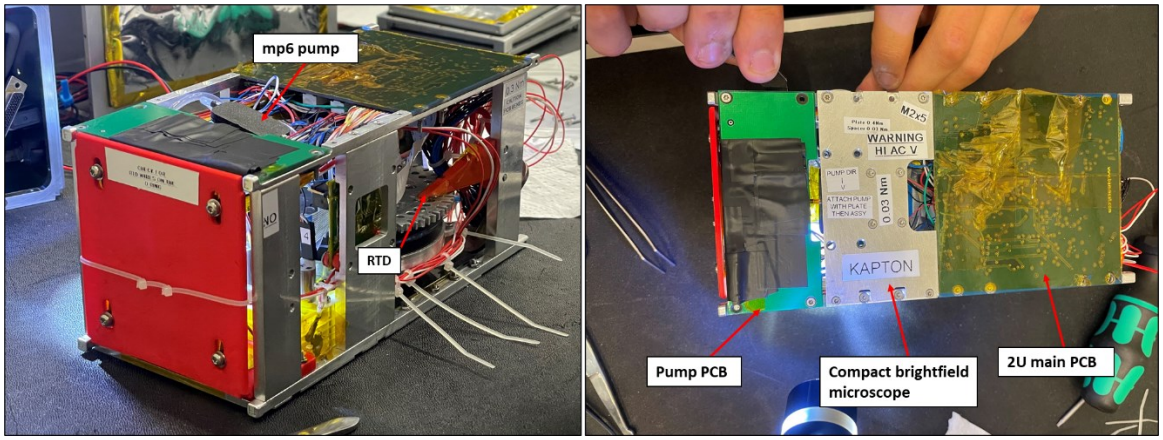

Figure 8-8. Images illustrating Step 13 to Step 15 of the assembly process**.**

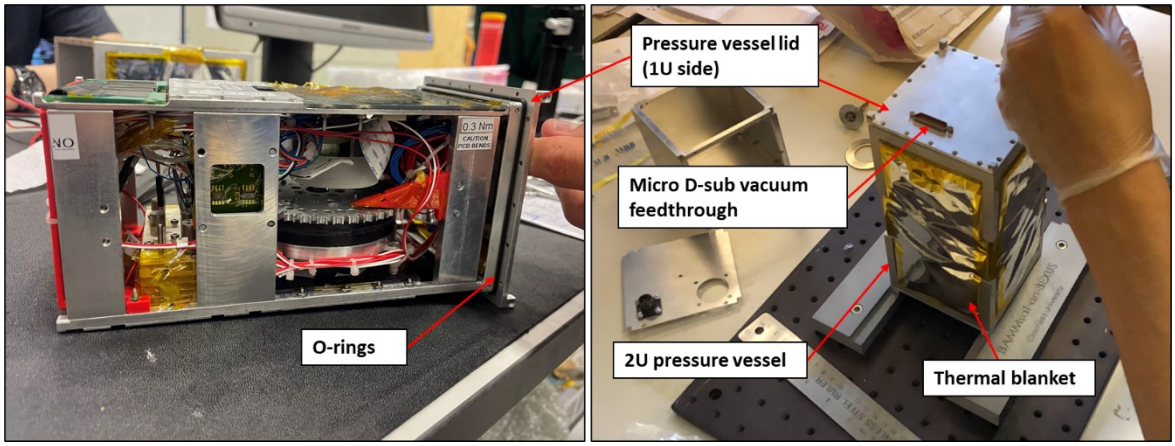

Figure 8-9. Images illustrating Step 16 to Step 19 of the assembly process.

8.7.2.2 Non-nominal AIT process – Issue encountered, and modification made

Several design issues arose during the AIT process. Some of the issues had caused design modifications that affected the design at this stage of the BoB mission. This section captures the design issue and the modification made during AIT in preparation to be shipped to Esrange Space Centre.

8.7.2.2.1 A large volume of the fluidic T-junction to fit into the 2U form factor

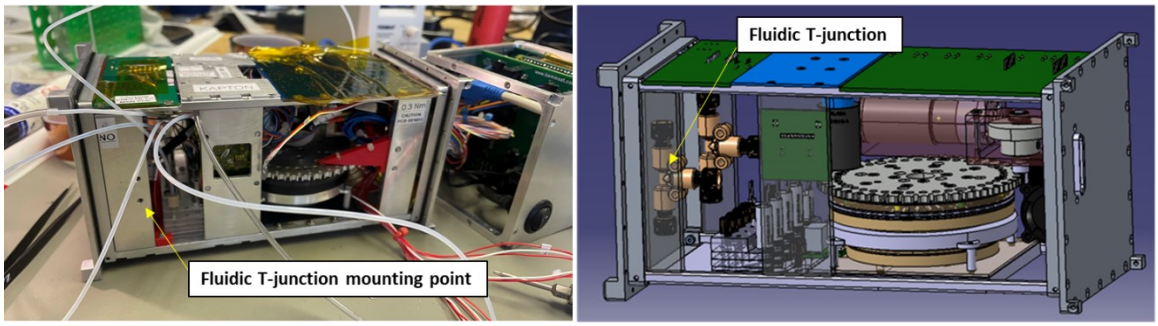

Figure 8-10. Left – Fully assembled BoB system without the pressure vessel. Right – CAD image showing the location of the fluidic T-junction

The fluidic T-junction enabled the splitting of the fluidic network for connection to a differential fluidic pressure sensor. The pressure sensor (ABPDRRT005PG2A5; Honeywell) was a dual-port differential pressure sensor. The initial design would have connected the end of the T-junction to each end of the pressure sensor port. It was initially designed so that the pressure sensor would measure the pressure difference between the inlet and the outlet of the mp6 pump. Unfortunately, during the AIT, the combination of two fluidic T-junctions and tubing was unable to be fitted inside the assembly. The volume comparison can be seen in Figure 8-10. The issue meant that the pressure sensor had to be removed from the system.

8.7.2.2.2 Issue with the dynamic instability of laser-cut polymer and an adhesive layer

During one end-to-end test of the fluidic subsystem, an issue with the design of the fluidic subsystem became apparent. The problem revolved primarily around the laser-cut polymer (PMMA) and the pressure-sensitive adhesive. The two

elements make up the entire structure of the selector valves manifold. The same issue with cracking (see Figure 8-11) became apparent when the MCSD and RV were bolted and unbolted on the manifold. Similarly, the same issues arose when the Diba fluidic connector was bolted and unbolted on the manifold.

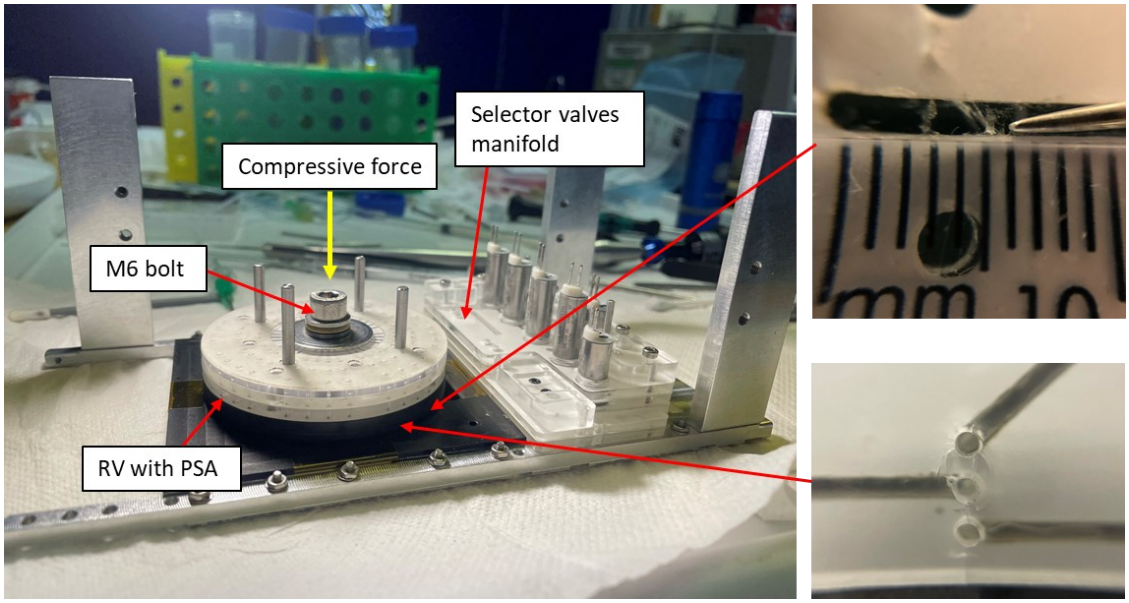

Figure 8-11. The compressive force from the bolting caused the polymer underneath to crack and cause leakage. It also caused the adhesive to seep and block the fluidic channel.

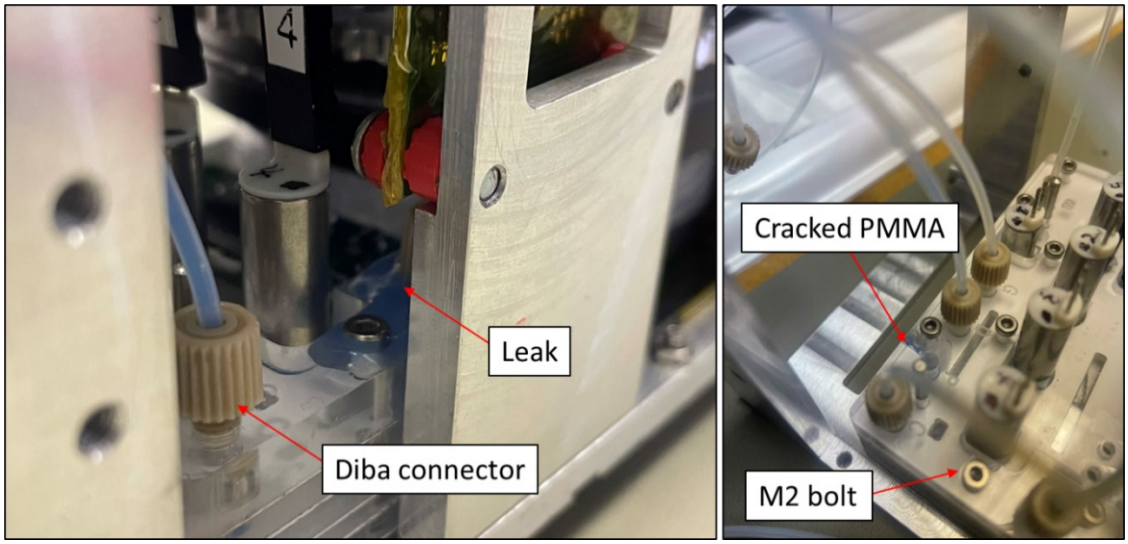

Figure 8-12. Left – Leaking at connector since sealing had to be judged by hand. Right – Polymer cracked during testing and caused fluidic leaking.

The first issue was caused by assembling and dissembling the MCSD and RV on the manifold. During bolting, the pressure from the surface of the RV caused the laser-cut polymer underneath to crack or the adhesive to seep into the channel, which caused the fluid to either leak or be blocked, respectively. The cracked PMMA layer can be seen on the bottom right image of Figure 8-11, and the adhesive seeping can be seen on the top right image of Figure 8-11.

The second issue was caused by assembling and dissembling the Diba fluidic connector on the manifold. The crack in Figure 8-12 (right image) was caused due to the opposing force from the M2 bolts and the Diba connecter. The M2 bolt provided the compressive force to hold the layers together (laser-cut PMMA and PSA). However, tightening the Diba connector pulled the layer apart since the Diba ferrule pushed against the polymer's surface when tightened.

The sealing from the Diba connector was achieved by tightening to push the ferrule against the layer. The connector was a Diba Click-N-Seal connector with torque control fitting. The connector was designed to produce a click sound once the proper torque and seal were achieved. However, the laser-cut PMMA cracked before the click occurred. An example of cracked PMMA can be seen in the right image of Figure 8-12. Since the design does not allow the Diba connector to achieve the optimum sealing, the sealing was achieved using hand judgment. This was proven to be challenging since not achieving a proper seal can lead to leaking (see left of Figure 8-12)

The result from the testing showed the fragility in the structural design of the laser-cut polymer-bonded by pressure-sensitive adhesive. The fragility became apparent when dynamic load was introduced into the design. At this stage of the BoB mission leading up to the flight campaign, fixing the issue required a significant redesign and was not feasible.

The bolting torque of the RV was kept at a low value of 0.5 Nm to mitigate damaging the manifold. For the Diba connector, the sealing was achieved by hand judgment to assess if the connector was tightened. The judgement built up after many trials and errors.

8.7.2.2.3 Issue with focusing the *C. elegans* in the full system

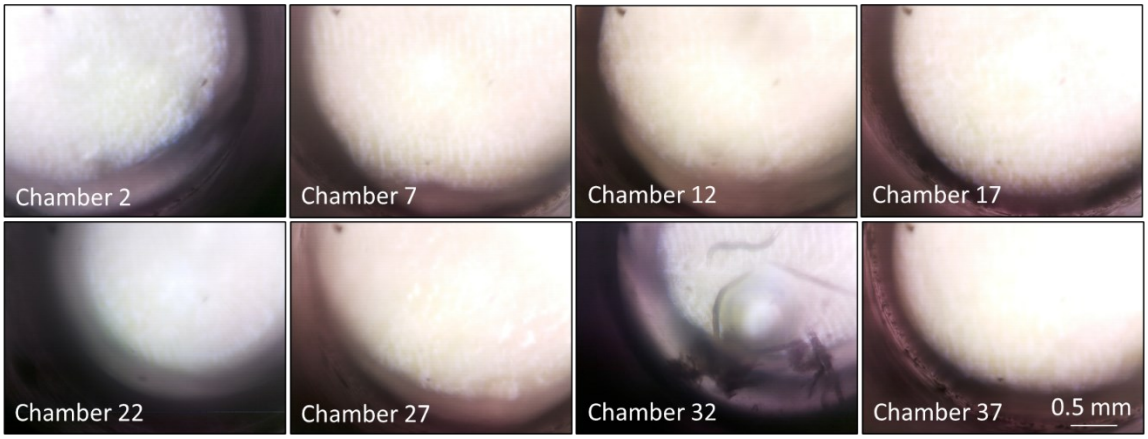

Figure 8-13. Snapshot of each quadrant of the MCSD during a full system rotation test with *C. elegans*.

A full system test with *C. elegans* was performed in preparation for Experiment Acceptance Review (EAR) within the BoB mission. The Experiment Acceptance Review was a formal review imposed by the REXUS/BEXUS programme to check experiment readiness and ensure compliance with their safety regulation. EAR was the final review before confirming that the BoB system was ready for flight. The test was performed using *C. elegans* and was performed to represent flight conditions.

During the test, an issue arose with the ability of the compact brightfield microscope to resolve the *C. elegans.* For the test, the entire 32 sample chambers were filled with *C. elegans*. Unfortunately, the result from the test showed that only one sample chamber resolved with *C. elegans*. It was sample chamber 32 in Figure 8-13. The other 31 chambers did not show any *C. elegans.*

A snapshot image of each quadrant of the MCSD is shown in Figure 8-13 to demonstrate the result. A quadrant represents a section of four chambers in the MCSD. An example of a quadrant is chamber 2 to chamber 5 of the MCSD. The reader can refer to Figure 8-4 for a full view of the MCSD.

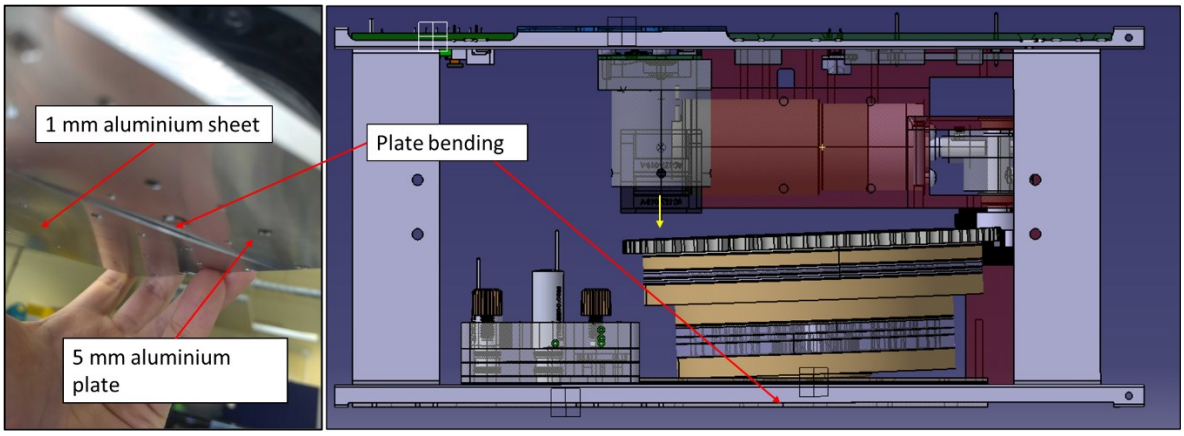

Figure 8-14. The issue with structural bending from bolting the MCSD and RV. The image on the right has an exaggerated tilting of the MCSD for visual purposes.

Further investigation of unresolved images found that the MCSD had a slight tilt, approximately at 2º from the centre of the MCSD, as shown in the right image of Figure 8-14. The structural sheet underneath the assembly deformed once the MCSD was bolted onto the structure. It was hypothesised that the bending caused a perspective error in the optics since the imaging plane was no longer parallel to the lens. The effect on the imaging plane was also evident in the captured images in Figure 8-13. In those images, the centre of the sample chamber was not aligned with the centre of the captured image.

The 1 mm aluminium sheet was too thin to resist the pressure from the bolt. The initial design had two pieces of 1 mm aluminium sheet and a 5 mm aluminium plate (see left of Figure 8-14). The 5 mm aluminium plate was threaded to bolt the MCSD and RV. While above the 1 mm sheet, the selector valve manifold was assembled on top of it. Since the sheet was too thin and was not supported by the plate, it deformed at its weakest point.

The base was redesigned into a single piece, and the thickness was increased from 1 mm to 3 mm to fix the issue with the sheet bending. The result after modification showed that it fixed the problem. No bending was evident, and the centre of the captured image was aligned with the centre of the sample chamber (see Figure 9-20).

8.8 Final design of the BoB system, ready for BoB flight campaign

This section summarises the final design of the BoB system after the AIT activities. It was no longer possible to iterate the design at this stage, and it was prepared for the BoB flight campaign. The design changes are summarised in Figure 8-15. For design comparison, the initial design can be viewed in section 8.3. The design changes are summarised in the text below.

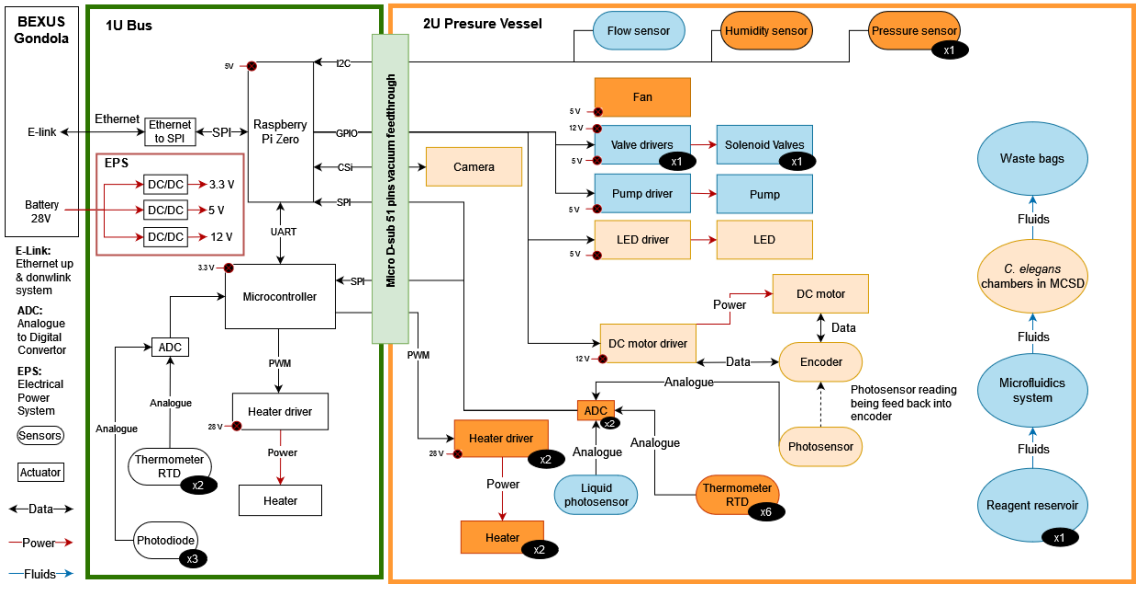

Figure 8-15. Block diagram of the BoB system ready to be shipped to the BoB flight campaign.

Compared to the initial design, one design change in the BoB system was the removal of the positioning sensors. These were the IMU and GNSS sensors, and they were deprioritised to simplify the BoB system to reduce the development workload.

The atmospheric pressure sensor was reduced from two to one because the pressure sensor (MS5607-02BA) was damaged due to short-circuit during laboratory testing at Cranfield University. The flown pressure sensor (Adafruit BME280) has integrated pressure, humidity, and temperature sensors.

The fan driver was removed to power the fan (RS OD2510). It had to be constantly powered directly from the 5V from the EPS PCB instead of PWM controlled as the fan driver was not supplying enough current across the MOSFET to operate the fan. The design included the fan to mitigate the effect during future microgravity spaceflight. Lack of buoyancy-driven convection could result in localised O_2 depletion of CO_2 build-up close to the gas-permeable membrane, given the lack of convective mixing. The fan's forced circulation/convection will improve the *C. elegans* breathability by circulating O_2 and CO_2.

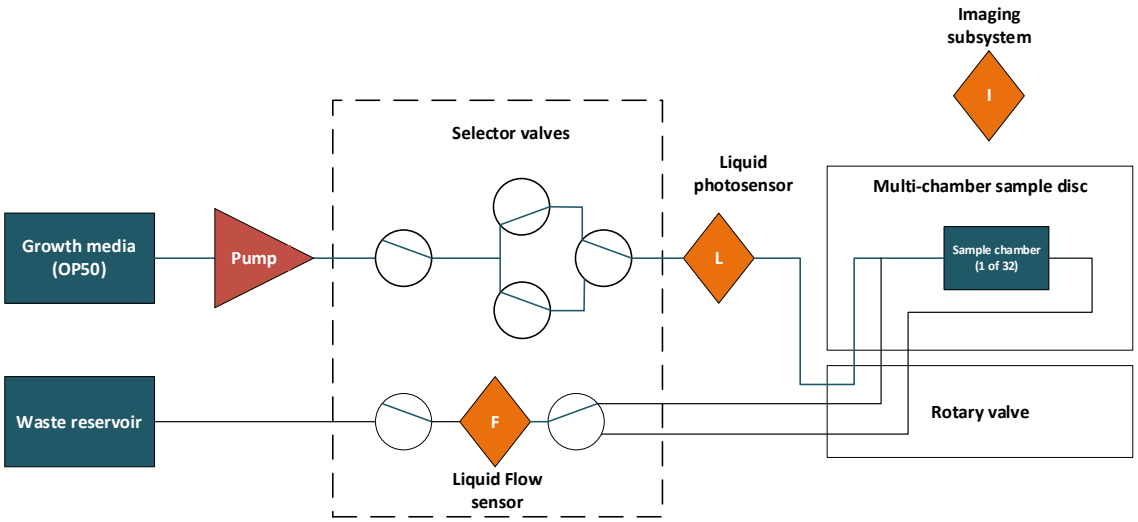

Figure 8-16. The fluidic subsystem's fluidic pathways; ready to be shipped for the BoB flight campaign.

Like the overall BoB system, the 2nd gen. BAMMsat bioCubeSat payload also had design changes after development and AIT. In general, it has reduced functionalities compared to the initial design. For design comparison, the initial design can be viewed in section 8.4. The design changes are summarised in the text below.

One of the critical design changes was removing the fluidic pressure sensor. The fluidic pressure was placed to measure the pressure difference across the pump. During AIT, it became apparent that the fluidic T-junction and the associated fluidic tubing were too large to be integrated into the full system. The removal

made it impossible to record the pressure difference and confirm the pump's actuation via the sensor. The removal is not detrimental to the BoB mission since pumping can be confirmed via the compact brightfield microscope and the liquid flow sensor.

Secondly, the pump's position was changed to push the liquid into the MCSD instead of pulling it across the MCSD. The changes were made because the pump could not pull the liquid without bubbles during the lab testing (see section 5.4.3.3). It can be assumed that this was due to poor sealing across the fluidic subsystem.

A few weeks before the BoB flight campaign, a fire broke out at Esrange Space Centre. It burnt the biological laboratory, and the laboratory was decommissioned for the BEXUS 30 flight campaign (Swedish Space Corporation, 2021). It meant that the fluidic reagent in the BoB system was reduced from three to one. The reduction removed the hazardous chemicals Sodium Azide and Glutaraldehyde from the BoB mission since they no longer could be handled safely during the flight campaign without access to the biological laboratory.

8.9 Verification matrix

The verification matrix for the BoB system can be referred to in Appendix B.

8.10 Discussion, summary, and future work

8.10.1 Discussion and summary

Chapter 8 discusses the integration of the subsystems and components constructed into the 2nd gen. BAMMsat bioCubeSat payload and, subsequently, the BoB system. The activities performed were described in the assembly, integration, and testing workflow.

One of the take-home messages from the chapter is the unreliability of fluidic manufacturing techniques using laser-cut polymer bonded by pressure-sensitive adhesive. Although this design has been flown into space by NASA Ames, the design did not work within BAMMsat since the design has dynamic loading on the polymer and the adhesive. In some cases, the polymer cracked, causing a leak, and the adhesive seeped into the fluidic channel and caused a blockage.

In summary, the completion of AIT showed that a functioning BoB system had been completed. Although, there was still an unknown with the imaging subsystem since a further test with *C. elegans* was required to assess if fixing the tilting also fixed the issue with focusing the *C. elegans* inside the sample chamber. However, at this stage of the BoB mission, the team was preparing to travel to Esrange Space Center and was unable to test again.

8.10.2 Future work

Immediate future works based on chapter 6 are to evaluate the two design issues which appeared during the testing in chapter 6

- Further testing will be required to understand the optical limitation with the compact brightfield microscope's ability to image live *C. elegans*; see section 8.7.2.2.3.
    - One potential was the 1 mm aluminium sheet bending. However, it could be due to a plethora of other reasons, and an in-depth diagnosis will be required to confirm cause and effect. Some examples could be due to the growth media changing the refractive index, the position of the C. elegans, the thickness of C. elegans,

variation in thickness of the optical system and the MCSD due to machining, manufacturer tolerance in the material, the thickness of the optical window, variation in the thickness of the *C. elegans*, and behaviour of the *C. elegans* (i.e., *C. elegans* either lie flat or loop away from the surface). The list highlights potential optical system issues that require tighter control during manufacturing and assembly. Note that the compact brightfield microscope has a short depth of field of <1 mm. One solution to mitigate this design issue is an adjustable motorised lens to change the focus quickly.

- Overcome the issue with the large volume of the T-junction; see section 8.7.2.2.1.
    - The 2nd gen. design has a differential pressure sensor with two fluidic ports to measure the pressure difference across the mp6 pump. Two split the fluidic
        - Explore the market for an alternative fluidic splitter. One solution would be the Bartels Mikrotechnik mp-y tubing connector.
        - Explore alternative design solutions such as removing the two ports differential pressure sensor into a two single port pressure. This design would remove the need for two fluidic splitters.

Long-term future work would include exploring new fabrication techniques for the selector valve manifold.

- Explore new microfluidic fabrication techniques to overcome the limitation of the fabrication by laser-cut polymer and pressure-sensitive adhesive.
    - One of the key research findings was the limitation of this fabrication technique. As shown in section 8.7.2.2, the adhesive blocked the fluidic channel and the polymer (acrylic) cracked under dynamic loading.

- There are established alternative microfluidic manufacturing fabrication techniques, such as PDMS etching (Gorissen et al., 2016) or polymer diffusion bonding (Brenan et al., 2000). There is also a new fabrication technique using state-of-the-art 3D printing (Prabhakar et al., 2021).

9 BAMMsat-on-BEXUS: Flight campaign summary, preliminary analysis of the flight results and lessons learnt

9.1 Introduction

This chapter introduces and presents the BAMMsat-on-BEXUS flight campaign launched on 30th October 2021 and reports a flight campaign summary, preliminary analysis, and lessons learned. The flight campaign was a technological and operational demonstration of the 2nd generation BAMMsat bioCubeSat payload, and the flight tested the subsystems developed in previous chapters of this thesis. The current chapter will present a preliminary analysis of the flight results and the lessons learnt that inform the 3rd generation BAMMsat bioCubeSat payload design.

Four terminologies are being re-introduced and used to describe BAMMsat-on-BEXUS throughout this chapter to help with the discussion.

- BAMMsat-on-BEXUS mission or BoB mission

The term BoB mission refers to activities that encompass a typical space mission. This term represents the activities and processes behind the overall mission aim of performing technology and operational demonstration of the 2nd gen. BAMMsat bioCubeSat payload on a stratospheric balloon flight.

- BAMMsat-on-BEXUS flight campaign or BoB flight campaign

The term BoB flight campaign refers to a series of activities performed during the flight campaign between the 24th of September – the 4th of October 2022 at ESRANGE Space Centre, Kiruna. The activities included pre-flight operations, flight operations and post-flight operations.

- BAMMsat-on-BEXUS system or BoB system

The term BoB system refers to the 3U CubeSat format system encompassing the 1U bus and the 2nd gen. BAMMsat bioCubeSat payload. The 1U bus was the "brain" of the BoB system and acted as the mechanical, electrical and data

interface between the 2nd gen. BAMMsat bioCubeSat payload and the BEXUS gondola.

- 2nd gen. BAMMsat bioCubeSat payload

The 2nd gen. BAMMsat bioCubeSat payload is the autonomous miniaturised laboratory at the core of the BAMMsat concept with the subsystems developed during this PhD. It is a 2U bioCubeSat payload system used to house and observe biological samples. It continued from the laboratory breadboard version (1st gen. BAMMsat bioCubeSat payload) in the 2nd gen. BAMMsat bioCubeSat payload, which flew into the stratosphere.

9.1.1 Why BEXUS?

The BEXUS programme provides a unique operational and natural extreme environment in the stratosphere that could not be easily replicated in the laboratory. The environment is appropriate for a technology and operation demonstration of the BAMMsat bioCubeSat payload since the biological samples imposed additional handling and thermal control requirements during pre-flight to ensure their viability. The BEXUS flight campaign could be used as an analogue of pre-flight, flight and post-flight operations similar to an orbital flight campaign.

The extreme environment in the stratosphere is an analogue of the physical spaceflight environment, such as reduced pressure in a near-vacuum environment. The atmospheric pressure could be reduced to approximately 5 - 25 mbar. Similarly, the thermal variation is another physical analogue. The temperature drastically decreases during ascent and reaches a cold temperature between -40°C to -80°C; see Figure 9-4. However, it has limitations since it is not a good analogue of weightlessness (microgravity) and ionising radiation.

BoB housed *C. elegans*, a model biological organism inside the multi-chamber sample disc (MCSD) within a 2U pressure vessel. The BoB flight campaign tested the BAMMsat bioCubeSat payload functionalities to provide a controlled thermal and fluidic environment with appropriate housekeeping control. The functionalities reflect the hardware's capability to maintain a viable biological sample.

The BoB system has a 3U CubeSat form factor with 2U allocated for the 2nd gen. BAMMsat bioCubeSat payload and 1U assigned as the BoB CubeSat bus. BoB system was the first complete prototype of the BAMMsat concept with a biological sample in a full flight campaign. The intention was to capture lessons learnt through the whole project lifecycle and flight operations before optimising the next iteration for BAMMsat 3rd generation for spaceflight.

REXUS, or the rocket counterpart of BEXUS, was considered as another flight option. However, the additional vibration requirement was perceived as a high risk for the first prototype. It was a student-led project with a lack of overall

resources, and the additional requirements could be detrimental to the completion of the project.

Table 9-1. BAMMsat-on-BEXUS mission's milestones and dates within the BEXUS programme.

Project milestones	Dates
Call for proposal open	17th June 2019
Proposal submission	14th October 2019
Selection workshop at ESTEC facility, Netherlands	26th November – 28th November 2020
Student training week and Preliminary Design Review	10th February – 14th February 2020
Critical Design Review	13th May 2020
Integration Progress Review	30th July 2020
Progress Review 1	21st September 2020
Progress Review 2	26th November 2020
Progress Review 3	26th March 2021
Experiment Acceptance Review	18th August 2021
Flight campaign at ESRANGE Space Centre, Sweden	24th September – 4th October 2021 (Flight date: 30th September 2021)

BEXUS programme replicates an entire space project lifecycle to provide the student with the experience within one year. The process started with a proposal submission in October and a flight in October the following year. During this duration, students had to defend the proposal. They also performed periodic reviews to check progressions with panels from national and aerospace agencies across Europe, such as SSC, SNSA, DLR, ZARM, MORABA and ESA. In each review, the team must submit an evolving document called Student Experiment Document (SED) and pass the review to proceed to the next stage.

It was an intensive programme considering the students must deliver working hardware and tests it to the flight requirements alongside the associated

documentation. The BAMMsat-on-BEXUS mission won the flight ticket for the BEXUS 30 flight campaign. Due to the COVID-19 pandemic, the BEXUS flight campaign had to be postponed from October 2020 to October 2021, with additional reviews up to the flight campaign. Table 9-1 summarises the BoB mission progress throughout the programme.

9.1.2 BEXUS system and gondola

The BEXUS system is a stratospheric balloon platform launched from the ESRANGE Space Centre in Kiruna, Sweden. It consists of a large balloon (12,000 m^3), a primary tracking system via EMPIRE (ESRANGE Multi-Purpose Iridium Relay), a parachute, a Flight Termination (a cutter to separate the balloon), Flight Train ATC (Air Traffic Control), and a Gondola which is used to mount the experiments (Frenea-Schmidt, 2021). An image representing the BEXUS flight train is shown in Figure 9-1.

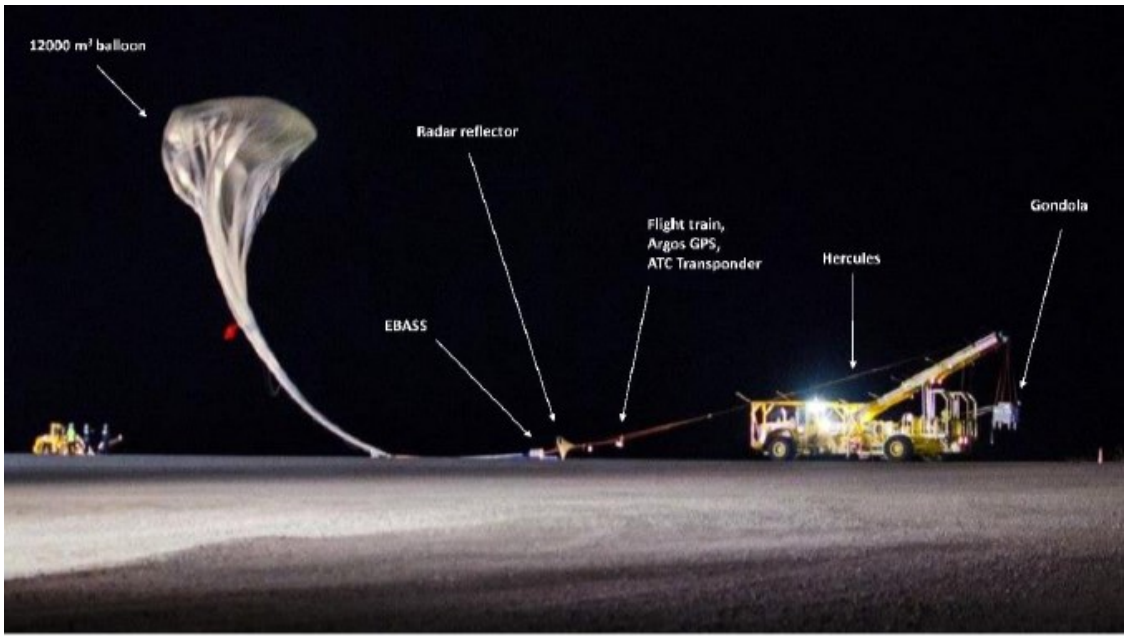

Figure 9-1. Image of the BEXUS 19 flight campaign during take-off at ESRANGE Space Centre in 2014[1].

[1] The EBASS unit has now been replaced by EMPIRE. Photo credit: SNSB – K. Dannenberg in (Carreno-luengo, 2015).

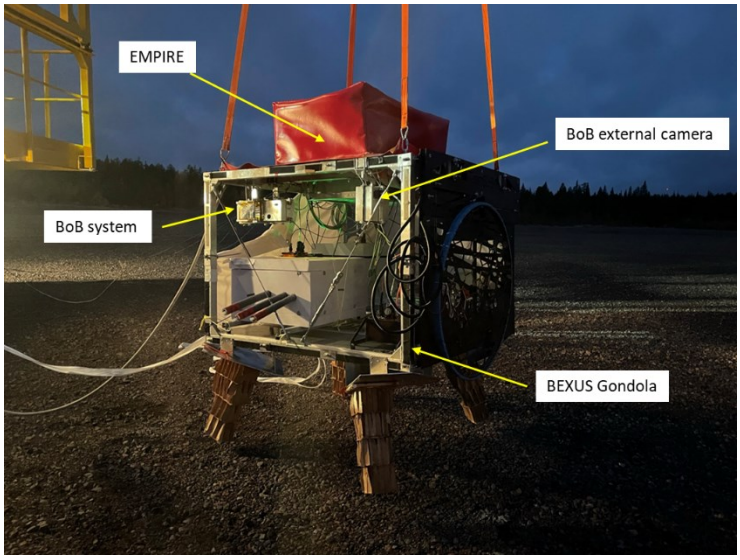

Figure 9-2. Image of the BEXUS 30 Gondola on the launch site preparing for launch.

In Figure 9-2, the Gondola mechanically mounts the experiments to the BEXUS system. Five experiments flew on the BEXUS 30 flight, i.e., BoB, ECO-WISE, ELFI, O-ZONE, and STARDUST. The experiments came from the United Kingdom, Greece, Germany, Italy, and Poland.

9.1.3 The environment experienced by the BoB system during pre-flight and flight operations

This section summarises the environment experienced by the BoB system during the flight campaign. The extreme environment was used to validate the BoB system functionalities and to extract environmental requirements and constraints which influenced the BoB system design. The environment considered the pre-flight and flight phases during the flight campaign. This discussion did not include the post-flight environmental phase since the *C. elegans* would have been injected with preservatives, and the temperature environment is no longer a concern. The flight operation was designed to end with the BoB system turned off before the descent sequence started.

During pre-flight, the BoB activities revolved around preparing and testing the BoB system in preparation for flight. The test involved interference testing in checking compatibility between the BEXUS gondola and other experiments.

During pre-flight operation, BoB systems were primarily placed indoors inside a large hanger with a temperature of around 20ºC ± 5ºC.

Once the experiments passed the flight reviews, the experiments were mounted on the BEXUS 30 gondola and brought to the launch pad, see Figure 9-2 for the image on the Gondola at the launch pad. At the launch pad, the BoB system was exposed to the external ambient environment. The temperature can vary from 0ºC to - 15ºC and experience up to several hours of exposure while waiting to be launched. Representative pressure, temperature and humidity environment profiles are shown in Figure 9-4 and Figure 9-5. The nominal BEXUS flight profile can be seen in Figure 9-3. These figures were extracted from the BEXUS User Manual (Frenea-Schmidt, 2021)

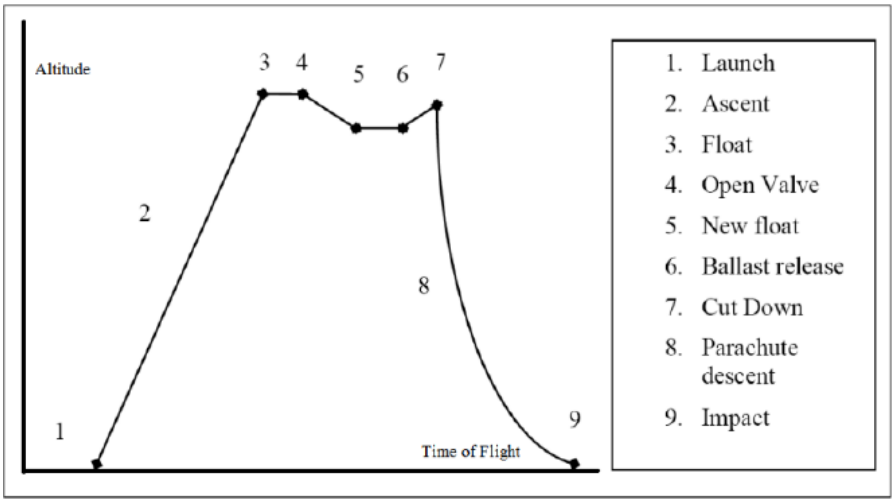

Figure 9-3. BEXUS nominal flight profile.

The balloon altitude can reach 25-33 km during the float phase and last between 1-5 hours. The external air temperature could go down to - 80ºC and, similarly, a pressure between 5 and 25 mbar (see Figure 9-3). The coldest environment will be in the tropopause with slightly higher temperature during float in the stratosphere (Frenea-Schmidt, 2021)

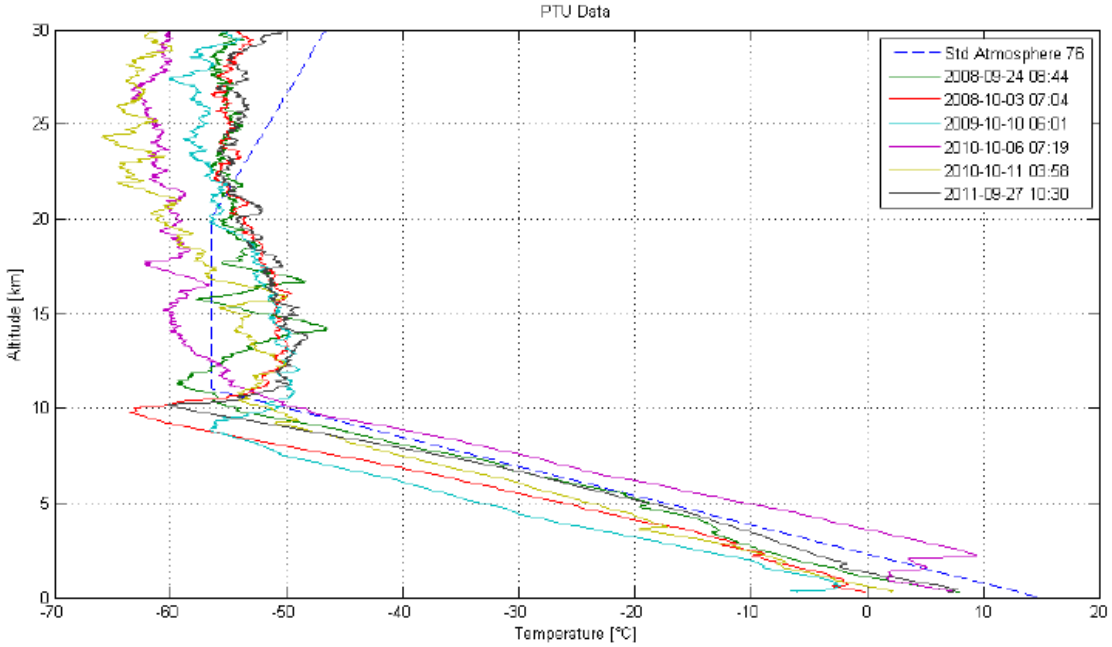

Figure 9-4. Previous BEXUS flight PTU (pressure, temperature, humidity) sondes flight data compared to Standard Atmosphere 1976 (Frenea-Schmidt, 2021).

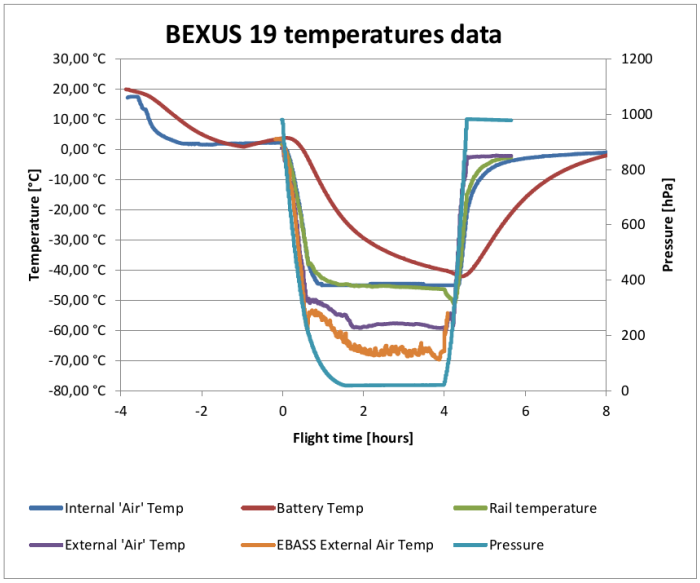

Figure 9-5. The local temperature around the Gondola can vary depending on its position across the Gondola (Frenea-Schmidt, 2021).

From Figure 9-4, the temperature started to drop linearly as the balloon was launched into the stratosphere. However, the temperature inside the Gondola is slightly warmer than the surrounding temperature (see Figure 9-5). This could be

due to the heat from the various experiments and the heat from the BEXUS flight system.

9.1.4 Why *C. elegans on BAMMsat-on-BEXUS mission*?

C. elegans was applied as the biological sample on the BAMMsat-on-BEXUS mission. Using a live biological system in the technological and operational demonstration was valuable for testing the BoB system in the real-world application as close to spaceflight.

C. elegans in BAMMsat was identified in 2018 when a complete science case was developed for a flight opportunity on the ISS. For the flight opportunity, the consortium of Cranfield University, University of Exeter and Kayser Space developed a science case to study the therapeutic efficacy of existing approved drug compounds against the molecular pathway involved in deleterious human effect spaceflight. *C. elegans* has never been flown in a standalone bioCubeSat, although the concept was proposed in 2004 as NemaSat (Levy, 2004). Previous bioCubeSats have opted for single cellular model organisms such as *E. coli* and *S. cerevisiae*.

A multicellular organism such as *C. elegans* could be a stepping stone for complex biological systems onboard a bioCubeSat, and could greatly benefit the scientific community. The challenge of flying such an organism is the issue of sample handling during pre-flight. Typically, a CubeSat flew as a secondary payload, and handover was performed weeks in advance with CubeSat turned off. The operation is not ideal for an organism requiring tighter thermal and fluidic control to remain viable.

C. elegans is a non-parasitic, multicellular nematode worm commonly found in soil. *C. elegans* and humans have highly conserved signalling and molecular pathways as 83% of *C. elegans* genes have human homologues, making it a model organism and a good representative of human physiology. *C. elegans* have been used to study genetics, development, ageing, muscle physiology and radiobiology (Ishioka & Higashibata, 2019). It also has flight heritage, previously

flown on the Space Shuttle, ISS, and the Chinese's Shijian and Shenzhou spacecraft. University of Exeter and UKSA have also flown *C. elegans* on the ISS to study muscle loss (UK Space Agency, 2021b).

9.2 BAMMsat-on-BEXUS mission aim and objectives

The BoB mission was envisioned to advance the development status of the BAMMsat concept to increase the likelihood of gaining access to spaceflight opportunities in LEO and beyond.

The BoB mission aims to perform an operational and technological demonstration of the BAMMsat bioCubeSat payload in a spaceflight representative context using a biological sample.

The aim can be broken down into three objectives.

1) *Develop and demonstrate the ability to handle, integrate and operate BAMMsat in a spaceflight representative context*
   a) Demonstrate the ability to extract data using *C. elegans* as a biological payload on a bioCubeSat and as a hosted payload on a larger spacecraft such as ISS and Bion satellite.
   b) Develop and implement protocols to handle and integrate *C. elegans* into the mission and flight operations of a BAMMsat-on-BEXUS mission.
   c) Develop and implement appropriate pre-flight, flight and post-flight operations compatible with the BEXUS stratospheric balloon flight mission.

The objective originated from the notion of making sure that the development of the BoB system will take into account the impact of applying biological samples to the mission. This is especially true during pre-flight operations, where biology will require special handling and attention to ensure it remains viable until the end of the mission.

The objective is considered met when the mission demonstrates a nominal/baseline of 24-hour pre-flight handover to the launch provider (BEXUS). The pre-flight operation needs to allow up to a 96-hour launch delay by maintaining viable *C. elegans* samples with minimal physical interaction.

The BoB mission would develop a pre-flight operation translatable to an orbital flight scenario, especially for the growing small satellite launch providers. The

biological payload viability can be verified by producing live worms' imagery during flight with the imaging system to record the motility and mobility of the *C. elegans*. The 24-hour up to 96-hour is to accommodate future flight opportunities, see Table 9-2.

Table 9-2. The various late access timing for current launch vehicles for CubeSats or CubeSat compatible missions.

Types of launch vehicle and space platform	**Late access timing**	**Reference**
CubeSat ride-sharing launch as a free-flying CubeSat	i. Two weeks based on SpacePharma Dido 2 and ISIS* ii. PharmaSat was delivered and integrated into Minotaur 1 rocket 6 weeks before launch	i. * Personal conversation between A. Shamsul with Innovative Solutions in Space (ISIS) at the IAC 2019 ii. (Antonio J. Ricco et al., 2011)
Hosted on larger spacecraft such as ISS or Bion satellite	i. Typically, 36 hours late access before the nominal ISS cargo launch on SpaceX Falcon** ii. Bion satellite late access was 8 to 10 hours before launch, with early retrieval 12 hours after landing	i. **A. Shamsul Personal conversation with Molecular Muscle Experiment team which flew on the ISS ii. (Fitton & Moore, 1996)
New Space launcher	Satellite to be delivered 8 hours to 4 days based on Blue Origin late access on New Shepard	(Erika B. Wagner, 2019)
BEXUS	CubeSat to be delivered 24 hours late access before the final flight review	(Frenea-Schmidt, 2021)

Unfortunately, CubeSat is still launched in a rideshare programme or as a secondary payload, and CubeSat is often delivered and integrated early in a power-off state. Currently, it is a challenge for space biological experiments for CubeSat, where environmental control, such as temperature, is vital.

2) *Demonstrate the key BAMMsat's ability to provide a controlled environment relevant to maintaining viable biological samples in extreme operational environments (specifically thermal and fluidic control together with appropriate housekeeping sensing).*
   a) Demonstrate fluidics functionality.
   b) Demonstrate internal thermal control within the 2U pressure vessel. During pre-flight, *C. elegans* shall be at a low metabolic rate temperature (i.e., +12°C ± 2 °C) and during flight operation, the *C. elegans* shall be at +20°C ± 2 °C.
   c) Demonstrate housekeeping sensor functionalities – i.e., for internal pressure vessel environmental control and fluidic operations.
   d) Demonstrate the ability to maintain *C. elegans* in a viable state during flight.
   e) Demonstrate a system with autonomous flight operations.

The objective is considered met if the BoB system demonstrates the ability to maintain a controlled environment in temperature, pressure, and fluidics application during pre-flight and flight. The demonstration of the Geneva drive, the microfluidics system injection, imaging, and data recovery will be implemented both pre-flight and in-flight.

The result can be determined by imaging the resulting changes in the *C. elegans* behaviour once the pressure vessel is sealed, thermal control activated, and fluidic subsystem activated. The successful ability to provide a controlled environment will be demonstrated if the C. elegans survive the flight. The initial design also included preserving *C. elegans* during recovery (preservative injected at the end of flight operations before shutdown telecommand for descent).

3) *Complete the development of a spaceflight relevant model version of BAMMsat suitable for the flight on BEXUS*
   a) Repackaging and reconfiguring the existing laboratory breadboard into a 2U CubeSat payload format.
   b) Reconfigure the existing BAMMsat laboratory breadboard to be compatible with an operation inside the 2U environmentally controlled pressure vessel

The success of this objective is based on configuring the BAMMsat bioCubeSat payload to be compatible with the standard 2U size CubeSat, ready for the launch on BEXUS. The final CubeSat will have a 3U format, with 1U being allocated for the CubeSat bus. Design is based on previous NASA and SpacePharma bioCubeSats. The BAMMsat system requires a pressurised, thermally controlled system to provide the internal atmosphere for O_2 and CO_2 exchange between the sample chamber and the localised environment inside the pressure vessel to ensure the survivability of the *C. elegans*. Thermal control is vital as biological samples can only survive a specific temperature range.

9.3 BAMMsat-on-BEXUS: The team, roles, management, and challenges

The following section briefly summarises the work packages involved during the BoB mission. This section was included to recognise the work performed by the various individuals during the BoB mission. It also highlights the complexity and the interdisciplinary fields required to deliver the mission.

9.3.1 Work packages and responsible personnel

The following text represents the division of the work packages, the person responsible, and the type of work performed during the BoB project.

I. Team Leader and BAMMsat bioCubeSat payload:

This work package was led by A. Shamsul (author of this document), a PhD student from the School of Aerospace, Transport and Manufacturing, Cranfield University. Given BAMMsat is his PhD research topic, Aqeel was responsible for leading and managing the team. He led the formation of the team, the proposal, and the recruitment of the team members. Because of his knowledge of BAMMsat, he produced the first version of the systems requirements and constraints to establish BoB's baseline design. He led the design, manufacturing, verification and testing of the 2nd generation BAMMsat bioCubeSat payload and interfaced it with the rest of the system and the biological aspect. As well as reviewing all engineering decisions, integrating and reviewing the Student Experiment Document (SED) submitted to the panel at each review process (see Table 9-1), and corresponding with the BEXUS panel and industrial sponsors.

II. Systems engineering

Work package led by A. Bolliand, MSc Astronautics and Space Engineering (MSc ASE) student cohort of 2019-20 in the School of Aerospace, Transport and Manufacturing, Cranfield University. He was responsible for managing the systems requirements and constraints in the subsequent versions alongside managing the power and communication data budget with software input from M.

Zalasiewicz. He was also responsible for managing the power and data budget interfacing with the BEXUS Gondola.

III. Biological payload

Work package led by M. Cooke, PhD student in Medicine, in the Department of Sport and Health Sciences, University of Exeter. M. Cooke was responsible for all biological aspects of this mission, such as biological handling from the lab to the launch campaign and vice versa, biocompatibility test, food concentration experiment, *C. elegans* age synchronisation, interfacing the biological requirements and constraints with the design of the BoB system, primarily with the BAMMsat bioCubeSat payload and active thermal subsystem.

IV. Electronics subsystem

G. Sinclair led the work package alongside N. Shetti, and H. Lleo. G. Sinclair was a 2019-20 MSc Astronautics and Space Engineering (MSc ASE) cohort at Cranfield University. In contrast, N. Shetti and H. Lleo were in the cohort of 2020-21. G. Sinclair designed, manufactured, verified, and tested all the PCBs. Hector Lleo and N. Shetti were recruited to spread the workload later in the project. H. Lleo developed the pump PCB, and N. Shetti was recruited to help with the assembly and testing of the PCBs. G. Sinclair was responsible for designing the valve actuating circuit for the fluidic subsystem in the BAMMsat bioCubeSat payload. A. Shamsul provided design input and selected the sensors and actuators of the BAMMsat bioCubeSat payload. Similarly, A. Bolliand provided active thermal subsystem design input and selected the sensors and heaters. Lastly, M. Zalasiewicz provided design input from an operating systems perspective to make sure the software could interface with the electrical design of the primary flight computer and microcontroller.

V. Mechanical

A work package led by A. Chabi, a student in MSc ASE, Cranfield University student cohort of 2019-20. He designed, manufactured, verified, and tested the overall mechanical structure of the BoB system, which included the 2U pressure

vessel for the BAMMsat bioCubeSat payload, 1U bus, and mechanical interface to the BEXUS Gondola.

VI. Thermal subsystem

The thermal subsystem work packages were split into two, i.e., active and passive thermal subsystems. A. Bolliand led the development of the active thermal subsystem, a feedback-controlled thermal heater, and he designed, manufactured, verified and tested the subsystem ready for flight. On the other hand, A. Chabi led the development of the passive thermal subsystem, primarily multi-layer insulation (MLI). He designed, manufactured, verified, and tested the MLI ready for flight.

VII. Project management

Work package led by M. Martinez De Bujo was a student in MSc ASE in the cohort of 2019-20, Cranfield University. A. Shamsul took over once M. Martinez De Bujo completed his study for the academic year of 2020-21. They both led the project management aspect of project scheduling, budgeting, securing grants, and arranging group meetings.

VIII. Software

Work package led by M. Zalasiewicz, a part-time MSc Astronautics and Space Engineering in the cohort of 2019-22, Cranfield University. M. Zalasiewicz was responsible for designing, verifying, and testing the flight operating system software for the BoB system and ground control software. He was also responsible for interfacing the software with the relevant BoB subsystems and BEXUS gondola electrical and telecommunication unit.

IX. Operations

Work package led by Adrien Bolliand. M. Cooke and A. Shamsul provided inputs on the biological handling and operation of the 2nd gen. BAMMsat bioCubeSat payload. The operation work package includes pre-flight operation, flight operations, and post-flight operation planning. It was seen as necessary since *C.*

elegans imposed specific requirements and constraints. M. Zalasiewicz implemented the flight operation via the flight operating system software.

X. Outreach

Various students handled the outreach work package at different stages of the project. The core personnel were N. Shetti, S. Raj (BSc in Biology, University Sains Malaysia), R. Panchal (MSc ASE 2021-22), T. Tonina (MSc ASE 2018-19), and J. Lucero (MSc ASE 2019-20). Other team members were heavily involved in providing content, blogs, and various supports throughout the project.

XI. External camera

R. Giroud, MSc ASE 2020-21, led the development of the external camera. The external camera is an independent system added midway through the two-year project. The system was added to take advantage of the extended timeline and include a camera to record the flight of BAMMsat-on-BEXUS. This was primarily for future outreach to visualise the flight, see Figure 1-2. R. Giroud led the design, verification, and testing of the external camera system, leveraging the experience of other team members, which helped shorten the development iterations.

9.3.2 Challenges in project management

The BAMMsat-on-BEXUS mission was a complicated and challenging project. Interaction and cooperation were required between various engineering and scientific disciplines to deliver the final system ready for flight. The project was challenging due to complications in project management (timeline and human resources) and technical development.

The text in this section attempts to capture the project's scope and how it was implemented and evolved. It was initially thought to be a one-year project that extended into two years to mitigate the COVID-19 pandemic. The lockdown meant that access to laboratories was restricted, and progress was hampered.

The flight was postponed from October 2020 to October 2021. The team, which started with a core of seven team members, then grew to fifteen team members

to mitigate the postponement, given some team members finished their Cranfield University studies in September 2020. New team members had to be recruited from the MSc Astronautics and Space Engineering (ASE) cohort of 2020-21 and later trained on the BoB mission and the system. The core team members came from the previous one-year MSc ASE cohort of 2021-22.

The final hurdle experienced by the team was a fire that broke out at Esrange Space Centre on 26th August 2021 (Swedish Space Corporation, 2021). A fire broke out during a scheduled static firing test of a solid rocket motor which damaged the building with the biological laboratory facility. The absence of a biological laboratory on-site during the flight campaign led to adjustment to the BoB mission, primarily on hazardous chemical use in fluidic operations. The hazardous chemicals were removed to remove the risks of handling the chemicals without the necessary equipment, such as a laminar flow cabinet.

The project also faced technical challenges throughout the programme. One of the feedbacks from the BEXUS panel on the project proposal stated, "*the experiment is complex and could be a challenge within the limit of the programme and resources of the team*" (REXUS/BEXUS, 2019). The technical challenge was due to the combination of the BAMMsat-on-BEXUS system being the first complete prototype plus the additional requirements and constraints associated with biological handling. At this stage of the project, many novel subsystems had to be developed and integrated into the full system. The system also had to be repackaged into a CubeSat format meeting the standardised CubeSat requirements and constraints to ensure future compatibility. The technical challenge, combined with a steep learning curve with the team being early-career engineers and scientists, meant many design iterations.

The initial plan for developing the BoB mission was to follow a typical project management V model and the waterfall model of a space or complex project lifecycle (Forsberg & Mooz, 1991). However, the development strategy quickly became a rapid iterative process as the project progressed.

The development cycle started with defining the requirements and constraints extracted from the mission objectives. The requirements were then extracted into baseline for subsystems and the lowest part of the sensors, actuators, and software elements. Readers interested in the list of requirements for the BoB mission can refer to Appendix A of this document. During the project lifecycle, periodic reviews were included to check progress and ensure the development was still within the scope of the mission timeline.

During the development, the project lifecycle was not as linear as was intended. In most cases, concurrent engineering was practised, where the development and tasks of different subsystems were performed in parallel. In some instances, system-level testing was conducted ahead of unit testing, which is not ideal, especially if the unit has not been thoroughly tested. Such a decision was due to limited resources and time-constraint where the system had to be put forth to pass the reviews. The project naturally became a bed of rapid iteration, where identified issues are quickly solved and incorporated into the full system.

9.4 Final flight design and operations

This section discusses the final BoB system design and flight operations implemented and launched from the Esrange Space Center on 30/09/2021 on the BEXUS 30 flight. This section was included because the BoB system evolved from the planned design (summarised in section 8.3). The final design had some last-minute modifications during the flight campaign due to the challenges experienced at Esrange during the pre-flight operation.

The final flight design had further modifications due to challenges in assembly, integration, and verification during the flight campaign. Table 9-3 provides an overview of the activities and challenges experienced during the flight campaign. The BEXUS 30 flight campaign was held from 24/09/2021 – 04/10/2021. BEXUS 30 with the BoB system launched on the 30th of September 2021.

There were two key issues during the flight campaign that imposed design modification.

- The issue with imaging where the *C. elegans* inside the sample chamber could not be focused.
- The issue with MCSD leakage.

Table 9-3. Overview of the activities and challenges experienced during the BEXUS 30 flight campaign.

Day	Date (D/M/Y)	Activity	Remarks
- 3	21/09/21	M. Cooke[1] arrived at Esrange	Prepared the laboratory and the *C. elegans* by growing and synching their lifecycle in preparation for flight
0	24/09/21	Nominal arrival of all team members	Nominal arrival and checked the status of the BoB system after transits. There was no observable damage to the system and subsystems
1	25/09/21	Preparation	The tasks during Day 1 included preparing the workstation and the BoB system, sterilising the relevant subsystems such as the MCSD, and calibrating optics to ensure it can resolve the *C. elegans*
2	26/09/21	Individual test	Mechanical fit on the BEXUS gondola and functional testing of the different subsystems. Subsystems functioned nominally, except some of the chambers dried out due to MCSD leaking; Figure 9-10 shows the leaks underneath the MCSD. The imaging system could not focus the C. elegans inside the sample chamber during the bench testing. To find a solution, various tests were performed by changing the working distance and back focal length distances. Another issue was encountered when the selector valve manifold was damaged. The team rushed into meeting the functional testing, and the MCSD was not bolted correctly. After the Individual test, A. Shamsul had to rebuild the manifold to fix the damage.
3	27/09/21	Interference test	Every experiment/system from all the teams on board BEXUS 30 was mounted on the BEXUS Gondola to check electrical and communication interference. At this stage, the imaging subsystem was still unable to resolve the *C. elegans*, as identified on Day 1. It was

[1] M. Cooke was the team biologist and *C. elegans'* expert. He arrived three days before the nominal arrival date to prepare a biological laboratory since the biological laboratory was damaged due to fire (Swedish Space Corporation, 2021)

			decided to change the lens to the Raspberry Pi camera v2.1 original lens. Figure 9-8 shows the modification made to the imaging subsystem with a makeshift optical mounting unit.
4	28/09/21	Flight Compatibility Test (Aborted)	The FCT was the final test before the flight. The aim was to replicate flight operations and ensure compatibility between the BEXUS system and all experiments. After FCT, it was impossible to change the BoB system. In preparation for flight, the age synchronised *C. elegans* was integrated into the MCSD using the planned configuration shown in Figure 6-4. The other teams had communication interference, and the FCT was aborted. The BoB team dismounted the BoB systems from the Gondola and transferred the BoB system into a portable incubator (Labcold; RPDF0012F); see Figure 9-6. The team performed the nominal feeding via telemetry in the evening and heard a low but audible screeching sound when rotating the Geneva gear. During feeding, downloaded videos showed that some of the chambers had dried out.
5	29/09/21	Flight Compatibility Test (Successful)	In the morning, a decision was made to disassemble the BoB system to assess the noise and replace the *C. elegans*. The noise came from the corroded axial bearing and caused the rotary valve to become loose. See Figure 9-27 to see the image of the corroded bearing. The corrosion was due to salt in the OP50 growth media. To mitigate leaks, the team reassembled the BoB system with an increased number of sample chambers with *C. elegans*. The BoB system was integrated and sealed at 07:55 UTC, and FCT was performed successfully at 12:35 UTC. After FCT, the BoB system was dismounted, placed in the Labcold incubator to keep at the temperature at +12ºC to lower the metabolic rate of *C. elegans*, and performed nominal feeding operations.

			Unfortunately, the screeching sound reappeared. After FCT, it was impossible to replace the *C. elegans* as changes were viewed as a risk to the flight.
6	30/09/21	Flight	Launch confirmed, and the launch sequence began at 02:00 UTC. BoB system remounted at 01:20 UTC, and the balloon was launched at 04:54 UTC, and the flight lasted for 5 hours 32 minutes.
7 to 10	1/10/21 – 4/10/21	Post-flight	BEXUS Gondola recovery and immediate post-flight analysis.

Figure 9-6. Image of the Dome building at ESRANGE on the left where all pre-flight operations were performed, i.e., assemble, integration, and verification.

The left image was taken when the Gondola was being transferred to the launch pad for flight on 30/09/2021. The fully assembled BoB system was housed after being dismounted from the Gondola inside the Labcold incubator to keep the temperature at 12°C, see Day 5 in Table 9-3. The incubator was a crucial instrument during pre-flight operations since it enabled temperature control of the BoB system at +12ºC to lower the metabolic activity of *C. elegans*.

9.4.1 Imaging problems and modification at Esrange space centre

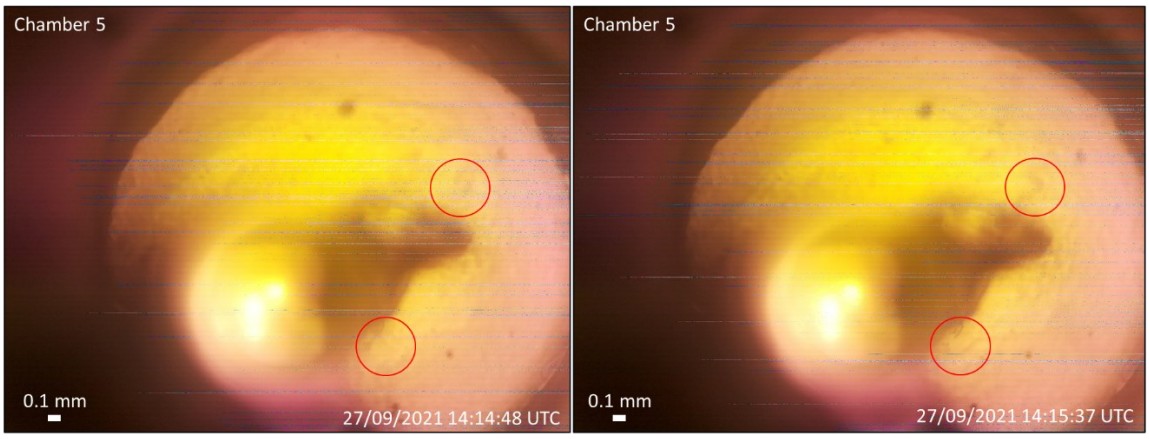

Figure 9-7. Uncropped images of Chamber 5 were taken during the Interference test via an autonomous operation on 27/09/2021.

One of the significant design modifications in the final flight configuration was the imaging subsystem. Figure 9-7 shows the captured image during the Interference test (Day 3). The image showed a poor resolution of the *C. elegans*. *C. elegans* in Figure 9-7 was confirmed via video analysis where *C. elegans* motility was evident during post-flight analysis. Various configurations were tested on days 2 and 3 by changing the working distance between the object and the lens, similarly, by changing the back focal length between the sensor and the lens to resolve the image. However, the various test confirmed that the different setups could not resolve the *C. elegans*. A decision was later made to revert to the original lens of the Raspberry Pi (RPi) v2.1 camera from the custom lens developed for the compact brightfield microscope.

The reason for the poor image quality captured during the flight campaign was that the imaging subsystem was not thoroughly tested with *C.* elegans and its growth media. The test with *C. elegans* in a flight system was only performed once before the flight campaign. This was due to complications with laboratory closure, COVID travel restriction, and travel distance between Cranfield University and the University of Exeter (see section 8.7.2.2.3 for the test results). Before the flight campaign, the number of planned optical testing was reduced to one testing to reduce the risk of COVID-19 infection and take national lockdowns

into account. The only testing of the entire BoB system with *C. elegans* with its growth media was performed during Experiment Acceptance Review (EAR) at Cranfield University. However, the EAR test result was inconclusive, where only 1 of 32 chambers image was resolved.

After the EAR, the following optical calibration with *C. elegans* had to be performed during the flight campaign. It was hypothesised that the issue could be solved by changing the working distance between the object and the lens, and the back focal length during the flight campaign. Unfortunately, the problem remained after various trials during Days 2 and 3 of the flight campaign. Further experimentation will be required to understand the reasons behind the poor image quality after the flight campaign.

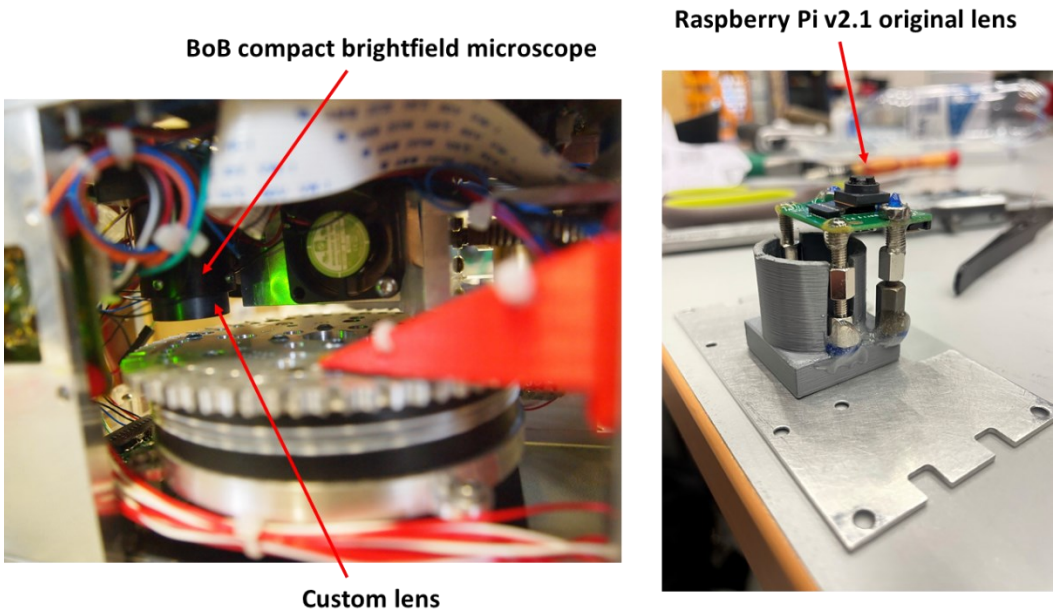

Figure 9-8. (Left) Compact brightfield microscope designed for the BoB system with the custom lens. (Right) An RPi v2.1 camera with its original lens.

The last design change made during the flight campaign to resolve the issue of poor image quality was to revert to the original lens of the RPi v2.1 camera. For reference, a custom compact brightfield microscope was developed for the BoB system (see section 4.7 for a complete discussion on the design). The change

was suggested based on previous work at the University of Exeter by M. Cooke, where the original lens was able to resolve the *C. elegans* at lower magnification.

A PCB spacer, 3D printed part, and BoB aluminium camera plate was combined to accommodate the last-minute design change. The makeshift mounting was required to house the RPi v2.1 camera with its original lens at the optimal working distance since it was a fixed focus lens. The lens was unscrewed from its factory setting to increase the back focal length distance between the sensor and the lens to increase magnification.

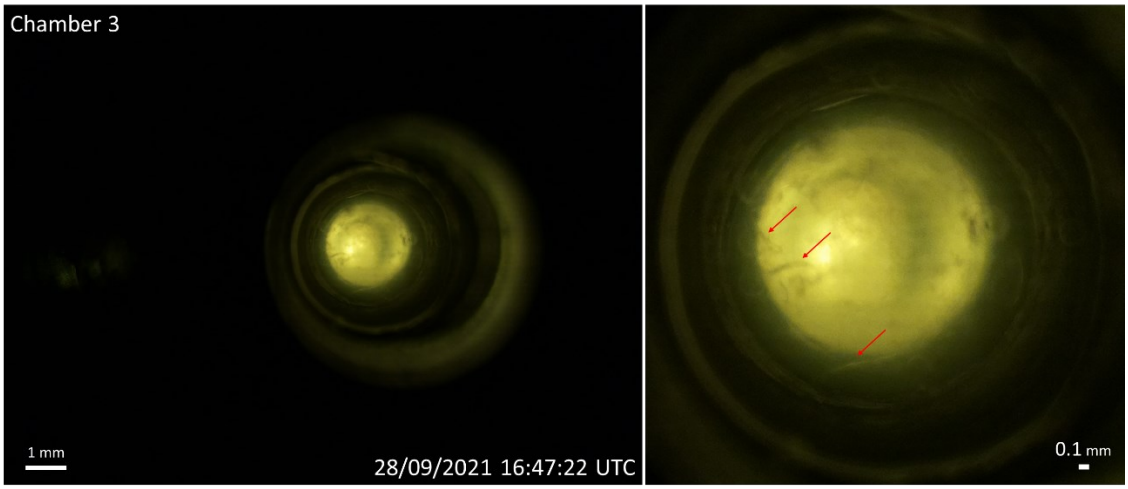

Figure 9-9. Captured image of chamber 3 showing *C. elegans* after aborted FCT[1].

A rapid performance test was conducted on a custom optical test bench to verify the image quality before proceeding with the design change. The new setup had a depth of field of approximately 2 mm and was not sensitive to tilting (perspective error). Formulation of the required working distance between the lens and the object was performed, and it was decided that reverting to the original lens would be advantageous for the mission objectives. Figure 9-9 shows one of the MCSD sample chambers captured with the RPi v2.1 camera with its original lens. The

[1] (Left) Uncropped image of chamber 3 taken on 28/09/2021 after the aborted FCT in Day 4. The image was captured to assess the viability and fed the *C. elegans* by pumping the OP50 growth media. (Right) Enlarged and cropped image from the left with arrows pointing towards *C. elegans* showed that the modification made to the imaging subsystems was encouraging.

image showed that it could resolve the *C. elegans* in its growth media in a complete system setup.

It is worth mentioning that the image (Figure 7-9) has very little to no noise compared to the image in Figure 9-7. The noise level depended on the bending of the cables. It was possible to capture an image with no noise by iterating the process of finding the minimal wire bending by assembling the 2U pressure vessel, capturing an image, downloading the image, disassembling, and repositioning the wire. Unfortunately, there was no time to iterate for the final flight configuration before the second FCT (Day 5). Hence, some of the flight images had noticeable noises.

9.4.2 Leakage issue and increased number of housed samples inside the 2nd gen. MCSD as a mitigation strategy

The second issue faced during the flight campaign was the leakage inside the 2nd gen. BAMMsat bioCubeSat payload. Leaking has been a persistent issue throughout the BoB study, and it was because of the limitation of the manufacturing technique. The chosen manufacturing technique kept the design cost low and accessible. However, the design was pushing the limit of its capability. This was evident in the MCSD, there were too many layers inside the MCSD, and each layer had to be aligned and bolted correctly to ensure fluidic sealing. Figure 3-17 shows the fully assembled layers of the 2nd gen. MCSD.

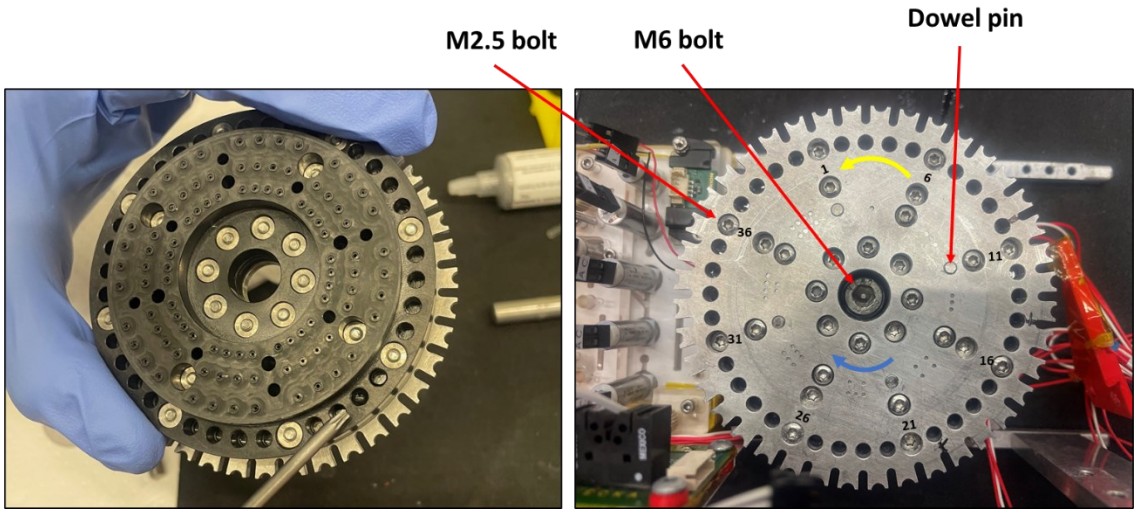

Figure 9-10. Left - A fully assembled MCSD ready for flight with leakage on the underside of one of the chambers.

During the pre-flight operation, when integrating the C. elegans into the MCSD, the bolt loosened during handling and caused leaks (Figure 9-10). The M2.5 bolts along the concentric circles on the MCSD were bolted at a torque of 0.1 Nm; see (right image). The torque was relatively low, and actions during handling, especially when inserting and removing the dowel pins, caused the bolt to loosen.

The dowel pins aligned the MCSD layer and the Geneva gear to the BAMMsat bioCubeSat payload. During the MCSD and *C.* elegans integration and later integration to the BAMMsat bioCubeSat payload assembly, the process would typically include the dowel pins being removed and replaced three times. Due to the tight tolerance of the dowel pins, the actions dislocated the bolts and loosened the sealing. The image on the right (Figure 9-10) showed the evidence of leaking from the MCSD assembled for flight on 30/09/2021. Unfortunately, this issue was identified late in the final flight campaign opportunity (Day 5) to replace the *C. elegans* inside the MCSD.

The leaking had a knock-on effect which was discovered on Day 5 to the axial bearing of the Rotary Valve. The high salt concentration growth media which leaked from the sample chamber caused the axial bearing of the rotary valve to

corrode. See Figure 9-27 for the corrosion image. The corrosion meant that the bearing was damaged and no longer rotated freely around the centre axis.

Figure 9-10 (right) shows the top view of the MCSD bolted to the RV via an M6 bolt. The M6 bolt was tightened by rotating the bolt clockwise (blue arrow) using a torque screwdriver at 0.5 Nm. The MCSD was designed to rotate counterclockwise (yellow arrow) via the Geneva gear mechanism. Essentially, rotating counterclockwise untightened the M6 bolt since the bearing does not have a free rotation due to increased friction. It meant that the two surfaces of the RV were no longer in compression and had fluidic sealing.

On Day 5, it was decided that the number of samples inside the MCSD should be increased to the maximum capacity of 32 chambers. This was an increased number of chambers from the planned 16 chambers. The decision was made to increase the probability of having viable *C. elegans* during the flight due to leaking during assembly. However, due to leaking during assembly, only 23 chambers had *C. elegans* inside the sample chambers survived the integration process, confirmed visually via a stereoscopic microscope. Figure 9-11 captured the final number of sample chambers with their respective sample type.

Another late design was an additional chamber with a "dye" in Chamber 2 (see Figure 9-11). The chamber was added during the flight campaign to visualise fluidic pumping to test the secondary objective of the BoB mission (see section 9.2). During bench testing at the flight campaign, it was not easy to evaluate if the pumping had occurred. The "dye" was added as an extra measure to confirm fluidic pumping during flight.

Although it is called a "dye", " it is particulates of varying sizes made from a dried down OP50 solution. It was believed that the addition of the dye could help better visualise the fluidic pumping actions. It was thought that during pumping, the fluidic agitation on the particulates could be captured in the video better than pumping growth media into the chamber with *C. elegans.*

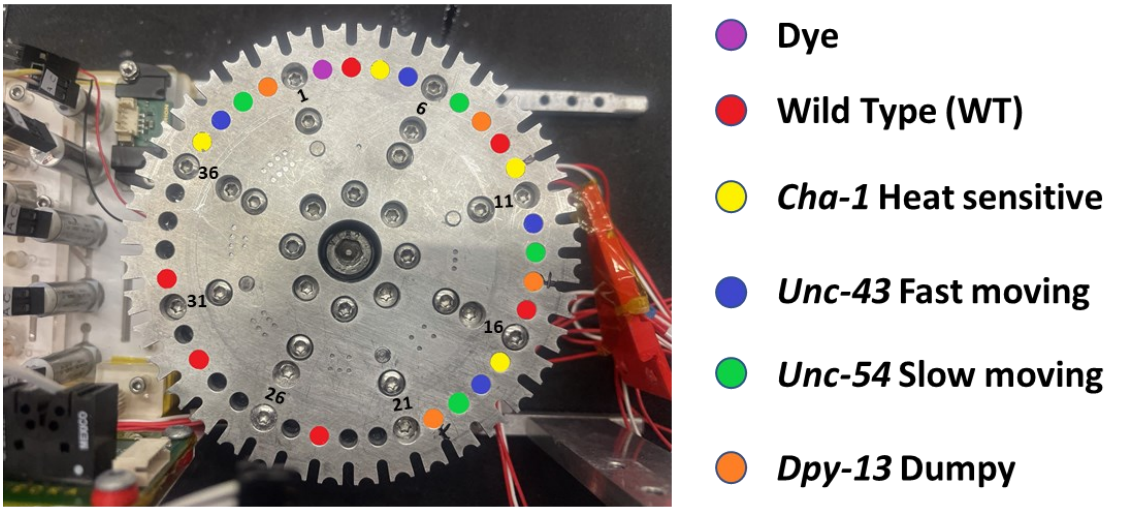

Figure 9-11. The final flight configuration with an increased number of sample chambers with *C. elegans* and the addition of a "dye" chamber.

9.5 Preliminary analysis of BAMMsat-on-BEXUS flight results

This section discusses the preliminary analysis of the flight result from the BAMMsat-on-BEXUS (BoB) flight that flew onboard the BEXUS 30 gondola. The BEXUS 30 gondola was launched into the stratosphere on 30/09/2021 from the Esrange Space Centre, Kiruna. At the time of writing (Jan 2022), there was only a short period for preliminary analysis between the end of the flight campaign and thesis submission. This section provides an overview of the flight and a brief insight into the performance of the BoB system. Other team members such as A. Bolliand, M. Zalasiewicz, M. Cooke and G. Sinclair have provided varying inputs alongside the author to help interpret the flight result.

The flight result showed some evidence of live *C. elegans,* demonstrating the capability of the BoB system to maintain a viable biological sample. There was also some evidence of autonomous fluidic pumping that demonstrated the BoB system's ability to perturb the biological sample. Both were discussed since they were part of the mission objective. Being a technology demonstration mission, the flight did encounter some issues. The flight encountered some issues with imaging and loss of thermal sensors, which impacted the ability to capture data and affected the health of *C. elegans.* The issue will be discussed in this section and used as a lesson learned for the 3rd gen. BAMMsat system.

9.5.1 Summary of flight timeline and flight path

This section provides an overview of the flight timeline before a detailed discussion. The flight lasted for approximately eight and a half hours, with the flight countdown starting at 02:00 UTC on 30/09/2021. Table 9-4 provided key events during the flight sequence to visualise the activities involved.

The flight sequence is separated into four phases, i.e., the Dome phase, Launch pad phase, ascent phase and float phase. The phases are introduced to assist with the discussion for the rest of this chapter.

Table 9-4. The table provides the extracted time for key events during the launch sequence on 30/09/2021[1].

Event	CEST (UTC +0200; hr:mm)	UTC time (hr:mm)
End of BoB system integration to the BEXUS 30 gondola	03:20	01:20
Beginning of flight countdown	04:00	02:00
Gondola picked up from the Dome[2] for line-up	04:44	02:44
Gondola flight train line-up[3]	05:00	03:00
Beginning of late access (access requested to turn on the BoB external camera	05:28	03:28
Balloon launched	06:54	04:54
Float phase began (at 27.3 km altitude)	08:30	06:30
Beginning of autonomous operation[4]	08:40	06:40
End of autonomous operation	09:30	07:30
Balloon cut off	11:55	09:55
Gondola communications connection lost (at 1.26 km altitude)	12:27	10:27
Landed	12:29	10:29

Before the flight, the BoB system was removed from the incubator and mounted to the BEXUS 30 Gondola at 01:20 UTC. The BoB system was remounted from the incubator to the Gondola at the latest possible time before the Gondola was

[1] CEST standard (local Swedish time) is being included as a reference, and the UTC standard was used to synchronise all flight data during post-flight analysis.
[2] Dome is a large building used as a preparation area
[3] Line-up was an action to line the BEXUS 30 flight train with the direction of the wind before release.
[4] Autonomous operation was a set of sequence during float phase which involved fluidic pumping, rotating the MCSD and image the *C. elegans.*

transferred to the launch pad. The decision was made to reduce exposure to the external temperature to maintain *C. elegans* viability.

After the autonomous operation, manual telecommands were sent from the ground station for data collection. Depending on the weather and flight path, the minimal float time of the BEXUS flight is 1 hour. M. Zalasiewicz developed the autonomous operation to ensure that the data collection occurred despite the loss of telemetry. BEXUS 30 flight was fortunate since the float phase was longer than expected, and it allowed the team to send telecommand to perform more data collection.

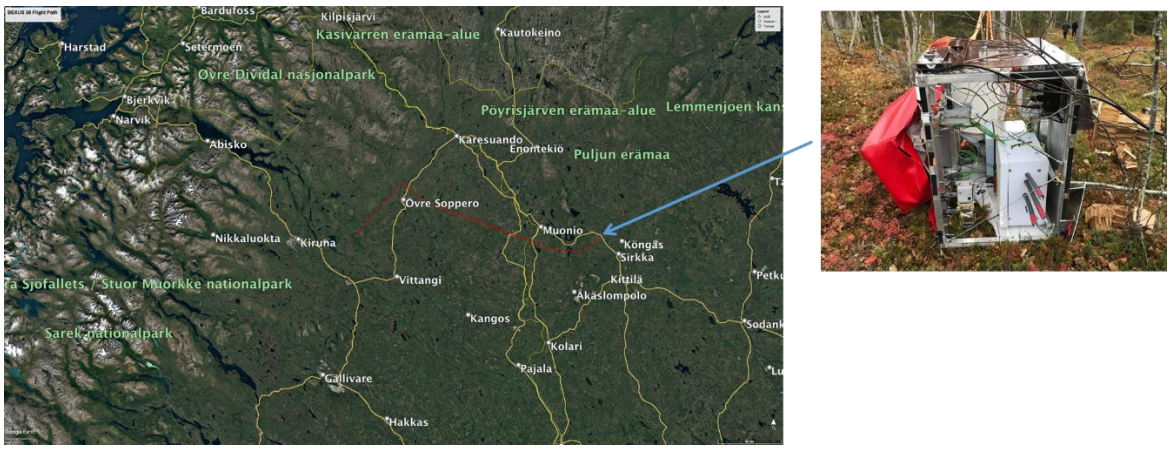

Figure 9-12. Summary of BEXUS 30 flight paths.

In general, the flight of BEXUS 30 was nominal. The balloon flew towards the east (right side of the image) into Finland. Compared to the mountainous terrain in the west, the flatter terrain allows easier post-flight recovery. The BEXUS 30 Gondola landed in Finland near the town of Sirkka.

9.5.2 Comparison between flight environment and internal BoB environment and its impact on the BoB system

9.5.2.1 Pressure environment

It is worth comparing the two different environments experienced during the BoB flight. The primary environment was the ambient environment experience by the BoB system, which started inside the Dome and later in the float phase in the stratosphere. The primary environment then affected the secondary environment, which was the environment inside the 2U pressure vessel. The 2U pressure vessel housed the biological samples, *C. elegans* and the 2nd gen. BAMMsat bioCubeSat payload. Both were tested in an extreme environment in a technology demonstration mission.

One of the objectives of BAMMsat-on-BEXUS was to access the harsh environment representative of spaceflight. The environment during the flight was challenging, particularly the dynamic pressure and thermal environment. These environments imparted stress on the system and will be discussed accordingly. Since the biological sample imposed additional requirements during pre-flight, the analysis also looked at pre-flight data to have an overall picture of the flight result.

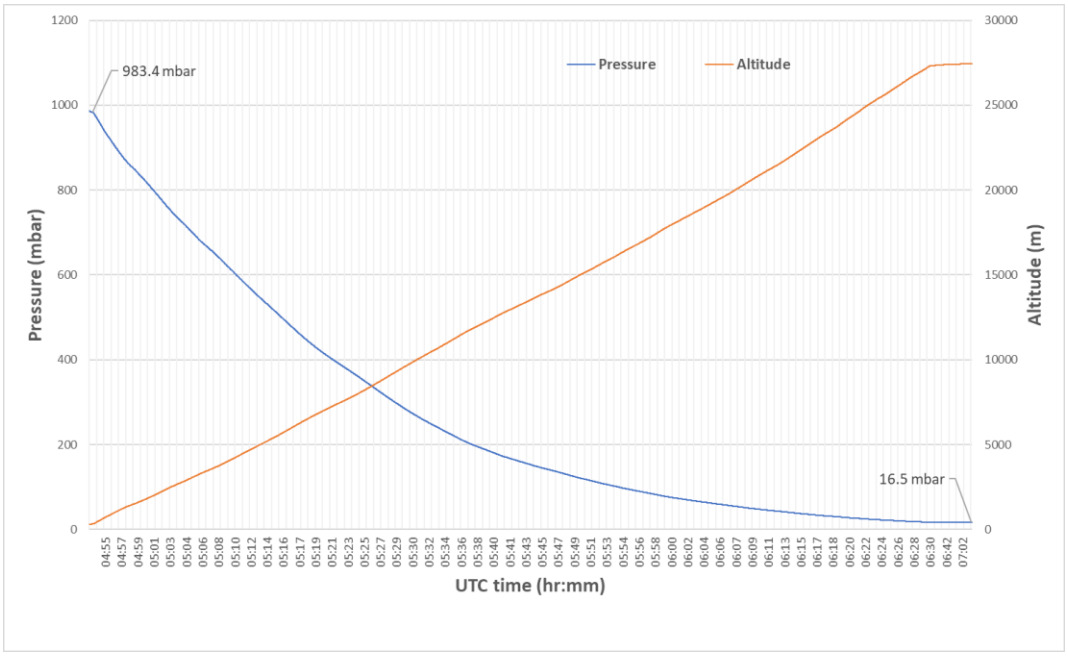

Figure 9-13. Pressure profile vs altitude of the BEXUS 30 flight during the ascent phase.

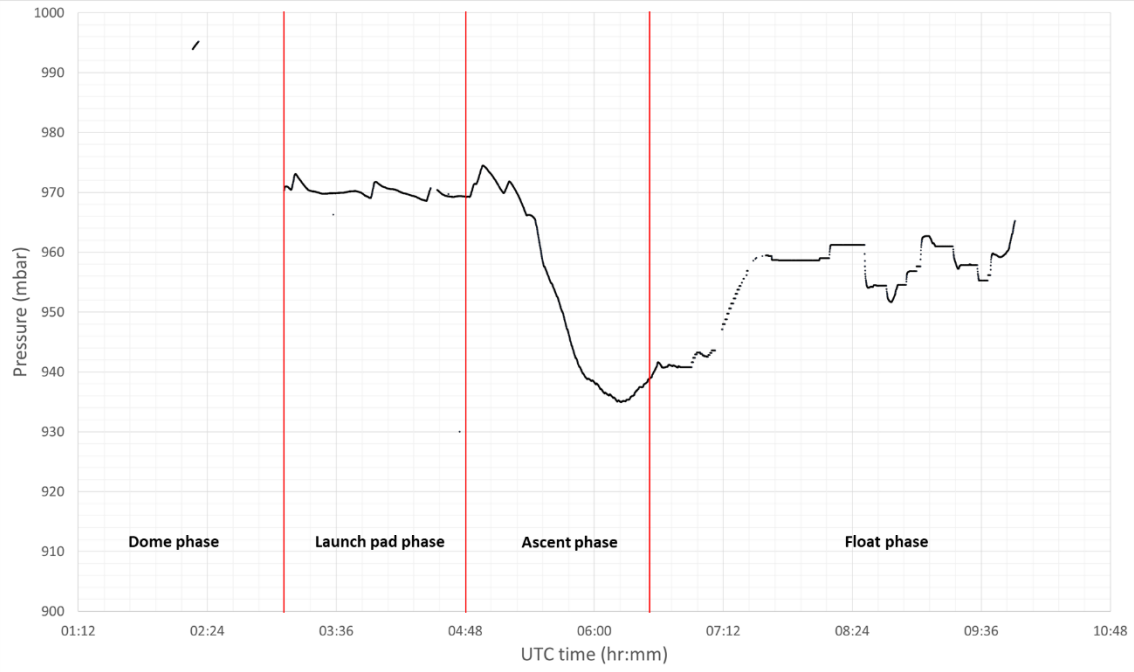

Figure 9-14. The pressure inside the 2U pressure vessel[1].

The graph is separated into four phases. The Dome phase was when the BoB system was tested and integrated with the BEXUS 30 gondola. The BoB system was sealed and contained with the local atmosphere at this stage. The launchpad phase was when the BEXUS 30 Gondola was grounded, pending launch. The ascent phase started once the Gondola was released and ascended into the float phase in the stratosphere.

The external environment pressure reading at the launch pad was recorded at 983 mbar and slowly decreased exponentially to 16.5 mbar during the float phase. The data in Figure 9-13 was provided by the launch from BEXUS 30 EMPIRE PTU.

In comparison, the 2U pressure vessel demonstrated that it contained the ground atmosphere. Figure 9-14 showed that the pressure vessel maintained the pressure between 930 mbar and 980 mbar with a negligible leak rate. The

[1] The data starts from inside the Dome into the float phase in the stratosphere. The system was shut down at the end of the float phase.

pressure dipped during the ascent phase. The dropped was because of the reduction in temperature, which meant a reduced average kinetic energy of the gaseous inside the 2U pressure vessel. The pressure profile followed the temperature profile inside the 2U pressure vessel when comparing Figure 9-14 and Figure 9-16.

9.5.2.2 Thermal environment

A. Bolliand developed the active thermal control subsystem. See section 9.3.1 for more detail on the work package breakdown of the BoB mission. Before the flight campaign, the BoB system was tested under a pseudo thermal vacuum chamber. The test was performed to understand the performance of the active thermal control subsystem, which is used as the basis for flight analysis. The work performed in this section by the author was produced as a continuation to work performed by A. Bolliand with some input by A. Bolliand to interpret the flight result.

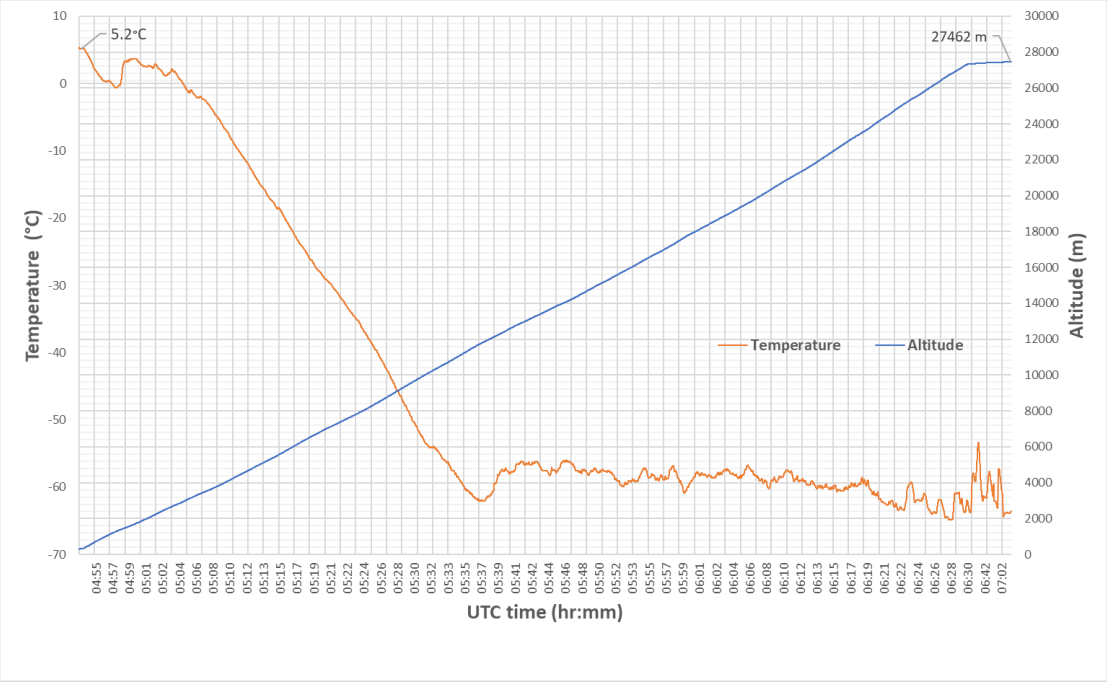

Figure 9-15. Graph of the external temperature vs altitude during the ascent phase of the BEXUS 30 flight.

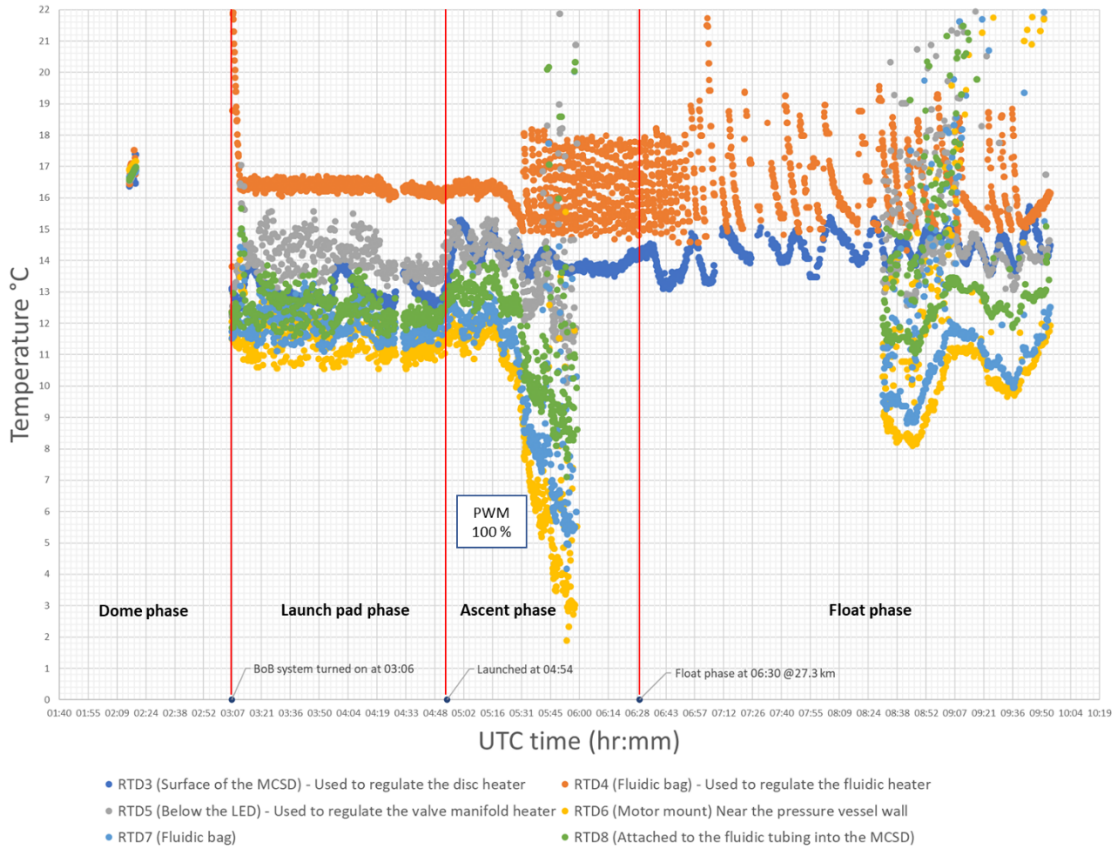

Figure 9-16. Temperature readings for all RTDs inside the 2U pressure vessel.

In Figure 9-15, the external temperature environment recorded a temperature of 5.2°C at the launch pad. Once launched, the temperature steadily decreased in the ascent phase, which took approximately 40 minutes. At above 11 km altitude, the temperature reached -60°C with the coldest temperature of -65°C in the stratosphere. The launch provider provided the temperature data in Figure 7-15 extracted from the BEXUS EMPIRE system and only offered the temperature data during the ascent phase.

The temperature at various points inside the 2U pressure vessel was 17 ± 0.5°C at the Dome phase. When the BoB system was turned on again at the launch pad, the temperature had a more considerable variation, demonstrated by the different RTDs shown in Figure 9-16. The lowest temperature during the ascent phase was around 10.5°C, and the highest temperature was around 16.5°C.

During the ascent phase, the thermal environment was challenging when the BoB system ascended through the troposphere into the stratosphere. During this period, the BoB system experienced an average external temperature of –60°C to -65°C (see Figure 9-15). The external temperature affected the temperature inside the 2U pressure vessel, where the lowest temperature closest to the vessel wall was 2°C (RTD6). The highest temperature during this phase was the fluidic bags (RTD4), with a temperature of around 16°C. The fluidic bags contained OP50 liquid culture, the growth media for the *C. elegans*. Since it contained water, it had a good specific heat capacity to retain the temperature.

At around 05:30 UTC, an interesting event occurred when the Gondola entered the stratosphere. At an altitude of about 10 km, the external temperature was approximately -55°C, and more importantly, four RTDs became anomalous during this period. In Figure 9-16, RTD5, RTD6, RTD7 and RTD8 did not provide value within the expected range of 0°C to 20°C. During the flight, it was thought these RTDs were damaged at the ground station from the telemetry data. During post-flight analysis, the RTD gave noisy temperature readings between 30°C and 80°C (see Figure 9-24). This was non-nominal and will be discussed later in section 9.6.1. The RTDs returned to the expected temperature range in the middle of the float phase at 08:30 UTC.

RTD 3 was a critical component in the BoB system as it was used to regulate the MCSD heater. The *C. elegans,* heater and RTD3 can be seen on the top right of Figure 9-17. RTD3 was located on the surface of the MCSD to control the MCSD heater underneath. Since the RTD3 was not located inside the sample chamber, the temperature of the *C. elegans* had to be extrapolated from RTD3.

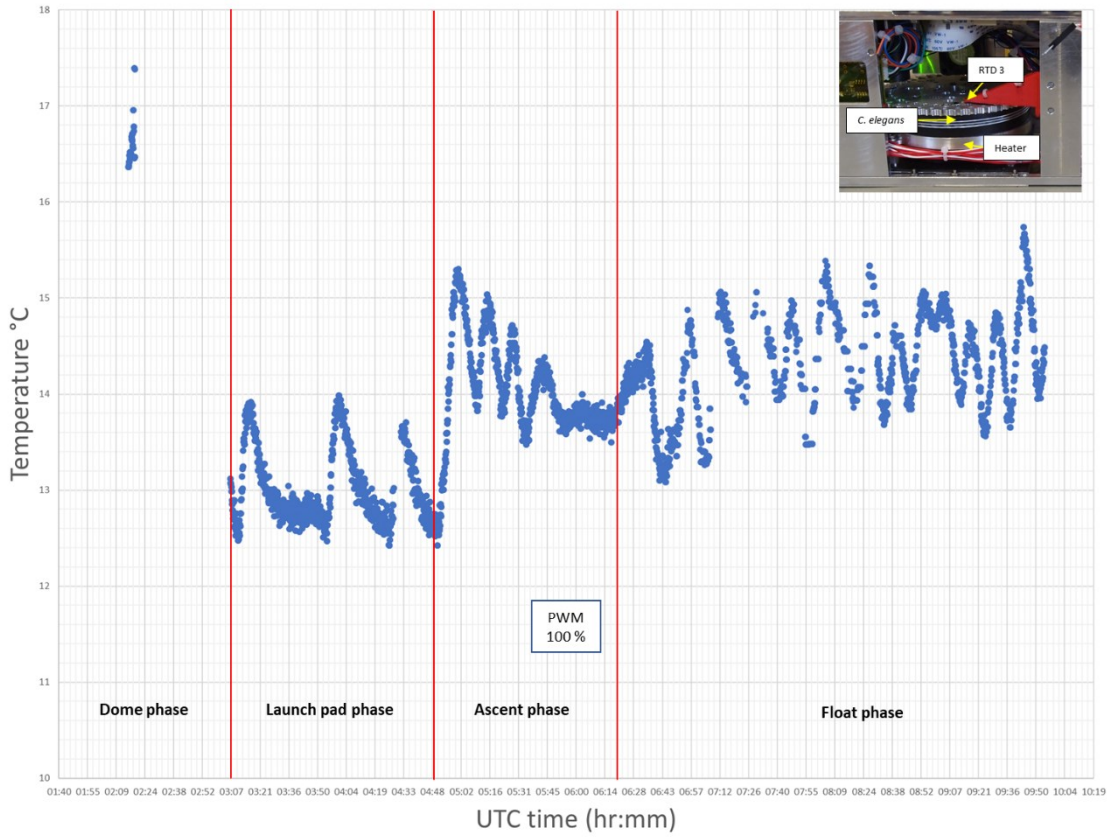

Figure 9-17. The RTD3 temperature sensor values in the four different phases during the flight.

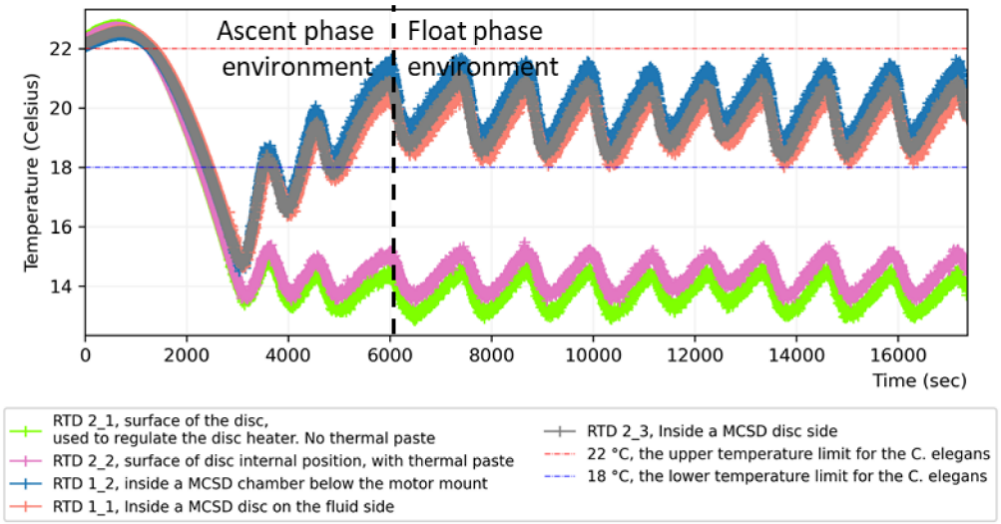

Figure 9-18. Temperature test results in the pseudo thermal vacuum chamber of the active thermal subsystem before the flight campaign for comparison (Bolliand, 2020).

The value inside the sample chamber can be extrapolated using the knowledge from the pseudo thermal vacuum chamber testing (see Figure 9-18). The test indicated that the temperature inside the sample chamber is often stable and remained at 6 to 7°C higher than the RTD reading on the surface of the MCSD, i.e., RTD3 in-flight configuration (Bolliand, 2020). This meant that during the flight, the temperature experienced by the *C. elegans* could be assumed to be between +18°C to +23°C. This temperature was the upper limit of the C. elegans thermal requirements, and this high temperature could have an impact on the health of *C. elegans*. It is worth noting that the extreme thermal environment experienced during ascent was never replicated in the laboratory due to facility limitations (Bolliand, 2020).

RTD3 and RTD 4 were within the expected range compared to the other four RTDs that were lost during the flight. It was hypothesised that the harsh environment imparted stress on the system and caused sensor readings errors. The rapid temperature decrease, with dynamic convection cooling from the wind and temperature below -60°C, was never tested in the lab. During this period, the loss of RTD readings was significant as the system was experiencing the coldest environment during flight.

The three sensor readings (RTD3, RTD4, RTD5) were used as temperature input into the active thermal bang-bang controllers (Bolliand, 2020). RTD3 controlled the MCSD heater, RTD4 controlled the fluidic bag heater, and RTD5 controlled the valve manifold heater. The loss meant that the thermal control for the valve manifold heater had to be adjusted manually from the ground station. Since RTD3 and RTD4 had the expected temperature behaviours, thermal management was performed nominally. The team manually overrides the heating parameters during the ascent and float phases by adjusting the PWM duty cycle. The PWM was set to 100% during ascent for the valve manifold heater, which meant that the heaters ran at total capacity. The heating was varied manually during the float phase based on the RTD5 reading as an input. However, without feedback from the complete system, the PWM parameters were estimations.

9.5.3 Flight results analysis

9.5.3.1 Evidence of *C. elegans* motility

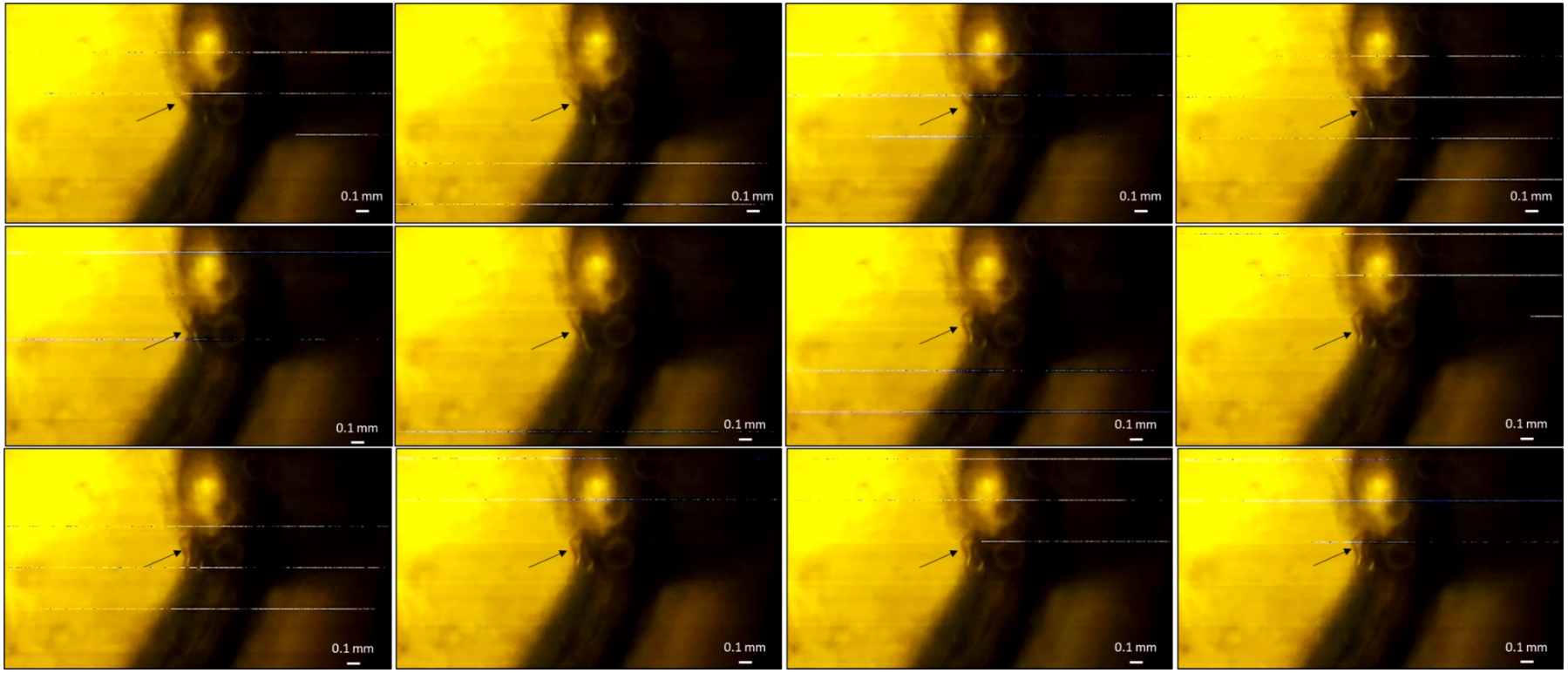

Figure 9-19. Extracted frame by frame video of Chamber 37 captured at 0.03 seconds apart (30 fps).

The location of the MCSD sample chambers flown during the flight can be viewed in Figure 9-11.

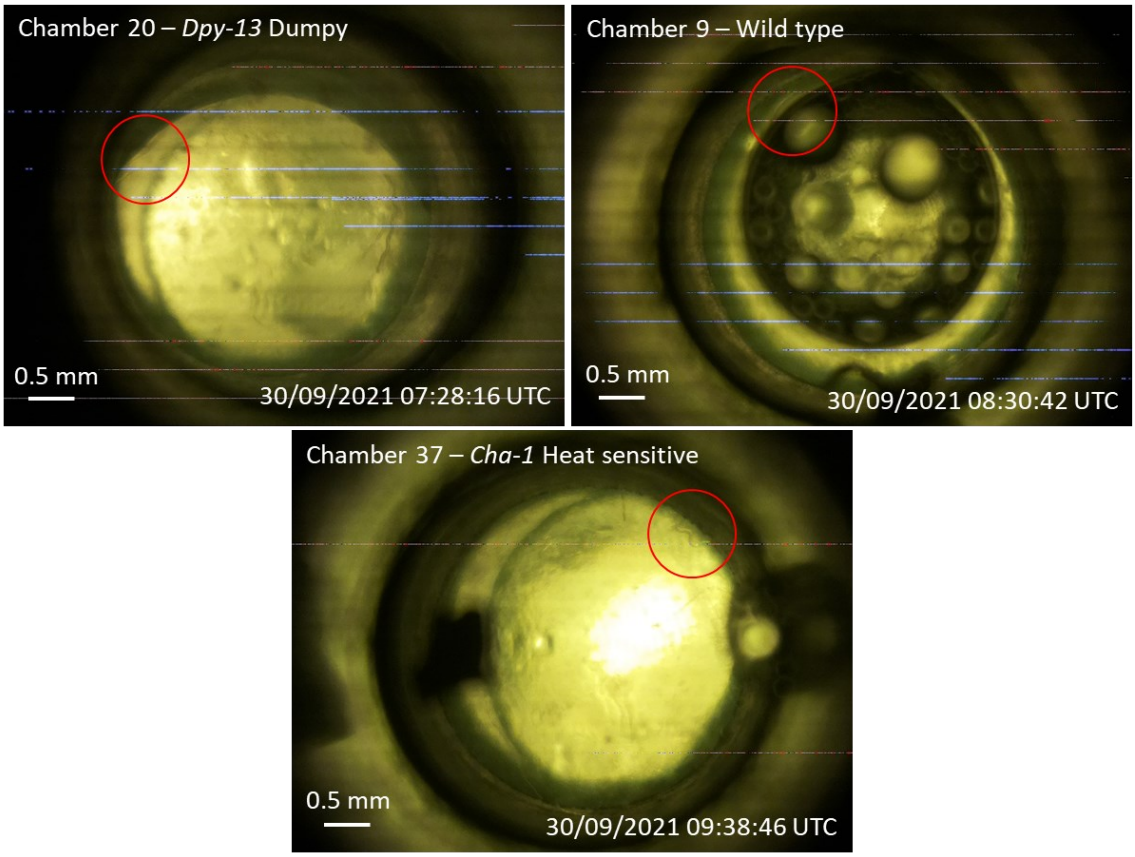

Figure 9-20. Example of three chambers with motile *C. elegans* captured at various stages during the float phase of the flight.

During the post-flight analysis of the flight imagery and video data, five chambers demonstrated motile *C. elegans*. Examples are shown in Figure 9-20, and the chambers with motile *C. elegans* are summarised in Table 9-5. The motile movement was confirmed via video analysis, as shown in Figure 9-19.

The imaging subsystem was set for image capture at 3280x2464 pixels resolution during the flight. The video capture was set to record 30 seconds at 1920x1080p resolution at 30 frames per second.

9.5.3.2 Evidence of fluidic pumping during flight

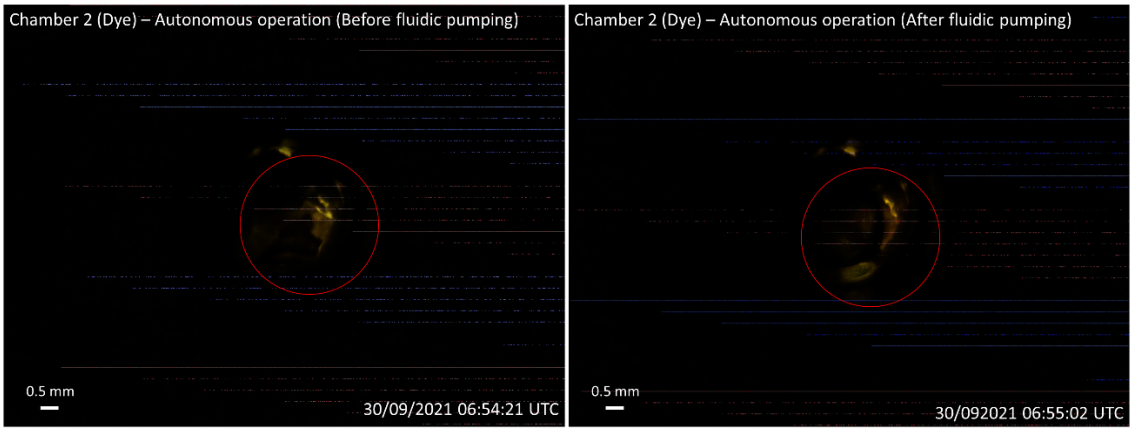

Figure 9-21. Uncropped images of Chamber 2 during the flight before and after fluidic pumping.

As mentioned in section 9.4.2, the chamber with a "dye" was an additional chamber added during the flight campaign. The location of the MCSD sample chambers flown during the flight can be viewed in Figure 9-11. The "dye" is made up of dried down OP50 (*C. elegans'* food source). The name "dye" was selected for reference purposes only. The idea with the "dye" was to have large particulates of OP50 actuated by fluidic pumping to confirm pumping since it was challenging to confirm fluidic actuation with *C. elegans* alone.

Figure 9-21 shows captured images of Chamber 2. The image on the right showed a shape change within the red circle. The change of shape was an image of moving particulates due to fluidic pumping actuation. Unfortunately, the image quality was poor because too many particulates blocked the light illumination from underneath the sample chamber.

9.5.3.3 The issue with high humidity

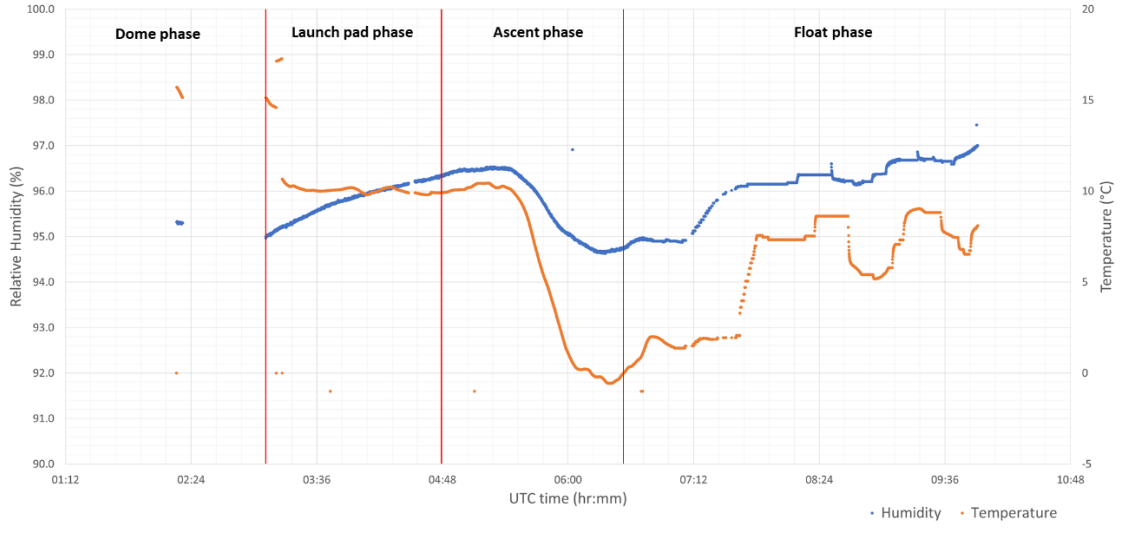

Figure 9-22. The relative humidity and temperature inside the 2U pressure vessel.

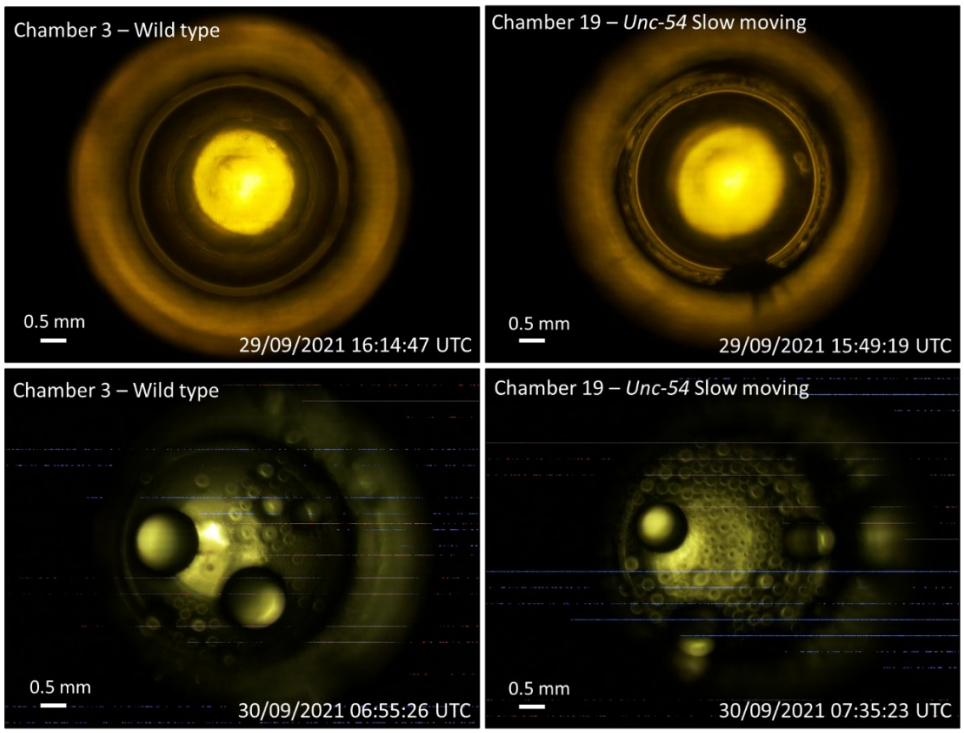

Figure 9-23. Images showing obstruction due to bubbles or water droplets[1].

[1] The images were cropped, resized, and captured from the same chambers taken before and during flight.

It is believed that the high humidity environment could have caused the issue with the imaging subsystem after analysing the flight data. Figure 9-23 shows the poor image quality of the sample chamber captured during the flight. There was a stark contrast between the two images' quality before and during the flight.

During the flight, there were bubbles or water droplets formation. Bubbles could have formed during integration or after the growth media pumping sequence. On the other hand, water droplets could have appeared along the optical line of sight. It could have appeared on the lens, on the top or the underside of the gas-permeable membrane. Previous lab testing showed that water droplets could form on the gas permeable membrane (see Figure 3-21).

Before sealing the 2U pressure vessel, the ambient relative humidity was recorded at 48% before closing the 2U pressure vessel. There is still a mechanism for water vapour to "leak" through the gas-permeable membrane in a leak-proof system. However, the rate and point at which equilibrium is reached are much slower. Previous lab tests performed showed that the sealed MCSD in a high humidity environment had a slower consistent rise and took six days and nine hours to reach 85% relative humidity. See section 3.9.2 for a discussion on the test performed.

The relative humidity remained consistently high once sealed. This was expected due to the leak inside the 2U pressure vessel from the fluidics subsystem; see discussion in section 9.4.2. The fluid was OP50 growth media in liquid form. Figure 9-22 shows the relative humidity inside the 2U pressure vessel maintained between 94.5% to 97% relative humidity from the Dome until the end of the flight. The relative humidity profile followed the temperature profile, where it was higher when it was colder and lower when it was hotter.

The majority of the captured images during flight showed the presence of bubbles or water droplets. The exact type, either bubble or water droplet, has not been fully identified at the time of writing and will require further investigation. Although the poor image quality appeared across the flown 23 chambers, it was still possible to assess the mobility and motility movement of the *C. elegans* during

post-flight image and video analysis. At the time of writing, it was identified via video analysis that chambers 9, 13, 20, 29 and 37 demonstrated motile *C. elegans.*

9.6 Flight campaign discussion, conclusion and lessons learnt

9.6.1 Flight campaign discussion

The flight results showed an insight into the performance of the BoB system during the flight campaign at Esrange space centre. The flight demonstrated motile *C. elegans* during the flight. Unfortunately, the flight video analysis only confirmed 5 out of 23 chambers with motile *C. elegans*.

The motility was confirmed when the videos showed that *C. elegans* was moving using its metabolic activity instead of being influenced by fluidic pumping or the gently rocking of the BEXUS 30 Gondola during the float phase. See Figure 9-19 as an example. In this case, a motile *C. elegans* is considered alive; however, the health status will require future investigation before they can be regarded as alive and healthy. Table 9-5 summarises the chamber position in the MCSD and its respective phenotypes.

Table 9-5. Chamber position of motile *C. elegans* in the MCSD and its respective phenotypes.

MCSD chamber position	***C. elegans* phenotype**
Chamber 9	Wild type
Chamber 13	*Unc-43* Fast moving
Chamber 20	*Dpy-13* Dumpy strain
Chamber 29	Wild type
Chamber 37	*Cha-1* heat-sensitive strain

Presently, the video analysis showed that the *C. elegans* in the other 18 chambers showed no sign of motility. Without clear imagery, it can be assumed that *C. elegans* did not survive pre-flight and flight operations. It can also be assumed that the *C. elegans* survived. Still, it was impossible to image them because bubbles and water droplets badly obstructed the optics to image any motile *C. elegans* during flight. In some videos, it was possible to image non-

motile *C. elegans* being mobile from the gentle rocking of the Gondola during flight.

Three possible justifications were considered on what could have caused the flight result.

- The first justification was that the C. elegans were experiencing high temperatures within the upper range of their viability, especially during pre-flight (see Figure 9-24).
- The second justification was that the *C. elegans* leaked out due to poor MCSD sealing during *C. elegans* integration (see Figure 9-10).
- Thirdly, the liquid leaking led to high humidity inside the 2U pressure vessel. Once the internal atmosphere rapidly cooled down, water vapour condensed and formed water droplets along the optical line of sight of the imaging subsystem, obstructing the image (see Figure 9-23).

9.6.1.1 Discussion on temperature variation and *C. elegans* survivability

The first justification was concluded by analysing the temperature data. The data highlighted that the *C. elegans* were experiencing temperature within the upper limit once the BoB system was sealed during FCT and in the Dome before the flight, see Figure 9-24.

During pre-flight operation, the BoB mission was designed with the C. elegans at low metabolic rate temperature (+12°C ± 2 °C). During the flight, the temperature will increase to +20°C ± 2 °C during flight for nominal temperature and metabolic activity. See section 9.2 and requirement DG-10 200 in appendix A.5 for more detail on the design requirements.

The requirement was designed to lower the metabolic rate of *C. elegans* during pre-flight to extend its lifecycle. This was designed to accommodate up to 96-hour pre-flight handover or launch delay. Once the launch sequence is confirmed, the temperature would have been increased to a nominal temperature of 20°C ± 2°C for the nominal *C. elegans* metabolic rate during flight.

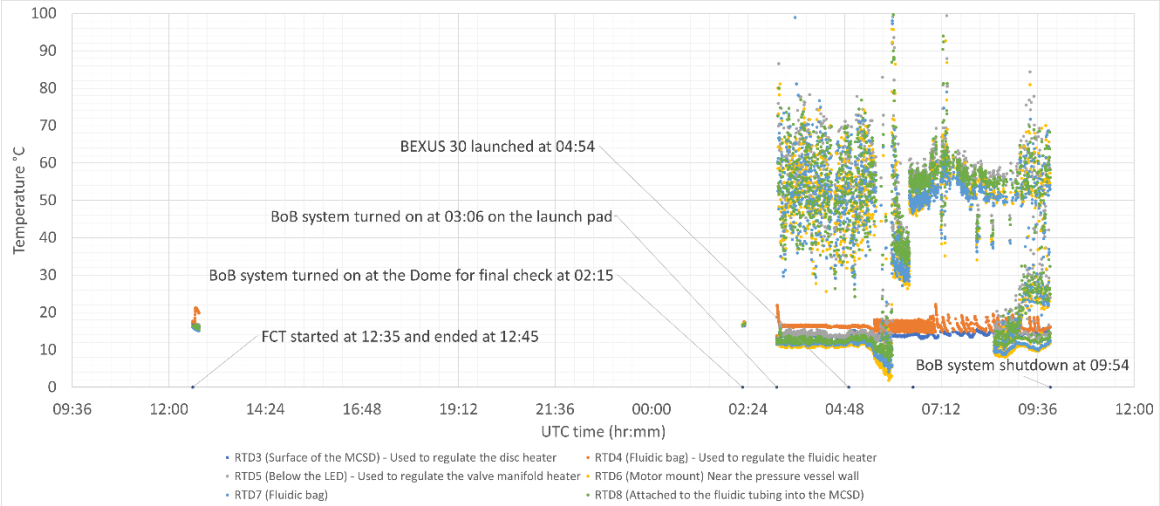

Figure 9-24. The temperature profile of the six RTDs inside the 2U pressure vessel across to flight campaign events during FTC (29/09/2021) and flight (30/09/2021)

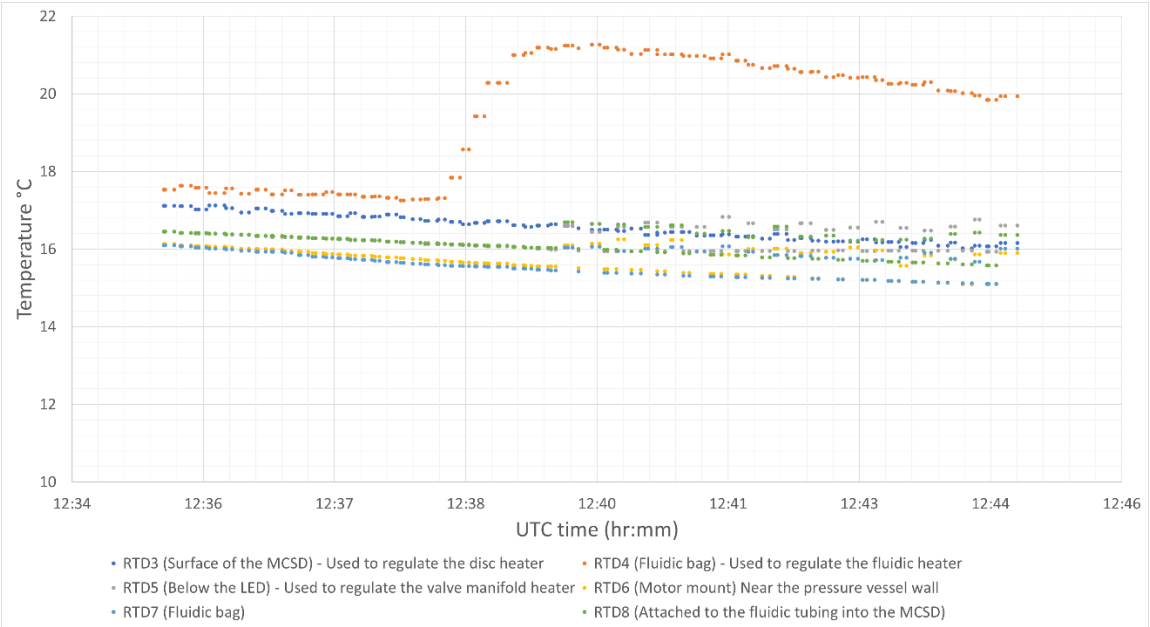

Figure 9-25. The temperature profile of the six RTDs inside the 2U pressure vessel during FCT[1].

The critical sensor data was the temperature reading of RTD3. RTD3 was located on the surface of the MCSD to control the MCSD heater underneath (see Figure 9-17 for the location of the sensor). Ideally, RTD 3 would have been located inside

[1] RTD3 is the temperature sensor closest to the *C. elegans* located on the surface of the MCSD.

the sample chambers as this reading will provide the actual temperature reading of the *C. elegans*. However, due to the heritage design of the MCSD, it was not feasible to redesign the MCSD with the sensor inside the chamber within the BoB mission timeline. It meant that the temperature of *C. elegans* had to be extrapolated from RTD3. Based on the previous testing, the *C. elegans* inside the chamber could be between 6°C – 7°C higher than the surface temperature (Bolliand, 2020).

Figure 9-24 showed that the *C. elegans* were experiencing temperatures between 22°C – 24°C during FCT and at the Dome before pick-up. This was within the upper limit of the *C. elegans* thermal requirements. In the worst scenario, the *C. elegans* temperature could have risen to 24°C, higher than the upper limit of the *C. elegans* thermal requirement at 22°C.

Looking at the FCT event, the final integration of the BoB system with the *C. elegans* was completed on 29/09/2021 at 07:55 UTC and later mounted on the Gondola. For FCT, the BoB system was brought to the launch pad on 29/09/2021 at 12:35 UTC (see Figure 9-24). After FCT, it was brought back to the Dome and later dismounted from the Gondola into the incubator at 13:21 UTC. The incubator maintains the *C. elegans* at 12°C. This total time between sealing the pressure vessel and placed inside the incubator was approximately six hours of exposure to non-nominal pre-flight temperature (+12°C ± 2 °C).

It is worth pointing out that some temperature data were missing at the time of writing. These were data when the BoB system (turned off) was mounted on the Gondola in the Dome waiting for FCT between 29/09/2021 at 07:55 UTC and after FCT in the evening during feeding (see Figure 9-24). It may be possible to extract missing data from granular data logs for future analysis. Because of the missing temperature data and no sensor inside the MCSD sample chamber, it is difficult to have an overall picture of the actual *C. elegans'* temperature. The final check was performed on 30/09/2021 at 02:15 UTC in the Dome before being picked up for transfer to the launchpad.

During the flight, the *C. elegans* were experiencing temperatures between 18°C to 23°C. Speculation could be made if the high temperature during pre-flight meant that some C. elegans could have entered the dauer larva state, minimising its movement or becoming deceased. The higher temperature could have also sped up the *C. elegans* lifecycle. At 22°C, it could take approximately 10 hours for the L4 stage to reach an Adult stage and 18 hours to reach the Adult stage capable of laying eggs (Altun & Hall, 2009). If that was the case, the *C. elegans* could have reached the Adult stage with eggs during flight or after the BEXUS 30 gondola landed, surviving the total flight.

During post-flight analysis, some *C. elegans* progeny was found in one of the fluidic channels indicating that could be the case (see Figure 9-26). The image was taken approximately 79 hours after the BoB system was sealed before the FCT. For the *C. elegans* to lay and hatch the eggs, the *C. elegans* would have survived and reached the Adult stage during flight or when the BEXUS 30 Gondola landed. The *C. elegans* was integrated into the MCSD at the L4 stage.

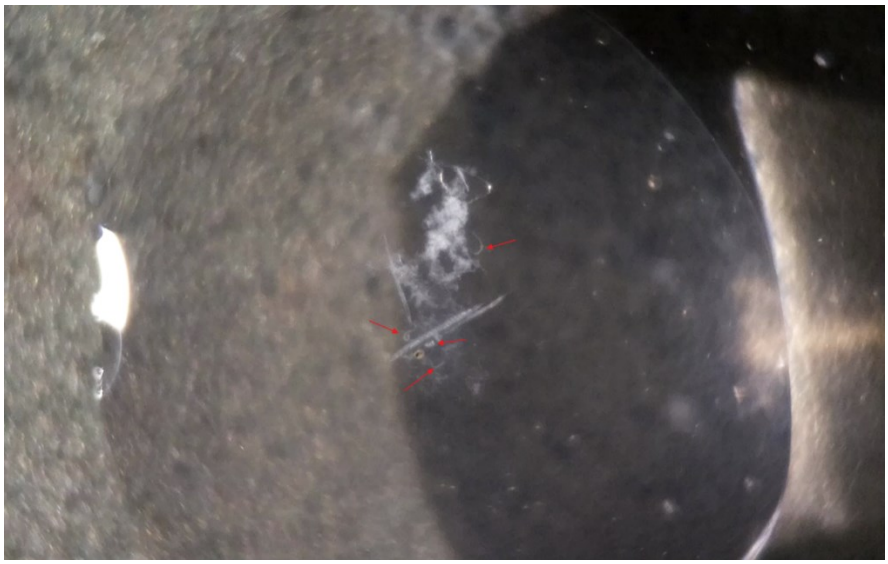

Figure 9-26. *C. elegans* progeny was found in one of the fluidic channels along Chamber 6 extracted, and placed on a petri dish[1].

[1] The image was taken around 02/10/2021 at 15:00 UTC via a custom test bench optical stand using Raspberry Pi camera V2.1 with an original lens.

Another observation from the flight result was the non-nominal sensor's behaviour started when the BoB system was turned on at the launchpad. Figure 9-24 shows the non-nominal temperature readings of the four RTDs (RTD5, RTD6, RTD7 and RTD8). The temperature was unusually noisy when the BoB system was turned on at 03:06 UTC, and some of the temperature readings were between 30°C to 80°C. The noisy temperature reading would have affected the active thermal control of *C. elegans*. The noisy reading became worse at 06:00 UTC, where the readings were beyond the expected range of 0°C to 20°C.

The noise meant that the RTD or the ADC could have been damaged. It could be many reasons that cause the damage. Some of the reasons could be damaged PCB or ADC from condensation, or the PCB could have suffered mechanical damages during handling. Further investigation will be required to understand the cause and effect fully.

9.6.1.2 Discussion on leaking inside the 2nd gen. BAMMSat bioCubeSat payload and its impact on the BoB system

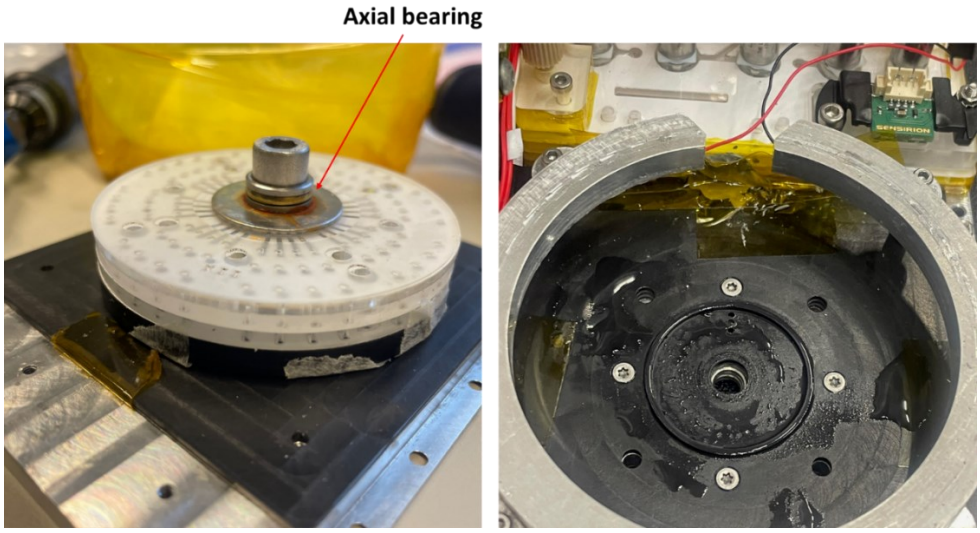

Figure 9-27. Images of post-flight analysis of the Rotary Valve demonstrating damage from leaking[1].

[1] (Left) Image of the spare rotary valve (RV) assembled on a test bench at the flight campaign for an investigation. (Right) The image of the RV being disassembled confirmed the leaking around the area during post-flight analysis.

The second and third justification of the flight result was due to leaking. Leaking was a persistent problem during the technological development and during the flight campaign. During the MCSD and *C. elegans* integration, there were apparent leaks around the MCSD; see section 9.4.2 for the complete discussion. During the integration of MCSD to the rest of the system, further leaks were observed, and this leak would have encountered the axial bearing of the rotary valve (RV), see Figure 9-27.

The contact with high salt concentrated OP50 growth media solution caused corrosion on the bearing. The corrosion loosened the sealing of the rotary valve, and when growth media was pumped, the growth media would leak and propagate around the side of the RV instead of going into the MCSD. Not able to pump growth media into the sample chamber meant that feeding was impossible. It can be speculated that due to the leak, the sample chamber could have dried, or *C. elegans* could have starved, entering the dauer larva state, minimising its movement or becoming deceased.

Leakage from the fluidic subsystem had a knock-on effect on the overall mission. It was believed that the high relative humidity inside the 2U pressure vessel, i.e., high water vapour content combined with the sudden decrease in temperature during the ascent phase, caused condensation. In principle, the sudden temperature drop would reduce the maximum water vapour that can be held in the water-saturated air inside the 2U pressure vessel. The water vapour was then condensed into water droplets inside the 2U pressure vessel as the temperature dropped.

The water droplet could be the reason behind the non-nominal sensor readings, as water droplets could have formed on the PCBs and affected the electrical circuit. The water droplet could have also appeared in the optics' line of sight, affecting the captured images. The bubble or water droplet obstruction only occurred during the flight float phase. It did not appear on the ground before the flight (see section 9.5.3.3 for discussion on the high humidity environment).

9.6.2 Flight campaign conclusion

In summary, the flight of BAMMsat-on-BEXUS onboard BEXUS 30 was challenging yet insightful. The BoB mission did not come without its challenges. There was the impact of the COVID-19 pandemic, the complexity of the systems, handling and integrating *C. elegans*, the burnt down biological laboratory at Esrange, and the challenges during the flight campaign.

Nonetheless, every team member responsible for every work package delivered a working subsystem into a version of the BAMMsat-on-BEXUS system, which flew into the stratosphere (see section 9.3.1 for the summary of work packages). It was the first complete prototype of BAMMsat, bringing it closer to spaceflight. Overall, the mission delivered its overarching aim - "*to learn from the technological development and operation in a real-world application in preparation for future spaceflight"*.

It is worth reviewing the set objectives in section 7.2 of this document to evaluate the mission's success.

1) *Develop and demonstrate the ability to handle, integrate and operate BAMMsat in a spaceflight representative context*
   a) Demonstrate the ability to extract data using *C. elegans* as a biological payload on a bioCubeSat and as a hosted payload on a larger spacecraft such as ISS and Bion satellite.
   b) Develop and implement protocols to handle and integrate *C. elegans* into the mission and flight operations of a BAMMsat-on-BEXUS mission.
   c) Develop and implement appropriate pre-flight, flight and post-flight operations compatible with the BEXUS stratospheric balloon flight mission.

The BoB mission did develop and demonstrate the minimum ability to handle, integrate, and operate BAMMsat in a spaceflight representative context. Further development in technology and operation will be required to meet this objective fully. In essence, flight and post-flight operations were adequate for this mission. The pre-flight operation had setbacks primarily due to biological laboratory and

equipment loss, which impacted the sterilisation procedure. The protocol for integrating *C. elegans* into MCSD and the rest of the system took longer than expected. This was because of the complexity of the design and assembly procedure. This design and assembly processes need to be simplified for the next generation.

Further development is required, especially in extracting data from biological payloads. The imaging subsystem was only able to capture 5 out of 23 chambers. Fundamentally, the system was not ready for flight due to a lack of testing with *C. elegans* in the laboratory. Plus, the imaging subsystem needs design improvement to be compatible with the high humidity environment.

2) *Demonstrate the key BAMMsat's ability to provide a controlled environment relevant to maintaining viable biological samples in extreme operational environments (specifically thermal and fluidic control together with appropriate housekeeping sensing).*
   a) Demonstrate fluidics functionality.
   b) Demonstrate internal thermal control within the 2U pressure vessel. During pre-flight, C. elegans shall be at a low metabolic rate temperature (i.e., 12°C ± 2 °C) and during flight operation, the C. elegans shall be at 20°C ± 2 °C.
   c) Demonstrate housekeeping sensor functionalities– i.e., for internal pressure vessel environmental control and fluidic operations.
   d) Demonstrate the ability to maintain *C. elegans* in a viable state during flight.
   e) Demonstrate a system with autonomous flight operations.

The BoB system demonstrated the minimal essential BAMMsat's ability to maintain biological samples in a controlled environment. The fluidic subsystem was able to pump growth media into the sample chambers. However, there were issues with leaking across the whole subsystem because of the design, material, and manufacturing choices. Housekeeping sensors for fluidics, such as pressure

sensor, was removed due to large mechanical volume, and the flow sensor was damaged during flight, possibly from liquid damage.

Thermally, the active and passive thermal design and control were able to control the temperature within a set range. However, during pre-flight, the operation overlooked the launch provider's operation, which involved waiting and exposure to higher external thermal environments for a long time. It was also challenging to extrapolate the viability of the *C. elegans* without knowing the actual temperature of the *C. elegans* and poor imaging data. Nonetheless, the BoB system performed the autonomous flight operation with no apparent issue.

3) *Complete the development of a spaceflight relevant model version of BAMMsat suitable for the flight on BEXUS*
   a) Repackaging and reconfiguring the existing laboratory breadboard into a 2U CubeSat payload format.
   b) Reconfigure the existing BAMMsat laboratory breadboard to be compatible with an operation inside the 2U environmentally controlled pressure vessel

Objective three can be considered met. The BAMMsat bioCubeSat payload was repackaged into a 2U format inside a 2U pressure vessel, albeit with complex assembly procedures and sub-optimal wire and fluidic harnessing. The atmospheric pressure was confirmed to be contained for the flight duration.

In conclusion, the BAMMsat-on-BEXUS mission was partially successful. The flight system had reduced functionalities, and the sub-systems did not perform to the required standard to successfully meet the mission objectives. Nonetheless, many technological and operational lessons were learnt that are vital for the next generation. These lessons could not be easily replicated in the laboratory environment, putting BAMMsat in a better position for future spaceflight opportunities.

9.6.3 Future work and lessons learnt

Immediate future work would include further analysis to test the hypotheses on the issues during the flight.

- Assess the health status of the *C. elegans* that demonstrated motility in the captured images and videos, and extract missing temperature data after FCT and Flight
    - The lesson learnt after the flight was that the biological mission started once the biology arrived at the launch site. It is vital to have a data management plan during pre-flight to record the necessary information to assess the viability of biology. During the post-flight analysis, the lack of data during the pre-flight operation made it challenging to evaluate the result. It is also essential to work closely with the launch provider to consider the timing for all the pre-flight testing and its associated external environment.
- Test the impact of the high humidity on the imaging subsystem and the MCSD to understand the effect of condensation.
    - One of the flight conclusions was that the high humidity had caused condensation across the system. The lesson learnt here was that for a system with liquids in an extreme environment, it is worth testing the impact of humidity on the system.

Long term future work would include tasks required to prepare BAMMsat for spaceflight.

- Redesign the packaging and mechanical assembly of the 2U BAMMsat bioCubeSat payload.
    - The 2U BAMMsat bioCubeSat payload flew on BEXUS 30 was the first complete prototype. The design philosophy was to keep the mechanical structure at a minimum and accessible if any modification was required. Unfortunately, the build was not optimised, and there were issues with electrical and fluidics harnessing. The lessons learnt from the harnessing experience

must be feedback in the following design, and the strategy should be to minimise tubing or wires. It is highly suggested that the different subsystems be modular, for instance, the PCBs and fluidic, to have their enclosure with a simple interface. The modularity will help with any issue and allow easy decoupling without affecting the rest of the system. The MCSD should be the last point of assembly to easily swap the disc and visual inspection of the biological specimen without being obstructed by the rest of the system.

- Address the leaking issues across the fluidic subsystem.
    - Leaking has been persistent throughout the development and the flight campaign. The issue came due to the design of the MCSD, which has too many layers. Similarly, the selector valve manifold also had many layers. Each layer is a point of failure where the leak can occur. The assembly of the MCSD was too complex, and each layer required a rigorous visible inspection for fluidic channel alignment. For the next generation, the MCSD needs to be remanufactured into a monolithic structure by exploring manufacturing techniques such as 3D printing and other microfluidics manufacturing techniques.
- Address the thermal design limitation of the current system.
    - One of the main challenges during the flight was not having enough information to assess the viability of the biological specimen. It is worth exploring the modification required for the MCSD to include the sensor close to the sample chamber in the next generation. It is also worth performing a full thermal simulation to understand heat distribution across the system, which is helpful when losing temperature sensors. Also, thorough testing and calibration of the system to establish a better relationship between the temperature inside a chamber and the closest temperature sensor will be beneficial.

- Test the imaging subsystem with rigorous optical testing standards with the biological specimen.
    - One of the significant changes in the design was the changes to the optical system during the flight campaign because the optical lens could not resolve and image *C. elegans* with enough contrast. The issue could have been determined by testing the biological specimen with its media and understanding its optical parameters in more detail.
- To perform a simulated pre-flight integration assembly before the flight campaign.
    - It is worth performing a simulated pre-flight integration assembly before the flight campaign for any future generation. This will help gauge the actual operation timeline since biological handling has many intricate nuances.
- Devise a test on the fluidic subsystem with a minimal leak to understand the volumetric flow rate across the fluidic subsystem.
    - Due to time limitations, a rigorous fluidic volumetric test in the full fluidic subsystem was not performed for this mission. The growth media stopped pumping into the sample chamber during the autonomous flight operation. Although it is most likely due to a leak, it was hard to gauge the volume of used media.
- Test the impact of bubbles in the chamber.
    - The trapped air inside the fluidic channels was pushed into the sample chamber during pumping, causing bubbles and obstructing the image. The efficacy of the system dealing with bubbles was never thoroughly tested. Bubble formation could be reduced by priming the fluidic channels with media and careful assembly to avoid trapped air.

- Integrate and test the track-etched membrane filter inside the MCSD with the fluidic subsystem.
    - Although planned, the filter was never thoroughly tested due to time limitations.
- Test the pressure vessel's long-term stability
    - To assess the pressure vessel's sealing integrity against various temperature cycles and radiation exposure.

10 Final discussion, future work, and conclusion

10.1 Final discussion

The motivation behind the PhD research was to advance the BAMMsat concept that has been in development within Cranfield University since 2012. The current research developed the 1st gen. laboratory breadboard into a version that flew onboard a stratospheric balloon platform as a technology demonstration under the BAMMsat-on-BEXUS (BoB) mission. As mentioned throughout the thesis, the author was responsible for developing the central aspects of the 2nd gen. BAMMsat bioCubeSat payload and other students were involved in the BoB mission, which developed the technologies required for the BoB system and some of the more peripheral aspects of the 2nd gen. BAMMsat bioCubeSat payload.

The 2nd gen. BAMMsat bioCubeSat payload embodied the core of the BAMMsat concept and was the focal point of the PhD research. The 2nd gen. BAMMsat bioCubeSat payload was built upon the underlying features of BAMMsat, which are to (i) house multiple samples, (ii) maintain samples in an appropriate local environment, (iii) perturb samples fluidically, and (iv) monitor samples. Combining these features with the CubeSat design philosophy and standardisation, the BAMMsat concept can produce an autonomous, miniaturised, scientific laboratory that can improve space research access.

These core functionalities, design process, and development process will be discussed in the final discussion here to evaluate the PhD research output. In essence, the PhD research attempted to advance the BAMMsat concept by developing the 1st gen. laboratory breadboard into a 2nd gen. technology demonstration hardware and bridging the gap towards a 3rd gen. spaceflight mission, currently planned to be on board the ISS.

The final discussion of the thesis will be discussed within the context of the PhD objectives to evaluate the research outputs against the set objectives. Before delving into the discussion, the author refers to the “bioCubeSat” terminology.

The author defines this as a CubeSat with a biological payload of experiments onboard the CubeSat. Note that a widely accepted terminology could not be established during the literature review. Each of the PhD objectives will be discussed individually for the remainder of this section.

"To summarise the state-of-the-art in the literature to inform the BAMMsat payload design for Bioscience, Astrobiology, Medicine and Material science experiment in space environments and extreme Earth environments."

The first objective is a standard workflow of a PhD research. The aim was to establish a baseline within the research field and determine the current state of the art in the community. The literature survey identified that the concept of bioCubeSat was introduced as early as 2002 (30 years ago) under the BioNano Satellite-1 concept (B. Twiggs & Kuroki, 2002). It highlighted that the progress within the bioCubeSat was progressing at a relatively slow rate despite being introduced during the early years of the CubeSat concept. NASA Ames has led the development with up to five bioCubeSat launched. Towards the fifth launch of NASA Ames (2017), a private company, SpacePharma, launched its bioCubeSat (2017).

Despite the promise of a lower cost of entry, bioCubeSats were still progressing at a slow rate. This is especially true in comparison with earth observation CubeSats, which are now being commercialised at scale with companies such as Spire Global and Planet Lab. The literature review did not identify any publication which explains the slow adoption of bioCubeSat. However, it can be speculated that the challenge is finding the value and application within life science and CubeSat that can support growth and research interest sustainably. More importantly, adding a biological system adds complexity through the logistic chain from the laboratory to launch, which added a hurdle for the concept to be adopted widely.

The concept is now starting to mature, with many universities developing their bioCubeSat concepts (D. J. Robson & Cappelletti, 2022). Similarly, the case for commercialising microgravity for life science is also increasing; see section 1.1. The literature survey highlighted the need to validate space-based models for terrestrial applications (Sharma et al., 2021). Perhaps this is where bioCubeSats

could be an asset and can grow as a concept and research area, leveraging its ability to be a high-throughput, autonomous, miniaturised research platform.

The key message from the literature review showed that the BAMMsat is still relevant and timely, especially with the ability to perform in-situ data measurement and sensory capabilities such as chemical sensors, fluorescent microscopes, and visible spectrometers. BAMMsat also has the potential as a high throughput platform with the rotary valves concept, which increases the density of the sample and sample chambers. Hence, increased experiments without the negative impact of increasing mass and volume.

In summary, the PhD research output met the set objectives. Chapter 2 summarised the current state of the art, and some of the design choices from the NASA Ames were being implemented in the 2nd gen. BAMMsat bioCubeSat payload design. For example, the track-etched membrane filter. The research output showed that bioCubeSat is a promising research field with growing interest within the community.

"To rectify design issues, re-design, manufacture and test the BAMMsat Multi-chamber Sample Disc (MCSD) and Rotary Valve (RV) for the 2nd gen. BAMMsat bioCubeSat payload."

The second objective was included to further the development of MCSD and the RV concept development. The design of the two components is coupled with one another. The two key design propositions enable BAMMsat to investigate a wider variety of samples and a higher number of experiments in the same 2U form factor than other bioCubeSats. Combining the two, each sample chamber can be individually addressed by intermittently rotating the chamber to access fluidic ports and sensors independently, e.g., microscope or visible spectrometer. The MCSD and RV allow several sample chambers to be designed compactly without the additional valving and wiring. In a conventional fluidic design, each chamber will require its own sensor, valves, and wiring.

The PhD research had advanced this concept from the 1st gen. developed partially from NASA design heritage into a 2nd gen. design that accommodates the payload AIV. The research outputs have been extensively discussed in Chapter 3. As a brief reminder, the design of the 1st gen. was based on laser-cut polymer bonded by interlayers of pressure-sensitive adhesive. The design is a common microfluidic construction technique and has spaceflight heritage used by NASA and SpacePharma. The 2nd gen. has the design features of the 1st gen. with the added functionality of being able to repeatably access the sample chambers with a mechanically assembled design instead of permanently bonded adhesive. The key advantage of the 2nd gen. is to overcome the limitation of sample exchange and retrieval during pre-flight and post-flight.

The PhD research began with solving a heritage design issue from the 1st gen. RV. As a reminder, the RV had a problem with the PTFE material, where it experienced cold creep under compression. Over time, the creeping caused liquid to leak between the two rotating surfaces. This design issue was rectified in the 2nd gen. using an alternative PEEK material. During the lab testing, the RV

with PEEK was functional. However, the RV did fail during the BoB flight due to bearing failure caused by leaking at the MCSD.

One of the design limitations of the mechanically assembled 2nd gen. MCSD was the potential of leaking between the layers as the bolt loosened during handling. The 2nd gen. had multiple layers of polymers, elastomers, and membranes arranged in a specific sequence, enabling the mechanically assembled features. These layers are then bolted together to create a 3D structure with a hollow fluidic channel between the layers. The issue with such a design was the complex assembly and verification process. Each layer had to be aligned to ensure correct compression along the fluidic channel to provide the seal. This can be complex and difficult to assemble, especially for a new user to start using the components., It increases the chances of mistakes during AIV, as evident during the BoB flight campaign when layers were not assembled correctly and caused leakage from the sample chamber. The high saline growth media leakage from the MCSD flowed towards the bearing and corroded the bearing, inhibiting free rotation at the RV and causing the RV to fail.

One of the key findings was the design limitation based on laser-cut polymer and adhesive bonding during the research. During the PhD research, a common issue at the laboratory and during the BoB flight campaign was that the adhesive blocked the fluidic channel. Similarly, the polymer (acrylic) also has a tendency to crack. The issue is specific to BAMMsat due to the dynamic loading of the rotary valve and fastening of the fluidic connectors. The issue highlighted that such a design is not suited for dynamic loading. Reviewing the NASA designed fluidic card, there isn't obvious evidence that the design is experiencing regular dynamic loading. For this reason, the design had a lower risk of damage compared to BAMMSat.

For the 3rd gen. MCSD and RV, it is suggested that the designer explore alternative microfluidic fabrication techniques such as PDMS etching (Gorissen et al., 2016) or diffusion bonding (Gorissen et al., 2016). A growing field of 3D printed microfluidics has an added advantage, such as rapid prototyping of

complex fluidic geometry or shorter lead time than PDMS etching or diffusion bonding techniques. An overview of various 3D printed microfluidics techniques has been published in the literature (Prabhakar et al., 2021). The techniques could produce a reduction from 20 layers to a much smaller number of “layers” – some of which may be 3D-printed monoliths. Having fewer layers means fewer failure points for leaking. The design options mentioned here are also valid for the iteration of the selector valve manifold.

Another issue worth highlighting is the issue with the current bolting strategy for the MCSD layers. Presently, it is being designed to be bolted at 0.1 Nm torque. The low-clamping toque was sensitive to handling and was the primary culprit of the MCSD leaking during the flight campaign. This design limitation will not survive the vibration from a rocket launch and will need to be addressed in the 3rd gen. The limitation can be overcome by using a thread locking compound as an immediate solution.

Lastly, the track-etched membrane filter was never fully integrated into the MCSD design, and this will be an essential design feature for spaceflight.

In summary, the PhD research output did re-design and manufacture a new concept of mechanically assembled MCSD and RV as highlighted in the 2nd gen. design. The design was able to perform at some-level fluidic actuation and incubation of biological systems as demonstrated in the laboratory and the BoB mission. However, the 2nd gen design did not completely rectify the issue with leaking, and the 3rd gen. might require exploration of new manufacturing techniques such as state-of-the-art 3D printing.

"To design, manufacture, and test a compact brightfield microscope for the 2nd gen. BAMMsat bioCubeSat payload."

The third objective was introduced specifically for the BoB mission. It was to develop a compact brightfield microscope to record imagery of the *C. elegans'* behaviour and health during the BoB mission. In the early design phase, it was believed that a compact brightfield microscope could provide enough information to record the movement of *C. elegans.* Therefore, the fluorescent capability was not required from the 1st gen.; hence the development was sidelined for the BoB mission. The 1st gen. would have also required larger financial and human resources beyond the scope of the BoB mission.

However, fluorescent imaging will be key for the growth of life science research in microgravity. Fluorescent imaging is a widely used technique in life science on Earth, and it is reasonable to expect a similar technique is required for space research. The 3rd gen. development should explore opportunities further to develop the 2U fluorescent microscope into a functional system.

During the PhD research, a design of a compact brightfield microscope was manufactured and completed. The final design was promising and could capture detailed images *of C. elegans*, revealing its inner anatomical structure. Considering *C. elegans* is a relatively transparent and low contrast biological sample, capturing such image quality with a brightfield microscopy technique was rather promising. Note that the image was captured on a thin microscope slide with dried *C. elegans* (immobile) using an optimum setting in the laboratory. In the final flight configuration, there are many uncontrollable variables.

One key lesson learnt in the optical design is the humidity environment within the system. With a combination of a high humidity environment and large temperature fluctuation, water could condense and appear along the optical line of sight, blocking the images of the biological sample. For a bioCubeSat system with relatively high liquid content, the humidity in the system will increase over time. For this reason, a humidity test in the full system with the optics is recommended for 3rd gen. development.

The design had some limitations, especially in the full system with the *C. elegans*. In the full system flight configuration, it was not possible to image *C. elegans.* Further testing will be required to understand the optical limitation; to provide some examples, it could be due to and not limited to growth media changing the refractive index, the position of the *C. elegans,* the thickness of *C. elegans,* and variation in the thickness of the MCSD layers. Note that the compact brightfield microscope has a short depth of field of <1 mm. One solution to mitigate this design issue is an adjustable motorised lens to change the focus quickly.

The key reason that this issue was not picked up was the lack of testing with *C. elegans*. Primarily, this was due to limited access to *C. elegans.* The BoB mission was enabled by Cranfield University and the University of Exeter, and the University of Exeter provided the biological resources and expertise. The COVID-19 pandemic meant that a full system with the *C. elegans* was only conducted once just prior to the BoB flight campaign. After the test, there was not enough time to evaluate and perform design iteration.

Nonetheless, the optical system design is still functional and could be used for cell culture application with a narrow depth of field or analysis using a stained biological system. Alternatively, a modified variant with a dark-field microscopy design could also be an alternative solution since dark-field imaging is preferable for low contrast samples such as *C. elegans*.

It is recommended to implement further rigorous standardised optical testing. It was very challenging for the author to perform comparison and design optimisation during the development without performing the test.

In summary, the PhD research output met the set objective: to design, manufacture, and test a compact brightfield microscope for the 2nd gen. BAMMsat bioCubeSat payload. However, the design had some limitations, especially in the full system with the *C. elegans,* which will require further evaluation.

"To repackage, design, manufacture, and test the sensors, fluidics, and associate mechanical supports for the 2nd gen. BAMMsat bioCubeSat payload."

The fourth objective was also proposed explicitly for the BoB mission. The objective was introduced to research and develop the fluidic subsystems, Geneva gear mechanisms, and mechanical housing. The evaluation of the PhD research output will be performed in sequence, starting from the 2nd fluidic subsystem, 2nd gen and with the Geneva gear mechanism and finishing with the 2nd gen. mechanical housing.

One of the PhD research outputs was the 2nd gen. fluidic subsystem. The fluidic subsystem enables one of the core features of BAMMsat, which was to perturb the sample fluidically. With fluidics, BAMMsat can transfer growth media within its system to maintain the biology's viability and transfer reagents to perform an experiment in flight. Without fluidics, it limits what BAMMsat can achieve as an autonomous miniaturised laboratory. During the PhD research, the work performed repackaged the fluidic sensors and actuator into a 2U form factor.

An important criticism of the design of the 2nd gen. BAMMsat bioCubeSat payload was the shortcoming of the fluidic subsystem. The fluidic subsystem was never thoroughly tested, and most of the testing was performed rapidly to meet the BoB mission timeline. The PhD research also failed to perform end-to-end fluidic subsystem tests to characterise the fluidic performance.

The primary reason that inhibited the testing was the leaking issue with the MCSD. The MCSD required many development efforts in the testing, manufacturing, and design iteration to address the leaking before a functional MCSD was available. Without a leakproof MCSD, it was challenging to characterise the end-to-end fluidic performance of the subsystem. By the time there was a functional MCSD, the was no time left to perform the end-to-end testing due to the BoB mission timeline.

The unpredictability of the flow sensor also inhibited the ability to characterise the fluidic performance. In essence, there is not enough information being recorded during the PhD research for a robust fluidic subsystem. Some of the key tests that would have been useful were fluidic dispersion / mixing inside the MCSD sample chamber and measuring various pressure and flow at different points of the fluidic subsystem.

The development of the 3rd gen. BAMMsat bioCubeSat payload should increase effort in developing microfluidic capabilities. This is especially true for the MCSD, RV, and selector valves manifold. Understanding the fluidic performance is vital to ensure that the fluidic subsystem functions in microgravity. Without gravity-driven convection, the liquid-liquid mixing is driven by diffusion during spaceflight. Without performing the end-to-end fluidic testing, it is difficult to predict the performance of the BAMMsat fluidic subsystem. The author recommends that the next BAMMsat development be tested on Earth-bound microgravity facilities such as parabolic flight. Some suggestions for the development are the ability to conduct precision delivery of reagents and handle bubble formation.

The second PhD research output for this objective was the 2nd gen. Geneva gear mechanism. The Geneva gear provided the intermittent rotary motion that the rotary valve required to be functional. The Geneva gear intermittent and locking / indexing rotary motion is inherently built into its mechanical design from its gear tooth profile. The Geneva gear mechanism was one of the subsystems that functioned with the least issue. There is a slight backlash that will require further investigation, and there was an issue with rotation during the flight as the bearing failed due to corrosion. However, the root cause was the fluidic leaking.

The 3rd gen. design will have to optimise the Geneva drive electric motor. As discussed in section 6.10.1, the motor was oversized with a large margin during the design phase to mitigate the unknown risk associated with the design. During the optimisation, the designer should consider the type of encoder. The 2nd gen. has an optical incremental encoder that interfaced with the proprietary motor drive. Information such as velocity or motor position was not provided. An

additional photosensor was included, which recorded the number of passes of the MCSD gear teeth through the photosensor. By doing so, the position of the MCSD can be determined. For a short duration BoB mission, it was deemed adequate. With limited human intervention during spaceflight, the designer will need to perform an in-depth trade-off on the encoder / determination of motor position / determination of MCSD positions as part of the motor optimisation for a spaceflight version.

For this objective, the third PhD research output was the 2nd gen. mechanical housing. In general, the mechanical housing was adequate for the BoB mission. However, for a spaceflight version, a significant re-design will be required on the entirety of the mechanical structure to optimise the location, housing, and mechanical load path. It is recommended that FEM is performed to minimise load toward the multi-chamber sample disc, the PCBs and the optical system. This is to minimise stress on the MCSD and RV, the PCBs and the optical system.

In summary, the PhD research output did meet the objectives, but it is not the ideal solution. Significant development will be required for the 3rd gen. fluidic subsystem, while the Geneva gear mechanism and the mechanical housing will require design optimisation.

"To perform systems integration and testing of the 2nd gen. BAMMsat bioCubeSat payload in preparation for the BEXUS flight."

The fifth objective brought together the PhD research outputs from the previous chapters / objectives and integrated the subsystems into the full assembly of the 2nd gen. BAMMsat bioCubeSat payload.

A general design assessment based on the experience during assembly and integration was the spatially tight interface between the different subsystems. Although the design had an open space concept, some subsystems still had a tight interface. A modification in one had repercussions in the other which made simple modifications difficult. Looser interactions could be achieved by using more compliant and well-defined interfaces.

For example, the MCSD and RV could be designed with their own assembly. The interface to the solenoid valve manifold is provided via fluidic connectors with flexible tubing. Compared to the current design, the MCSD and RV were mounted on the mechanical assembly of the solenoid valve manifold. During the development, fixing the issue with aluminium sheet bending was challenging since it impacted the height of the MCSD and the subsequent compact brightfield microscope. Where possible. The next-generation assembly and integration aim to have independent (de-coupled) and modular subsystems. In some cases, it may not be possible. The author suggests that the designer for the next gen. BAMMsat to perform an FMECA analysis and produce an interface map to understand these relationships.

Another suggestion to improve the gear alignment of the MCSD and the Geneva gear mechanism is to mount both subsystems on the same chassis. Mounting on the same chassis meant that both subsystems had the same reference. This reduced chain of tolerances and reduced the possible issue of misaligning the gears.

In summary, the assembly and integration for the 2nd gen. BAMMsat bioCubeSat payload was fit for purposes. The lesson learnt here should be incorporated into the next generation.

"To summarise the BAMMsat-on-BEXUS flight and preliminary analysis of the flight result."

The final PhD objective was included to perform a preliminary analysis and summary of the BoB mission, and the research output has been extensively discussed in Chapter 9.

The BAMMsat-on-BEXUS (BoB) flight was a good exercise in the technology development of a bioCubeSat concept within a space system context. The programmatic reviews, access to a flight in an extreme environment, access to a team resource, and access to finance help develop the BAMMsat concept. Without the flight opportunity, it would have been challenging to advance the concept at the same level during the PhD research.

The BoB flight was used to demonstrate the BAMMsat's technology. The dynamic stratospheric environment helped validate the hardware with stressors not easily replicated in the laboratory. Although there were issues with the design, many lessons learnt will input towards the 3rd gen. design.

One of the main advantages was the operation during the BoB flight campaign. The biological system often has additional requirements and constraints, particularly in biological handling and temperature control. This impacts the pre-flight operations at the launch site. Performing these pre-flight operations is an analogue to an orbital spaceflight and building operation know-how for future spaceflight.

It is also a good analogue for integration on a larger platform. In the future space flight context, BAMMsat could be hosted inside the ISS via CubeSat hosting facilities such as ICECUBE and NanoRacks.

In summary, the BoB flight helped to de-risk and informed the design process for a 3rd gen that is expected to be flown on the ISS and hosted inside a facility such as ICE Cubes.

10.2 Future work

For the 2nd gen BAMMsat, the immediate future work has already been discussed in previous sections of this chapter and elsewhere in the thesis. The final discussion in this chapter has also included suggested future design work for the 3rd gen. BAMMsat bioCubeSat payload.

10.3 Conclusion

The PhD research conducted was a multidisciplinary research field that combines the fields of space systems, fluidics, optics, mechanics, electrical, and software to develop an autonomous miniaturised laboratory.

At the start of the PhD, BAMMsat was developed into a laboratory breadboard. The PhD advanced the concept into a 2U CubeSat payload version which flew in the stratosphere via a stratospheric balloon system seen as an analogue for future in-orbit flight.

During the PhD, five different subsystems were developed: the multi-chamber sample disc, rotary valve, compact brightfield microscope, fluidic subsystem, Geneva gear mechanism, and mechanical housing. These subsystems were packaged into a 2U CubeSat payload version of BAMMsat.

As part of research and development, issues are rarely avoidable and ***should not be considered a failure***. The PhD research various testing in the laboratory captured, discussed, and suggested solutions to the design issue, which can be referred to throughout the PhD that can input to the 3rd gen. development.

With the growth of space commercialisation and growing life science in microgravity, bioCubeSats could play an important role. The BAMMsat concept addresses the knowledge gap by providing the flexibility to perform a broader range of scientific experiments and biological systems than other bioCubeSats. BAMMsat in-situ measurements via autonomous 2U fluorescent, visible spectrometer, and chemical sensors could support a range of experiments to support early validation data. There is potential for high-throughput experiments using the BAMMsat rotary valve concept. Combining high throughput capability

with machine learning capability for life science in microgravity could open a wide field of new therapeutics, drug discovery and space biomanufacturing that can positively impact our society.

With regards to the BoB mission, BAMMsat-on-BEXUS was the first full prototype of BAMMsat in a flight model CubeSat format. It was a multidisciplinary field development, and despite time constraints and challenges, including COVID-19, the BoB team managed to deliver an end-to-end hardware

The BoB mission was focused on a technology demonstration. The key advantage of the BoB mission was that it sped up the development of the BAMMsat concept. The stratospheric environment combined with interfacing to the host platform and operation within an analogue spaceflight system is hard to replicate in the laboratory, especially the pre-flight operation, which gave insight that is otherwise unattainable.

The subsequent development BAMMsat is to perform an initial in-orbit demonstration with life science partners in application in organ-on-a-chip, protein crystallisation and targeting new pathways for drug development. Successful demonstration of BAMMsat functionalities in orbit could help commercialise BAMMsat, enabling it to be widely adopted within the community.

REFERENCES

Altun, Z. ., & Hall, D. . (2009). INTRODUCTION TO C . elegans ANATOMY. In *WormAtlas* (pp. 1–15). https://www.wormatlas.org/hermaphrodite/introduction/mainframe.htm

Amselem, S. (2019). Remote Controlled Autonomous Microgravity Lab Platforms for Drug Research in Space. *Pharmaceutical Research*, *36*(12). https://doi.org/10.1007/s11095-019-2703-7

Antylia Scientific Blog Team. (2015). *How to Sterilize Your Laboratory Plasticware - from Antylia Scientific Blog*. https://www.coleparmer.ca/blog/2015/08/20/how-to-sterilize-your-laboratory-plasticware/

Banerjee, S. S., & Bhowmick, A. K. (2015). Experimental study on the CO2 laser cutting of novel polyamide 6/fluoroelastomer thermoplastic elastomeric blends. *Rubber Chemistry and Technology*, *88*(1), 125–137. https://doi.org/10.5254/rct.14.85960

Beatty, S. (2022). *6 simple search tips: Lessons learned from the Scopus Webinar*. Scopus (Blog). https://blog.scopus.com/posts/6-simple-search-tips-lessons-learned-from-the-scopus-webinar

Bickford, J. H. (1998). Handbook of Bolts and Bolted Joints. In *Handbook of Bolts and Bolted Joints*. CRC Press. https://doi.org/10.1201/9781482273786

Bolliand, A. (2020). *Requirements, Design, Build and Verification of an active thermal subsystem for BAMMsat-on-BEXUS*. Cranfield University.

Boone, T., Cohen, A., Chin, M., Chinn, T., Friedericks, C., Jackson, E., Keyhan, M., Lera, M., Matin, A. C., Mayer, D., Middour, C., Parra, M., Ricco, A., Spremo, S., & Field, M. (2014). E . coli AntiMicrobial Satellite (EcAMSat): Science Payload System Development and Test. *Proceedings of the AIAA/USU Conference on Small Satellites*.

Braddock, M. (2019). From Target identification to Drug Development in Space: Using the Microgravity Assist. *Current Drug Discovery Technologies*, *16*(March). https://doi.org/10.2174/1570163816666190112150014

Bramall, N. E., Quinn, R., Mattioda, A., Bryson, K., Chittenden, J. D., Cook, A., Taylor, C., Minelli, G., Ehrenfreund, P., Ricco, A. J., Squires, D., Santos, O., Friedericks, C., Landis, D., Jones, N. C., Salama, F., Allamandola, L. J., & Hoffmann, S. V.

(2012). The development of the Space Environment Viability of Organics (SEVO) experiment aboard the Organism/Organic Exposure to Orbital Stresses (O/OREOS) satellite. *Planetary and Space Science*, *60*(1), 121–130. https://doi.org/10.1016/j.pss.2011.06.014

Brenan, C. J. H., Domansky, K., Kurzawski, P., & Griffith, L. G. (2000). BioMEMS applied to the development of cell-based bioassay systems. *Micro- and Nanotechnology for Biomedical and Environmental Applications*, *3912*(March 2000), 76–87. https://doi.org/10.1117/12.379564

Brouwer, H. De, & Bogerd, J. Van Den. (2011). LEXAN * POLYCARBONATE FOR OPTICAL APPLICATIONS. *EUROTEC*.

California Polytechnic State University. (2015). *CubeSat Design Specification (CDS) REV 13*. The CubeSat Program, California Polytechnic State. https://doi.org/http://dx.doi.org/10.1155/2015/681901

Calleja, G., Jourdan, A., Ameduri, B., & Habas, J. P. (2013). Where is the glass transition temperature of poly(tetrafluoroethylene)? A new approach by dynamic rheometry and mechanical tests. *European Polymer Journal*, *49*(8), 2214–2222. https://doi.org/10.1016/j.eurpolymj.2013.04.028

Carreno-luengo, H. (2015). *Global Navigation Satellite Systems Reflectometry (GNSS-R): A New Tool for Earth Remote Sensing with Improved Spatio-Temporal Resolution* (Issue September). Universitat Politècnica de Catalunya (UPC).

Chabi, A. (2020). *Requirements, Design, Analysis, Manufacturing and Testing of the BAMMsat on BEXUS Payload overall Structure, Pressure Vessel, Thermal Passive Control and Gondola Mechanical Interface*. Cranfield University.

Chen, X., & Hui, S. (2005). Ratcheting behavior of PTFE under cyclic compression. *Polymer Testing*, *24*(7), 829–833. https://doi.org/10.1016/j.polymertesting.2005.07.006

Cohen, J., & Stodieck, L. (2016). Rodent Research Contributes to Osteoporosis Treatments. *Spinoff*, 30–33. http://spinoff.nasa.gov/Spinoff2016/pdf/hm_1.pdf

Cook, A. M., Mattioda, A. L., Quinn, R. C., Ricco, A. J., Ehrenfreund, P., Bramall, N. E., Minelli, G., Quigley, E., Walker, R., & Walker, R. (2014). Sevo on the ground: Design of a laboratory solar simulation in support of the O/OREOS mission. *Astrophysical Journal, Supplement Series*, *210*(2). https://doi.org/10.1088/0067-0049/210/2/15

Crombrugghe, G. De, & Pletser, V. (2017). Emerging Microgravity Platforms and their Capabilities Compared to the Traditional Offering. *67th International Astronautical Congress (IAC)*, *September*.

Cullen, D. C., Longley, J., Kingston, J., Lee, D., Black, M., Pearson, D., Waring, C., & Pink, R. (2016). BAMMSAT: DEVELOPMENT STATUS OF A PLATFORM FOR BIOSCIENCE, ASTROBIOLOGY, MEDICAL AND MATERIALS SCIENCE ON CUBESATS AND CUBESAT-LIKE PAYLOADS. *The 4S Symposium*.

De Brouwer, H., Van Den Bogerd, J., & Hoover, J. (2015). Color stability of polycarbonate for optical applications. *European Polymer Journal*, *71*, 558–566. https://doi.org/10.1016/j.eurpolymj.2015.08.031

Department of Space Indian Space Research Organisation. (2017). *PSLV-C37 / Cartosat -2 Series Satellite*. https://www.isro.gov.in/launcher/pslv-c37-cartosat-2-series-satellite

Dhall, A., Masiello, T., Butt, L., Strohmayer, M., & Hemachandra, L. P. M. (2016). Simulating Fluid Flow through a Culture Chip for Cell Migration Studies in Microgravity. *Proceedings of the 2016 COMSOL Conference in Boston*, *July 2018*, 2–7.

Diaz-Aguado, M. F., Minnelli, G., Ghassemieh, S., Beasley, C., & Schooley, A. (2011). O/OREOS and PharmaSat – Thermal Lessons Learned on Small Class D Spacecraft. *4th Conference on Environmental Systems*, *July*, 1–10. https://doi.org/10.2514/6.2011-5028

DiFrancesco, J. M., & Olson, J. M. (2015). The economics of microgravity research. *Npj Microgravity*, *1*, 1–6. https://doi.org/10.1038/npjmgrav.2015.1

Edmund Optics. (2022a). *Introduction to Modulation Transfer Function | Edmund Optics*. Application Notes. https://www.edmundoptics.eu/knowledge-center/application-notes/optics/introduction-to-modulation-transfer-function/%0Ahttps://www.edmundoptics.de/resources/application-notes/optics/introduction-to-modulation-transfer-function/

Edmund Optics. (2022b). *Lens Spacers , Shims and Focal Length Extenders | Edmund Optics*. https://www.edmundoptics.eu/knowledge-center/application-notes/imaging/lens-spacers-shims-and-focal-length-extenders/

Edwards, E. S., & Roux, S. J. (1998). Influence of gravity and light on the developmental

polarity of Ceratopteris richardii fern spores. *Planta*, *205*(4), 553–560. https://doi.org/10.1007/s004250050355

Ehrenfreund, P., Ricco, A. J., Quinn, R., Bramall, N., Bryson, K., Chittenden, J., Cook, A., Mancinelli, R., Mattioda, A., Minelli, G., Nicholson, W., Santos, O., Squires, D., Friedericks, C., Kitts, C., & Rasay, R. (2011). O/OREOS: A successful mission of NASA's astrobiology small payload program. *62nd International Astronautical Congress 2011, IAC 2011*. https://www.scopus.com/inward/record.uri?eid=2-s2.0-84864103002&partnerID=40&md5=424b85989e30dbb5df41ff6c9adb0a08

Ehrenfreund, P., Ricco, A. J., Squires, D., Kitts, C., Agasid, E., Bramall, N., Bryson, K., Chittenden, J., Conley, C., Cook, A., Mancinelli, R., Mattioda, A., Nicholson, W., Quinn, R., Santos, O., Tahu, G., Voytek, M., Beasley, C., Bica, L., … Young, A. (2014). The O/OREOS mission-Astrobiology in low earth orbit. *Acta Astronautica*, *93*, 501–508. https://doi.org/10.1016/j.actaastro.2012.09.009

Erika B. Wagner. (2019). New Shepard Payload Accommodations and Flight History. *70th International Astronautical Congress (IAC)*.

ERIKS. (2005). *TECAPEEK*. https://solutions-in-plastics.info/en/products/high-performance-plastics/peek/

EuroLaunch. (2020). *BEXUS User Manual v7-5*.

Fitton, B., & Moore, D. (1996). National and international space life sciences research programmes 1980 to 1993 - and beyond. In *Biological and Medical Research in Space* (pp. 432–541). https://doi.org/10.1007/978-3-642-61099-8_8

Fluorocarbon. (2020a). *PTFE vs PCTFE*. https://fluorocarbon.co.uk/news-and-events/post/57/ptfe-vs-pctfe

Fluorocarbon. (2020b). *PTFE vs PEEK*. https://fluorocarbon.co.uk/news-and-events/post/55/ptfe-versus-peek

FLUOROTHERM. (2022). *PCTFE Properties*. https://www.fluorotherm.com/technical-information/materials-overview/pctfe-properties/

Forsberg, K., & Mooz, H. (1991). The Relationship of System Engineering to the Project Cycle. *INCOSE International Symposium*, *1*(1), 57–65. https://doi.org/10.1002/j.2334-5837.1991.tb01484.x

Frenea-Schmidt, A. (2021). *BEXUS User Manual - BX_REF_BEXUS_User*

Manual_v8_03June21. https://rexusbexus.net/bexus/bexus-user-manual/

Glick, Y. (2018). *Health On Earth Made In Space – Vision to Reality*. International Micro Nano Conference 2018. https://fhi.nl/app/uploads/sites/57/2018/12/SpacePharma-iMNC-Health-on-earth-made-in-space-vision-to-reality-Dec-2018.pdf

Glick, Y., & Eyal, S. (2021). Future of Drug Development in Space: Unmanned Satellites and Vehicles. *Handbook of Space Pharmaceuticals*, 1–29. https://doi.org/10.1007/978-3-319-50909-9_46-1

Golkar, A. (2020). Experiential Systems Engineering Education Concept Using Stratospheric Balloon Missions. *IEEE Systems Journal*, *14*(2), 1558–1567. https://doi.org/10.1109/JSYST.2019.2917823

Goodfellow. (2022a). *Fluorinated Ethylene Propylene Copolymer - Film (FP341050)*.

Goodfellow. (2022b). *Polymethylpentene - Film TPX® (ME31-FM-000100)*. https://www.goodfellow.com/uk/en-gb/displayitemdetails/p/me31-fm-000100/polymethylpentene-film

Gorissen, B., Van Hoof, C., Reynaerts, D., & De Volder, M. (2016). SU8 etch mask for patterning PDMS and its application to flexible fluidic microactuators. *Microsystems and Nanoengineering*, *2*(March), 1–5. https://doi.org/10.1038/micronano.2016.45

Hollows, G., & James, N. (2022). *Understanding Focal Length and Field of View*. http://www.edmundoptics.de/resources/application-notes/imaging/understanding-focal-length-and-field-of-view/

Honess, D., & Quinlan, O. (2017). Astro Pi: Running your code aboard the International Space Station. *Acta Astronautica*, *138*(December 2016), 43–52. https://doi.org/10.1016/j.actaastro.2017.05.023

Hovell, C. (2017). *SpacePharma Informational Presentation*. NSF/NIH/ISS NATIONAL LAB INFORMATIONAL WEBINAR. https://doi.org/10.15713/ins.mmj.3

Ibeh, C. C. (2011). Thermoplastic Materials. In *Thermoplastic Materials*. https://doi.org/10.1201/b13623

Innovative Solutions In Space. (n.d.). *ISIS gets 101 CubeSats launched during recordbreaking PSLV launch*. Retrieved March 26, 2019, from https://www.isispace.nl/news/dutch-nanosatellite-company-gets-101-cubesats-launched-recordbreaking-pslv-launch/

Ishioka, N., & Higashibata, A. (2019). Space Experiments Using C. elegans as a Model Organism. In *Handbook of Space Pharmaceuticals*. https://doi.org/10.1007/978-3-319-50909-9_3-1

Johann, U., & Reiland, W. (1988). Stratospheric balloons as a testbed for optical space communications technology. *International Journal of Satellite Communications*, *6*(2), 225–230. https://doi.org/10.1002/sat.4600060217

John, O., Ian, W., Terry, O., & FranÃ§ois, P. (2000). Investigation of the Alamar Blue (resazurin) fluorescent dye for the assessment of mammalian cell cytotoxicity. *European Journal of Biochemistry*, *267*(17), 5421–5426. http://dx.doi.org/10.1046/j.1432-1327.2000.01606.x

Jones, H. W. (2018). The Recent Large Reduction in Space Launch Cost. *48th International Conference on Environmental Systems*, *July 2018*, 81. https://ttu-ir.tdl.org/handle/2346/74082

Kitts, C. (n.d.). *Initial Flight Results from the PharmaSat Biological Microsatellite Mission*. Retrieved March 15, 2019, from http://digitalcommons.usu.edu/cgi/viewcontent.cgi?filename=0&article=1288&context=smallsat&type=additional

Kitts, C., Hines, J. W., Agasid, E., Ricco, A. J., Yost, B., Ronzano, K., & Puig-Suari, J. (2006). The GeneSat-1 Microsatellite Mission : A Challenge in Small Satellite Design. *20th Annual AIAA/USU Conference on Small Satellites*, 1–6. https://doi.org/SSC06-IV-8

Kitts, C., & Quinn, N. (2004). An Interdisciplinary Field Robotics Program for Undergraduate Computer Science and Engineering Education. *ACM Journal on Educational Resources in Computing*, *4*(2), 3. https://doi.org/10.1145/1071620.1071623

Kitts, C., Ronzano, K., Rasay, R., Mas, I., Acain, J., Neumann, M., Bica, L., Mahacek, P., Minelli, G., Beck, E., Li, S., Gamp, B., Agnew, S., Shepard, J., Hines, J., Agasid, E., Friedericks, C., Piccini, M., Parra, M., … Mcginnis, M. (2009). Initial Flight Results from the PharmaSat Biological Microsatellite Mission. *23nd Annual AIAA/USU Conf on Small Satellites*, *January*. https://doi.org/SSC08-II-4

Kitts, C., Ronzano, K., Rasay, R., Mas, I., Williams, P., Mahacek, P., Minelli, G., Hines, J., Agasid, E., Friedericks, C., Piccini, M., Parra, M., Timucin, L., Beasley, C.,

Henschke, M., Luzzi, E., Mai, N., Mcintyre, M., Ricks, R., … Ricco, A. (2007). Flight Results from the GeneSat-1 Biological Microsatellite Mission. *2007 AIAA Small Satellite Conference*, *May 2014*, 1–11. https://doi.org/SSC08-II-4

Levine, L. M., Campbell, T., & Beach, R. (2007). Combining Additive and Subtractive Techniques in the Design and Fabrication of Microfluidic Devices. *2007 NSTI Nanotechnology Conference and Trade Show - NSTI Nanotech 2007*, *m*, 385–388. http://www.alineinc.com/pdf/NASA_Fluidic_Card_for_Cell_Culture.pdf

Levy, D. (2004). *Worms in space*. Stanford Report. https://news.stanford.edu/news/2004/february4/worms-24.html

Mai, T.-A., & Nguyen, N.-T. (2002). Fabrication of micropumps with Q-switched Nd:YAG-lasers. *Second International Symposium on Laser Precision Microfabrication*, *4426*(February 2002), 195. https://doi.org/10.1117/12.456871

Marcucci Ribeiro, M. C. (2004). Materials and reactors systems having humidity and gas control. In *United States - Patent Application Publication*.

Martinez, A. (2014). *SporeSat*. 11th Annual CubeSat Developers Workshop. http://mstl.atl.calpoly.edu/~bklofas/Presentations/DevelopersWorkshop2014/Martinez_SPORESAT.pdf

Matin, A. C., Wang, J. H., Keyhan, M., Singh, R., Benoit, M., Parra, M. P., Padgen, M. R., Ricco, A. J., Chin, M., Friedericks, C. R., Chinn, T. N., Cohen, A., Henschke, M. B., Snyder, T. V., Lera, M. P., Ross, S. S., Mayberry, C. M., Choi, S., Wu, D. T., … Spremo, S. M. (2017). Payload hardware and experimental protocol development to enable future testing of the effect of space microgravity on the resistance to gentamicin of uropathogenic Escherichia coli and its σs-deficient mutant. *Life Sciences in Space Research*, *15*(May), 1–10. https://doi.org/10.1016/j.lssr.2017.05.001

Minelli, G., Kitts, C., Ronzano, K., Beasley, C., Rasay, R., Mas, I., Henschke, M., Luzzi, E., Mai, N., Mcintyre, M., Ricks, R., Squires, D., Storment, C., Tucker, J., Yost, B., & Defouw, G. (2008). Extended Life Flight Results from the GeneSat-1 Biological Microsatellite. *22nd Annual AIAA/USU Conference on Small Satellites*.

Minelli, G., Ricco, A., Beasley, C., & Hines, J. (2010). O/OREOS nanosatellite: A multi-payload technology demonstration. *24th Annual AIAA/USU Conference on Small Satellites*. http://digitalcommons.usu.edu/smallsat/2010/all2010/32/

Moradi, M., Mehrabi, O., Azdast, T., & Benyounis, K. Y. (2017). Enhancement of low power CO2 laser cutting process for injection molded polycarbonate. *Optics and Laser Technology*, *96*, 208–218. https://doi.org/10.1016/j.optlastec.2017.05.022

NASA. (2006). *Bigelow Spacecraft Carries NASA "GeneBox" to Orbit*. https://www.nasa.gov/centers/ames/multimedia/images/2006/genebox.html

NASA. (2014). *NASAfacts: SporeSat*. https://www.nasa.gov/sites/default/files/sporesat_factsheet_031214.pdf

Nicholson, W. L., Ricco, A. J., Agasid, E., Beasley, C., Diaz-Aguado, M., Ehrenfreund, P., Friedericks, C., Ghassemieh, S., Henschke, M., Hines, J. W., Kitts, C., Luzzi, E., Ly, D., Mai, N., Mancinelli, R., McIntyre, M., Minelli, G., Neumann, M., Parra, M., … Young, A. (2011). The O/OREOS Mission: First Science Data from the Space Environment Survivability of Living Organisms (SESLO) Payload. *Astrobiology*, *11*(10), 951–958. https://doi.org/10.1089/ast.2011.0714

Padgen, M. (2017). *EcAMSat and BioSentinel : Autonomous Bio Nanosatellites Addressing Strategic Knowledge Gaps for Manned Spaceflight Beyond LEO*. SUNY Polytechnic Inst. (College of Nanoscale Science + Engineering) CNSE Colloquium Series. https://ntrs.nasa.gov/search.jsp?R=20170009842

Padgen, M. R., Chinn, T. N., Friedericks, C. R., Lera, M. P., Chin, M., Parra, M. P., Piccini, M. E., Ricco, A. J., & Spremo, S. M. (2020). The EcAMSat fluidic system to study antibiotic resistance in low earth orbit: Development and lessons learned from space flight. *Acta Astronautica*, *173*(January), 449–459. https://doi.org/10.1016/j.actaastro.2020.02.031

Padgen, M. R., Lera, M. P., Parra, M. P., Ricco, A. J., Chin, M., Chinn, T. N., Cohen, A., Friedericks, C. R., Henschke, M. B., Snyder, T. V., Spremo, S. M., Wang, J.-H., & Matin, A. (2019). EcAMSat spaceflight measurements of the role of σs in antibiotic resistance of stationary phase Escherichia coli in microgravity. *Life Sciences in Space Research*, *24*(October 2019), 18–24. https://doi.org/10.1016/j.lssr.2019.10.007

Pagnutti, M., Ryan, R. E., Cazenavette, G., Gold, M., Harlan, R., Leggett, E., & Pagnutti, J. (2017). Laying the foundation to use Raspberry Pi 3 V2 camera module imagery for scientific and engineering purposes. *Journal of Electronic Imaging*, *26*(1), 013014. https://doi.org/10.1117/1.jei.26.1.013014

Park, J., Salmi, M. L., Wan Salim, W. W. A., Rademacher, A., Wickizer, B., Schooley, A., Benton, J., Cantero, A., Argote, P. F., Ren, M., Zhang, M., Porterfield, D. M., Ricco, A. J., Roux, S. J., & Rickus, J. L. (2017). An autonomous lab on a chip for space flight calibration of gravity-induced transcellular calcium polarization in single-cell fern spores. *Lab on a Chip*, *17*(6), 1095–1103. https://doi.org/10.1039/c6lc01370h

Pereiro, I., Fomitcheva Khartchenko, A., Petrini, L., & Kaigala, G. V. (2019). Nip the bubble in the bud: A guide to avoid gas nucleation in microfluidics. *Lab on a Chip*, *19*(14), 2296–2314. https://doi.org/10.1039/c9lc00211a

Poly-Tech Industrial Inc. (2022a). *PEEK (Polyetheretherketone)*. https://www.polytechindustrial.com/products/plastic-stock-shapes/peek

Poly-Tech Industrial Inc. (2022b). *PTFE (Unfilled)*. https://www.polytechindustrial.com/products/plastic-stock-shapes/ptfe-unfilled

Powell, J. (1998). *CO2 Laser Cutting* (2nd ed.). Springer London. https://doi.org/https://doi.org/10.1007/978-1-4471-1279-2

Prabhakar, P., Sen, R. K., Dwivedi, N., Khan, R., Solanki, P. R., Srivastava, A. K., & Dhand, C. (2021). 3D-Printed Microfluidics and Potential Biomedical Applications. *Frontiers in Nanotechnology*, *3*(March), 1–16. https://doi.org/10.3389/fnano.2021.609355

Princeton University Environmental Health and Safety. (n.d.). *Compatible / Incompatible Materials*. Retrieved May 24, 2022, from https://ehs.princeton.edu/laboratory-research/biological-safety/autoclave-use/compatibleincompatible-materials

Puchalt, J. C., Sánchez-Salmerón, A. J., Guerola, P. M., & Martínez, S. G. (2019). Active backlight for automating visual monitoring: An analysis of a lighting control technique for Caenorhabditis elegans cultured on standard Petri plates. *PLoS ONE*, *14*(4), 1–18. https://doi.org/10.1371/journal.pone.0215548

Rae, P. J., & Dattelbaum, D. M. (2004). The properties of poly(tetrafluoroethylene) (PTFE) in compression. *Polymer*, *45*(22), 7615–7625. https://doi.org/10.1016/j.polymer.2004.08.064

Raspberry Pi Foundation. (2022). *Introducing the Raspberry Pi Cameras*. https://www.raspberrypi.com/documentation/accessories/camera.html

Rasperry Pi Foundation. (2015). *Raspberry Pi Camera Module*. 0–6.

https://www.raspberrypi.org/documentation/raspbian/applications/camera.md

Reichert, P., Prosise, W., Fischmann, T. O., Scapin, G., Narasimhan, C., Spinale, A., Polniak, R., Yang, X., Walsh, E., Patel, D., Benjamin, W., Welch, J., Simmons, D., & Strickland, C. (2019). Pembrolizumab microgravity crystallization experimentation. *Npj Microgravity*, *5*(1), 1–8. https://doi.org/10.1038/s41526-019-0090-3

REXUS/BEXUS. (2019). *FEEDBACK FOR PROPOSAL TO REXUS/BEXUS PROGRAMME - Team: BoB*.

REXUS/BEXUS. (2021). *The REXUS/BEXUS programme Rocket and Balloon Experiments for University Students*. https://rexusbexus.net/bexus/

Ricco, A. J., Agasid, E., Barker, V., Fahlen, T., Hines, J. W., Levine, L., Mancinelli, R., Oswell, D., Ricks, R., Ronzano, K., Squires, D., Storment, C., Swaiss, G., Timucin, L., Udoh, U., & Yost, B. (2005). INTEGRATED SYSTEM TO ANALYZE THE GENETIC EFFECTS OF THE SPACE ENVIRONMENT ON LIVING CELLS IN CULTURE: GENESAT. *Micro Total Analysis Systems*.

Ricco, A J, Hanel, R., Bhattacharya, S., Boone, T., Tan, M., Mousavi, A., Padgen, M., Gentry, D., Maria, S. S., Marina, D., Lewis, B., Sanchez, H., Chartres, J., Mcintosh, D., Lusby, T., Gavalas, S., Wheeler, S., & Group, R. (2016). The Biosentinel Bioanalytical Microsystem: Characterizing Dna Radiation Damage in Living Organisms Beyond Earth Orbit. *Hilton Head Workshop 2016: A Solid State Sensors, Actuators, and Microsystems Workshop*, 352–355.

Ricco, Antonio J. (n.d.). *Integrated Microfluidic Systems in Challenging Environments : Biological Studies in Earth Orbit*. Retrieved February 23, 2022, from https://studylib.net/doc/12062434/integrated-microfluidic-systems-in-challenging-environmen...

Ricco, Antonio J. (2011). *Autonomous Space Science on Small Satellites*. https://spacescience.arc.nasa.gov/microbes/STEP/documents_2011/lectures/STEP 2011-Ricco.pdf

Ricco, Antonio J., Parra, M., Niesel, D., Piccini, M., Ly, D., McGinnis, M., Kudlicki, A., Hines, J. W., Timucin, L., Beasley, C., Ricks, R., McIntyre, M., Friedericks, C., Henschke, M., Leung, R., Diaz-Aguado, M., Kitts, C., Mas, I., Rasay, M., … Yost, B. (2011). PharmaSat: Drug dose response in microgravity from a free-flying

integrated biofluidic/optical culture-and-analysis satellite. *Microfluidics, BioMEMS, and Medical Microsystems IX*, *7929*(February 2011), 79290T-79290T – 9. https://doi.org/10.1117/12.881082

Ricco, Antonio J, Hines, J. W., Piccini, M., Parra, M., Timucin, L., Barker, V., Storment, C., Friedericks, C., Agasid, E., Beasley, C., Giovangrandi, L., Henschke, M., Kitts, C., Levine, L., Luzzi, E., Ly, D., Mas, I., Mclntyre, M., Oswell, D., … Yost, B. (2007). Autonomous genetic analysis system to study space effects on microorganisms: Results from orbit. *TRANSDUCERS and EUROSENSORS '07 - 4th International Conference on Solid-State Sensors, Actuators and Microsystems*, 33–37. https://doi.org/10.1109/SENSOR.2007.4300065

Ricco, Antonio J, Parra, M., Piccini, M., Ly, D., Niesel, D., M, M., Kudlicki, A., Hines, J. W., Timucin, L., Beasley, C., Ricks, R., Mcintyre, M., Friedericks, C., Henschke, M., Leung, R., Diaz-Aguado, M., Kitts, C., Mas, I., Rasay, R., … Yost, B. (2010). PharmaSat: Drug dose dependence results from an autonomous microsystem-based small satellite in low Earth orbit. *Solid-State Sensors, Actuators, and Microsystems Workshop*, *January 2015*, 110–113.

Robson, D., Cappelletti, C., Segal, J., Williams, P., & Szewczyk, N. (2020). Development of a Cubesat Platform for Biomedical and Pharmaceutical Leo Experiments. *5th IAA Conference on University Satellite Missions and CubeSat Workshop*.

Robson, D. J., & Cappelletti, C. (2022). Biomedical payloads: A maturing application for CubeSats. *Acta Astronautica*, *191*(October 2021), 394–403. https://doi.org/10.1016/j.actaastro.2021.11.017

Samburski, G. (2018). Remote Controlled Miniaturized Lab Platform for Space Research. *69th International Astronautical Congress*.

Santa Maria, S. R., Marina, D. B., Massaro Tieze, S., Liddell, L. C., & Bhattacharya, S. (2020). BioSentinel: Long-Term Saccharomyces cerevisiae Preservation for a Deep Space Biosensor Mission . *Astrobiology*, *January*. https://doi.org/10.1089/ast.2019.2073

Sartowska, B. A., Orelovitch, O. L., Apel, P. Y., Blonskaya, I. V., & Presz, A. (2012). Nanopores with controlled profiles in track-etched membranes. *Nukleonika*, *57*(4), 575–579.

Schreurs, D., Nagels, S., Cardinaletti, I., Vangerven, T., Cornelissen, R., Vodnik, J.,

Hruby, J., Deferme, W., & Manca, J. V. (2018). Methodology of the first combined in-flight and ex situ stability assessment of organic-based solar cells for space applications. *Journal of Materials Research*, *33*(13), 1841–1852. https://doi.org/10.1557/jmr.2018.156

Serrano, M. A., & Moreno, J. C. (2020). Spectral transmission of solar radiation by plastic and glass materials. *Journal of Photochemistry and Photobiology B: Biology*, *208*(April), 111894. https://doi.org/10.1016/j.jphotobiol.2020.111894

Sharma, A., Clemens, R. A., Garcia, O., Taylor, D. L., Wagner, N. L., Shepard, K. A., Gupta, A., Malany, S., Grodzinsky, A. J., Kearns-Jonker, M., Mair, D. B., Kim, D.-H., Roberts, M. S., Loring, J. F., Hu, J., Warren, L. E., Eenmaa, S., Bozada, J., Paljug, E., … Wagner, W. R. (2021). Biomanufacturing in low Earth orbit for regenerative medicine. *Stem Cell Reports*, *17*(1), 1–13. https://doi.org/10.1016/j.stemcr.2021.12.001

Sims, M. R., Cullen, D. C., Rix, C. S., Buckley, A., Derveni, M., Evans, D., Miguel García-Con, L., Rhodes, A., Rato, C. C., Stefinovic, M., Sephton, M. A., Court, R. W., Bulloch, C., Kitchingman, I., Ali, Z., Pullan, D., Holt, J., Blake, O., Sykes, J., … Holm, N. (2012). Development status of the life marker chip instrument for ExoMars. *Planetary and Space Science*, *72*(1), 129–137. https://doi.org/10.1016/j.pss.2012.04.007

Sinclair, G. T. B. (2020). *Requirements, design, manufacture and build of the electrical system for the BAMMsat on BEXUS payload and further consideration of the solenoid valve, photodiode and Electrical Power Subsystems*. Cranfield University.

Smith, D. J., & Sowa, M. B. (2017). Ballooning for Biologists: Mission Essentials for Flying Life Science Experiments to Near Space on NASA Large Scientific Balloons. *Gravitational and Space Research*, *5*(1), 52–73. https://doi.org/10.2478/gsr-2017-0005

Space Tango. (2022). *CubeLab*. https://spacetango.com/cubelab/

SpacePharma. (n.d.). *SPumP The SpacePharma Microgravity Miniaturized Pump*. Retrieved April 1, 2019, from http://spump.github.io/

SpacePharma. (2017). *SPuMP Report Summary*. https://cordis.europa.eu/project/rcn/203195/factsheet/en

Spremo, S. (2018). *EcAMSat Spacecraft Mission: The Success Story of NASA's First 6U*

CubeSat. 15th Annual CubeSat Developers Workshop.

Swedish Space Corporation. (2021). *INCIDENT MESSAGES - The Esrange Fire on 26 August*. https://sscspace.com/news-activities/incident-information/

Tan, M. X., Piccini, M., & Ricco, A. J. (2011). Integrated Fluidic System for Growth and Fluorescence Imaging of Multicellular Organisms in Nanosatellite Applications. *15th International Conference on Miniaturized Systems for Chemistry and Life Sciences*, 1719–1721.

Tilley III, J. N., Friedman, E. J., Ford, H. C., & Bely, P. Y. (1995). POST: a stratospheric testbed for testing new space telescope technologies. *Space Telescopes and Instruments*, *2478*(June 1995), 89–100. https://doi.org/10.1117/12.210915

Twiggs, B., & Kuroki, S. (2002). BioExplorer Bus - Low Cost Approach. *IEEE Aerospace Conference*, 427–434.

Twiggs, R. (2009). Origin of CubeSat. In H. Helvajian & S. . Janson (Eds.), *Small Satellites: Past, Present and Future* (pp. 151–173). The Aerospace Press. https://doi.org/doi:10.2514/4.989223

UK Space Agency. (2021a). *Announcement of Opportunity : Call for Ideas UK Microgravity Experiments*. https://assets.publishing.service.gov.uk/government/uploads/system/uploads/attachment_data/file/668930/AO_for_National_Experiments.pdf

UK Space Agency. (2021b). *Worms on a mission to research muscle loss in space*. https://www.gov.uk/government/news/worms-on-a-mission-to-research-muscle-loss-in-space

ul Haque, A., Rokkam, M., De Carlo, A. R., Wereley, S. T., Roux, S. J., Irazoqui, P. P., & Porterfield, D. M. (2007). A MEMS fabricated cell electrophysiology biochip for in silico calcium measurements. *Sensors and Actuators, B: Chemical*, *123*(1), 391–399. https://doi.org/10.1016/j.snb.2006.08.043

Wadsworth, J., Cockell, C. S., Murphy, A. S. J., Nilima, A., Paling, S., Meehan, E., Toth, C., Scovell, P., & Cascorbi, L. (2020). There's Plenty of Room at the Bottom: Low Radiation as a Biological Extreme. *Frontiers in Astronomy and Space Sciences*, *7*(August), 1–14. https://doi.org/10.3389/fspas.2020.00050

Waller, J. M., Newton, B. E., Beeson, H. D., & Haas, J. P. (2001). Comparison of the

Dimensional Stability of Kel-F 81 and Neoflon CTFE M400H Polychlorotrifluoroethylenes Used in Valve Seat Applications. *ASTM Special Technical Publication*, *1395*, 21–37. https://doi.org/10.1520/stp12485s

Walsh, R. A. (2001). Handbook of Machining and Metalworking Calculations. In *Metalworking*. george_hoare@mcgraw-hill.com

Wan Salim, W. W. A., Park, J., Rickus, J. L., Rademacher, A., Ricco, A. J., Schooley, A., Benton, J., Wickizer, B., Martinez, A., Mai, N., Rasay, M., Porterfield, D. M., Brownston, L., Cote, M., Defouw, G., Henschke, M., Kitts, C., Luzzi, E., Perez, M., … Sweet, A. (2014). Sporesat : a Nanosatellite Platform Lab-on-a-Chip System for Investigating Gravity Threshold of Fern-Spore Single-Cell Calcium Ion Currents. *Hilton Head*, 111–114.

Yamin, Y. (2016). *SPACEPHARMA: Remote-Controlled Miniaturized Microgravity Solutions*. Technical Presentations Made at the 53rd Session of UNOOSA Scientific and Technical Subcommittee. http://www.unoosa.org/oosa/en/ourwork/copuos/stsc/technical-presentations.html

Yost, B., Hines, J., Agasid, E., Engelbert, D., Ricco, A., & Kitts, C. (2005). The GeneSat-1 Test Demonstration Project: A Unique Use of Smallsats. *Proceedings of the AIAA/USU Conference on Small Satellites*, 1–7. https://doi.org/SSC05-V-3

Yuri. (2022). *Our Service*. https://www.yurigravity.com/our-service#right-hardware

Zea, L., Maria, S. R. S., & Ricco, A. J. (2021). CubeSats for microbiology and astrobiology research. In C. Cappelletti, S. Battistini, & B. K. Malphrus (Eds.), *Cubesat Handbook From Mission Design to Operations*. Acadmic Press.

APPENDICES

Appendix A BAMMsat-on-BEXUS requirements and constraints

A.1 Naming convention

The naming convention has been created to organise the requirements. It has the following format:

- XX (2 consonants to define the type of requirement)
- 00 000 (5 numbers to identify the requirements)
- c (stands for condensed as this is a condensed version)
- Main Requirement IDs are multiples of 10, sub-requirement IDs are multiples of 1
- E.g. FC-01 100c for the 1st FunCtional condensed requirement

A.2 Nomenclature

CHAMBERS	**REFERS TO THE INDIVIDUAL CHAMBERS INSIDE THE MULTI-CHAMBER SAMPLE DISC (MCSD) WHERE *C. ELEGANS* WILL BE INCUBATED.** 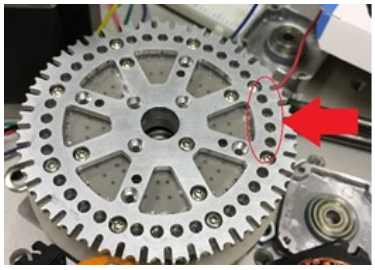 **FIGURE A - MCSD DISC WITH FOUR CHAMBERS BEING HIGHLIGHTED**
EXPERIMENT OPERATION	Start at launch and end during the float phase before the cut-off at "the end of operation". The experiment will be designed with a baseline operation to meet our experiment objectives within 1-hour as per minimum float time. In the event of extended float time, we will have an extended operation to perform other system performance verification.
EXTERNAL ENVIRONMENT STATUS	The term refers to temperature, absolute pressure outside the pressure vessel and solar illumination at a fixed time.
FCT	Flight Compatibility Test. After this event, the BoB team handover experiment to the launch provider.

GROWTH MEDIUM	The term refers to a liquid medium, containing non-pathogenic OP50 *E. coli*, designed to support the growth of the *C. elegans*.
HEALTH STATUS	The team refers to the population status, mobility speed, motility speed, gross observable phenotypes and size of the *C. elegans.*
HOUSEKEEPING DATA	Refer to internal and external environmental parameters.
INTERNAL ENVIRONMENT	Refers to the environmental parameters that *C. elegans* worms are experiencing at a fixed time. In other words, it is the environment inside the MCSD chambers and not necessarily the environment of the rest of the experiment. This include: • Temperature • Absolute pressure • Humidity • Fluidic pressure • Fluidic volumetric flow rate
MCSD	Multi-chamber sample disc.
PRE-FLIGHT OPERATIONS	Start by loading the worms to the MCSD and end at launch.
SYSTEM	Refers to the assembly of BAMMsat hardware that will be flying on BEXUS only. The “system” is composed of an experiment assembly or payload (*C. elegans* and a pressurised environment) and a bus (that will support the payload).

A.3 Functional Requirements

Requirement ID	Description	WP
FC-01 100c	**The system shall provide a viable and nutritious internal environment to ensure the viability and a low metabolic rate of the C. elegans during the pre-flight operations.** *The internal environment refers to the environmental parameters in which the C. elegans worms evolve. This includes temperature, absolute pressure, humidity, O2 concentration in fluids, fluidic pressure, fluidic volumetric. The required nutrients will be provided by a growth fluidic media. The system and pre-flight operation will be designed to be able to hand over the system with C. elegans to the launch provider 24 hours in the best case, to 96 hours in the worst case, before launch.*	2000/3000/ 5000
FC-01 200c	**The system shall provide a viable and nutritious internal environment to ensure the viability of the C. elegans during experiment operation.**	2000/3000/ 5000
FC-02 100c	**Deleted** *This requirement is expanded below*	
FC-02 110c	**The system shall measure and log internal temperature during pre-flight and experiment operation.**	3000
FC-02 130c	**The system shall measure and log internal pressure during pre-flight and experiment operation.**	3000
FC-02 140c	**The system shall measure and log internal relative humidity during pre-flight and experiment operation.**	3000
FC-02 160c	**The system shall measure and log the fluid pressure during pre-flight and experiment operation.**	3000/5000
FC-02 170c	**The system shall measure and log the fluidic volumetric rate during pre-flight and experiment operation.**	3000/5000
FC-02 200c	**Deleted** *This requirement is expanded below*	3000
FC-02 210c	**The system shall measure and log the external temperature during pre-flight and experiment operation.**	3000
FC-02 220c	**The system shall measure and log the external absolute pressure during pre-flight and experiment operation.**	3000
FC-02 230c	**The system shall measure and log the external solar illumination during pre-flight and experiment operation.**	3000
FC-03 100c	**The system shall take and log static images and video of the C. elegans inside the MCSD via an imaging system during pre-flight operation and experiment operation to evaluate the health status of the C. elegans.** *The health status of the C. elegans can be defined by imaging its population density, mobility, motility, behaviour and size. The imaging system consists of a camera, imaging lenses, and illumination source. The pre-flight imaging is to confirm the viability of the C. elegans before starting the experiment and confirm the pre-flight experiment procedure*	5000

FC-03 200c	**The system shall be able to take and log videos of a chamber while the last media is being replaced.** *This will enable us to see in real-time the impact of the drug that we will pump it into the chamber. The drug is an anaesthetic; therefore, it is expected to see C. elegans slowing their movement.*	3000/5000
FC-04 100c	**The system shall determine which side is being illuminated by the sun.** *To understand which side of the system is being heated up by the solar irradiance and evaluate the performance of the thermal regulation.*	3000
FC-05-100c	**The system shall segregate the C. elegans population in chambers in the MCSD**	5000
FC-05 200c	**The system shall pump different type of media inside the MCSD.** *To feed, give a drug or fix the C. elegans. Dye solutions are being considered.*	5000
FC-05 300c	**The system shall pump different type of media out the MCSD into a fluidic waste reservoir.**	5000
FC-05 400c	**The system shall measure and log the angular position of the MCSD in reference to the imaging system.**	5000
FC-06 100c	**The system shall transmit internal and external status data to the ground station via the BEXUS E-Link during pre-flight operation and experiment operation.**	3000
FC-06 200c	**The system shall be able to receive and execute commands from the ground station via the BEXUS E-Link.**	4000/3000
FC-06 300c	**The ground support system shall have a user interface to display housekeeping information, operational sequences during pre-flight and experiment operation.**	4000/3000
FC-06 400c	**The ground support system shall have a user interface to transmit override commands sequence to the systems during pre-flight and experiment operation.**	4000/3000
FC-07 100c	**The system shall rotate the MCSD via a Geneva drive to address independent chamber for fluidic and imaging.**	3000/5000
FC-08 100c	**The Pressure vessel shall be able to contain a leak of media from the fluidic system that would happen after the FCT.**	2000/50000

A.4 Performance Requirements

Requirement ID	Description	WP
PR-01 100	**The system shall segregate the C. elegans population into 16 groups of 10 ±5 L4 stage C. elegans.** *5 strains/ conditions in total. Three chambers per strain which total to 16 chambers. One strain will the wild type control strain.*	5000
PR-02 100	**Deleted**	
PR-02 200	**Deleted**	
PR-02 300	**Deleted**	
PR-03 100	**The pressure vessel shall maintain the internal atmospheric pressure when closed at the ground in a range of ±0.2 bar during the pre-flight and experiment operation.** *The ~1 bar will be approximate to the atmospheric pressure at ESRANGE during the flight campaign. A margin of 0.2 bar will be safe for C. elegans and internal hardware.*	3000/2000
PR-04 100	**The system shall measure the internal temperature between +0 °C and +30°C.**	3000
PR-04 110	**The system shall measure and log the internal temperature at least every second.**	3000
PR-04 120	**The system shall measure the internal temperature with a ± 1 °C accuracy.** *Should be precise enough to enable thermal regulation and validate PR-02 10c, PR-02 20c and PR-02 30c. 0.1oC is a common precision.*	3000
PR-04 200	**The system shall measure the external temperature between -80 °C and +30 °C**	3000
PR-04 210	**The system shall measure and log the external temperature at least every 10 seconds.**	3000
PR-04 220	**Deleted** ~~*"The system shall measure the external temperature between ± 1 °C accuracy."*~~ It was recognized that the system does not need to measure external temperature in order to fulfil its objectives. The requirement was rejected.	3000
PR-05 100	**The system shall measure the internal absolute pressure between 500 hPa and 2500 hPa.** *Shall be precise enough to validate PR-03 10c. Should be precise enough to validate PR-03 11c. 0.03hPa is a common precision*	3000
PR-05 110	**The system shall measure the internal absolute pressure at least every second.**	3000
PR-05 120	**The system shall measure the internal absolute pressure with ± 200 Pa accuracy.**	3000
PR-05 200	**Deleted** ~~*"The system shall measure the external absolute pressure between 1 hPa and 1500 hPa."*~~ It was recognized that the system does not need to measure the absolute external pressure in order to fulfil its objectives. The requirement was rejected.	3000

PR-05 210	**Deleted** ~~*"The system shall measure the external absolute pressure at least every 10 seconds."*~~ It was recognized that the system does not need to measure the absolute external pressure in order to fulfil its objectives. The requirement was rejected.	3000
PR-05 220	**Deleted** ~~*"The system shall measure the external absolute pressure with ± 200 Pa accuracy."*~~ It was recognized that the system does not need to measure the absolute external pressure in order to fulfil its objectives. The requirement was rejected.	3000
PR-06 101	**The system should measure the relative humidity of the internal environment between 5% and 100%.** *The humidity and resultant condensation should not be a problem. It has been computed that the total volume of water trap in the vessel if the relative humidity is 50 % at room temperature is around a quarter of a ml. But a dry environment could lead to some media evaporation, and it could be interesting to monitor the humidity even with a coarse prescion of ± 5%.*	3000/2000
PR-06 111	**The system should measure the relative humidity of the internal environment at least every 60 sec.**	3000/2000
PR-06 121	**The system should measure the relative humidity of the internal environment with a 5% accuracy.**	3000/2000
PR-07 100	**The system shall take and log static images of the C. elegans with a resolution of 0.025 mm over C. elegans with at least 3280 x 2464 pixels.** *The number of pixels was based on the Raspberry Pi camera capabilities*	5000
PR-07 200	**The system shall capture and log video with a minimum resolution of 0.075 mm over C. elegans with at least 1080 x 1920 pixels.** *Numbers based on the Raspberry Pi camera capabilities*	5000
PR-07 210	**The system shall capture and log video with a minimum of 30 images per second.** *Shall be enough to identify C. elegans type of motility/mobility*	5000
PR-08 200	**The system shall measure the fluidic pressure between the inlet and outlet of the pump between 0 and 20 000 Pa.** *The pressure sensors are placed to measure the pressure difference across the pump for any sudden pressure lost*	5000/3000
PR-08 210	**The system shall measure and log the fluidic pressure between the inlet and outlet of the pump at least every second.** *Every second - to precisely detect a failure.*	5000/3000
PR-08 220	**The system shall measure the fluidic pressure between the inlet and outlet of the pump with a ±200 Pa accuracy for each chamber pumped.**	5000/3000
PR-08 300	**The system shall measure and log the fluidic mass flow rate passing through the multi-chamber sample disc between 0 µL/min and 1000 µL/min.** *This allows us to fill the chamber with the right quantity of media*	5000/3000

PR-08 310	**The system shall measure and log the fluidic mass flow rate passing through the multi-chamber sample disc at least every second.** *every second - to precisely detect a failure*	5000/3000
PR-08 320	**The system shall measure and log the fluidic mass flow rate passing through the multi-chamber sample disc with a ± 50 µL/min accuracy.**	5000/3000
PR-09 100	**Once connected to the BEXUS E-Link, the system shall transmit via BEXUS E-Link housekeeping data from the internal environment at least every second except imaging data.** *In case of failure, a detail dataset may be needed for accident investigation.*	3000/4000
PR-09 200	**Once connected to the BEXUS E-Link, the system shall transmit via BEXUS E-Link data from the external environment at least every 10 sec.** *Will be needed to evaluate the behaviour and performance of the thermal regulation*	3000/4000
PR-10 100	**The system shall carry on-board a minimum of 10 ml of media. ~ 6 ml of growth media + ~1 ml of fixative + margin.** *This is sufficient to validate all mission objectives*	5000
PR-10 101	**The system should carry on-board a minimum of 95 ml of media. ~ 80 ml of growth media + ~ 5 ml of drudged media + ~5 ml of fixative + margin.** *This would enable procedures for extensive testing of the system*	5000
PR-11 100	**Deleted** ~~*"The system shall survive transient excitation of -10g vertically and ± 5 g horizontally during landing as specified in the BX_REF_BEXUS_User Manual_v7-4_04Dec18 [1]."*~~ *See DG-11-400.*	2000

A.5 Design Requirements

Requirement ID	Description	WP
DG-01 100	**The material used in MCSD shall be biocompatible with the C. elegans.**	5100
DG-01 200	**The system shall have a filter that retains the C. elegans within its chambers and allows fluid exchange.** *The system shall have a filter that retains the C. elegans within its chambers*	5100
DG-02 100	**The electric motor shall use an encoder.** *This combined with the abutment of the MCSD will allow the system to know which chamber is being analyse by the imaging system and connected to the fluidic system*	3000/5000
DG-02 200	**The electric circuit for the motor driving the Geneva drive shall have safety circuit to prevent any voltage and current spike.**	3000/5000
DG-03 101	**The fluidic network should have a bubble trap to prevent bubbles from going inside the sample chamber.**	5000
DG-03 201	**The plane side of the MCSD and the imaging plane should be perpendicular to the direction of gravity.** *In this orientation, the sedimentation doesn't obstruct the imaging system*	5000
DG-03 300	**The Fluidic system below the MCSD shall be aligned with the imaging system. This will enable FC-03 20c and allow us to see in real-time the impact of the drug that we will pump it into the chamber.**	5000
DG-04 100	**The dimension of the pressure vessel shall not exceed a 2U CubeSat format.** *A 2U CubeSat format is defined as 20cm×10cm×10cm*	2000
DG-04 200	**The pressure vessel shall be designed to statically hold the experiment assembly.** *Extra requirements likely to follow underneath*	2000
DG-04 300	**The system shall be rigidly mountable to the BEXUS gondola.The BEXUS manual** (EuroLaunch, 2020) **stated that stress calculation or load analysis needs to be shown that the mounting is strong enough.**	2000
DG-04 400	**deleted** ~~*The pressure vessel shall be designed to comply with the Swedish Law AFS 2016:1.*~~ *After studying the law, it was not applicable for the system.*	
DG-04 500	**The pressure vessel shall be designed with at least 2 x safety factor as specified by the BEXUS organiser.**	2000
DG-05 100	**The dimension of the system shall not exceed a 3U CubeSat format.** *(2 U pressure vessel + 1U bus) A 3U CubeSat format is defined as 30cm×10cm×10cm*	2000
DG-06 100	**The system shall have a panel-mounted with a 4 pin, male, box mount receptacle MIL–C-26482P series 1 connector with an 8-4 insert arrangement (MS3112E8-4P) to connect the system to the BEXUS power bus. The specification is determined by the BX_REF_BEXUS_User Manual_v7-4_04Dec18 [1]. A suggested connector is Amphenol PT02E8-4P. Refer to Chapter 6.2 in the manual.**	3000

DG-07 100	**The system shall have a panel-mounted with RJF21B with a CODE A insert to connect to the BEXUS E-link via an RJ45 cable mated to the MIL-C-26482-MS3116F-12-10P. Refer to BX_REF_BEXUS_User Manual_v7-4_04Dec18 [1] in Chapter 6.3. The RJ45 mated to the MIL-C-26482-MS3116F-12-10P will be provided by the SSC.**	3000
DG-07 200	**The system shall connect to the inside of the RJF21B using an RJ45 cable.** *This connection connects the experiment to a connector on the RJF21B which is connected to another RJ45 that connect to the BEXUS E-Link*	3000
DG-08 101	**The system except for the C. elegans, growth media and preservative should be reusable between testing phases and flight campaign.** *Reusable design is needed to perform tests at "low-cost."*	5000/2000/3000
DG-09 100	**The system shall have an override function to control the system from the ground station.** *In the event non-nominal experiment operation*	4000/3000
DG-09 200	**A safe mode shall be implemented.** *In the case of failure, it will ensure reboot of the system, a minimal level of temperature regulation and that data is safe*	4000
DG-10 100	**The temperature of the internal environment with C. elegans shall never be at a temperature below +10 C until end of experiment operation.** *Otherwise, the survival rate would be too low for the total number of worms. WARNING The CubeSat may be outside mounted on the gondola without any power for at least 30 min*	2000
DG-10 200	**The system shall maintain the internal environment at +12°C ±2°C during pre-flight operation.** *The medium-full life cycle of a C. elegans is around 15 days. At that low temperature, C. elegans would be in a low metabolic state, and they will age more slowly. This enables us to experiment on C. elegans at the stage that we want during operation while handing over the system with worms up to 96 hours before launch*	2000
DG-10 300	**The system shall maintain the internal environment at +20°C ±2°C during experiment operation.** *At this temperature, C. elegans metabolic rate is nominal and they behave normally*	2000
DG-11 100	**The experiment shall operate nominally within the temperature profile of a BEXUS flight as stated in BX_REF_BEXUS_User Manual_v7-4_04Dec18 [1]** *All system including the blanket*	2000/3000
DG-11 200	**The system should function and perform nominally in pressure environment between 1 bar and 5 mbar as stated in BX_REF_BEXUS_User Manual_v7-4_04Dec18 [1]** *the system excluding the blanket*	2000/3000

DG-11 300	**The system shall and perform nominally when the environment of DG-11 100 and DG-11 200 are combined as suggested in BX_REF_BEXUS_User Manual_v7-4_04Dec18 [1]** *the system excluding the blanket*	2000/3000
DG-11 400	**The system shall be compatible with the pre-flight, count down, flight and post-flight vibration environment as detailed in the BX_REF_BEXUS_User Manual_v7-4_04Dec18 [1]** *the system excluding the blanket*	2000/3000
DG-11 500	**The system shall cope with a static load of at least 10 times the weight of the functional system as stated in the BX_REF_BEXUS_User Manual_v7-4_04Dec18 [1]** *the system excluding the blanket*	2000
DG-12 100	**CubeSats materials shall have a Total Mass Loss (TML) < 1.0 %** *P POD requirement a list of NASA approved low out-gassing materials can be found at: http://outgassing.nasa.gov*	2xxx
DG-12 200	**The 1 U bus shall accommodate ascent vent**	2000/3000
DG-13 100	**Deleted**	
DG-14 100	**Deleted** ~~*The system shall have a filter that retain the C. elegans within its chambers*~~	
DG-15 100	**The system shall not consume at any time more than 40 W.**	3000/5000
DG-15 110	**The average consumption of the system shall be less than 25 W during pre-flight and experiment operation**	3000/5001
DG-15 200	**The system shall not consume at any time more than 2 A on the BEXUS battery**	3000/5002
DG-15 210	**The systems shall not consume on average more than 1 A on the BEXUS battery**	3000/5003
DG-16 100	**Deleted** ~~*"The pressure vessel shall accommodate a pressure inlet allowing to overpressure vessel to a minimum of 2 bar under atmospheric condition outside the system."*~~ This inlet would be unpractical for the system. The inlet would have enable to verify the DG-04-500 using flight elements of BAMMsat exclusively, but it was decided to implement a lid with a pressure inlet only for test T 07, and BAMMsat will fly with a flat lid.	2000
DG-17 100	**The material that will be in contact with a chemical or have to contain a leak shall be compatible with the chemical. This includes compatibility under operating shocks, vibration, pressure, temperature and reactivity as suggested in the Esrange Safety manual v8.1.**	2000/5000

A.6 Operational Requirements

Requirement ID	Description	WP
OP-01 100	**The operation and experiment procedure shall comply with any Swedish and UK law for handling and experimenting with C. elegans.** *Because a scientific experiment on living organisms can raise ethical concerns among the public, we would like to mention that there is no ethic guideline associated with C. elegans.*	1000
OP-01 200	**The design, test and qualification procedure for the pressure vessel shall be approved by the ESRANGE Safety Board:**	1000
OP-03 100	**The vibration of the system during transport shall be monitored from Cranfield to Esrange.** *To be able to testify the integrity of the hardware*	1000
OP-04 100	**On the ground, before launch and after integration, the system shall be able to evaluate the health status of C. elegans worms.**	1000
OP-06 100	**Any part of the system that will be in contact with the C. elegans shall be sterilised before assembly.**	5000
OP-07 100	**The system shall be mounted on the gondola behind the gondola frame for protection and to expose the system to dynamic solar irradiance.**	1000
OP-08 100	**The system shall be capable of actively heating the temperature of the internal environment before the start of the experiment.** *Heating-up the system changes the C. elegans from being in low metabolic phase to active phase to increase metabolic activity in preparation of experiment operation.*	2000
OP-09 100	**The system shall perform the nominal experiment sequence autonomously from the start of the experiment to the end of the experiment.**	4000
OP-10 100	**At FCT the system shall be handed over to SSC and not physically access after until retrieval. Only applicable if the launch is performed on day 5 or 6 or 7**	5000/1000

A.7 Constrains

Requirement ID	Description	WP
CT-01 100	**The system described above shall be designed, manufactured, tested, operated by a team of students from Cranfield University and Exeter University.**	all
CT-02 100	**The system described above shall be designed, manufactured, tested, operated between December 2019 and October 2020.**	all
CT-03 100	**The system shall fit the outer dimensions of a 3 U CubeSat without the tuna can antenna. (300 * 100 *100 mm)**	2000

Appendix B BAMMsat-on-BEXUS verification matrix

ID	Requirement text	Method	status
FC-01 100c	The system shall provide a viable and nutritious internal environment to ensure the viability and a low metabolic rate of the C. elegans during the pre-flight operations.	**Error! Reference source not found.**: Check health status of *C. elegans* by verifying motility through imaging system	V
FC-01 200c	The system shall provide a viable and nutritious internal environment to ensure the viability of the C. elegans during experiment operation.	**Error! Reference source not found.**: Check health status of *C. elegans* by verifying motility through imaging system	V
FC-02 110c	The system shall measure and log internal temperature during pre-flight and experiment operation.	**Error! Reference source not found.**: Check that the temperature sensor is giving correct readings	V
FC-02 130c	The system shall measure and log internal pressure during pre-flight and experiment operation.	**Error! Reference source not found.**: Check that the pressure sensor is giving correct readings	V
FC-02 140c	The system shall measure and log internal relative humidity during pre-flight and experiment operation.	**Error! Reference source not found.**: Check that the humidity sensor is giving correct readings	V

FC-02 160c	The system shall measure and log the fluid pressure during pre-flight and experiment operation.	**Error! Reference source not found.**: Check that the fluid pressure sensor is giving correct readings	Waived
FC-02 170c	The system shall measure and log fluidic volumetric rate during pre-flight and experiment operation.	**Error! Reference source not found.**: Check that the fluidic volumetric rate sensor is giving correct readings	V
FC-02 210c	The system shall measure and log the external temperature during pre-flight and experiment operation.	**Error! Reference source not found.**: Check that the temperature sensor is giving correct readings	V
FC-02 220c	The system shall measure and log the external absolute pressure during pre-flight and experiment operation.	**Error! Reference source not found.**: Check that the pressure sensor is giving correct readings	Waived
FC-02 230c	The system shall measure and log the external solar illumination during pre-flight and experiment operation.	**Error! Reference source not found.**: Check that the photodiodes are providing proper readings	Partially verified
FC-03 100c	The system shall take and log static images and video of the C. elegans inside the MCSD via an imaging system during pre-flight operation and experiment operation to evaluate the health status of the C. elegans.	**Error! Reference source not found.**, **Error! Reference source not found.**: Check that the imaging system is providing images and video of C.elegans	V

FC-03 200c	The system shall be able to take and log videos of a chamber while the media of this last one is being replaced.	**Error! Reference source not found.**,**Error! Reference source not found.**: Check that the imaging system is providing images and video of media replacement	V
FC-04 100c	The system shall determine which side is being illuminated by the sun.	**Error! Reference source not found.**: Compare the position of the Sun with the readings of the photodiodes	Waived
FC-05-100c	The system shall segregate the *C. elegans* population in chambers in the MCSD	Review that the design is suitable to segregate *C. elegans* in chambers. **Error! Reference source not found.**: Check that the system is able to properly segregate the *C. elegans* in the chambers.	V
FC-05 200c	The system shall pump different type of media inside the MCSD.	**Error! Reference source not found.**: Check that the fluidic system is capable of pumping different types of media into the chambers	Waived
FC-05 300c	The system shall pump different type of media out the MCSD into a fluidic waste reservoir.	**Error! Reference source not found.**: Check that the fluidic system is capable of pumping different types of	Waived

		media out of the chambers into a fluidic waste reservoir	
FC-05 400c	The system shall measure and log the angular position of the MCSD in reference to the imaging system.	**Error! Reference source not found.**: Check that position of the MCSD calculated by the system represents the position of the MCSD	V
FC-06 100c	The system shall transmit internal and external status data to the ground station via the BEXUS E-Link during pre-flight operation and experiment operation.	**Error! Reference source not found.**: Check the transmission of the data to the ground station	V
FC-06 200c	The system shall be able to receive and execute commands from the ground station via the BEXUS E-Link.	**Error! Reference source not found.**: Check that the commands sent from the ground station are received and executed	V
FC-06 300c	The ground support system shall have a user interface to display housekeeping information, operational sequences during pre-flight and experiment operation.	Review that the design of the ground support system includes a user interface to display housekeeping information, operational sequences during pre-flight and experiment operation. **Error! Reference source not found.**: Check that the ground support	V

		system displays correctly housekeeping information, operational sequences during pre-flight and experiment operation. **Note – currently only using command line user interface.**	
FC-06 400c	The ground support system shall have a user interface to transmit override commands sequence to the systems during pre-flight and experiment operation.	Review that the design of the ground support system includes a user interface to transmit override commands. **Error! Reference source not found.**: Check that the override functionality of the ground support system works	V
FC-07 100c	The system shall rotate the MCSD via a Geneva drive to address independent chamber for fluidic and imaging.	**Error! Reference source not found.**: Check that the system can rotate the Geneva drive to address independent chamber for fluidic and imaging	V
FC-08 100	The Pressure vessel shall be able to contain a leak of media from the fluidic system that would happen after the FCT.	Review of the design of the pressure vessel, ensuring can contain a leak	V

PR-01 100	The system shall segregate the *C. elegans* population into 16 groups of 10 ±5 L4 stage *C. elegans.*	Verification by inspection that the MCSD includes at least 16 individual chambers. Inspection will be performed at launch site during biological integration with flight hardware. Check that the amount of *C. elegans* contained in each chamber is in the range 10±5 in each well	NV
PR-03 100	The pressure vessel shall maintain the internal atmospheric pressure when closed at the ground in a range of ±0.2 bar during the pre-flight and experiment operation.	**Error! Reference source not found.**: Check that the pressure vessel can maintain the internal pressure when closed in a range of 1±0.2 bar while inside a vacuum chamber. **Error! Reference source not found.**, **Error! Reference source not found.**: Check that the internal pressure is maintained in a range of ±0.2 bar during the pre-flight and experiment operation.	V
PR-04 100	The system shall measure the internal temperature between +0 °C and +30°C.	Review of the range of operation of the	V

		temperature sensors within the specifications provided by the supplier	
PR-04 110	The system shall measure and log the internal temperature at least every second.	Review of the software for the measurement and log of the temperature sensors. **Error! Reference source not found.**: Check that the temperature is measured and logged at least every second.	V
PR-04 120	The system shall measure the internal temperature with a ± 1 °C accuracy.	**Error! Reference source not found.**: Check that the temperature sensors are capable of measuring temperature with an accuracy of ± 1 °C	V
PR-04 200	The system shall measure the external temperature between -80 °C and +30 °C with.	Review of the range of operation of the temperature sensors within the specifications provided by the supplier	V
PR-04 210	The system shall measure and log the external temperature at least every 10 second.	Review of the software for the measurement and log of the temperature sensors. **Error! Reference source not found.**: Check that the	V

		temperature is measured and logged at least every 10 seconds.	
PR-05 100	The system shall measure the internal absolute pressure between 500 hPa and 2500 hPa.	Review of the range of operation of the pressure sensors within the specifications provided by the supplier	V
PR-05 110	The system shall measure the internal absolute pressure at least every second.	Review of the software for the measurement and log of the pressure sensors. **Error! Reference source not found.**: Check that the pressure is measured and logged at least every second.	V
PR-05 120	The system shall measure the internal absolute pressure with ± 200 Pa accuracy.	Review of the accuracy of the pressure sensors within the specifications provided by the supplier	Waived
PR-06 101	The system should measure the relative humidity of the internal environment between 5% and 100%.	Review of the range of operation of the humidity sensors within the specifications provided by the supplier	V

PR-06 111	The system should measure the relative humidity of the internal environment at least every 60 sec.	Review of the software for the measurement and log of the humidity sensors. **Error! Reference source not found.**: Check that the humidity is measured and logged at least every 60 seconds.	V
PR-06 121	The system should measure the relative humidity of the internal environment with a 5% accuracy.	Review of the accuracy of the humidity sensors within the specifications provided by the supplier	V
PR-07 100	The system shall take and log static images of the *C. elegans* with a resolution of 0.025 mm over *C. elegans* with at least 3280 x 2464 pixels.	**Error! Reference source not found.**: Check that the imaging system can take and log static images of the C. elegans with a resolution of 0.025 mm over C. elegans with at least 3280 x 2464 pixels.	V
PR-07 200	The system shall capture and log video with a minimum resolution of 0.075 mm over *C. elegans* with at least 1080 x 1920 pixels.	**Error! Reference source not found.**: Check that the imaging system can capture and log video with a minimum resolution of 0.075 mm over C. elegans	V

		with at least 1080 x 1920 pixels.	
PR-07 210	The system shall capture and log video with a minimum of 30 images per second.	**Error! Reference source not found.**: Check that the imaging system can capture and log video with a minimum of 30 images per second.	V
PR-08 200	The system shall measure the fluidic pressure between the inlet and outlet of the pump between 0 and 20 000 Pa.	Review of the range of operation of the fluidic pressure sensors within the specifications provided by the supplier	V
PR-08 210	The system shall measure and log the fluidic pressure between the inlet and outlet of the pump at least every second.	Review of the software for the measurement and log of the fluidic pressure sensors. **Error! Reference source not found.**: Check that the fluidic pressure is measured and logged at least every second.	V
PR-08 220	The system shall measure the fluidic pressure between the inlet and outlet of the pump with a ±200 Pa accuracy for each chamber pumped.	Review of the accuracy of the fluidic pressure sensors within the specifications provided by the supplier	Waived
PR-08 300	The system shall measure and log the fluidic mass flow rate passing through the multi-	Review of the range of operation of the fluidic	V

	chamber sample disc between 0 µL/min and 1000 µL/min.	mass flow rate sensors within the specifications provided by the supplier	
PR-08 310	The system shall measure and log the fluidic mass flow rate passing through the multi-chamber sample disc at least every second.	Review of the software for the measurement and log of the mass flow rate sensors. **Error! Reference source not found.**: Check that the mass flow rate is measured and logged at least every second.	V
PR-08 320	The system shall measure and log the fluidic mass flow rate passing through the multi-chamber sample disc with a ± 50 µL/min accuracy.	Review of the accuracy of the fluidic mass flow rate sensors within the specifications provided by the supplier	Waived
PR-09 100	Once connected to the BEXUS E-Link, the system shall transmit via BEXUS E-Link housekeeping data from internal environment at least every second except imaging data.	Review of the design of the software for the transmission of data of the internal environment. **Error! Reference source not found.**: Check that the system can transmit housekeeping data from internal environment at least every second except imaging data.	V

PR-09 200	Once connected to the BEXUS E-Link, the system shall transmit via BEXUS E-Link data from external environment at least every 10 sec.	Review of the design of the software for the transmission of data of the external environment. **Error! Reference source not found.**: Check that the system can transmit housekeeping data from external environment at least every 10 sec.	V
PR-10 100	The system shall carry on-board a minimum of 10 ml of media. ~ 6 ml of growth media + ~1 ml of fixative + margin.	Review of the design to ensure that the system can carry a minimum of 10 mL of media. Inspection of the quantity of media that the system is capable of carrying.	V
PR-10 101	The system should carry on-board a minimum of 95 ml of media. ~ 80 ml of growth media + ~ 5 ml of drudged media + ~5 ml of fixative + margin.	Review of the design to ensure that the system can carry a minimum of 95 mL of media. Inspection of the amount of the media that the system is capable of carrying.	Waived
PR-11 100	The system shall survive transient excitation of -10g vertically and ± 5 g horizontally during	**Error! Reference source not found.**: Check that the system is capable of	Waived

	landing as specified in the BX_REF_BEXUS_User Manual_v7-4_04Dec18 [1].	withstanding a transient excitation of -10g vertically and ± 5 g horizontally	
DG-01 100	The material used in MCSD shall be biocompatible with the C. elegans.	**Error! Reference source not found.**: Check the biocompatibility of the MCSD	V
DG-01 200	The system shall have a filter that retains the C. elegans within its chambers and allows fluid exchange.	**Error! Reference source not found.** and **Error! Reference source not found.**. Check that the pore size of the filter is capable of retaining the *C. elegans* within the chamber while allowing fluid exchange.	Waived
DG-02 100	The electric motor shall use an encoder.	Review of the design of the motor to ensure that it has an encoder	V
DG-02 200	The electric circuit for the motor driving the Geneva drive shall have safety circuit to prevent any voltage and current spike.	Review of the design of the electric circuit for the motor driving the Geneva drive, ensuring that it has a safety circuit	V
DG-03 101	The fluidic network should have a bubble trap to prevent bubble coming inside the sample chamber.	Review of the design of the fluidics, making sure that it includes a bubble trap to	Waived

		prevent bubble coming inside the sample chamber.	
DG-03 201	The plane side of the MCSD and the imaging plane should be perpendicular to the direction of gravity.	Review of the design of the positioning of the MCSD and the imaging plane. Inspection of the positioning of the MCSD and the imaging plane with respect to the direction of gravity.	V
DG-03 300	The Fluidic system below the MCSD shall be aligned with the imaging system. This will enable FC-03 20c and allow us to see in real time the impact of the drug that we will pump it into the chamber.	Review of the positioning of the fluidic system. Inspection of the positioning of the fluidic system, making sure that it is below the MCSD and aligned with the imaging system.	V
DG-04 100	The dimension of the pressure vessel shall not exceed a 2U CubeSat format.	Review of the dimensions of the pressure vessel	V
DG-04 200	The pressure vessel shall be designed to statically hold the experiment assembly.	Review of the mechanical design of the pressure vessel. Analysis using FEA of the static stresses and deformations of the pressure vessel	V

DG-04 300	The system shall be rigidly mountable to the BEXUS gondola. BX_REF_BEXUS_User Manual_v7-4_04Dec18 [1] stated that stress calculation or load analysis needs to be shown that the mounting is strong enough.	Review of the mechanical design of the gondola mounting structure. Analysis using FEA of the static stresses and deformations of the full system, including the gondola mounting structure	V
DG-04 500	The pressure vessel shall be designed with at least 2 x safety factor as specified by the BEXUS organiser.	**Error! Reference source not found.**: Check that the pressure vessel can withstand an overpressure of 2x the nominal pressure difference during flight	V
DG-05 100	The dimension of the system shall not exceed a 3U CubeSat format.	Review of the dimensions of the system	V
DG-06 100	The system shall have a panel mounted with a 4 pin, male, box mount receptacle MIL–C-26482P series 1 connector with an 8-4 insert arrangement (MS3112E8-4P) to connect the system to the BEXUS power bus. The specification is determined by the BX_REF_BEXUS_User Manual_v7-4_04Dec18 [1]. A suggested connector is Amphenol PT02E8-4P. Refer to Chapter 6.2 in the manual.	Review of the design of the BEXUS power bus connection. Inspection of the BEXUS power bus connection.	V
DG-07 100	The system shall have a panel mounted with RJF21B with a CODE A insert to connect to the	Review of the design of the BEXUS E-link connection.	V

	BEXUS E-link via an RJ45 cable mated to the MIL-C-26482-MS3116F-12-10P. Refer to BX_REF_BEXUS_User Manual_v7-4_04Dec18 [1] in Chapter 6.3. The RJ45 mated to the MIL-C-26482-MS3116F-12-10P will be provided by the SSC.	Inspection of the BEXUS E-link connection.	
DG-07 200	The system shall connect to the inside of the RJF21B using an RJ45 cable.	Review of the design of the connection to the inside of the RJF21B. Inspection of the connection to the inside of the RJF21B.	V
DG-08 101	The system except the *C. elegans*, growth media and preservative should be reusable between testing phases and flight campaign.	Review of the design of the system elements, ensuring their reusability	V
DG-09 100	The system shall have an override function to control the system from the ground station.	Review of the software, ensuring that an override function is implemented. T19: Check that the override function can successfully control the experiment from the ground support system	V
DG-09 200	A safe mode shall be implemented.	Review of the software, ensuring that a safe mode is implemented. T19: Check that the safe mode has	V

		been implemented correctly	
DG-10 100	The temperature of the internal environment *with C. elegans* shall never be at a temperature below +10 ^{o}C until end of experiment operation.	**Error! Reference source not found.**, **Error! Reference source not found.**: Check that the temperature of the internal environment with C. elegans is never at a temperature below +10 C. Thermal analysis of the experiment operation including the thermal control system to ensure the capability to control the temperature to maintain it in the required range	V
DG-10 200	The system shall maintain the internal environment at +12°C ±2°C during pre-flight operation.	**Error! Reference source not found.**: Check that the temperature of the internal environment is maintained at +12°C ±2°C during pre-flight operation. Thermal analysis of the pre-flight operation including the thermal control system to ensure the capability to control the temperature to maintain it at +12°C ±2°C	V

DG-10 300	The system shall maintain the internal environment at +20°C ±2°C during experiment operation.	**Error! Reference source not found.**: Check that the temperature of the internal environment is maintained at +20°C ±2°C during flight operation. Thermal analysis of the flight operation including the thermal control system to ensure the capability to control the temperature to maintain it at +20°C ±2°C	V
DG-11 100	The experiment shall operate nominally within the temperature profile of a BEXUS flight as stated in BX_REF_BEXUS_User Manual_v7-4_04Dec18 [1]	**Error! Reference source not found.**: Check that the experiment can operate nominally within the temperature profile of a BEXUS flight as stated in BX_REF_BEXUS_User Manual_v7-4_04Dec18 [1]. Thermal analysis of the flight operation including the thermal control system to ensure the capability to control the temperature within the temperature profile of a BEXUS flight as stated in	V

		BX_REF_BEXUS_User Manual_v7-4_04Dec18 [1]	
DG-11 200	The system should function and perform nominally in pressure a environment between 1 bar and 5 mbar as stated in BX_REF_BEXUS_User Manual_v7-4_04Dec18 [1]	**Error! Reference source not found.**: Check that the experiment can operate nominally within the pressure profile of a BEXUS flight as stated in BX_REF_BEXUS_User Manual_v7-4_04Dec18 [1]. Mechanical analysis of the flight operation within the pressure profile of a BEXUS flight as stated in BX_REF_BEXUS_User Manual_v7-4_04Dec18 [1]	V
DG-11 300	The system shall perform nominally when environment of DG-11 100 and DG-11 200 are combined as suggested in BX_REF_BEXUS_User Manual_v7-4_04Dec18 [1]	**Error! Reference source not found.**: Check that the system can perform nominally when environment of DG-11 100 and DG-11 200 are combined	V
DG-11 400	The system shall be compatible with the pre-flight, count down, flight and post flight vibration environment as detailed in the BX_REF_BEXUS_User Manual_v7-4_04Dec18 [1]	**Error! Reference source not found.**: Check that the mounted system is compatible with the pre-flight, count down, flight	V

		and post flight vibration environment.	
DG-11 500	The system shall cope with a static load of at least 10 time the weight of the functional system as stated in the BX_REF_BEXUS_User Manual_v7-4_04Dec18 [1]	**Error! Reference source not found.**: Check that the system can cope with a static load of at least 30 time the weight of the functional system	V
DG-12 100	CubeSats materials shall have a Total Mass Loss (TML) < 1.0 %	Similarity analysis of the materials used in for the system, comparing them with materials used in previous missions	WAIVED
DG-12 200	The 1 U bus shall accommodate ascent vent	Review of the design of the 1U bus, ensuring that it accommodates an ascent vent. Inspection of the 1U bus, ensuring that it accommodates an ascent vent	V
DG-15 100	The system shall not consume at any time more than 40 W.	**Error! Reference source not found.**, **Error! Reference source not found.**: Check the instantaneous power consumption during pre-flight and flight operations, ensuring it does not surpass	V

		40 W. Analysis of the peak power consumption that is expected considering multiple scenarios.	
DG-15 110	The average consumption of the system shall be less than 25 W during pre-flight and experiment operation	**Error! Reference source not found.**, **Error! Reference source not found.**: Check the average power consumption during pre-flight and flight operations, ensuring it does not surpass 25 W. Analysis of the average power consumption that is expected considering multiple scenarios.	V
DG-15 200	The system shall not consume at any time more than 2 A on the BEXUS battery	**Error! Reference source not found.**, **Error! Reference source not found.**: Check the intensity consumption on the battery during pre-flight and flight operations, ensuring it does not surpass 2 A	V
DG-15 210	The systems shall not consume on average more than 1 A on the BEXUS battery	**Error! Reference source not found.**, **Error! Reference source not found.**: Check the intensity consumption	V

		on the battery during pre-flight and flight operations, ensuring it does not surpass 1 A	
DG-17 100	The material that will be in contact with a chemical or have to contain a leak shall be compatible with the chemical. This includes compatibility under operating shocks, vibration, pressure, temperature and reactivity as suggested in the Esrange Safety manual v8.1.	Review of the design of the materials and chemicals used in the experiment by comparing stability and reactivity of chemicals using MSDS sheets	V
OP-01 100	The operation and experiment procedure shall comply with any Swedish and UK law for handling and experimenting with C. elegans.	Review of the operation and experiment procedure to ensure compliance with Swedish and UK law for handling and experimenting with C. elegans.	V
OP-01 200	The design, test and qualification procedure for the pressure vessel shall be approved by the ESRANGE Safety Board:	Review of the approval by the ESRANGE Safety Board of the design, test and qualification procedure for the pressure vessel	V
OP-03 100	The vibration of the system during transport shall be monitored from Cranfield to Esrange.	Review of the set up to monitor vibration during transportation of the system	V

OP-04 100	On ground, before launch and after integration the system shall be able to evaluate the health status of C. elegans worms.	Review of the operations to evaluate the health status of the *C. elegans* before launch and after integration the system	V
OP-06 100	Any part of the system that will be in contact with the C. elegans shall be sterilised before assembly.	Review of the operations to sterilise any part of the system that will be in contact with the C. elegans	V
OP-07 100	The system shall be mounted on the gondola behind the gondola frame for protection and to expose the system to dynamic solar irradiance.	Review of the positioning of the system on the gondola, making sure it is placed behind the gondola frame for protection and is exposed to dynamic solar irradiance. Inspection of the position of the system on the gondola, making sure it is placed behind the gondola frame for protection and is exposed to dynamic solar irradiance	V
OP-08 100	The system shall be capable of actively heat up the temperature of the internal environment before the start of the experiment.	**Error! Reference source not found.**: Check that the thermal control system is capable of heating up the temperature of the internal	V

		environment before the start of the experiment. Thermal analysis of the experiment operation including the thermal control system to ensure the capability to heat up the temperature of the internal environment before the start of the experiment	
OP-09 100	The system shall perform the nominal experiment sequence autonomously from the start of the experiment to the end of the experiment.	**Error! Reference source not found.**: Check that the system is capable of performing the nominal experiment sequence autonomously from the start of the experiment to the end of the experiment.	V
OP-10 100	At FCT the system shall be handed over to SSC and not physically access after until retrieval. Only applicable if the launch is performed on day 5 or 6 or 7	Review of the operations at ESRANGE	V
CT-01 100	The system described above shall be designed, manufactured, tested, operated by a team of students from Cranfield University and Exeter University.	Review of the team involved in the project	V

CT-02 100	The system described above shall be designed, manufactured, tested, operated between December 2019 and October 2020.	Review of the timeline of the project	Waived
CT-03 100	The system shall fit the outer dimensions of a 3 U CubeSat without the tuna can antenna. (300 * 100 *100 cm)	Review of the dimensions of the design of the experiment	V

Appendix C Thorlabs MAP051919-A datasheet

	ITEM	THORLABS P/N	MATERIAL
A , B	DOUBLET 1 & 2	AC127-019-A	N-BAF10 & N-SF6HT
C	HOUSING	-	BLACK ANODIZED 6061-T6 ALUMINUM
D	RETAINING RING	SM05RR	BLACK ANODIZED 6061-T6 ALUMINUM

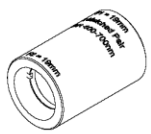

ISOMETRIC VIEW

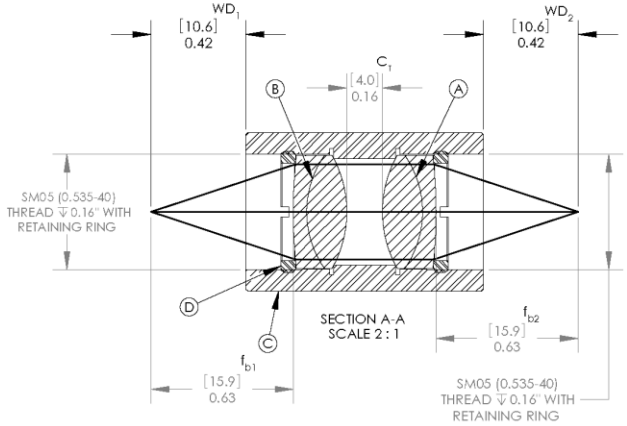

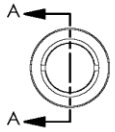

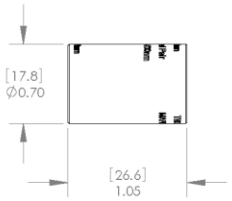

NOTES/SPECIFICATIONS:
1. FOCAL LENGTH: f1= 19.0mm f2= 19.0mm
2. MAGNIFICATION: 1:1
3. CLEAR APERTURE: > 90% OF LENS DIAMETER (Ø12.7mm)
4. DESIGN WAVELENGTHS: 486.1nm, 587.6nm, 656.3nm
5. AR COATING: BBAR Ravg < 0.5% FROM 400 - 700nm

DIMENSIONS ARE IN [mm] / in

THIS DRAWING IS FOR INFORMATION ONLY
NOT INTENDED FOR MANUFACTURING

	NAME	DATE
DRAWN	BAG	11/24/2009
ENG APPR.	SFG	12/14/2009
MFG APPR.	PM	12/14/2009

PROPRIETARY AND CONFIDENTIAL
THE INFORMATION CONTAINED IN THIS DRAWING IS THE SOLE PROPERTY OF THORLABS, INC. ANY REPRODUCTION IN PART OR AS A WHOLE WITHOUT THE WRITTEN PERMISSION OF THORLABS, INC. IS PROHIBITED.

THORLABS INC. PO BOX 366 NEWTON NJ

TITLE: 1:1 MATCHED ACHROMATIC PAIR
f_1= 19.0mm f_2= 19.0mm

MATERIAL: SEE TABLE | SIZE A | REV. D

SCALE: 1:1 | SHEET 1 OF 1

DWG. NO. 20563-E01 | PART NO. MAP051919-A

5 4 3 2 1

Appendix D BoB custom lens assembly

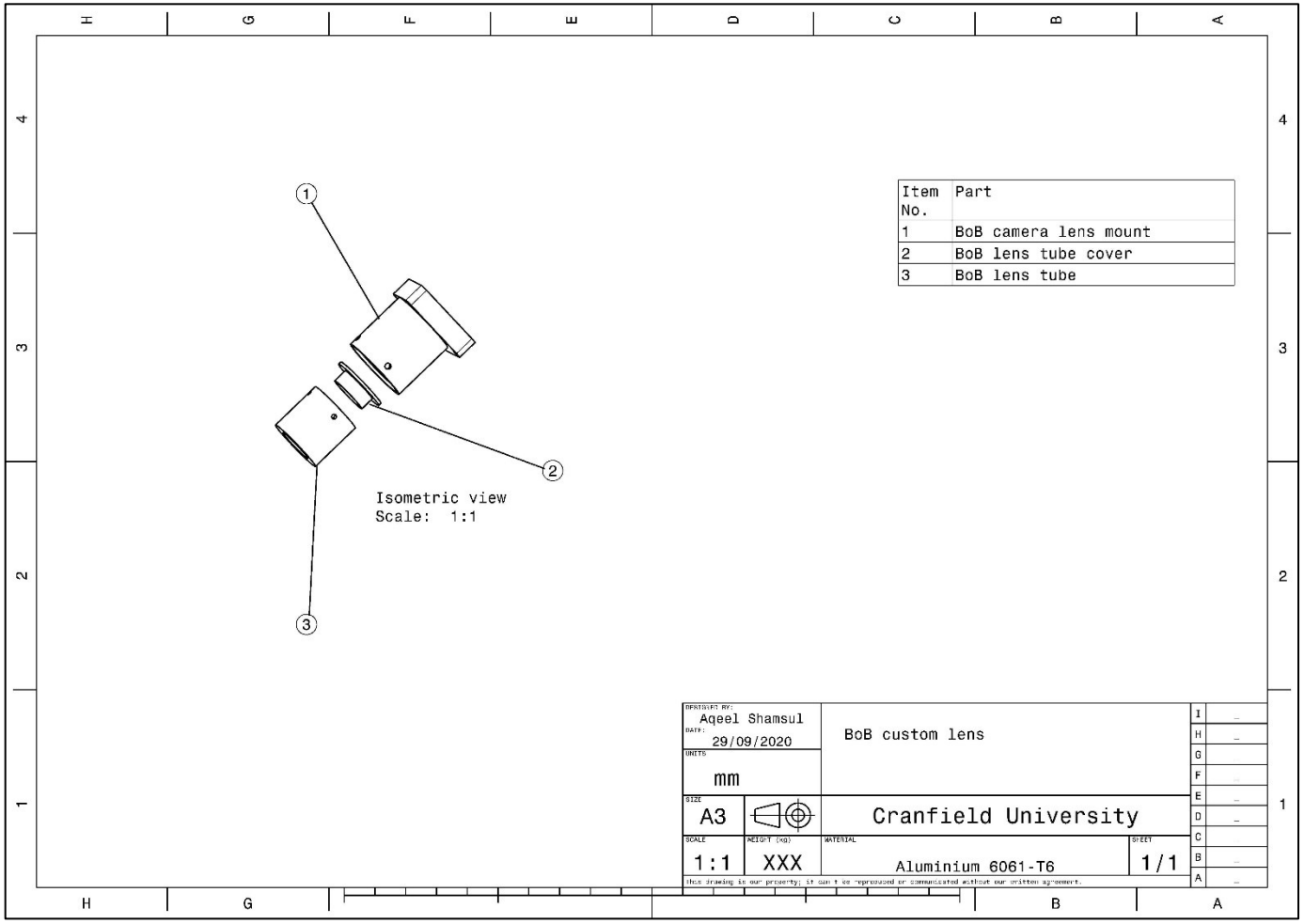

Appendix E BoB custom camera mount

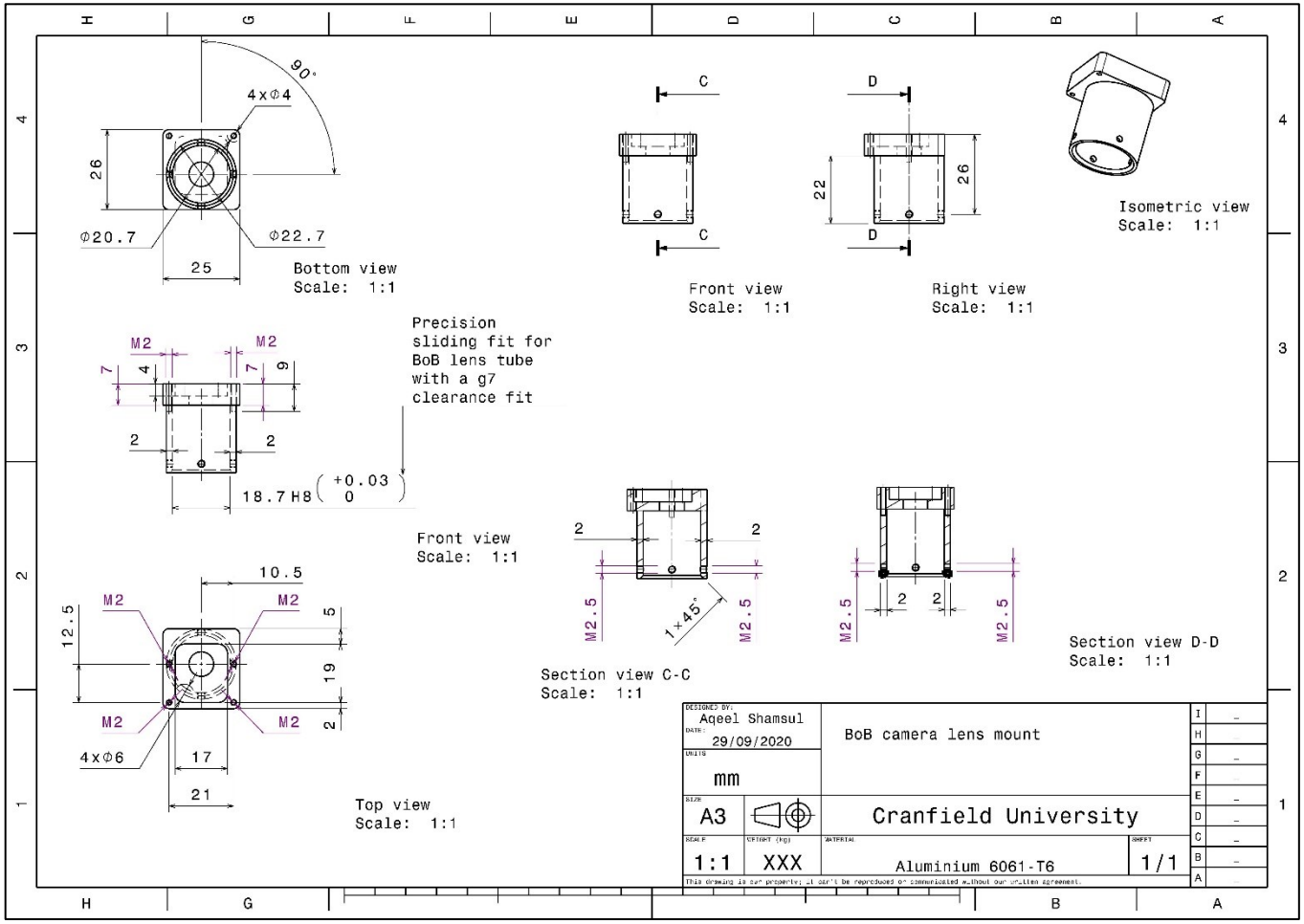

Appendix F BoB custom lens tube

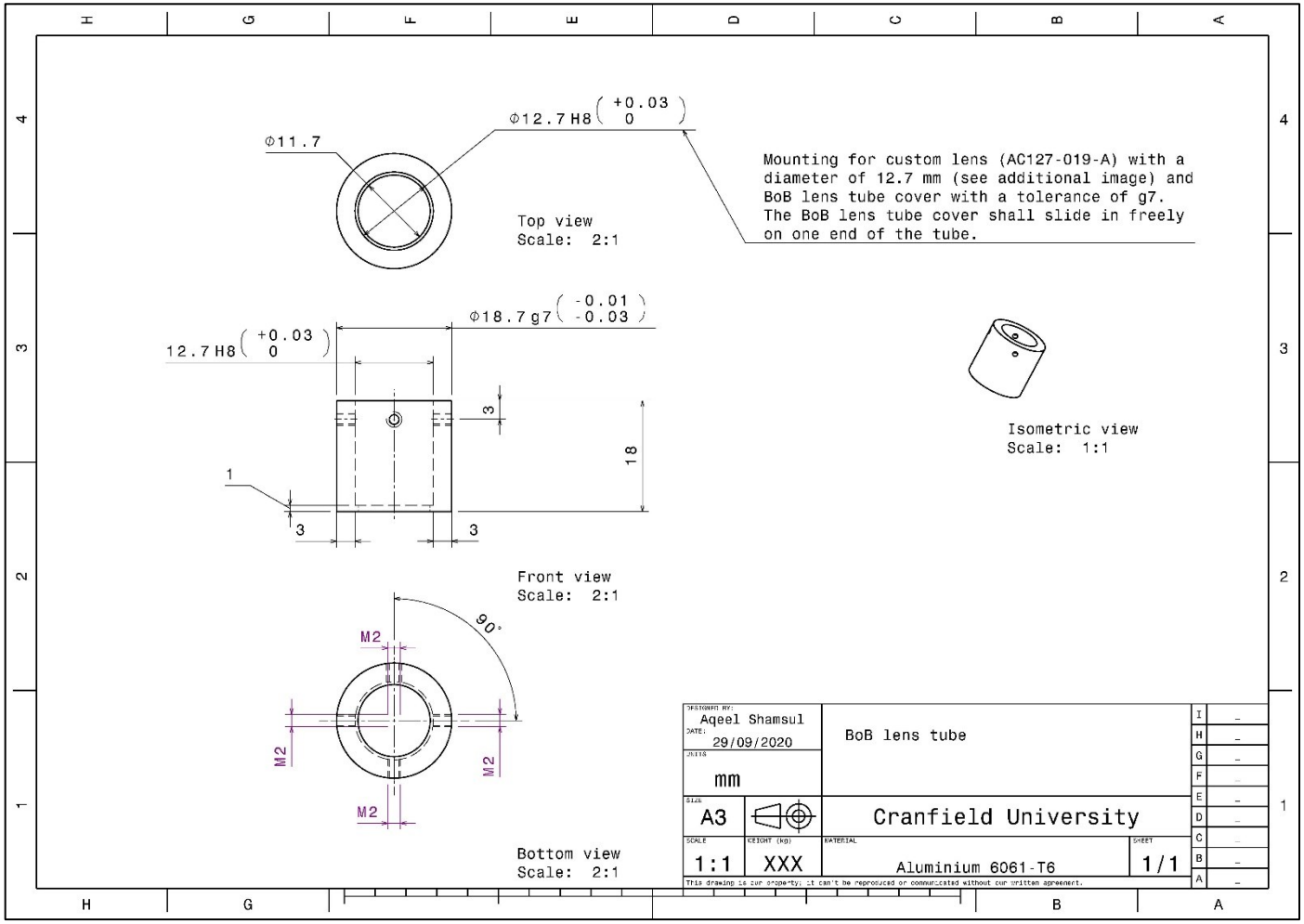

Appendix G List of publications by the author throughout the PhD research

- Shamsul, A., Sinclair, G., Bolliand, A., Chabi, A., Martinez, M., Zalasiewicz, M., Cooke, M., Cullen, D. C., Szewczyk, N., & Etheridge, T. (2021). A versatile miniaturised hardware platform to enable bioscience research in space. Journal of British Interplanetary Society, 74(10), 386–395.
- Shamsul, A., Sinclair, G., Bolliand, A., Chabi, A., Bujo, M. M. De, Zalasiewicz, M., & Cullen, D. C. (2020). BAMMsat-on-BEXUS: A technology and operation demonstration of a bioCubeSat platform on a stratospheric balloon flight educational program. 34th Small Satellite Conference.
- Shamsul, A., Cullen, D., Etheridge, T., Cooke, M., & Millard, T. (2019). BAMMsat recent development: A bioCubeSat hardware platform to enable biological studies in space. 70th International Astronautical Congress (IAC).

Appendix H Bartels Mikrotechnik mp6 datasheet

microComponents

3 The mp6-OEM controller

The mp6-OEM is a small, easy to use driving circuit developed for the micropumps of the mp6-series. It generates up to 270 Vpp voltage from a 3-5 V supply.

Its low power consumption makes it ideal for battery powered handheld devices or even solar powered devices.

The module can be integrated into a PCB design like a 14 pin DIL package.

The build-in interface allows the user to adapt frequency and/or amplitude to its application by the use of a few additional components or a microcontroller.

In order to locate Pin 1, please refer to the following figure. The pin is marked with a white spot.

3.1 Technical specifications mp6-OEM

mp6-OEM controller	Order code: mp6-OEM
The OEM-controller drives the micropump at adjustable performance in a package similar to an integrated circuit. It enables integration into system electronics or on a PCB.	
Dimensions	10.5 x 20.5 x 6 mm 0.4134 x 0.8070 x 0.2362 in.
Pumping media	liquids, gases
Max. volume flow (DI-water)	4.9 ml/min @ 3 VDC supply; 100 Hz 7 ml/min @ 5 VDC supply; 100 Hz
Adjustable parameters	amplitude, frequency
Amplitude range	85 – 270 Vpp [1]
Frequency range	25 - 226 Hz (Frequencies up to 1000 Hz are possible; please note that the amplitude will decrease in that case. Frequencies down to 1 Hz are possible with an external clock generator.)
Signal form	similar to rectangular
Power supply	2.5 – 5.5 VDC (5 V recommended for optimized performance)
Pumping media	ca. 30 mA at 5 V
Pin arrangement	DIL 14; horizontal ~2.54 mm, vertical ~7.62 mm
[1] Before May 2014: mp6-OEM have an amplitude range of 85 – 235 Vpp	

Bartels mikrotechnik

Bartels Mikrotechnik GmbH, Konrad-Adenauer-Allee 11, 44263 Dortmund, Germany
www.bartels-mikrotechnik.de, info@bartels-mikrotechnik.de
Tel: +49-231-47730-500, Fax: +49-231-47730-501

microComponents

3.2 Electrical Characteristics

Applies to a connected micropump and the internal defined frequency and slew rate.

Parameter	Symbol	Conditions	Min	Typ.	Max	Unit
Supply voltage	VDD		2.5		5.5	V
Average current consumption	IDD	VDD = 5 V (1)		30		mA
Setting range AMPLITUDE			0.35		1.3	VDC
min. voltage at pump	Vpump	AMPLITUDE = 0.5 VDC	80	85	90	Vpp
max. voltage at pump (2)	Vpump	AMPLITUDE = 1.3 VDC	260	270	280	Vpp
PWM-range AMPLITUDE			0,2		1	MHz
Frequency output	F	VDD = 5 V (1)	90	100	110	Hz
Digital Low-Signal				0		V
Digital High-Signal			2		VDD	V
Capacitance CLOCK			1.0	2.2	10	nF
Input current AMPLITUDE			1		3	µA
Operating current during Shutdown Mode				1.6		µA

(1) The signal output is determined by internal components.

(2) Before May 2014: mp6-OEM have an amplitude range of 85 – 235 Vpp, typ.

3.3 Pin layout

VDD	Supply voltage
GND	Ground
SHUTDOWN	If the micropump should be switched off, the mp6-OEM has to be set to the Shutdown Mode. Then AMPLITUDE **and** SHUTDOWN have to be set to 0 V.
CLOCK	Predefined clock signal. Frequency will be set to the nominal 100 Hz, when this pin is connected to CLOCK_INT (see image "Schematic 1" in chapter 3.6.1). (The internal capacitor is 2.2 nF.) A capacitor of 1 to 10 nF can be placed between CLOCK and GND to define other frequencies (see image "Schematic 2" in chapter 3.6.2). It is also possible to connect an external clock signal with a **quadruplicated** frequency of the micropumps frequency.
CLOCK_INT	When connected to CLOCK the frequency is set to 100 Hz.
AMPLITUDE	The amplitude can be set either with an analogue voltage between 0.35 V to 1.3 V, or with an equivalent pulse-width modulation (PWM) at a voltage level of 5 V and a pulse

microComponents

	frequency of 0.2 to 1 MHz.
SLEWRATE	Setting of the slew rate. This pin will be connected to SLEW_INT.
SLEW_INT	Internal resistor against GND for set the slew rate.
	(The internal resistor is 360 kΩ.)
GND2, GND3	Connected internally with ground (GND). No need to connect.
+P1	Piezo actuator 1, positive electrode (see chapter 3.6)
-P1	Piezo actuator 1, negative electrode (see chapter 3.6)
+P2	Piezo actuator 2, positive electrode (see chapter 3.6)
-P2	Piezo actuator 2, negative electrode (see chapter 3.6)

3.4 Typical flow behavior

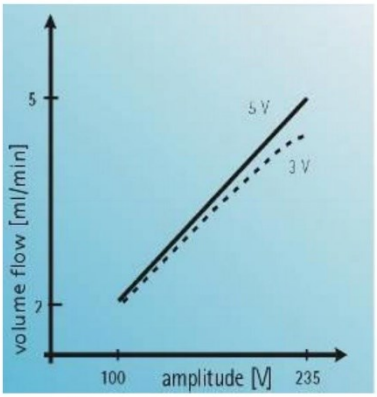

3.5 Connecting the micropump with the mp6-OEM

The micropumps of the mp6-series can be connected with the mp6-OEM via a FCC connector. More information concerning this connector and the pin layout of the micropump can be found in manual of the micropump mp6-series.

DANGER

THE "MICROPUMP OUT" CONNECTOR CAN CARRY HIGH VOLTAGE!
PLUG IN THE MICROPUMP CONTROL CABLE ONLY WHEN THE MP-X CONTROLLER IS SWITCHED OFF!

Bartels mikrotechnik

Bartels Mikrotechnik GmbH, Konrad-Adenauer-Allee 11, 44263 Dortmund, Germany
www.bartels-mikrotechnik.de, info@bartels-mikrotechnik.de
Tel: +49-231-47730-500, Fax: +49-231-47730-501

microComponents

3.6 Examples of circuiting the mp6-OEM

3.6.1 Operation with fixed settings

The mp6-OEM can operate the micropumps of the mp6-series without further external components. In this case, frequency and amplitude to the micropump are predefined to **270 V and 100 Hz** by the internal circuit.

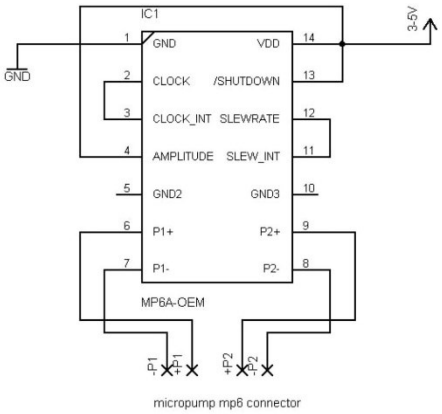

Schematic 1: Predefined amplitude of 270 V and frequency of 100 Hz by internal circuit.

3.6.2 Operation with variable settings via external components

In this example, frequency and amplitude to the micropump will be defined by external components. The amplitude can be varied in the range from 85 Vpp to 270 Vpp, the frequency from 25 Hz to 226 Hz. With frequencies above 226 Hz it is possible that the maximal amplitude will decrease. Frequencies below 25 Hz are possible too, however, the stability of the signal form has to be verified then!

Using a potential divider it is possible to change the amplitude, see image "Schematic 2" below. The voltage at the AMPLITUDE-Pin can be calculated with this formula:

$$V_{AMPLITUDE} = V_{DD} \cdot \frac{R1}{R1 + R2}$$

As an alternative to the potential divider, an appropriate potentiometer (e.g. 10 kΩ) is possible too.

Bartels Mikrotechnik GmbH, Konrad-Adenauer-Allee 11, 44263 Dortmund, Germany
www.bartels-mikrotechnik.de, info@bartels-mikrotechnik.de
Tel: +49-231-47730-500, Fax: +49-231-47730-501

microComponents

The relation of the voltage at the AMPLITUDE-Pin to the output voltage is shown in image "OEM-Behavior 1" below.

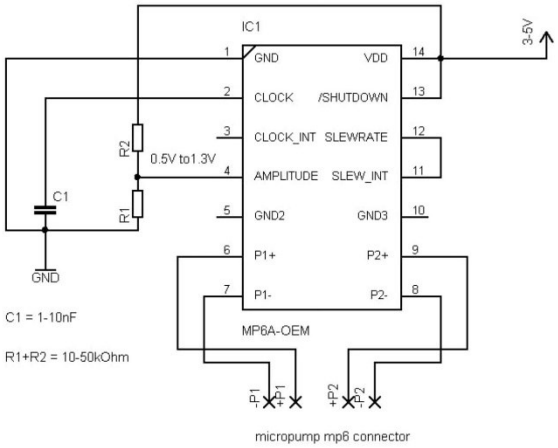

Schematic 2: Defining frequency and amplitude with external components.

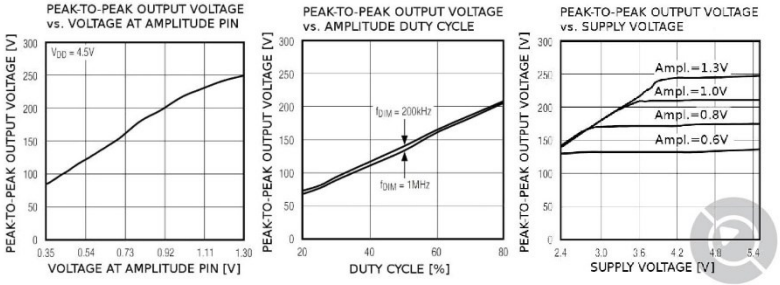

OEM-Behavior 1: Output voltage changed with external components.

Variation of frequency is realized with a capacitor of 1 to 10 nF. Typical capacitances are shown in the image "OEM-Behavior 2" below.

For frequencies lower than 25 Hz an external frequency signal has to be uses, as explained in chapter 3.6.3!

Bartels Mikrotechnik GmbH, Konrad-Adenauer-Allee 11, 44263 Dortmund, Germany
www.bartels-mikrotechnik.de, info@bartels-mikrotechnik.de
Tel: +49-231-47730-500, Fax: +49-231-47730-501

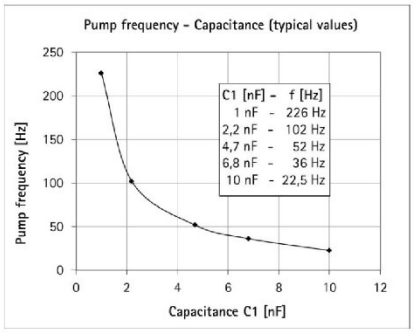

OEM-Behavior 2: Typical capacitances for different frequencies.

3.6.3 Operation with variable settings via microcontroller

Using a microcontroller to operate the micropump, a quadruplicated frequency of the final micropumps frequency has to be connected to the CLOCK Pin. With this procedure, single-digit frequencies can be achieved.

Please take into account to set the pulse-width of the frequency duty cycle at a level of 95% when operating at frequencies lower than 25 Hz.

The amplitude can be set either with an analogue voltage between 0.35 V to 1.3 V, or with an equivalent pulse-width modulation (PWM) at a voltage level of 5 V and a pulse frequency of 0.2 to 1 MHz at the pin AMPLITUDE.

The PWM signal must have an amplitude of at least 1.3 V and maximal the same as the supply voltage to ensure that the output voltage is only dependent on the duty cycle!

For minimizing the power consumption, the mp6-OEM can be switched off. One way is to set the mp6-OEM into the Shutdown Mode; then AMPLITUDE and SHUTDOWN have to be set to 0 V. The other way is to interject the power supply.

Bartels Mikrotechnik GmbH, Konrad-Adenauer-Allee 11, 44263 Dortmund, Germany
www.bartels-mikrotechnik.de, info@bartels-mikrotechnik.de
Tel: +49-231-47730-500, Fax: +49-231-47730-501

Appendix I Sensirion LPG10 datasheet

SENSIRION
THE SENSOR COMPANY

LPG10-1000 Liquid Flow Sensor

Digital Planar Package Sensor

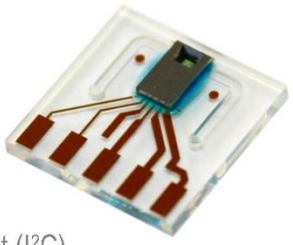

- Ultra small size
- Excellent repeatability
- Bio-compatible & inert materials
- Calibrated and temperature compensated digital output (I^2C)

Product Summary

Unique CMOSens® planar packaging technology enables non-invasive measurement of liquid flow inside a cost-effective planar form factor. The flow channel passes through the planar substrate and is connected to fluidic channels via a manifold. The fluid is only in contact with the glass channel. The digital microsensor chip provides the full signal processing functionality for a fully calibrated, temperature-compensated digital output.

Integration of the LPG10-1000 Liquid Flow Sensor

Due to the dramatically reduced size and downmount fluidic connections, the LPG10-1000 allows an outstandingly compact mechanical, fluidic, and electronic integration. To receive support and acceleration on initial testing, please contact Sensirion about existing integration solutions.

1 Sensor Performance

Table 1: Performance of LPG10-1000 (all data for medium H_2O, 23 °C, 1 bar_{abs} unless otherwise noted)

Parameter	LPG10-1000	Unit
Full scale flow rate	1000	µl/min
Sensor output limit[a]	1500	µl/min
Accuracy below full scale (whichever error is larger)	5 0.25	% of measured value % of full scale
Repeatability error from zero to full scale (whichever error is larger)	0.5 0.025	% of measured value % of full scale
Temperature coefficient (additional error / °C; whichever is larger)	0.1 0.005	% of measured value / °C % of full scale / °C
Flow detection response time τ_{63}	40	ms
Response time on power-up	120	ms
Operating temperature	+5 ... +50 (+41 ... +122)	°C (°F)
Operating humidity	0...95%, non-condensing	% RH
Storage temperature[b]	-40 ... +60 (-40 ... +140)	°C (°F)
Storage humidity	0...95%, non-condensing	% RH
Recommended maximum operating pressure[c]	3 (43)	bar (psi)
Burst pressure[c]	7 (101)	bar (psi)

[a]Flow rate at which the sensor output saturates, see section 2 for performance specifications between full scale and saturation point
[b]Flow path empty
[c]Pressures listed are mechanical limits of the glass substrate; Burst pressure of manifold assembly depends on actual manifold seal design.

2 Specifications Chart

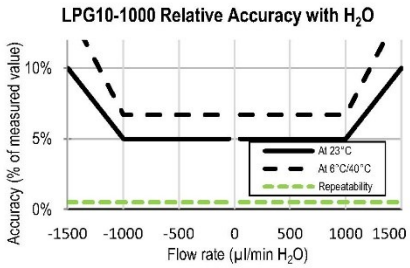

Figure 1: Sensor accuracy and repeatability (% of measured value) across the sensor's flow range

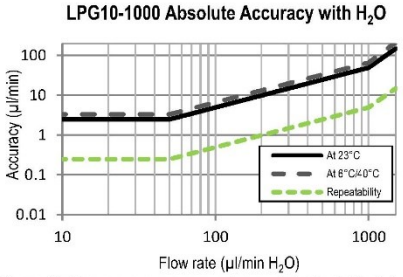

Figure 2: Sensor accuracy and repeatability (µl/min) across the sensor's flow range

3 Communication with the Sensor

The OEM flow sensor LPG10-1000 shows bi-directional, linear transfer characteristics. The product comes fully calibrated for water.

Digital sampling time, 16 bit	74 ms
Digital sampling time, 9 bit	1 ms

3.1 Electrical Specifications

Table 2: DC Characteristics

Parameter	LPG10-1000
Operating voltage	3.3– 3.6 V_{DC} (Recommended: 3.4-3.5 V_{DC})
Operating current	< 6 mA typical in operation

The electrical connection to the LPG10-1000 flow sensor is illustrated in the schematic drawing shown in section 3.2.

3.2 Sample Circuitry

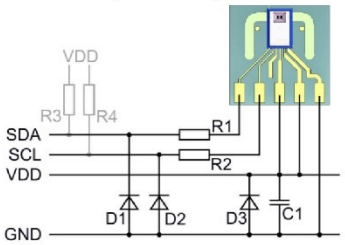

D1, D2, D3: ESD5Z5.0T1G
R1, R2: 47R
C1: 1uF, 25V, X7R, place as close as possible to the sensor pads

Table 3: Pad assignment from left to right:

Pad	Assignment
1	SDA, data
2	SCL (bi-directional), clock
3	VDDA, analog supply voltage
4	VDDD, digital supply voltage
5	GND, ground

The electrical connection to the pads can be realized in different ways, e.g. using spring contacts.

3.3 Digital Communication via I²C-Bus

Digital communication between a master and the LPG10-1000 sensor runs via the standard I²C-interface. The physical interface consists of two bus lines, a data line (SDA) and a clock line (SCL) which need to be connected via pull-up resistors to the bus voltage of the system. By default, the I²C address is set to 64 (hexadecimal: 40, binary: 1000000).

These lines can be used on a 3.3 V level with a clock frequency of 100 kHz. For the detailed specifications of this I²C communication, please refer to specific I²C Application Notes from Sensirion.

4 Fluidic Connection

Table 4: Fluidic Specifications and Pressure Rating

Parameter	LPG10-1000
Wetted materials:	
• Internal substrate flow channel material	Borosilicate glass
Fluidic connection	Downmount
Pressure drop (at full scale flow rate, H_2O, 23°C)	0.1 mbar
Total internal volume	~11.7 µl

5 Mechanical Specifications

Table 5: Mechanical Specifications (for tolerances please see the drawings below)

Parameter	LPG10-1000
Largest dimensions	10 x 10 x 2.25 mm
Total mass	0.32 g
Cross section flow channel	0.9 x 0.9 mm

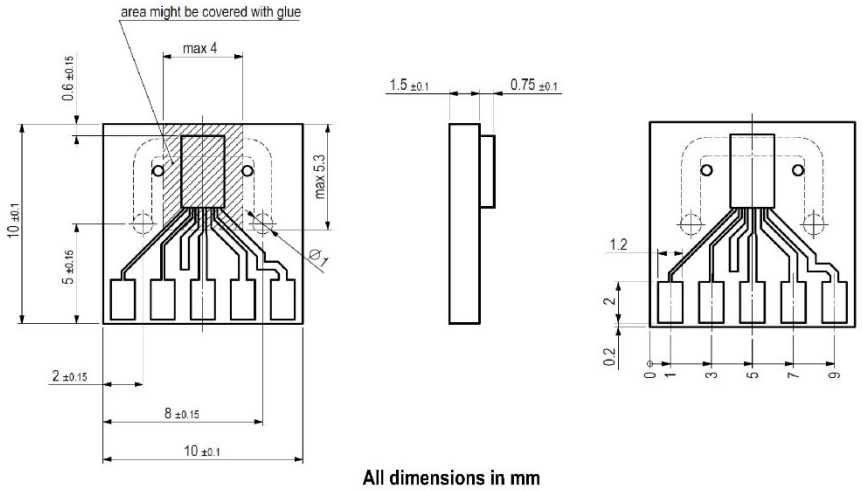

All dimensions in mm

Attention fragile!	
Mechanical shocks and touching of the glass surface may lead to stress on the chip and may damage the glass package. • The thin-walled top layer can easily break. Thus, do not touch the planar glass package on the top surface with your fingers or tools (e.g. tweezers). • Respect the burst pressure specification. Be aware that injecting fluid by hand with a syringe can lead to large pressure peaks. • Do not exert pressure on the chip. Mechanical structures must not be in contact with the sensor chip (see tolerances above). • Do not operate the liquid flow sensor when the contact pads have been wetted. Dry first.	!

6 Ordering Information

Standard shipment includes only the sensor, neither cables nor fluidic connection material.

For easy testing, an Evaluation Kit is available. The kit contains:
An LPG10-1000 sensor, preassembled in a fluidic manifold (PMMA), featuring ¼ -28 flat bottom fluidic fittings. The fluidic seal between sensor and manifold is ensured using two O-Rings (FPM). The included connector cap secures the sensor to the manifold and features a 4-pin Molex connector. The included Molex adapter cable, USB-cable and software allow for easy evaluation using a PC. When using the Evaluation Kit, the wetted materials include PMMA (manifold) and FPM (O-Rings), as well as borosilicate glass (LPG10 sensor).

For customers who wish to evaluate their own manifolds, we offer a Connectivity Kit containing:
The connector cap featuring a 4-pin Molex connector, O-Rings (FPM) for fluidic sealing, a flat ribbon cable (30 cm) and M2.5x8 screws for fixation.

Contact Sensirion for more information on the Evaluation or the Connectivity Kit.

Product	Article No	MOQ	Packaging Unit
LPG10-1000	1-101126-01	100	20
Evaluation Kit LPG10-1000	1-101319-01	1	n/a
Connectivity Kit LPG10 Series	1-101500-01	1	n/a

Important Notices

Warning, personal injury

Do not use this product as safety or emergency stop devices or in any other application where failure of the product could result in personal injury (including death). Do not use this product for applications other than its intended and authorized use. Before installing, handling, using or servicing this product, please consult the datasheet and application notes. Failure to comply with these instructions could result in death or serious injury.

If the Buyer shall purchase or use SENSIRION products for any unintended or unauthorized application, Buyer shall defend, indemnify and hold harmless SENSIRION and its officers, employees, subsidiaries, affiliates and distributors against all claims, costs, damages and expenses, and reasonable attorney fees arising out of, directly or indirectly, any claim of personal injury or death associated with such unintended or unauthorized use, even if SENSIRION shall be allegedly negligent with respect to the design or the manufacture of the product.

ESD Precautions

The inherent design of this component causes it to be sensitive to electrostatic discharge (ESD). To prevent ESD-induced damage and/or degradation, take customary and statutory ESD precautions when handling this product.

Warranty

SENSIRION warrants solely to the original purchaser of this product for a period of 12 months (one year) from the date of delivery that this product shall be of the quality, material and workmanship defined in SENSIRION's published specifications of the product. Within such period, if proven to be defective, SENSIRION shall repair and/or replace this product, in SENSIRION's discretion, free of charge to the Buyer, provided that:

- notice in writing describing the defects shall be given to SENSIRION within fourteen (14) days after their appearance;
- such defects shall be found, to SENSIRION's reasonable satisfaction, to have arisen from SENSIRION's faulty design, material, or workmanship;
- the defective product shall be returned to SENSIRION's factory at the Buyer's expense; and
- the warranty period for any repaired or replaced product shall be limited to the unexpired portion of the original period.

This warranty does not apply to any equipment which has not been installed and used within the specifications recommended by SENSIRION for the intended and proper use of the equipment. EXCEPT FOR THE WARRANTIES EXPRESSLY SET FORTH HEREIN, SENSIRION MAKES NO WARRANTIES, EITHER EXPRESS OR IMPLIED, WITH RESPECT TO THE PRODUCT. ANY AND ALL WARRANTIES, INCLUDING WITHOUT LIMITATION, WARRANTIES OF MERCHANTABILITY OR FITNESS FOR A PARTICULAR PURPOSE, ARE EXPRESSLY EXCLUDED AND DECLINED.

SENSIRION is only liable for defects of this product arising under the conditions of operation provided for in the datasheet and proper use of the goods. SENSIRION explicitly disclaims all warranties, express or implied, for any period during which the goods are operated or stored not in accordance with the technical specifications.

SENSIRION does not assume any liability arising out of any application or use of any product or circuit and specifically disclaims any and all liability, including without limitation consequential or incidental damages. All operating parameters, including without limitation recommended parameters, must be validated for each customer's applications by customer's technical experts. Recommended parameters can and do vary in different applications.

SENSIRION reserves the right, without further notice, (i) to change the product specifications and/or the information in this document and (ii) to improve reliability, functions and design of this product.

Copyright © 2001-2017, SENSIRION.

CMOSens® is a trademark of SENSIRION.

All rights reserved

REACH, RoHS and WEEE Statement

The LPG10-1000 complies with requirements of the following directives:

- EU Directive 1907/2006/EC concerning Registration, Evaluation, Authorization and Restriction of Chemicals (REACH)
- EU Directive 2002/96/EC on waste electrical and electronic equipment (WEEE), OJ13.02.2003; esp. its Article 6 (1) with Annex II.
- EU Directive 2002/65/EC on the restriction of certain hazardous substances in electric and electronic equipment (RoHS), OJ01.01.2011

Headquarters and Subsidiaries

SENSIRION AG
Laubisruetistr. 50
CH-8712 Staefa ZH
Switzerland

phone: +41 44 306 40 00
fax: +41 44 306 40 30
info@sensirion.com
www.sensirion.com

Sensirion Taiwan Co. Ltd.
info@sensirion.com
www.sensirion.com

Sensirion Inc., USA
phone: +1 805 409 4900
info_us@sensirion.com
www.sensirion.com

Sensirion Japan Co. Ltd.
phone: +81 3 3444 4940
info-jp@sensirion.com
www.sensirion.co.jp

Sensirion Korea Co. Ltd.
phone: +82 31 337 7700-3
info-kr@sensirion.com
www.sensirion.co.kr

Sensirion China Co. Ltd.
phone: +86 755 8252 1501
info-cn@sensirion.com
www.sensirion.com.cn

To find your local representative, please visit www.sensirion.com/contact

Appendix J Sensirion LPG10 Basic Performance Check

SENSIRION
THE SENSOR COMPANY

Basic Performance Check

Application Note for Liquid Flow Sensors

Preface

This application note gives guidelines on how to run a simple and quick test of a liquid flow sensor's accuracy. Besides the flow sensor and Sensirion's free Sensor Viewer Software, only a low cost, off-the-shelf plastic syringe is required. Please note that the emphasis is on simple and quick testing. The results of the described experiments should solely be used to decide on further test procedures and should not be the basis of any performance or quality evaluation.

1 Applicability

This document is applicable to all Sensirion liquid flow sensors. However, the described method works best for flow sensors with a max flow rate in the milliliter per minute range.

2 Background

Sensirion's liquid flow sensors are high precision devices with unique measurement capabilities such as high sampling speed and accurate measurement of low and ultra-low flow rates. They provide access to flow information in a fluidic system on the millisecond-time scale. In complex setups, the sensor's measurement may differ from the expected behavior or the user's intuition. A typical example of such unexpected measurements are e.g. oscillations in the flow rate at frequencies in the range of a few Hz to a few 10s Hz. These are picked up and recorded by the sensor, even if the flow looks "constant and smooth" to the naked eye.

It is possible for sensors that are used for experiments in a laboratory environment, to show varying results or report a flow rate, which declines or drifts over time. In such situations, the user may question whether the observed behavior corresponds to the true behavior of the system, or if the sensor's reading has drifted. Such drift occurs, for example, if the fluidic system, including the sensor, is contaminated by a biofilm (typical after prolonged use in systems with recirculating water) or has acquired a deposit inside (typical if used with adhesives or other materials which may produce deposits on the inside walls of the fluidic system).

Even though, Sensirion liquid flow sensors are designed to be robust, they are high precision devices. If the sensor has suffered a drop or impact, the user might be unsure if the sensor was damaged in the event.

In all these situations, the user would like to verify the sensor's performance, i.e. check, that the sensor is still "OK". While it requires a highly sensitive and sophisticated setup to precisely verify the sensor's performance and factory calibration over the entire flow range, a set of simple checks can already detect (or rule out) the majority of sensor failures and hence allow the user to decide if the sensor is right or wrong.

Alternatively, when the application requires using the sensor with other liquids than those for which it was calibrated (e.g. H_2O or IPA), it will be beneficial to evaluate the sensor's performance in response to this liquid and estimate the measurement deviation.

Whenever there is doubt about the sensor's performance, we strongly recommend removing it from the system in which it is installed and verify its performance independently, thus removing as many external factors as possible. Experience shows that even seemingly simple integrated setups can show problematic effects that make them unreliable to determine a sensor's accuracy.

This document provides a recipe on how to perform a simple verification measurement of your sensor's performance using only readily available materials and the Sensirion Liquid Flow Meter Kit.

3 Required Materials

- Sensirion Liquid Flow Meter Kit including the sensor, the SCC1-USB Sensor Cable, and fluidic fittings
- (windows) PC with a free USB port and the USB-RS485 Sensor Viewer[1] software installed.
- Clean beaker, cup or the like
- Two short plastic tubes about 30 cm (1 ft.) each.
- Plastic syringe, 250µl, 1 ml, 2 ml, 5 ml, 10 ml, or 50 ml, depending on the sensor's flow range.
- For low flow rate sensors: a suitable fluidic restriction: small ID tube or syringe needle/cannula

Tubes, plastic syringes and syringe needles are readily available in most drugstores.

4 Basic Idea

At each flow measurement instance, the totalizer function of the Sensor Viewer software calculates the amount of liquid (volume) that passed through the sensor since the last measurement instance. By summing up these volumes, the total volume is calculated.
When a known volume, in this case the fill level of a syringe, is ejected through the sensor, the volume measured by the totalizer should agree with the ejected volume if the flow rate did always stay within the sensor's measurement range.

For flow rates of more than ~ 10 ml/min, it is possible to maintain a relatively constant ejection flow rate using a hand driven syringe and the measurement graph of the Sensor Viewer as visual feedback. Simply match the strength used to push in the plunger to your desired flow rate. You should be able to maintain a flow rate within 10-20% of the target flow rate.

Contamination and damages of Sensirion liquid flow sensors typically affect the sensor's measurement accuracy over the full measurement range. The effect on the maximum flow rate is typically a bit higher than for lower flow rates.

Therefore, we recommend doing the first test at about 70-80% of the sensor's full-scale flow rate:

- This makes it easy to control the flow by hand,
- gives enough room for small variations,
- and is very likely to confirm inaccuracies.

5 General procedure

In order to verify the sensor's performance, 3 steps are needed:

1. Verify the sensor reading for an (approximately) constant forward flow
2. Verify the sensor reading for an (approximately) constant backward flow.
3. Measure the sensor's offset (zero-flow reading)

These will be described in more detail below.

[1] https://www.sensirion.com/en/download-center/

SENSIRION
THE SENSOR COMPANY

6 Detailed Procedure

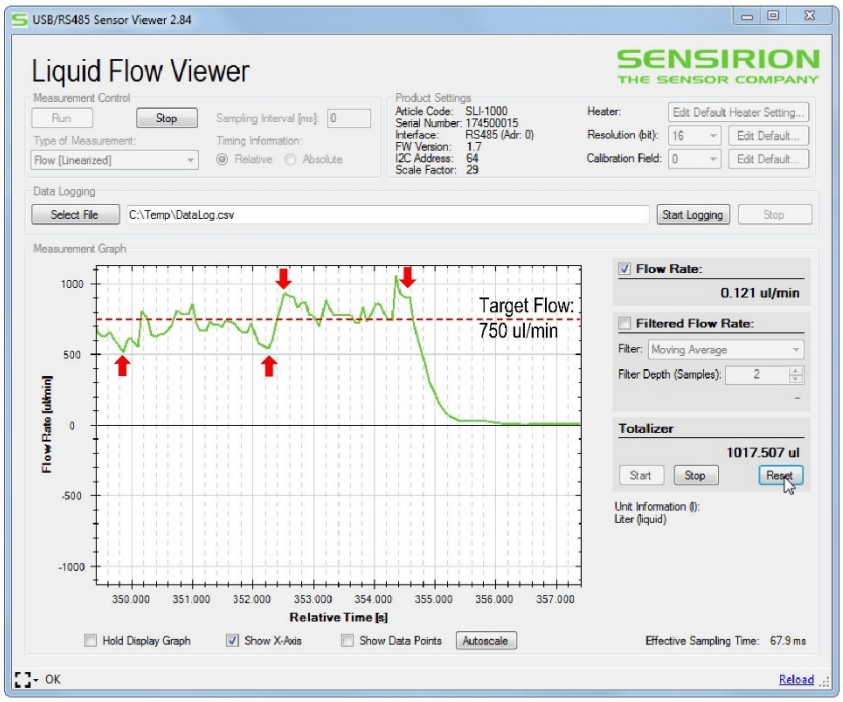

Figure 1: Sensor Viewer with Totalizer showing the measured volume after ejection of a 1 ml syringe

Step 1: Connect the sensor via the SCC1-USB cable with a PC and start the measurement in the Sensor Viewer software.
Step 2: Connect a tube to the sensor's outlet (downstream side) and hang it into a beaker filled with liquid.
Step 3: Draw up a syringe from the liquid in the beaker and push out any air and air bubbles.
Step 4: Connect the syringe to the sensor's inlet (upstream side) and push the liquid with relatively high force through the sensor to push out any air and bubbles that are caught in the sensor or tubing. Draw up the syringe and repeat until no more bubbles escape the tubing into the beaker.
Step 5: Draw the syringe up to the maximum fill volume.
Step 6: Start the Sensor Viewer's totalizer function. (Reset first if it does not show zero).
Step 7: Push the liquid slowly out of the syringe while viewing the flow rate on the screen and try to maintain the flow rate close to the target flow rate.
Step 8: Stop the totalizator once the syringe is empty.

Repeat this procedure for backward flow by installing the sensor in the opposite direction.

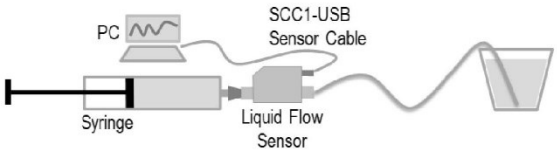

Figure 2: Suggested setup for performance testing

7 Low Flow Sensors

At lower flow rates than approximately 10 ml/min, it is difficult maintaining a constant flow rate with a low cost syringe by hand. This can be solved by introducing a flow restriction right after the sensor. Due to the low flow rates, this must be a capillary with a small inner diameter of 0.25 mm (0.01 inch). Such capillaries with 1/16" outer diameter made from PEEK are typical for micro fluidic and HPLC applications and can be bought from many suppliers. Due to the $R \sim d^4$ dependency of the restriction on the diameter, a capillary with 0.5 mm inner diameter will not work.
Alternatively, a better syringe or lubricating the plunger might help, too.

8 Recommended Syringes and Restrictions

A syringe with a volume one to three times the sensor's full-scale flow rate (multiple by one minute, i.e. a 40 ml/min full scale sensor requires at least a 40 ml syringe) offers a good trade-off between the time needed for the performance test and the accuracy provided.

	H_2O Calibration		IPA (Hydrocarbon) Calibration[2]	
Sensor Type	Syringe	Restriction	Syringe	Restriction
SLF3S-1300F	50 ml	not necessary[3]	50 ml	not necessary[3]
SLF3S-0600F	2 - 5 ml	Pressure Drop: ~ 100 kPa Capillary: L: ≈ 350 mm, ID: 0.25 mm, or Capillary: L: ≈ 20 mm, ID: 0.12 mm, or Needle: L: ≥ 10 mm, ID: 0.1 mm (i.e. 32G)	2 -5 ml	Pressure Drop: ~ 100 kPa Capillary: L: ≈ 350 mm, ID: 0.25 mm, or Capillary: L: ≈ 20 mm, ID: 0.12 mm, or Needle: L: ≥ 10 mm, ID: 0.1 mm (i.e. 32G)
SLS-1500	50 ml	not necessary[3]	n/a	n/a
SLI-2000	1 - 10 ml	Pressure Drop: ~ 30 kPa Capillary: L: ≈ 200 mm, ID: 0.25 mm, or Needle: L: ≥ 10 mm, ID: 0.15 – 0.25 mm (i.e. 25G - 30G)	50 ml	not necessary[3]
SLI-1000	1 ml	Pressure Drop: ~ 70 kPa Capillary: L: ≈ 500 mm, ID: 0.25 mm, or Capillary: L: ≈ 30 mm, ID: 0.12 mm, or Needle: L: ≥ 10 mm, ID: 0.1 mm (i.e. 32G)	1 - 10 ml	Pressure Drop: ~ 30 kPa Capillary: L: ≈ 200 mm, ID: 0.25 mm, or Needle: L: ≥ 10 mm, ID: 0.15 – 0.25 mm (i.e. 25G - 30G)
SLI-0430	250 ul[4]	Pressure Drop: ~ 70 kPa Capillary: L: ≈ 300 mm, ID: 0.12 mm	1 ml	Pressure Drop: ~ 70 kPa Capillary: L: ≈ 500 mm, ID: 0.25 mm, or Needle: L: ≥ 10 mm, ID: 0.1 mm (i.e. 32G)
LD20-2600B	50 ml	not necessary[3]	n/a	n/a
LD20-0600L	1 ml[4]	Pressure Drop: ~ 70 kPa Capillary: L: ≈ 300 mm, ID: 0.12 mm	n/a	

Table 1: Suggested syringes and flow restrictions

[2] For testing a sensor with a liquid with higher viscosity than water or IPA, the restriction should be reduced proportionally in length to maintain the pressure drop. Viscosity and length affect the restriction's pressure drop linearly.
[3] Depending on the quality of the syringe, a small restriction might be helpful.
[4] At flow rates far below 1 ml/min it is difficult to maintain a stable flow manually.

SENSIRION
THE SENSOR COMPANY

9 Zero-flow Offset Measurement

Follow the steps described in the above procedure with a slight modification to obtain a precise zero-flow reading.

- Follow steps 1 to 5 to setup and prime the system.
- Then put the syringe down on the table and don't touch the system or the test bench.
- Wait until the flow rate stabilizes at or around zero. Use the "autoscale" button in the viewer SW to zoom in to the y-axis. Note that the sensor can detect very low flow rates. It may take up to a minute for the flow to stabilize.
- Start the totalizer in the viewer software.
- Wait *exactly* one minute. Use a stopwatch or timer.
- Stop the totalizer in the viewer software.
- Divide the value of the totalizer by the time (1 minute or 60 seconds) to get the average flow rate during the test.

10 Interpretation of Measurement Results

If the zero flow offset as well as forward and backward flow measurements are within the sensor's specification according to the datasheet, the sensor is OK. Otherwise, please contact Sensirion for support.

11 Optional

The aim of this document is to describe the simplest testing method that is accessible to almost any user. If you have other equipment at hand, it can be improved in many ways. For example, with a precision balance or a precision syringe pump as reference or flow source.
However, even if such equipment is available, the presented method still offers a quick test to decide whether it is worthwhile setting up a more elaborate test.

Copyright© 2020, SENSIRION.
CMOSens® is a trademark of Sensirion.
All rights reserved.

12 Headquarters and Subsidiaries

Sensirion AG
Laubisruetistr. 50
CH-8712 Staefa ZH
Switzerland

phone: +41 44 306 40 00
fax: +41 44 306 40 30
info@sensirion.com
www.sensirion.com

Sensirion Taiwan Co. Ltd
phone: +886 3 5506701
info@sensirion.com
www.sensirion.com

Sensirion Inc., USA
phone: +1 312 690 5858
info-us@sensirion.com
www.sensirion.com

Sensirion Japan Co. Ltd.
phone: +81 3 3444 4940
info-jp@sensirion.com
www.sensirion.co.jp

Sensirion Korea Co. Ltd.
phone: +82 31 337 7700~3
info-kr@sensirion.com
www.sensirion.co.kr

Sensirion China Co. Ltd.
phone: +86 755 8252 1501
info-cn@sensirion.com
www.sensirion.com.cn

To find your local representative, please visit www.sensirion.com/distributors